Advanced Characterisation of Turbochargers with the focus of Modelling Two-stage Turbocharging Systems

Avola, Calo

Award date:
2017

Awarding institution:
University of Bath

Advanced Characterisation of Turbochargers with the focus of Modelling Two-stage Turbocharging Systems

Calogero Avola

A thesis submitted for the degree of Doctor of Philosophy

University of Bath

Department of Mechanical Engineering

August 2017

Abstract

Two-stage sequential turbocharging systems are adopted in automotive powertrains, in order to enhance torque level and transient response of the internal combustion engine. High pressure (HP) and low pressure (LP) turbochargers are placed in sequence, with exhaust gasses expanding through LP and HP turbines; while, air is compressed by LP and HP compressors, respectively, before being forced into the engine intake. In order to maximise performance and flexibility of the internal combustion engine, regulating valves are implemented into the turbocharging system. In order to investigate the interaction between the boosting system and the internal combustion engines, one-dimensional (1D) model simulations are considered a fundamental tool. In this scenario, turbomachinery performances are imposed into the model through compressor and turbine maps, to analyse the complete power unit. The adoption of standard gas-stand maps would be omitting the flow non-uniformity effects on a turbomachine due to bends and the presence of heat transfer in turbochargers could influence enthalpy level at boundaries. In addition, specific to two-stage turbocharging systems, the high degree of swirling flows and temperatures at the inlet of the HP compressor induced by the upstream turbomachine can influence significantly the performance of the two-stage system. Therefore, it has been fundamental to perform this study on the advanced characterisation of turbochargers, focussing on the modelling two-stage turbocharging systems.

In order to perform the research study, a new engine gas-stand facility has been developed, mapping turbochargers compressors under steady flows. In addition, in the unsteady layout, the introduction of pressure pulsations at the compressor under real engine pulsations has shown a significant shift of the surge line towards lower mass flows. In order to quantify the effects occurring in a sequential two-stage turbocharging system, an equivalent mapping approach has been developed, aiming to the improvement of accuracy in performance characterisation, accounting for inter-stage flows and heat transfers effects. Equivalent two-stage compressor maps have differed from the stand-alone mapping approach below 23Krpm due to poor accuracy of stand-alone maps at low compressor speeds. On the turbines side, maximum differences of 10% between equivalent and stand-alone maps persist in turbine efficiency, due to turbine isentropic power.

Acknowledgments

I would like to thank my primary supervisor, Dr. Colin Copeland, for the opportunity given in undertaking this PhD and his support throughout the journey. His mentorship has been excellent, producing highly efficient and constructive discussions in meetings.

Moreover, I would have to congratulate my line manager and co-supervisor, Dr. Richard Burke, for allowing me adequate time in performing the PhD studies while having a full-time position.

Nonetheless, I have to thank Prof. Chris Brace, Dr. Sam Akehurst and the entire PVRC team for their contribution in making me the professional engineer and researcher I am today. This could not have been possible outside the great environment they have created throughout the years.

In addition, I would like to thank Dr. Alessandro Romagnoli for hosting me at NTU during my visiting time as a researcher under the Future Research Leaders Incubator Scheme. For this, I thank the University of Bath and the Institute of Mechanical Engineers (IMechE) for the financial support.

Furthermore, I acknowledge the research consortium, *TurboCentre2*, for the constructive meetings and financial support. This thesis would have been just an illusion, otherwise.

A great thank goes to all my colleagues at the PVRC for the friendly support, help and the petrol-head discussions, keeping up pace and passion. In addition, it is impossible to exclude Bob, Jim, Martin, James and Tom for the help in the test cell. Thank you for the help in clearing up all my mess, including that time I let the *fire man* personality taking advantage.

Finally, I would have to thank my parents and sister for their support in the choices I have made. Moreover, a lovely thank goes to my fiancée, Luana, for being with me during this journey and providing me the brightness even in the darkest noon.

Contents

Nomenclature

Abbreviations

1D	One-dimensional
2D	Two-dimensional
3D	Three-dimensional
ABB	ASEA Brown Boveri Co.
AFR	Air-fuel ratio
ASME	American Society of Mechanical Engineers
BMEP	Brake mean effective pressure
BSFC	Brake specific fuel consumption
CAD	Crank angle degree
CAN	Controller area network
CB	Compressor back-pressure
CBP	Compressor by-pass
CHT	Conjugate heat transfer
CO	Carbon oxide
COT	Compressor outlet temperature
CoV	Coefficient of Variation
CR	Compression ratio
CRF	Compressor restricting flow
DAQ	Data acquisition
DoE	Design of Experiment
EC	Electric compressor
ECU	Engine control unit
EGR	Exhaust gas recirculation
EGS	Engine gas-stand
EHTR	Equivalent heat transfer resistance
EIVC	Early intake valve closing
FE	Fuel efficiency
FFT	Fast Fourier Transform
GS	Gas-stand

HC	Hydrocarbons
HP	High pressure
HT	Heat transfer
I/C	Intercooler
IHI	Ishikawajima-Harima Heavy Industries Co.
KKK	Kühnle, Kopp & Kausch Co.
LP	Low pressure
MAF	Mass air Ffow
NA	Not available
NEDC	New European driving cycle
NOx	Nitrogen oxides
P	Pressure
PID	Proportional, integral and derivative
PR	Pressure ratio
PRT	Platinum resistance thermometer
RAC	Swirl ratio for volute B
RAS	Swirl ratio for volute A
SAE	Society of Automotive Engineers
SC	Mechanical supercharger
T	Temperature
TBP	Turbine by-pass
TC	Turbocharger (in figure 2.1)
TC	Thermocouple
TIT	Turbine inlet temperature
TOT	Turbine outlet temperature
T-s	Total-to-static
TST	Two-stage turbochargers
T-T	Total-to-total
TWG	Turbine wastegate
V	Version
VGT	Variable geometry turbocharger
VTC	Virtual thermocouple

VTS	Virtual temperature sensors
VVT	Variable valve timing
WC	Water-cooled
WLTC	Worldwide harmonised light vehicles test cycle

Definitions

$\bar{h}$	Convective heat transfer coefficient (W/m^2 K)
$\dot{Q}$	Heat transfer rate (J/s)
$\dot{m}$	Mass flow rate (Kg/s)
a	Speed of sound (m/s)
C	Absolute air velocity at compressor inlet (m/s)
c_p	Specific heat capacity at constant pressure (J/K)
c_v	Coefficient of variation (%)
D2	Impeller tip diameter (m)
g	Gravitational acceleration (m/s^2)
Gr	Grashof number (-)
h	Enthalpy (J/Kg)
kc	Non-dimensional heat transfer coefficient (-)
L	Characteristic length (m)
Lambda	air-to-fuel concentration relative to the stoichiometric reaction (-)
M	Higher sample value (bar) and (Kg/s)
m	Lower sample value (bar) and (Kg/s)
Mu2	Tip speed Mach number (-)
N	Turbocharger speed (rpm)
Nu	Nusselt number (-)
Pr	Prandtl number (-)
q	Specific heat transfer (J/Kg)
R	Gas constant (J/Kg K)
Re	Reynolds number (-)
s	Entropy (J/Kg K)
SD	Standard Deviation (bar) and (Kg/s)

U	Rotor tangential velocity (m/s)
$u2$	Impeller blade tip speed (m/s)
V	Velocity of the fluid (m/s)
w	Absolute relative velocity at compressor inlet (m/s)
wt	Specific shaft work (J/Kg)
β	Coefficient of volume expansion (K)
γ	Ratio of specific heats (-)
η	Efficiency (-) and (%)
θ	Maximum amplitude (bar) and (Kg/s)
Θ	Temperature difference between surface and fluid (K)
κ	Thermal conductivity (W/m K)
λ	Enthalpy rise (J/Kg)
μ	Dynamic viscosity of the fluid (Pa s)
ρ	Density (Kg/m^3)
ϕ	Flow coefficient (-)
ψ	Mean value (bar) and (Kg/s)

Subscripts

1	Compressor Inlet
12	Compression process (1 to 2)
2	Compressor Outlet
2st	Two-stage
3	Turbine Inlet
34	Expansion process (3 to 4)
4	Turbine Outlet
adia	Adiabatic
app	Apparent
c	Compressor
corr	Corrected
dia	Diabatic
eff	Effective
eq	Equivalent

f	Friction
H	Housing
in	Inlet
in-st	Inter-stage
is	Isentropic
m	Mean
nc	Convection
oc	Conduction
out	Outlet
R	Radiation
red	Reduced
ref	Reference
s	Static
t	Total
T	Turbine
tc	Turbocharger
t-s	Total-to-static
t-t	Total-to-total
wc	Water-cooled

Superscripts

“	Inch
*	Position of thermocouple at turbine inlet
^	Position of pressure sensor
.	First derivative

Symbols

a,b,c,d,e,f	Constants (-)
n	Total samples (-)
x_i	Sample (-)
Δ	Difference

Further publications

The work in this thesis has been presented at various conferences and published in peer-reviewed articles. The list of publications related to the content of this thesis is reported below.

Review of Turbocharger Mapping and 1D Modelling Inaccuracies with specific focus on Two-Stage Systems

Avola, C. et al., 2015. SAE paper 2015-24-2523. 10.4271/2015-24-2523

Preliminary DoE analysis and control of mapping procedure for a turbocharger on an engine gas-stand

Avola, C. et al., 2016. ASME GT2016-56466. 10.1115/GT2016-56466

Numerical Investigation of Two-Stage Turbocharging Systems Performance

Avola, C. et al., 2016. ASME ICEF2016-9449. 10.1115/ICEF2016-9449

Compressor surge for fully and semi fluctuating automotive turbochargers

Avola, C. et al., 2017. GPPF 2017-136. http://www.pps.global/forum/zurich17/zurich17-proceedings/papers/radial_turbomachinery/GPPF_2017_paper_136.pdf

Effect of inter-stage phenomena on the performance prediction of two-stage turbocharging systems

Avola, C. et al., 2017. *Journal of Energy*, Vol. 134, pp. 743-756

List of figures

List of tables

Chapter 1 – Introduction

In this chapter, an introduction to the thesis is reported. Specifically, three sections are included as follows:

1. Background and motivation for conducting this research project on the advanced characterisation for modelling of two-stage turbocharging systems.

2. Definition and list of research objectives. In this section the project aim is also described.

3. For a more comprehensive view of the thesis, an introduction for each of the chapters is presented in the form of a list.

1.1 Background and motivation

1.1.1 Perspective

The rise in world population and the number of driven vehicles is leading policy makers towards the restriction of tailpipe emissions for new selling vehicles. Emission regulations, such as, the EURO 6 and the future EURO 7 [1] from the European Union, are setting limits on the release of harmful gaseous and solid pollutants from vehicles powered by internal combustion engines. Specifically, allowable levels of NO_x, HC, CO and particulates are defined for vehicles tailpipes during a controlled driving cycle. However, researchers have shown that the unique New European Driving Cycle (NEDC) could not represent the real world emissions of vehicles, due to low loads and speeds being required by the powertrain [2]. Therefore, a new driving cycle, knows as the Worldwide harmonized Light vehicles Test Cycle (WLTC), has been defined for incorporating restrictions on emissions also at medium/high load and speed of the engine [3].

Furthermore, these limits on emissions and the requirements on fuel consumptions and CO_2 [4] have led to investigation of new engine technologies, such as boosting devices. In this scenario, two-stage turbocharging systems could become a viable solution for improving powertrain efficiency. In addition, regulated two-stage systems can be more flexible, in regards to the constraints of a single stage compressor even in conjunction with variable geometry turbines (VGT), due to the different operation ranges of high and low pressure turbochargers. It is important to notice that single stage turbocharging systems, including VGT, are cheaper and simpler solutions than regulated two-stage systems. On the other side, the smaller HP turbocharger in the two-stage system would be able to improve transient response and reduce turbo-lag, because of lower rotating inertia. Due to growing presence of two-stage turbocharging systems in the automotive industry, performance characterisations for evaluation of this technology have become a necessity. In order to investigate performance of two-stage turbocharged powertrains, 1D simulations are implemented, as an inexpensive and resourceful tool for engine system development.

In 1D models, compressors and turbines of turbochargers are represented by performance maps. In addition, 1D models are not able to solve flow motion at inter-stage connecting ducts, due to the three-dimensional (3D) nature. However, 3D

simulations would require a significant amount of time to perform the thermodynamic analysis. Therefore, this project investigates a methodology to account for inter-stage effects and interactions with turbomachine for representing two-stage systems in 1D simulations, without recurring to the use of more complex 3D models.

1.1.2 Principles of automotive turbochargers

The adoption of turbochargers in internal combustion engines allows useful energy to be extracted from the exhaust gases, instead of being wasted, in order to increase the engine specific power. The higher air density at the engine intake leads to a rise in engine torque and power, due to the possibility to inject more fuel, without producing harmful pollutants. In this way, the specific power of each cylinder is increased together with the overall efficiency of the engine. Moreover, for constant engine power, a turbocharged engine can reduce the number of cylinders by decreasing friction and moving masses, applying the downsizing philosophy. The birth of turbochargers was signed with the patent published by the Swiss engineer Alfred Büchi, in 1905. This described a turbocharger as a turbine and a compressor coupled by a common shaft [5]. The unit was meant to be installed in a way that the exhaust gases could expand and make the turbine rotating. Consequently, the extracted mechanical power would be transferred to the compressor, pressurising the air delivered to the engine. Later in 1924, Brown Boveri (BBC) developed and installed the first turbocharger on a large Diesel engine [5]. Since then, the technology has been subjected to continuous improvements, with new modelling tools and experimental techniques being developed [6].

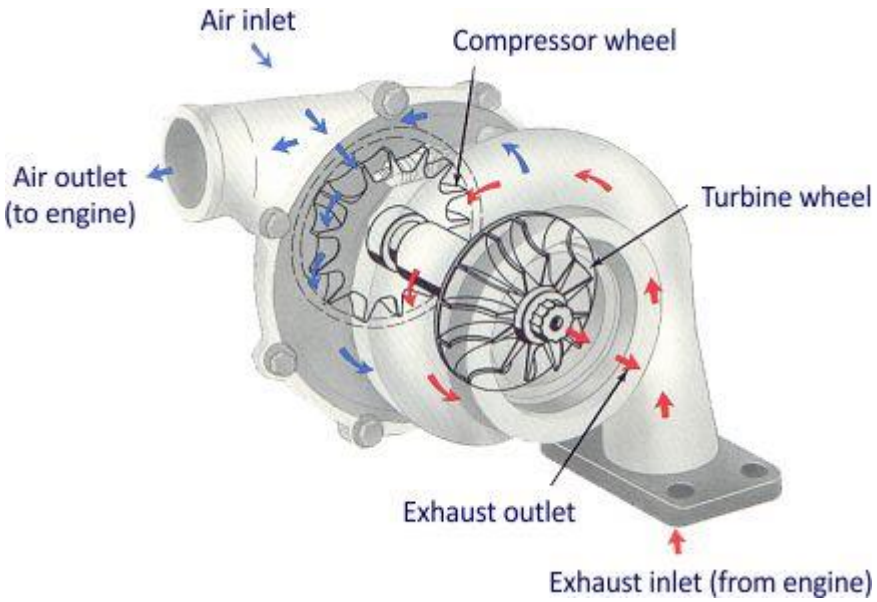

Figure 1. 1: Schematics of an automotive turbocharger

In figure 1.1, an automotive turbocharger is shown, including compressor and turbine. Compressor and turbine are connected through a mechanical shaft, rotating on an oil lubricated bearing system. In addition, in order to offer a flexibility over pressure control of the turbocharging unit, a control system is included. This is represented by a wastegate valve on the turbine volute, whose responsibility is to reduce turbine inlet pressure when activated, by-passing the turbine flow directly to the turbine outlet. Therefore, the adoption of a wastegate at the turbine can represent a control feature over the maximum admissible speed of the turbocharger, turbine inlet and compressor outlet pressures.

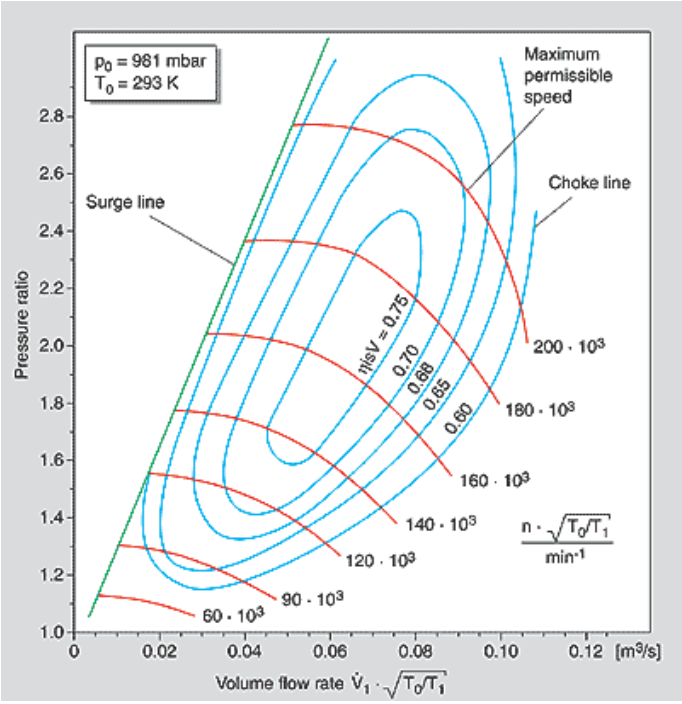

Figure 1. 2: Example of a compressor performance map, including constant speed lines and efficiency islands [7]

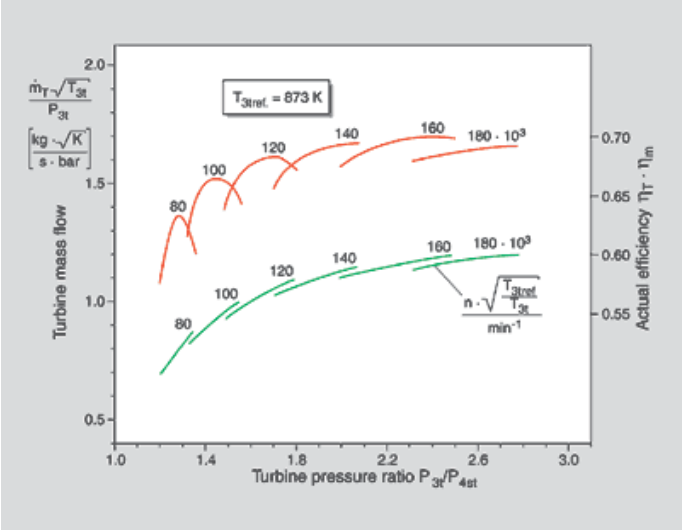

Figure 1. 3: Example of a turbine performance map, including swallowing capacity and efficiency lines [7]

Performance of compressors and turbines could be collected in flow and efficiency maps, with examples of these shown in figures 1.2 and 1.3. In compressor maps, stable operating regions are limited by lines of surge, choke and maximum speed. Specifically, at low mass flows, the compressor can reach instability when unable to deliver the desired pressure ratio, generating reversing flow at the inlet, due to

surge. At high flows, choke could occur in the compressor, reducing downstream pressure. In addition, for each stable operating point, rotational speed and efficiency of the compressor can be identified. Moreover, turbine performance are represented by the swallowing capacity (green lines in figure 1.3) and the efficiency lines (red lines in figure 1.3). In addition, operations of the turbine could be represented by several speed lines as in figure 1.3. In order to reduce dependency of compressor and turbine performance from temperature and pressure at the inlet of the turbomachine, corrected flow parameters and speed values are adopted in maps.

The elevated rotational speeds of the turbocharger shaft (up to 260000 rotation per minute) and exhaust gas temperatures entering the turbine, the bearing system at the turbocharger core would have to work hard to provide adequate lubrication and cooling power. In figure 1.4, the internal oil passages of the bearing system can be visualised. Furthermore, due to the maximization of turbocharging levels in downsized engines, water-cooling passages are often installed to reduce heat flux from turbine to compressor. In fact, although the high temperatures would be beneficial for enhancing power extraction at the turbine, heat to the compressor would translate into increased cooling demand for the after-cooler. In addition, in order to reduce friction losses, ball bearing systems are offered by turbo manufacturers, instead of oil lubricated journal bearings, in order to reduce turbocharger friction.

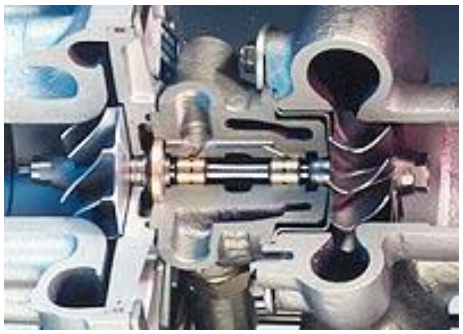

Figure 1. 4: Oil bearing system of an automotive turbocharger [7]

1.1.3 Turbochargers in automotive powertrain

In order to increase air density at the inlet without increasing engine intake temperature, a charge air cooler is positioned between the turbocharger and the

engine intake ports. In figure 1.5, a simplified layout of a turbocharged engine is shown, including a charge air cooler at the intake.

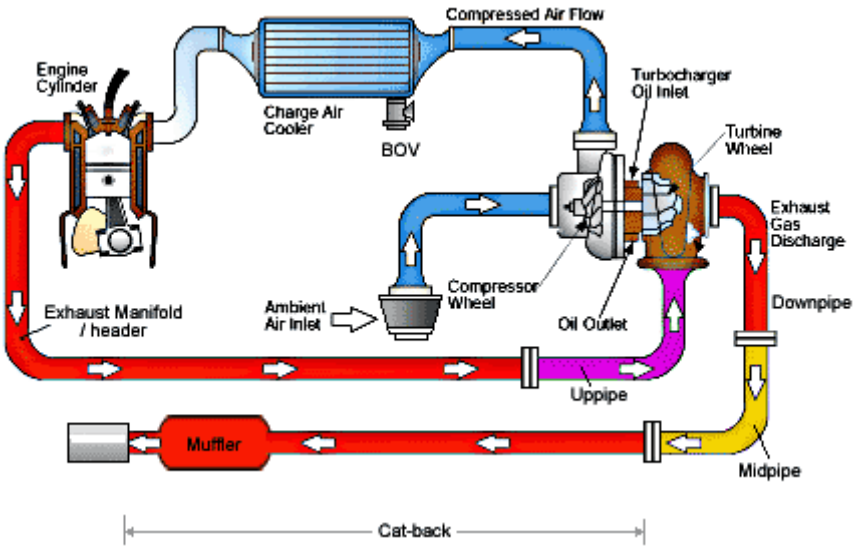

Figure 1. 5: Layout of a turbocharged internal combustion engine

Furthermore, the requirement for automotive turbochargers to deliver high boost pressure at the engine intake at low engine speed, improving low end torque of the engine, has led the development of variable geometry turbines (VGT). In figure 1.6, the turbine rotor/wheel is located downstream the pivoting vanes of the variable geometry, regulating the opening area of the turbine nozzle via an external actuator. Therefore, flow velocity can be maintained at the inlet of the turbine rotor, increasing the rotational speed of the turbocharging unit. In order to reduce volumes between the turbocharger unit and the internal combustion engine, turbocharger turbines are positioned in proximity of the engine exhaust, favouring transient operations. However, in engines with overlapping exhaust valve events of different cylinders, i.e. four cylinder engines with unique exhaust manifold, engine gas exchange would be reduced. In this scenario, twin scroll turbines, shown in figure 1.7, could maximise the pulsing effect of the exhaust gas, reducing the risk for flow interference between cylinders at the exhaust.

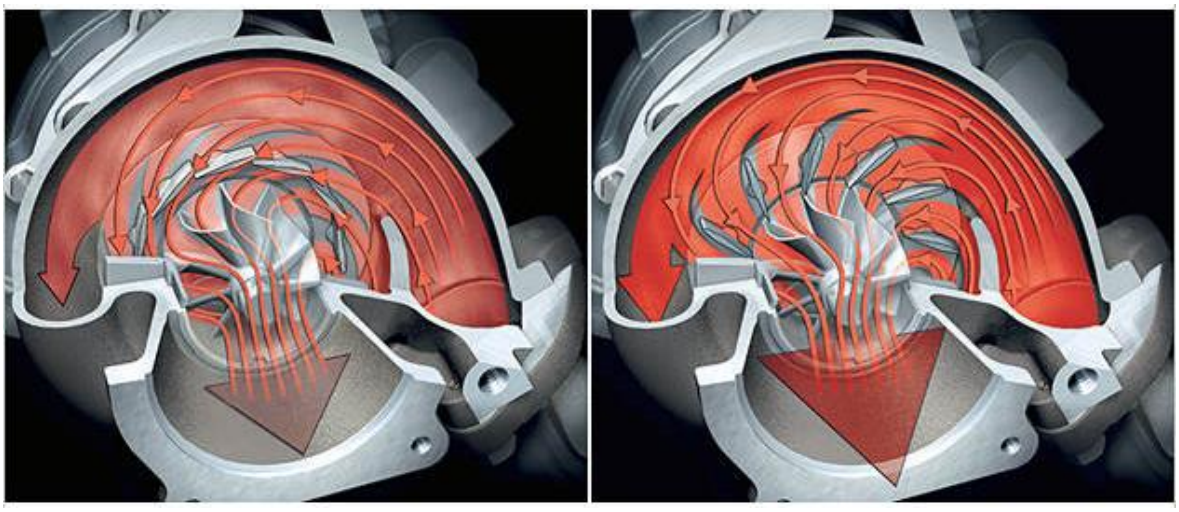

Figure 1. 6: Variable geometry turbine (VGT) turbocharger for improved variability

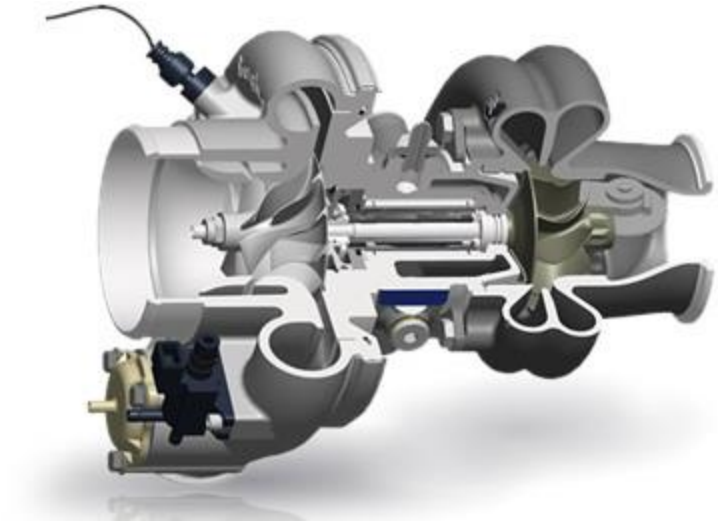

Figure 1. 7: Twin scroll turbine turbocharger for improved efficiency under pulsating flows [7]

Moreover, high level of boost pressure at engine intake could require the adoption of two-stage turbocharging systems, in order to match the target values of mass flow and pressure. In two-stage systems, turbochargers of different sizes are sequentially positioned in the air-path, as visible in figure 1.8. In addition, in order to maintain the optimum operation ranges of the two compressors and turbines, regulating by-pass valves are located in the system. However, due to packaging restrictions in vehicles bonnets, the adoption of bends in the ducting system would be necessary, generating flow disturbances at the inlet of the turbomachines. This

could also lead to a change in compressor/turbine performance, in comparison to the installation with straight ducts at boundaries.

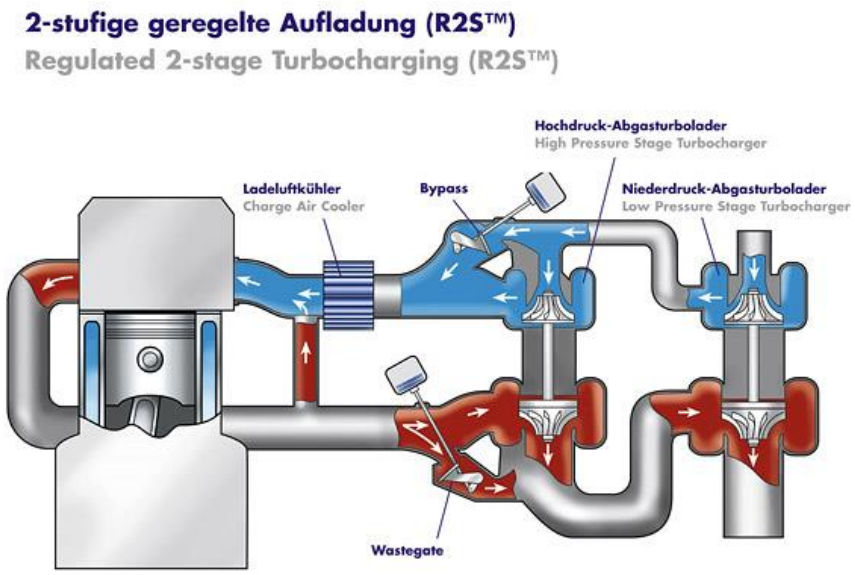

Figure 1. 8: Regulated two-stage turbocharging system for internal combustion engine [7]

1.1.4 Basis of fluid-dynamic simulations in automotive powertrains

In order to investigate the system performance of a turbocharged internal combustion engine, 1D simulation tools, such as Ricardo WAVE® [8] and GT-Suite® [9], could be implemented. Figure 1.9 shows an example of a turbocharged engine system model, consisting of intake and exhaust systems, engine combustion chambers and crankcase, turbochargers compressors and turbines.

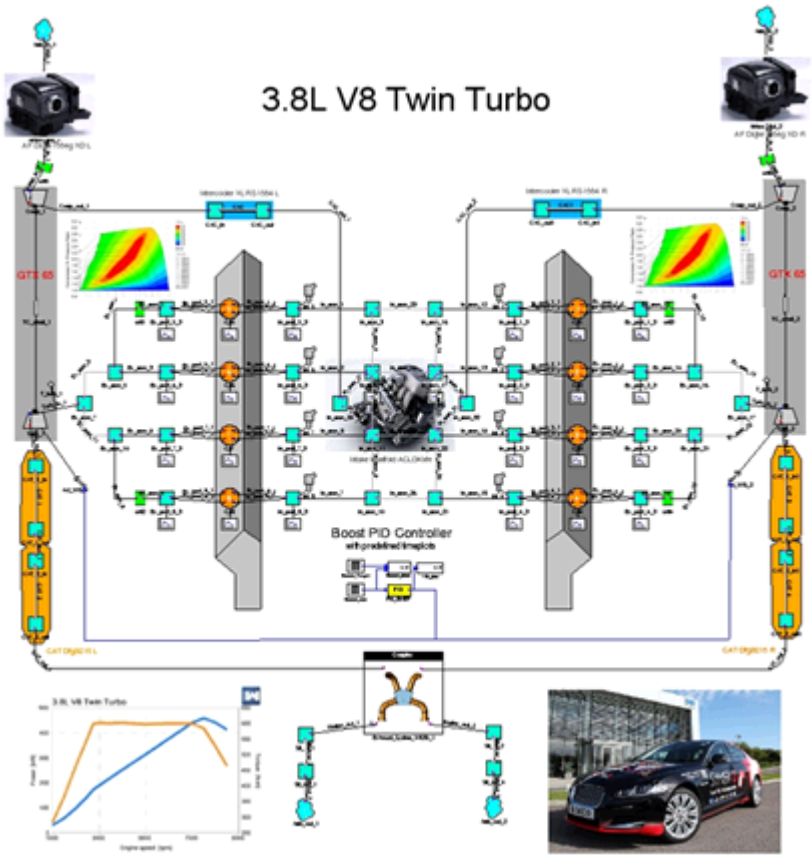

Figure 1. 9: Example of 1D powertrain simulation model [8]

In order to simulate the flow dynamics of intake and exhaust ducts, the air-path system would have to be represented, considering the actual geometries. In addition, boundary conditions would have to be defined, in order to perform the evaluation. In this way, along each duct, the governing equations of conservation of mass, Newton's second law (the change of momentum equals the sum of forces on a fluid particle) and the first law of thermodynamics (conservation of energy) are imposed, considering that fluid and gas are treated as continuums [10]. In addition, in-cylinder combustion is modelled as an exothermic reaction, inducing in-cylinder pressure rise and heat transfer to the cylinder wall. In figure 1.10, an example of the in-cylinder combustion phenomenon is reported, including instantaneous cylinder pressure and burned fuel fraction.

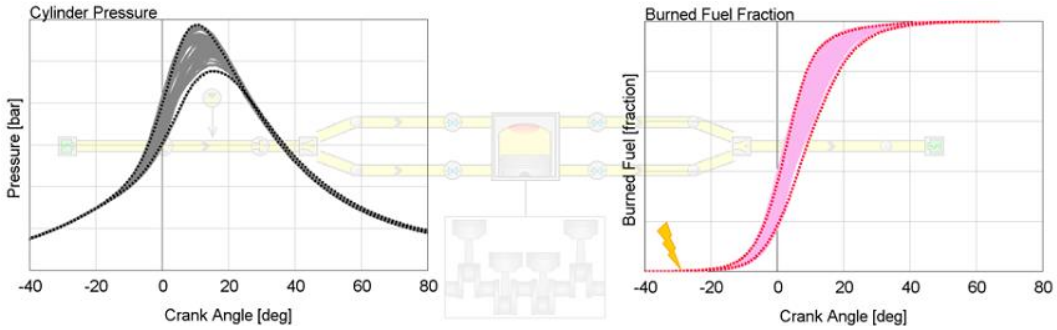

Figure 1. 10: In-cylinder combustion is represented as pressure rise and exothermic reaction [9]

Moreover, turbochargers components can be represented by compressor and turbine maps. In this scenario, measured performance data are imposed as inputs of the powertrain model, including corrected mass flow, pressure ratio, efficiency and corrected reference speed values for both compressor and turbine. In figures 1.11, it is possible to visualize compressor and turbine operating conditions, respectively to the various engine loads and speeds. In this way, compressors and turbine operations could be predicted, assessing that unstable operations are not induced in the turbocharger, such as surge, choke and maximum speed. Moreover, the 1D simulation tool could provide fundamental information in relation to the selection of the perfect turbocharger for an engine specific application.

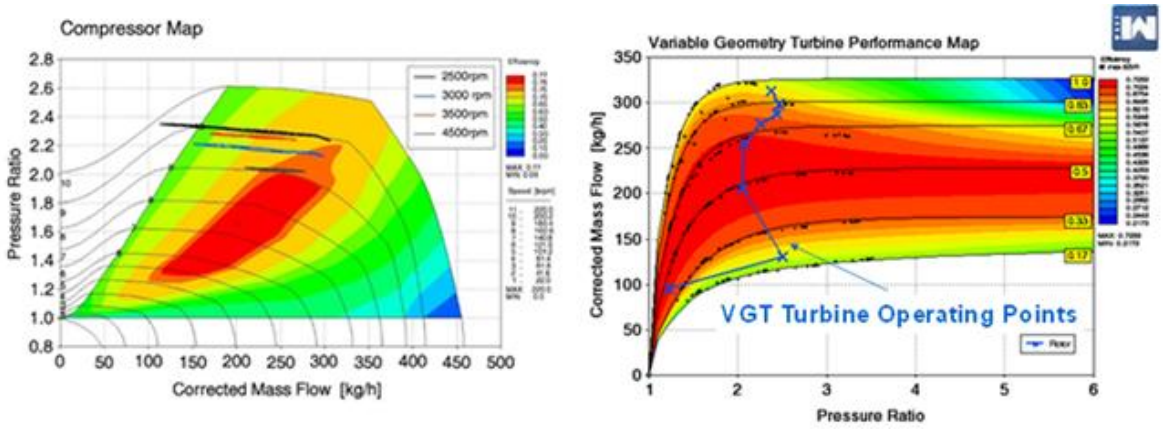

Figure 1. 11: Operating points on compressor and turbine maps for turbocharged internal combustion engine [8]

1.2 Aim, objectives and scope

The aim of this project has been the investigation and evaluation of two-stage turbocharging systems performance. The main focus is the analysis of inter-stage aero-thermal effects on the performance of the two turbochargers. In fact, the project has attempted in the evaluation of performance maps for the complete two-stage system as a single device. In order to perform the analysis, a number of steps have been required, such as the development of an engine gas-stand to evaluate turbochargers performance under steady, unsteady and transient flows.

Therefore, in order to achieve this project aim, specific project objectives have been defined and a complete list can be drawn below:

1. Review of flow and heat transfer effects influencing the performance maps of turbochargers and approaches for modelling two-stage turbocharging systems into 1D simulations.

2. Develop a unique engine gas-stand facility to explore performance of turbochargers.

3. Attempt the development of a methodology to interpret pulsating turbine performance measurements from the engine gas-stand, to capture turbine outlet temperatures into 1D models.

4. Develop a methodology to identify surge onset under steady and pulsating flows of the compressor, identifying the influence on stability range.

5. Investigate performance of regulated two-stage turbocharging systems under real powertrain operations, in order to identify the system operation.

6. Define a novel mapping methodology for two-stage turbocharging systems, reducing the errors in performance predictions, due to inter-stage effects.

7. Evaluate the effectiveness of equivalent maps in representing two-stage system performance.

The scope of this thesis is to investigate the effectiveness of a dedicated mapping approach for two-stage turbocharging systems. The presence of elevated swirling flows at the inlet of the HP compressor could generate a variation in the compressor map and the turbocharging system performance. In order to evaluate the benefits of equivalent maps for LP and HP turbochargers under steady and pulsating flows, an engine gas-stand facility had to be developed. Due to the relevance of surge line in the compressor map and turbine performance under pulsating flows in automotive powertrains applications, investigations have been performance for single turbochargers, in order to be transferred to the two-stage turbocharging system.

1.3 List of chapters

In this thesis, a total of eight chapters attempt to address the project aim and objectives, while, chapters 1 and 10 consist of the thesis introduction and conclusion, respectively. Specifically, a short description of chapters defining the thesis body is included below:

- **Chapter 2** includes a review of the modelling methodologies regarding two-stage turbocharging systems. Additionally, effects of swirling flows at turbomachine inlet and heat transfer across the turbocharger shaft are included. In particular, heat transfer models to account for the variation in apparent efficiency in compressor and turbine are reported. In conclusion, a methodology to incorporate the effects into an equivalent two-stage system has been proposed.

- **Chapter 3** describes the development of the engine gas-stand facility to investigate turbochargers performance. The chapter shows that compressor maps can be generated under steady flows, highlighting the effect of turbine inlet temperature on the temperature measured efficiency. Furthermore, the difficulties in acquiring turbine performance maps under unsteady flows are reported, due to lack of fast-response temperature and mass flow instrumentations.

- **Chapter 4** shows the adoption of a turbine model for representing performance under unsteady flows into 1D models. In fact, due to the absence of instantaneous mass flow and temperature information from the engine gas-stand facility, the turbine model shows the difficulties in interpreting instantaneous behaviour.

- **Chapter 5** explores the compressor surge behaviour under steady and unsteady flows in the engine gas-stand. In particular, the chapter shows the description of the unsteady turbocharger gas-stand. In fact, insurgence of instabilities of mass flow and outlet pressure at the compressor are explored. In particular, due to limits in controllability of the engine gas-stand, the steady

flow experiments are performed in a steady turbocharger gas-stand allowing higher degree of control of compressor mass flow. Surge onset is measured through amplitude and frequency of oscillations and compared to unsteady measurements

- **Chapter 6** discusses the attempt in defining the equivalent mapping approach for two-stage turbocharging systems through 1D simulations. In this chapter, the equivalent two-stage map is presented. Influence of turbine by-pass is explored, evaluating the optimal definition of two-stage speed.

- **Chapter 7** highlights and explains the equivalent mapping approach in the steady turbocharger gas-stand. Moreover, the equivalent mapping approach is compared to combined stand-alone turbochargers map to describe the complete two-stage system behaviour. Benefits and lacks of each approach are detailed.

- In **chapter 8**, equivalent maps are applied to 1D powertrain models to describe engine gas-stand operations under steady and transient operations. Furthermore, the simulation results are compared to experimental measurements and simulations from stand-alone maps for high and low pressure turbochargers.

- **Chapter 9** summarises the thesis outcomes, including a main summary of the project, conclusions for each of the defined objectives and outlook of the project and future work.

Chapter 2 - Review of mapping and modelling of two-stage systems

This chapter performs a literature review on performance measurements, mapping methodologies and modelling approaches of two-stage turbocharging systems for application in automotive powertrains. Initially, the analysis focuses on available literature information regarding modelling of two-stage turbocharged internal combustion engines. Subsequently, the chapter considers the variation of thermodynamics operation of compressors and turbines owing to flow perturbation at turbomachine inlet. Additionally, influence on temperature based efficiency of turbomachine owing to heat transfer across the turbocharger shaft is reported. Conclusively, a methodology to account for actual two-stage system performance through measurement and one-dimensional modelling application is highlighted.

Furthermore, analyses and findings included in this chapter have been published in the SAE paper 2015-24-2523 at the SAE 13th International Conference on Engines & Vehicles [11].

2.1 Two-stage turbocharging systems in automotive powertrains

The reduction of fuel consumption and improvement of thermal efficiency in automotive powertrains are common targets for generating a cleaner transportation system. Downsizing of internal combustion engines is one of the key strategies to satisfy power demand and emissions requirements of light duty vehicles in the near future [12]. The cutting of the number of cylinders in internal combustion engines is beneficial for the improvement of overall efficiency. This gives directly a major decay on mechanical losses as masses and point of contacts which could cause internal friction are reduced. However, a smaller engine is capable of swallowing less air in the combustion chamber, resulting in a reduction of deliverable engine torque and power. Coupling turbocharging systems with internal combustion engines can overcome this lack of torque and power by increasing the air density in the intake ducts [13] and allowing more fuel to be burned in accordance to air/fuel ratio (AFR) requirements.

Two-stage turbochargers in a sequential layout can deliver the required level of boost at the entire operating range of automotive engines. Pflueger [14] included a two stage sequential turbocharging system in a heavy duty diesel engine which provided substantial improvements in torque, fuel consumption and smoke. Additionally, higher rated power than in a single turbocharged configuration was achieved at a lower speed without exceeding the limiting maximum in-cylinder pressure. Absolute boost pressure of 3bar could be controlled by mean of a by-pass valve on the HP turbine. In this way, the HP stage could be completely by-passed and constant speed could be maintained in the turbocharger. The two-stage turbocharging system including a low pressure (LP) and a HP turbochargers could improve fuel consumption as underlined by Kang et al. [15]. In this case, the best brake specific fuel consumption (BSFC) was recorded for the LP stage providing the entire boost needed by the engine in full load conditions at 2500rpm. In this scenario, the HP turbocharger was by-passed, reducing the load on the exhaust of the internal combustion engine.

Although, the benefits of a two-stage regulated system by Kühnle, Kopp & Kausch (KKK) Co. were only analysed for steady state conditions [14], it is also important to investigate powertrain system behaviours under transient conditions, representing daily driving scenarios. Saulnier and Guilnain [16] showed that, in transient

operations, two-stage systems associated with a 1.5L engine could not be able to match acceleration of a natural aspirated 2.0L engine. In this study, combustion system and burning rate were left unchanged from the naturally aspirated configuration. On the other hand, enhancements in transient response were recorded by Choi et al. [17] when two sequential turbochargers were couple to a diesel engine originally equipped with a single variable geometry turbocharger. Supporting the better response to change in load, an exergy analysis proved that more energy could be extracted from the exhaust gases using two turbochargers in series, instead of single rotating machine and, favourably, a better transient response was also shown [18].

Furthermore, two-stage systems have been adopted in various powertrain systems with small and large internal combustion engines. The combination of boosting systems and different technologies that influence the air flow in the engine could improve overall efficiency. The application of Miller cycle in a two-stage turbocharged heavy duty engine lowered in-cylinder temperatures which resulted in 50% less soot and slightly higher power when the compression ratio (CR) was reduced from 17:1 to 16:1 [19]. In a 1MW marine engine, NO_x emissions were also reduced when a Miller cycle was adopted in combination with a CR of 9:1 [20]. However, at low load, early intake valve closure (EIVC) could not deliver benefits in efficiency terms due to the presence of longer ignition delays. Therefore, a variable valve timing (VVT) system was installed in a two-stage turbocharged engine, in order to improve efficiency and transient response at low loads [21]. In fact, the reduced peak of pressure generated during combustion cycles at low loads with Miller cycle would lead to deterioration of the engine torque and power.

In order to satisfy the requirements for elevated pressure ratio and mass flow ranges, regulated two-stage systems could be adopted. Sauerstein et al. [22] showed that HP and LP turbochargers should be coupled to the engine, in order to obtain the highest possible efficiency at low and medium speeds for the small turbomachine (HP) and at high speed and load for the larger turbocharger (LP). Moreover, Codan and Huber [23] stated that the LP stage remained important for generating higher pressure ratios. In this way, the HP turbocharger could rapidly achieve the maximum extraction capacity and target efficiency. This study focused on the part load region of the powertrain system and repartition of the stages might be different under various conditions.

Discussed studies showed that the characterisation of the single turbocharger in two or multi-stage systems is of primary importance. This involves an accurate identification of turbine and compressor performance in a two-stage system which could be addressed by 1D fluid-dynamics simulations. Therefore, high confidence has to be conveyed into the performance maps of each component in a two-stage system, allowing an acceptable modelling approach.

2.2 Modelling approaches of two stage sequential turbocharging systems in powertrains

1D fluid-dynamics modelling approaches could be implemented to evaluate complete powertrain units. Turbochargers performances and efficiencies are input in the model as they are previously measured in turbocharger gas stands [24]. 1D models of two stage turbocharged engines can provide information on boost pressure achievable in relation to engine breathing characteristics. For a first evaluation, [25] turbocharger maps can be easily sized whether compressors and turbines should not be appropriately matched for the engine. In case of regulated two stage systems, bypass valves and wastegated turbines can be modelled by considering pressure losses of the flow [25].

Boost pressure analysis could be analysed using a flatness model where engine is represented as a pump and a heat exchanger. Weber et al. [26] investigated step load changes and the effects of volumes in the air path and the exhaust. A model was developed for evaluating the air path and the fluid dynamics which was validated against steady state measurements. In order to have more precise representation of the system, the flow through the turbine by-pass (TBP) valve was replicated. From the analysis, it was shown that a reduction in intake manifold volume would have a small influence on transient performance [26]. However, this modelling approach could not consider the pressure losses in the path that could affect the turbochargers performance and, ultimately, the entire powertrain.

Characterisation of internal combustion engine with a zero-dimensional (0D) model could provide information on turbochargers and engine interaction. Lee et al. [27] analysed various two-stage boosting technologies in a 4.5L V6 diesel engine of a four-wheel drive truck with a weight of 4.7tons under transient conditions. The complete vehicle model showed that the combination of a fixed geometry (TC) and a variable geometry (VGT) turbochargers was able to achieve best transient performance as shown in figure 2.1. In addition, an electric compressor (EC) of 8KW, a mechanical supercharger (SC) and an EIVC cycle were analysed.

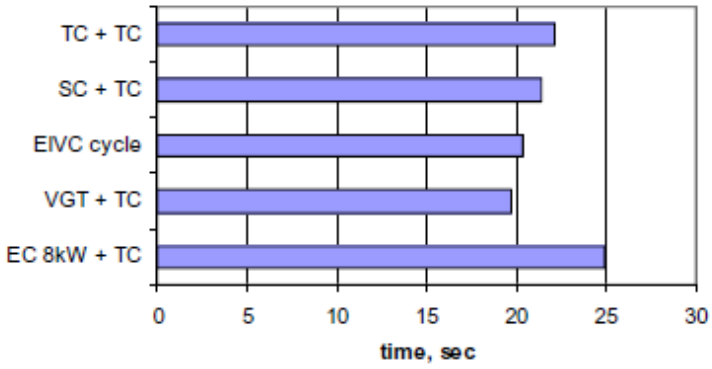

Figure 2. 1: Comparison of two stage boosting technologies in vehicle acceleration from 0 to 60 mph [27]

Galindo et al. [28] investigated a two stage turbocharging system using a 0D model, reducing the entire system to a filling and emptying model with the engine behaving as a pump and heat generator. In this way, it was found that lowering gas exhaust temperature and compressor efficiency could cause negative effects on powertrain thermal efficiency. However, gas dynamics effects were not considered and effects of chemical combustion on turbomachinery could not be taken into account. Therefore, these represented the handicap of 0D modelling approaches.

Full powertrain simulation including gas-dynamics and combustion events was performed by Amann and Ouwenga [29]. A 1.2L engine was studied and coupled to different two stage boosting systems in order to achieve best BSFC. The comparison of the different cases showed that two turbochargers in series were able to extract more energy from the exhaust gases and, so, reduce fuel consumption. In addition, it was possible to improve BMEP at full load. From using 1D simulation, it is also clear that high pressures developed by the charge at the intake could lead to advanced knocking conditions. Moreover, a reduction of CR was considered a possible strategy to avoid uncontrolled combustion events [19, 29]. The lowest CR was adopted in three-cylinder engine using two sequential turbocharges in the exhaust system. However, the variation of the engine geometry could affect negatively on the thermal efficiency of the engine. Table 2.1 shows the results achieved by the 1D simulation from single and two-stage boosting systems which improved consistently fuel efficiency (FE) in all the driving cycles, US06, NEDC and FTP75 [29].

Table 2. 1: Fuel efficiency (FE) results for four-cylinder and three-cylinder engines adopting single and two stage boosting technologies [29]

		4-Cyl TC	4-Cyl SC	3-Cyl TC-TC	3-Cyl SC-TC	3-Cyl TC-SC
US06	Fuel [g]	928	907	906	901	903
	Distance [m]	12852	12854	12854	12854	12854
	FE [lit/100km]	9.52	9.33	9.33	9.26	9.30
	FE [mpg]	24.7	25.2	25.2	25.4	25.3
	% change FE		2.0%	2.0%	2.8%	2.4%
FTP75	Fuel [g]	1110	1099	1050	1039	1041
	Distance [m]	17660	17662	17663	17663	17663
	FE [lit/100km]	8.22	8.17	7.81	7.74	7.75
(combined)	Weighted FE [mpg]	28.6	28.8	30.1	30.4	30.4
	% change FE		0.7%	5.2%	6.3%	6.1%
NEDC	Fuel [g]	677	666	642	636	637
	Distance [m]	10936	10935	10934	10934	10934
	FE [lit/100km]	8.20	8.06	7.76	7.69	7.71
	Weighted FE [mpg]	28.7	29.2	30.3	30.6	30.5
	% change FE		1.7%	5.6%	6.6%	6.3%

As 1D models are vastly used for powertrain evaluation, the account for flow non-uniformity and heat transfer seem fundamental in order to increase simulation fidelity. Analysis on the effects obtained in two-stage turbocharging systems needs to be experimentally investigated. Consequently, these effects have to be incorporated in the simulative models.

2.3 Experimental characterization and mapping of two stage turbocharging systems

Current practice for evaluating two-stage turbocharged engines using 1D fluid-dynamics simulations consists of assuming turbochargers performances [12, 25, 29]. These are previously measured in turbocharger gas-stands in according to existing standard of practice [24]. Therefore, straight ducts upstream and downstream of compressor and turbine are placed, in order to direct a uniform flow to the turbocharger. Thermocouples and pressure transducers are placed in the measurements sections at inlet and outlet of the turbomachines. It is important to notice that the SAE standard for measuring turbocharger maps does not specify any guideline for multi-stage systems [24].

Performance of a two-stage turbocharging system was measured in a hot gas stand by using by-pass valves and wastegates to isolate the turbo-components [30, 31]. Turbochargers maps were measured in stand-alone and complete two-stage system package. In fact, peak pressure ratio and efficiency of the LP turbine and HP compressor were also measured when the complete system was installed in the gas stand. It was shown that pressure losses could be affected by the aerodynamics performances, as visible in figure 2.2.

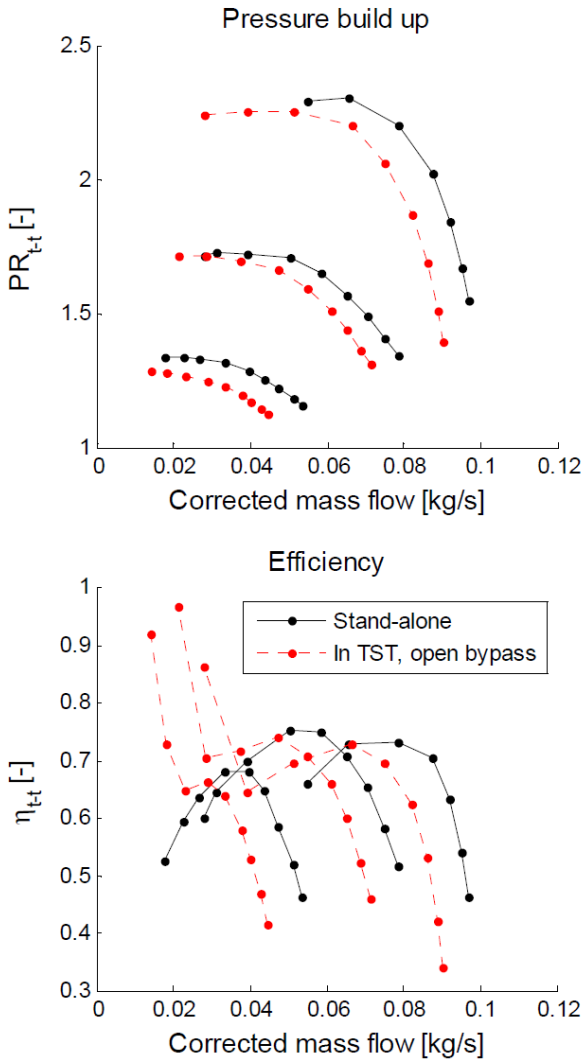

Figure 2. 2: HP compressor pressure ratio and efficiency maps for stand-alone and two-stage system (TST) with by-passed LP turbocharger [30, 31]

The entire compressor map was moved to the left to lower mass air flow and pressure ratio was down-shifted. Differences in compressor efficiencies between stand-alone and two stage system with LP wastegate open were measured. In case of two-stage configuration, the elevated values of compressor efficiency could be caused by the positioning of the temperature sensors, being close to the compressor entry, capturing flow recirculation [30, 31]. In addition, the efficiency variation at high mass flow are caused by the different isentropic power and apparent powers recorded in two-stage turbocharger layout, as pressure drops of the system are also included. The total compression (real) map was measured and compared to the composed map of the two alternatively by-passed stand-alone turbochargers, as shown in figure 2.3 [30, 31]. Differences between the system composed map,

obtained by the performance of the two isolated machines and the real full system map were recorded.

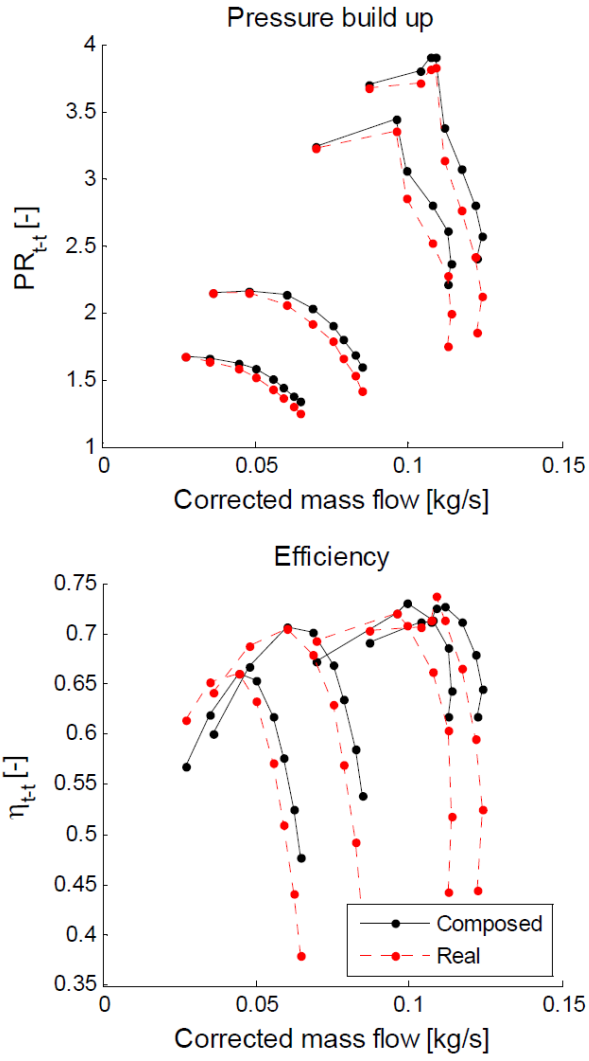

Figure 2. 3: Real and composed compressor maps of the two-stage turbocharging system [30, 31]

In figure 2.3, the speed lines for both maps were measured at constant speed of the HP turbocharger. Differences in pressure ratio and efficiency could be explained by non-uniformities of the flow at the entry of the HP compressor caused by the first compressor and the bends in the duct. In fact, 3D fluid-dynamics analysis suggested that swirl at the compressor entry introduced errors in the prediction of the performance [31].

Moreover, a complete system mapping approach was adopted in a specifically designed hot gas stand by ABB Turbocharging [32] for analysing the performance

of a two stage sequential system with a compression ratio of 12:1. Parameters related to two-stage applications were defined as the equivalent efficiency representing the complete turbocharging system including an intercooler between the two compression stages. The equivalent efficiency ($\eta_{TC,eq}$) was compared to the mean efficiency ($\eta_{TC,m}$) which represented the two-stage turbochargers performance without any other subsystem. Figure 2.4 shows the gas stand developed to incorporate two stage turbocharging system mapping [32].

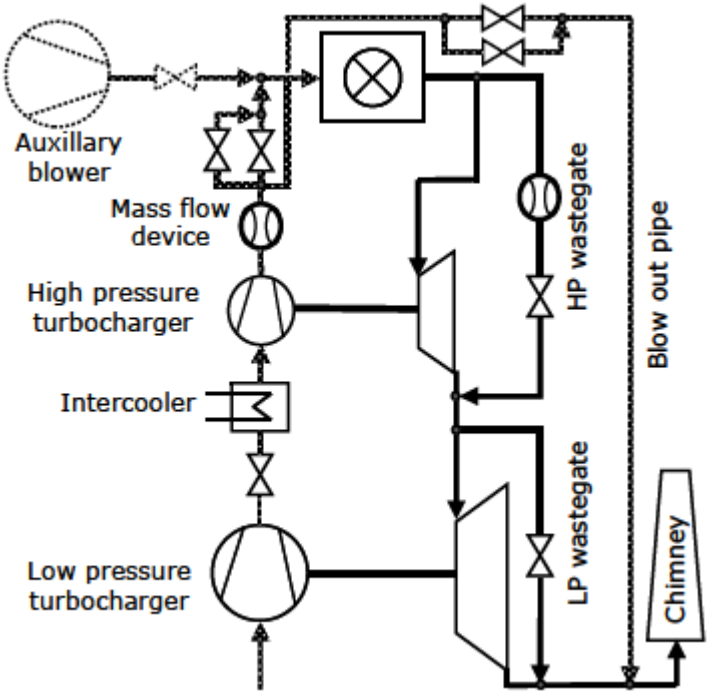

Figure 2. 4: Two-stage turbocharging gas stand from ABB Turbocharging [32]

The conducted analysis showed that the presence of bends between HP and LP turbochargers could cause a reduction in global system performance. The equivalent efficiency ($\eta_{TC,eq}$) was defined as full turbocharger system efficiency including the intercooler and the intermediate bends [32]. This efficiency differed from the mean turbocharger efficiency ($\eta_{TC,m}$) which considered the two units without the intermediate enthalpy alterations. The ratio between the equivalent and the mean efficiencies was defined as two-stage system efficiency ($\eta_{TC,2st}$). As shown in figure 2.5, the equivalent efficiency resulted lower than the mean efficiency due to pressure losses in the bends between the stages. Moreover, the inclusion of an intercooler between the compressors improved equivalent efficiency at high load [32]. In some conditions, the adoption of inter-stage cooling in the two-stage system

could show an increase in equivalent efficiency, as in pressure ratio between HP compressor outlet and LP compressor inlet above 4.5. It is important to consider that the two-stage system efficiency ($\eta_{TC,2st}$) is a ratio between equivalent and mean efficiencies. Therefore, the elevated values in figure 2.5 are representing a ratio of the two efficiencies.

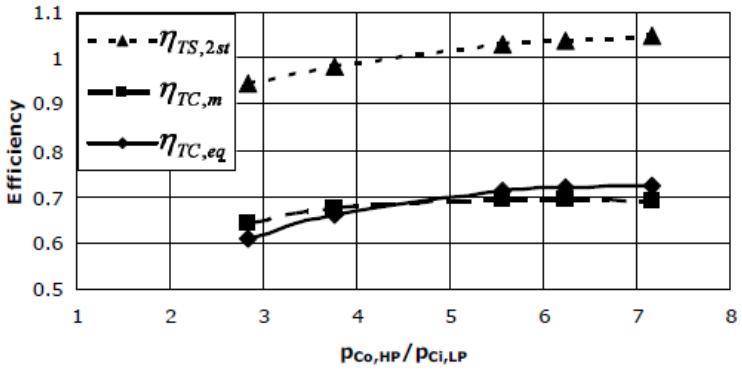

Figure 2. 5: Comparison between mean, equivalent and two-stage efficiencies for various compression loads [32]

This study from Fitzky et al. [32] refers to a two-stage system including an inter-stage cooler, reducing the non-uniformity of the flow entering the HP compressor. Therefore, the variation of performance for the two-stage system could be related to the cooling inter-stage effect.

2.4 Heat transfer in turbochargers

In two-stage systems, it is important to understand the nature of compression and expansion processes occurring in the various stages. In this way, it would be possible to define efficiencies and the correct delta of enthalpies (*Δh*) for turbo-components. This is important because turbochargers could perform differently depending on the temperature of gas accessing turbine and compressor [33]. In fact, adiabatic conditions at compressor and turbine can be achieved when fluids at compressor and turbine entry are approximately at the same temperature. In addition, oil is also commonly provided for cooling of the bearing pack and it has to be kept at the constant temperature with the other fluids [34]. Due to limits in maximum flow temperatures at compressor entry and avoidance of possible water condensation at turbine outlet, temperatures of about 90degC are usually imposed across the turbocharger for measuring isentropic efficiencies of turbine and compressor in turbochargers [34]. Isentropic efficiency is defined by the enthalpy differences of compression/expansion processes under constant entropy and adiabatic conditions. Equations 2.1 and 2.2 show the isentropic efficiencies for turbine and compressor, respectively [35].

$$\eta_{T,t-s} = \frac{(h_{t3} - h_{s4})}{(h_{t3} - h_{s4,is})} \tag{2.1}$$

$$\eta_{C,t-t} = \frac{(h_{t2,is} - h_{t1})}{(h_{t2} - h_{t1})} \tag{2.2}$$

In regards to turbine efficiency ($\eta_{T,t\text{-}s}$), the change between total enthalpy at inlet (h_{t3}) and static enthalpy at outlet (h_{s4}) of turbine is compared to the isentropic enthalpy process (h_{t3} - $h_{s4,is}$). Moreover, in the case of compressor, the change between total enthalpy at outlet (h_{t2}) and total enthalpy at inlet (h_{t1}) of compressor is compared to the isentropic enthalpy process ($h_{t2,is}$ – h_{t1}). Additionally, the increment of temperature difference between compressor and turbine could cause the turbocharger to perform under non-adiabatic conditions [34, 36, 37] by questioning the validity of equations 2.1 and 2.2 due to the presence of heat transfer. Shaaban and Seume [34] noticed that, introducing hot air through the turbine, heat transfer was generated from turbine to compressor. This resulted in a variation of compression and expansion processes compared to adiabatic conditions, due to

heat flux affecting measured temperatures and efficiencies. Specifically, compressor efficiency was subjected to an apparent reduction from the isentropic value for rotating speed ($N_{red,c}$) below 120krpm. In fact, compressor efficiency differed significantly at low speed and matched isentropic conditions at higher speeds, as shown in figure 2.6 [34]. Specifically, the apparent variation of measured compressor efficiency ($\eta_{dia,c}$) could be explained by the heat flux at the compressor from the hot turbine casing.

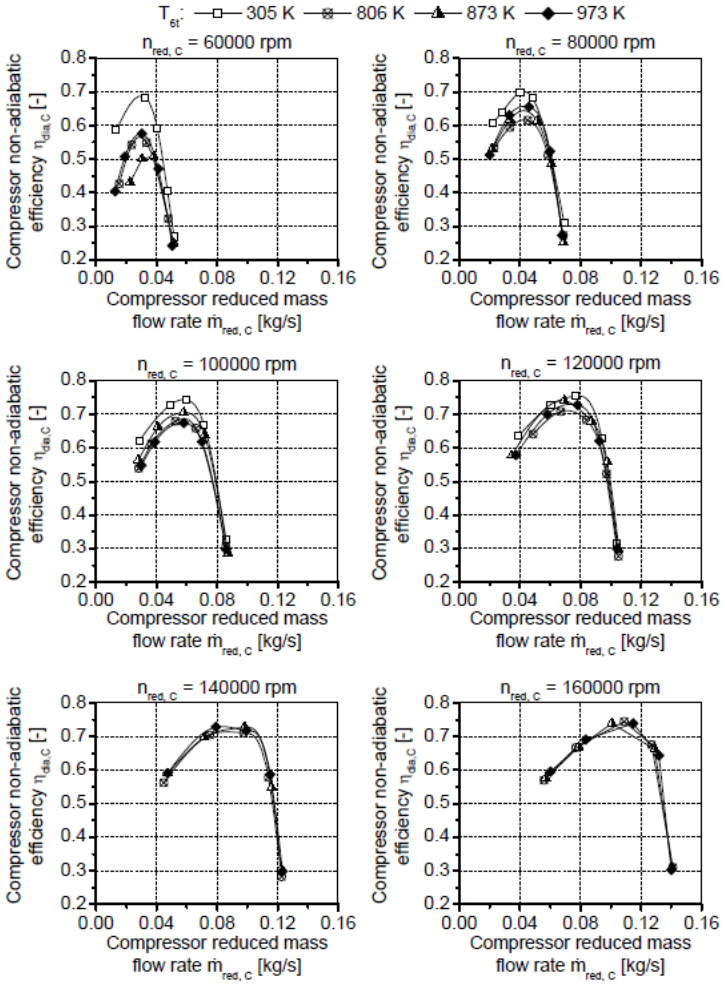

Figure 2. 6: Compressor efficiencies measured at different compressor speeds and turbine inlet temperatures [8]

The increment of turbine inlet temperature (TIT) led to variation of adiabatic efficiencies but also isentropic efficiencies measured under cold conditions [33]. In details, Serrano et al. [33] stated that the rise of TIT improved adiabatic efficiency of the turbine and its capacity to extract work. This was also supported by enhanced isentropic efficiencies for elevated temperatures. In fact, figure 2.7 shows that the

entropy (*s*) loss could be reduced in the expansion process when temperatures are elevated. This is principally caused by the diverging constant pressure lines [33].

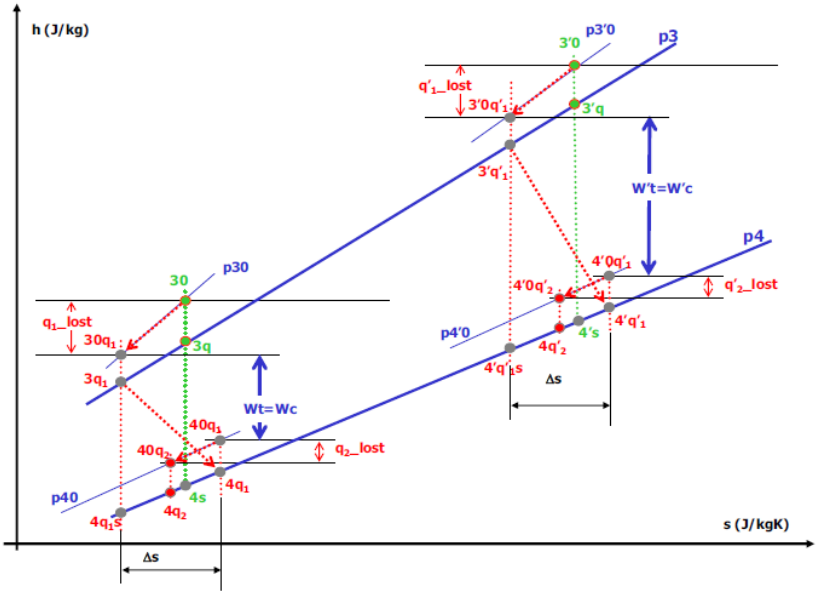

Figure 2. 7: Non-adiabatic expansion at different turbine inlet temperatures [33]

Moreover, in figure 2.7, the presence of heat transfer was expressed as losses of enthalpy (*h*), energy contained in the system, and entropy (*s*), capacity of a system to perform useful work, in the expansion process which took place in the turbine. Assuming at total thermodynamic condition of *30* at turbine inlet, heat (q_1_lost) could be diffused to the ambient and surroundings upstream the turbine wheel. Therefore, the extractable power would be limited to ($30q_1 – 40q_1$), assuming additional heat losses at the wheel outlet (q_2_lost). In this case, heat was considered to be wasted at the entry (q_1) and at the outlet (q_2) of the turbine [33]. This would be dependant of the geometry of the turbine housing and the convective factors [38]. In the case of a fixed geometry turbocharger, this was only related to the adiabatic expansion and it was not influenced by heat losses apart from the fact that the fluid entering the turbine could have a lower enthalpy (from *30* to $30q_1$). Furthermore, the increase in temperature of the fluid at the turbine inlet would lead to higher extraction capacity ($W'_t > W_t$).

In conjunction with figure 2.8, adiabatic turbine efficiency resulted higher in cases where TIT (T_3 in graph) was increased from the adiabatic conditions. In the two VGT opening position (10% and 60%), turbine efficiency at several turbine corrected speeds were investigated. In figure 2.8, efficiency under adiabatic conditions is

indicated via corrected speed values. Moreover, the rise of TIT would cause a shift from adiabatic operations and an increase of the temperature measured turbine efficiency. On the other side, adiabatic compressor efficiency at low and medium shaft speed decreased due to the rise of TIT from 305K to 973K [33]. In fact, 30% reduction of compressor efficiency was recorded at 60krpm.

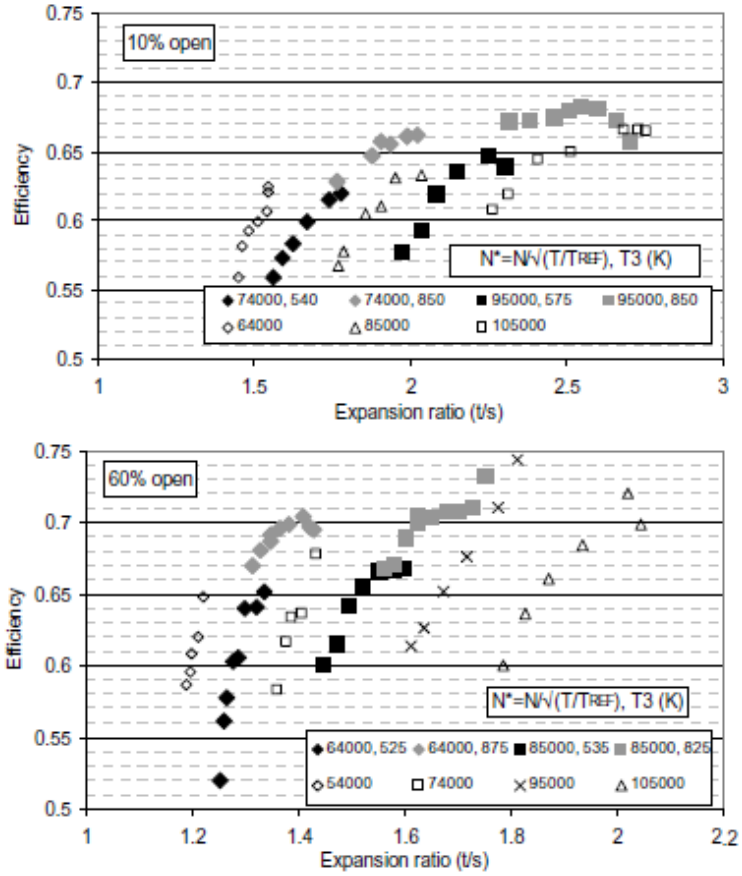

Figure 2. 8: Turbine efficiency expressed as (speed, TIT) at 10% and 60% opening position of the variable geometry vanes [33]

Under conditions of heat transfer in the turbocharger, the equation for isentropic efficiency would still be considered. However, the adiabatic temperature estimation around the turbo-components would be extremely difficult due to the presence of heat transfer. Specifically, this could mask the useful work extracted by the turbine and making equations 2.1 and 2.2 not relevant due to combination of turbomachine work and heat transfer. Therefore, compressor diabatic (non-adiabatic conditions) efficiency was defined by subtracting the heat transfer term to the compressor adiabatic enthalpy [36]. The heat transfer term was considered as constant and introduced in the diabatic efficiency equation. In fact, cause of non-adiabatic

expansion is the heat transfer from turbine to compressor which shifted the compressed flow to higher temperatures. Diabaticity performance of the compressor is caused by the temperature difference and the heat transfer which could quantified as defined by Grigoriadis et al. [37]. Therefore, a diabaticity criterion was expressed as heat exchange over enthalpy of fluid at turbine inlet. In this way, the divergence from the isentropic efficiency could be quantified and correlated to heat transfer.

Furthermore, due to the adjustments required for the efficiency calculation, the estimation of turbocharger power directly at the shaft could raise the need for defining temperature based efficiencies which could be inaccurate. In this way, the actual power of the turbocharger could be measured without account for heat transfer. A methodology was proposed by IHI Charging Systems [39] consisting of a contactless torque sensor directly installed at the shaft. Although this methodology could allow for measurements of turbocharger torque at the shaft comprehensively of friction, modifications on the turbocharger package are required in order to install the sensor.

2.4.1 Modelling of heat transfer from turbine to compressor

As highlighted in the previous section, it is important to evaluate heat transfer from turbine to compressor case occurring at significant temperature differences between turbine and compressor inlets. In relation to the thermodynamics principle of heat transfer [38], heat contained in the exhaust gasses can be transmitted to colder internal surface of turbine through convection. Subsequently, conduction and radiation dissipate heat to the rest of turbocharger surfaces and ambient air. The use of lubricating oil in the bearing pack can extract additional heat instead of being transferred to the compressor [40]. Moreover, due to increasing TIT, the need for a water-cooled turbocharger case could be fundamental for temperature reduction [41].

Casey and Fesich [36] assumed that a heat transfer law could be applied to the compressor for different turbocharger operating conditions. In [36, 42], the apparent enthalpy rise (λ_{app}) due to heat transfer (q_{12}) taking place was calculated as in equation 2.3. The apparent enthalpy rise is defined as ratio between the specific enthalpy change (Δh_{12}) and tip speed (u_2). In case of non-adiabatic turbocharger

operations, the specific enthalpy change results from the sum of shaft work (wt_{12}) and heat transfer (q_{12}).

$$\lambda_{app} = \frac{\Delta h_{12}}{u_2^2} = \frac{wt_{12} + q_{12}}{u_2^2} = \lambda + \frac{q_{12}}{u_2^2} \tag{2.3}$$

In order to calculate the heat transfer flux, the mass through the compressor ($\dot{m}$) would have to be defined, in equation 2.4, as product of air density at inlet (ρ_1), flow coefficient (ϕ_1), tip speed (u_2) and compressor diameter (D_2). Moreover, the heat flux could be calculated as function of heat transfer power ($\dot{Q}$) and mass flow ($\dot{m}$), in equation 2.5.

$$\dot{m} = \rho_1 \phi_1 u_2 D_2^2 \tag{2.4}$$

$$q_{12} = \frac{\dot{Q}}{\rho_1 \phi_1 u_2 D_2^2} \tag{2.5}$$

Under non-adiabatic conditions, the heat from the turbine could increase the value of the apparent enthalpy rise (λ_{app}), in comparison to the real enthalpy rises (λ_{eff}) across the compressor. The heat flux element to the compressor can be expressed in equation 2.6, substituting the tip speed of the compressor wheel with the Mach number (M_{u2}) and the speed of sound (a_2).

$$\lambda_{app} - \lambda_{eff} = \frac{q_{12}}{u_2^2} = \frac{\dot{Q}}{\rho_1 \phi_1 u_2^3 D_2^2} = \frac{\dot{Q}}{\rho_1 \phi_1 a_2^3 M_{u2}^3 D_2^2} \tag{2.6}$$

Therefore, a coefficient (k_c) dependant on the rate of heat transfer per unit area going into the compressor was defined. In this way, equation 2.6 can be rewritten as equation 2.7, defining the relationship between enthalpy change and flow and speed operations of the compressor.

$$\lambda_{app} - \lambda_{eff} = k_c \frac{1}{\phi_1 M_{u2}^3} \tag{2.7}$$

In the case of turbocharger operations at TIT of 873K, the relationship between enthalpy rise due to heat transfer and the product between flow coefficient and cubic power of the Mach number is visible in figure 2.9. In regards to different types of turbochargers, the function based on constant k_c equal to 0.01 is shown in figure 2.9. In this case, a constant heat flux was imposed to the model for two different turbocharger and at different conditions [36]. It was evident that at high Mach numbers, the difference between apparent and real enthalpy rises was relatively small due to lower impact of heat transfer.

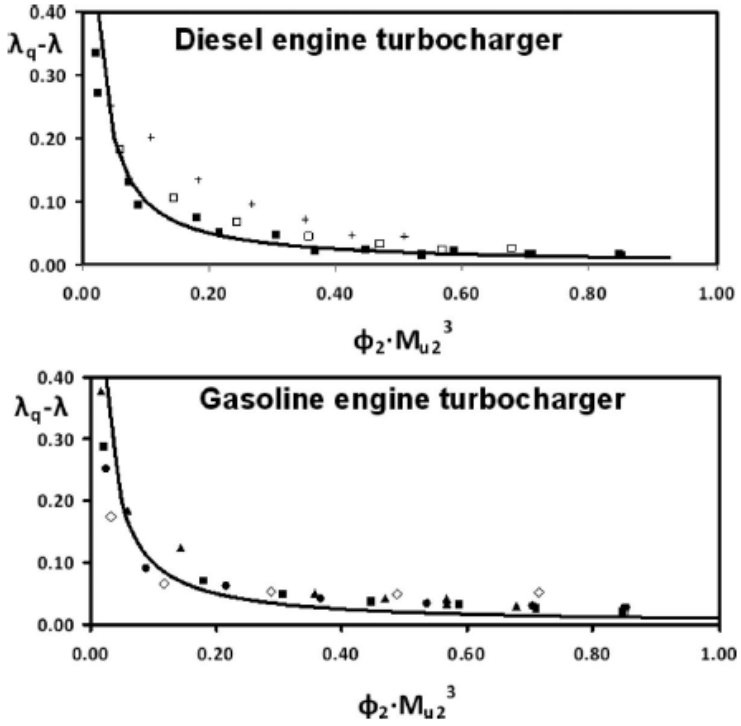

Figure 2. 9: Difference between apparent and real enthalpy rises for two turbochargers in a gas stand with TIT of 873K and constant heat transfer model. Speed lines are represented by different symbols [36]

A 3D conjugate flow and heat transfer (CHT) analysis of a turbocharger at various hot air condition at the turbine inlet showed that the heat flux varies along compressor and turbine [40]. In this study, surface and flow temperatures were quantified in the experiments and used as boundary conditions for the simulating the cases. In this way, it was possible to estimate the convective terms and the heat flux after estimating the Nusselt number (ratio between total heat transfer and conductive heat transfer). Bohn et al. [40] explained that the heat flux to the compressor case (Q_c) increased inversely to mass air flow through the compressor

($\dot{m}_c$), as shown in figure 2.10. In addition, the heat flux depended on the TIT ($\vartheta_{oT,1}$) and resulted maximum at higher temperatures than reference conditions ($\vartheta_{o,ref}$).

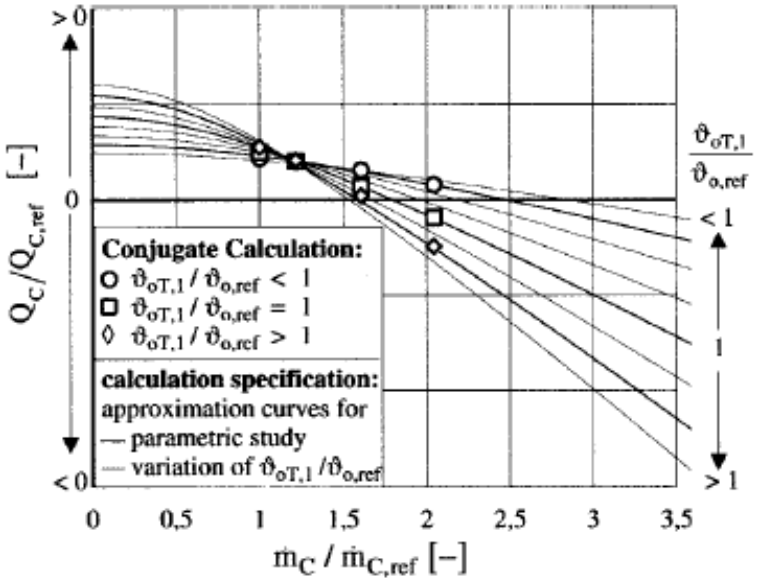

Figure 2. 10: Relationship between TIT, heat flux and mass air flow to compressor [40]

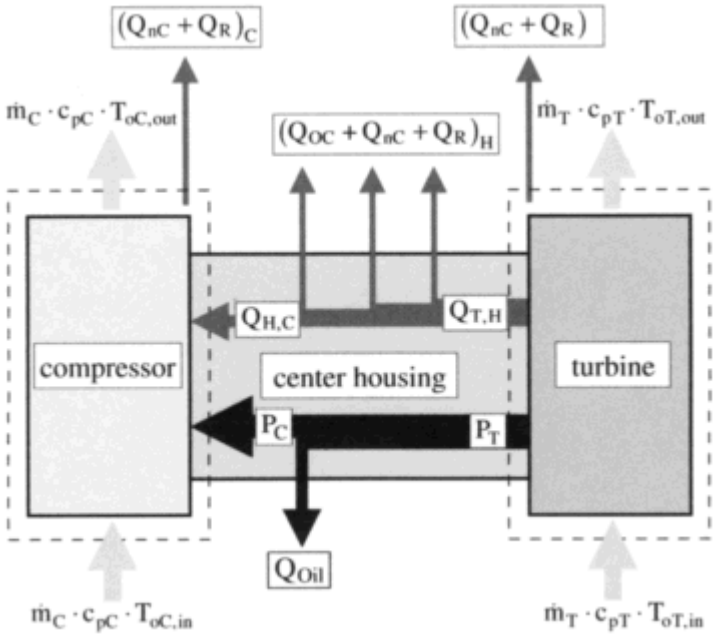

Figure 2. 11: Heat fluxes processes in a turbocharger [40]

A simplified heat transfer correlation was proposed by the Ecole Central de Nantes [43] where heat fluxes were defined in a concept similarly to Bohn et al. [40] as represented in figure 2.11. Heat fluxes from turbine ($Q_{T,H}$) to compressor ($Q_{H,C}$) were

defined by assuming an equivalent surface for compressor and turbine. In regards to power equilibrium, turbine power (P_T) is equal to the sum of compressor power (P_C) and friction in the oil lubricated bearing housing (Q_{Oil}). Furthermore, heat is transferred across the bearing housing via conduction (Q_{OC}), convection (Q_{nC}) and radiation (Q_R). Importantly, convection and radiation to ambient is assumed from the surfaces of turbine and compressor cases. Inlet and outlet enthalpies for turbine and compressor are defined, in figure 2.11, as product of mass flow ($\dot{m}$), specific heat capacity at constant pressure (c_p) and temperature. In addition, convective coefficients were calculated using the Dittus and Boelter correlation for Nusselt number estimation [44].

Regarding heat transfer analysis for correct turbocharger power estimation at non-adiabatic operations, three simple methods were proposed for predicting compressor outlet temperature and efficiency based on various assumptions [43]. However, heat flux to compressor had to be estimated and compressor efficiency prediction was not successfully achieved. In fact, a different model was lately implemented by the same institution [45] which consisted of an estimation of heat transfer process through an electric circuit analogy. The Equivalent Heat Transfer Resistance (EHTR) method associated conduction and convective coefficients to resistances in an equivalent electric circuit [45]. Non-insulated and insulated conditions were simulated to calculate heat power in compressor and turbine. Natural convection to ambient was considered when non-insulated conditions were imposed. Moreover, the model was able to capture compressor and turbine powers under transient conditions with an acceptable degree of accuracy [45].

A detailed explanation of heat transfer occurring in turbochargers was possible in the study of three different turbochargers [46]. Estimation of convective coefficients in turbochargers could be possible when temperatures in fluids and materials are measured and known. Forced convection was imposed for inner and back surfaces of turbo-components and oil in the bearing pack, on the basis of the Nusselt number (*Nu*) dependency from Reynolds (*Re*) and Prandtl (*Pr*) numbers. For the outer surfaces, free or forced convections were assumed and the Nusselt number resulted dependant from Grashof (*Gr*) and Prandtl numbers. Specifically, equations 2.8-2.13 list the laws governing free (2.12) and forced (2.8) convections.

$$Nu = a\, Re^{b} Pr^{c} \tag{2.8}$$

$$Nu = \bar{h}L/\kappa \quad (2.9)$$

$$Re = \rho uL/\mu \quad (2.10)$$

$$Pr = c_p\mu/\kappa \quad (2.11)$$

$$Nu = d\ Gr^e Pr^f \quad (2.12)$$

$$Gr = \beta g\rho^2 L^3 \Theta/\mu^2 \quad (2.13)$$

The Nusselt (*Nu*) number relates the total heat transfer to the conductive heat transfer term. In equation 2.9, $\bar{h}$ refers to the convective heat transfer coefficient, *L* refers to the characteristic length and the thermal conductivity is represented by *κ*. In addition, a relation exists between Nusselt (*Nu*), Reynolds (*Re*) and Prandtl (*Pr*) numbers, as visible in equation 2.8. In particular, the Reynolds number is the ratio between inertial and viscous forces of a fluid. This is expressed in equation 2.10 as the ratio between the fluid density (*ρ*), the velocity of the fluid (*v*), characteristic length (*L*) and the dynamic viscosity of the fluid (*μ*). On the other side, in equation 2.12, the Prandtl number refers to the ratio between the viscous and thermal diffusion rates, where c_p is the specific heat at constant pressure, *μ* is the dynamic viscosity of the fluid and *κ* is the thermal conductivity. Furthermore, *Nu* can be expressed as function of Grashof (*Gr*) and Prandtl (*Pr*) numbers in equation 2.12. Specifically, *Gr* considers the ratio between buoyancy and viscous forces in free convection. In equation 2.13, *β* is the coefficient of volume expansion, *g* is the gravitational acceleration, *ρ* is the density of the fluid, *Θ* is the temperature difference between surface and fluid and *μ* is the dynamic viscosity of the fluid. Moreover, for three different turbochargers, it was noticed that convection coefficients remained similar in case of free convection and varied when forced convection was considered as shown in table 2.2 which suggested geometrical dependency [46].

Table 2. 2: Convective terms of natural and forced convection regarding three different turbochargers [46]

	Turbocharger A			Turbocharger B			Turbocharger C		
Forced convection constants	***a***	***b***	***c***	***a***	***b***	***c***	***a***	***b***	***c***
Turbine housing inner surface	0.032	0.7	0.43	0.032	0.7	0.43	0.032	0.7	0.43
Turbine housing outer surface	0.6	0.4	0.33	0.6	0.4	0.33	0.6	0.4	0.33
Compressor housing inner surface	0.032	0.62	0.43	0.032	0.62	0.43	0.032	0.62	0.43
Compressor housing outer surface	0.032	0.8	0.43	0.032	0.8	0.43	0.032	0.8	0.43
Turbine back face	0.6	0.4	0.33	0.6	0.4	0.33	0.8	0.4	0.33
Compressor back face	0.032	0.8	0.43	0.032	0.8	0.43	0.032	0.8	0.43
Oil	0.04	0.8	0.43	0.04	0.8	0.43	0.08	0.8	0.43
Free convection constants	***d***	***e***	***f***	***d***	***e***	***f***	***d***	***e***	***f***
Turbine housing outer surface	0.2	0.25	0.25	0.1	0.25	0.25	0.1	0.25	0.25
Compressor housing outer surface	0.678	0.25	0.25	0.2	0.25	0.25	0.2	0.25	0.25

A 1D lumped heat transfer model was implemented in Valencia which further developed the concept introduced with the EHTR model [47]. Turbine and compressor were represented by two nodes and the bearing pack was defined by three nodes. Interfaces between compressor, turbine, oil and bearing pack were implemented to represent a more realistic 0D heat flow from turbine to compressor. In this way, it was possible to capture the temperature values at the nodes when turbochargers were fully insulated. Every node was associated to a metal capacitance which was linked to conductive and convective terms. These were calculated from experimental data recorded in a turbocharger gas stand [48].

Experiments on turbocharger operations under engine conditions showed that the turbine outlet temperature was subjected to change whether the turbomachine was kept insulated [49]. The importance of external radiation was highlighted by studying the influence of insulation on fluid temperature. In the experiments, the external surfaces facing turbine and compressor were also insulated with heat shields. In this way, it was possible to quantify the effect of radiation from turbine to compressor on total heat transfer. Moreover, the accountancy for heat transfer in the maps allowed the authors to reduce the maps multiplier used in 1D simulation tools to emulate the loss in efficiency of compressor and turbine [49].

Turbochargers in automotive powertrains are not kept fully insulated. Therefore, external radiation and convection could represent a significant part of the total heat flux. In this scenario, Payri et al. [50] developed a 1D model to account for external heat losses in turbochargers. Geometry assumptions were made in order to define the emissivity factors of turbine, compressor and bearing housing. It was highlighted that a significant amount of radiation escaped to the surroundings and only one-twentieth of the total flux went to the compressor case, when the turbocharger was coupled to a diesel engine [50].

On engine analysis of the turbocharger heat transfer model developed in Valencia [51] showed that the turbine outlet temperature could be predicted with acceptable accuracy. The temperature at the nodes reacted to transient condition of the engine which varied the temperature of the exhaust gases as shown in figure 2.12. Moreover, this model showed an improvement in prediction of turbine outlet temperature (TOT) when turbocharger are tested in gas-stands [52].

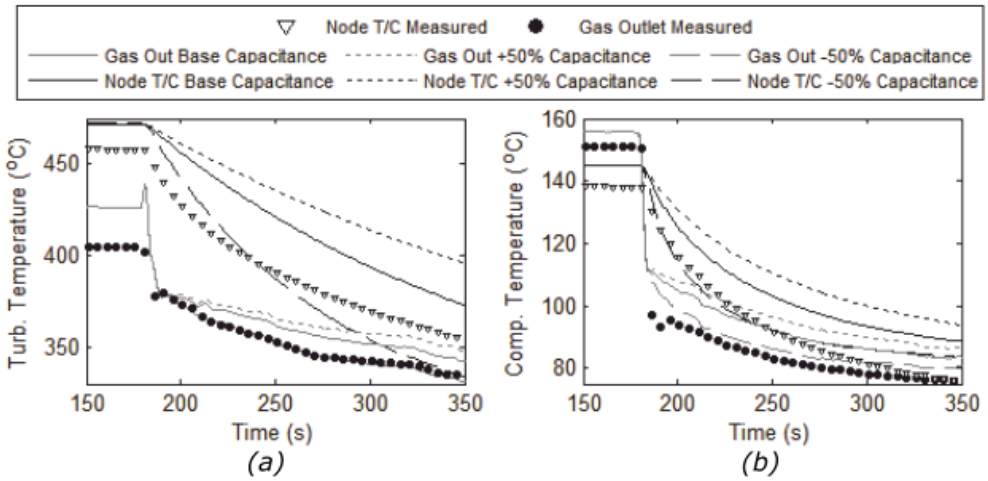

Figure 2. 12: Turbine and compressor node and relative capacitances temperatures under transient [51]

It is clear that heat transfer modelling has a certain importance in the prediction of turbocharger efficiency and behaviour [28, 48, 49, 52] in gas stand and automotive powertrains. Ideally, 3D fluid-dynamics models are capable of solving heat fluxes when boundary conditions surfaces are set correctly without incurring in efficiency over-estimations [53]. Thermal conjugate heat transfer analysis were able to provide information on temperature distribution by solving heat transfer equations [40, 54]. A complete thermal simulation of automotive exhaust systems recorded a maximum

of 30degC difference between measured and predicted temperatures on the turbine volute [55]. This model consisted in coupling finite difference and element methods to account for convection, conduction and radiation phenomena [55, 56]. In fact, 3D modelling approaches could improve the prediction of compression and expansion efficiencies. However, high level of details and computational power are often required.

On the other hand, iterative models for calculating heat transfer coefficients and non-adiabatic efficiency could reduce the computational time. Romagnoli and Martinez-Botas [57] used the geometry information and adiabatic efficiency to calculate turbine and compressor outlet temperatures. The convergence criterion consisted in the computation of heat fluxes to give a consistent turbine outlet temperature. Another iterative method was developed by Burke [58] and consisted in the assumption of convective coefficients, in order to calculate compressor outlet and surface temperature. In this case, it was possible to show the potential of turbocharger heat transfer model on non-adiabatic efficiency calculation of turbochargers in engines as for temperature prediction shown in figure 2.13.

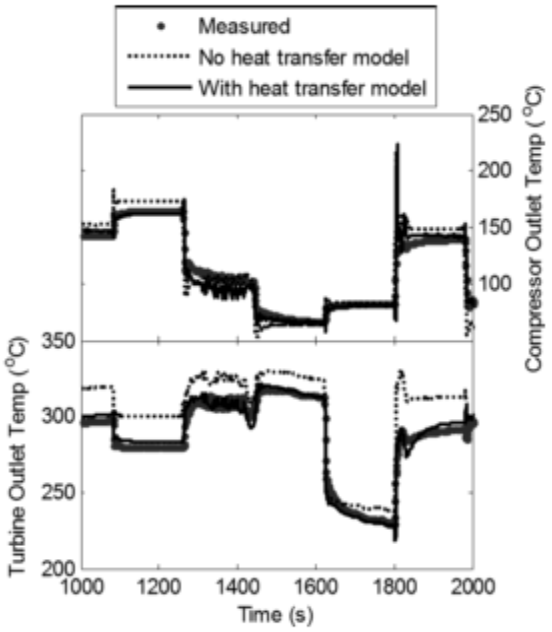

Figure 2. 13: Comparison of measured, predicted and heat transfer modelled turbine and compressor outlet temperatures in transient conditions [58]

The extensive analysis conducted by Scharf indicated that the heat flux to the compressor from the turbine could be calculated from balancing the energy equation

between enthalpy and friction power [59, 60]. The ratio between turbine expansion enthalpies at 363K and 873K of turbine inlet temperature were important for quantifying heat flux to compressor. In this case, the non-adiabatic compressor efficiency could be adjusted by adding the heat flux to the compression enthalpy measured under adiabatic conditions. The adoption of this heat transfer modelling approach in powertrain simulations gave an improvement in estimation of turbine outlet temperature as visible in figure 2.14 [61].

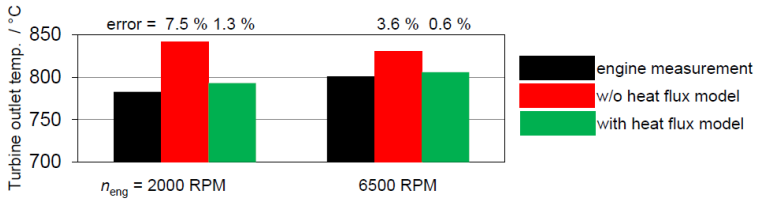

Figure 2. 14: Comparison of measured, predicted and heat transfer modelled turbine outlet temperature for engine speed of 2000 and 6500rpm [61]

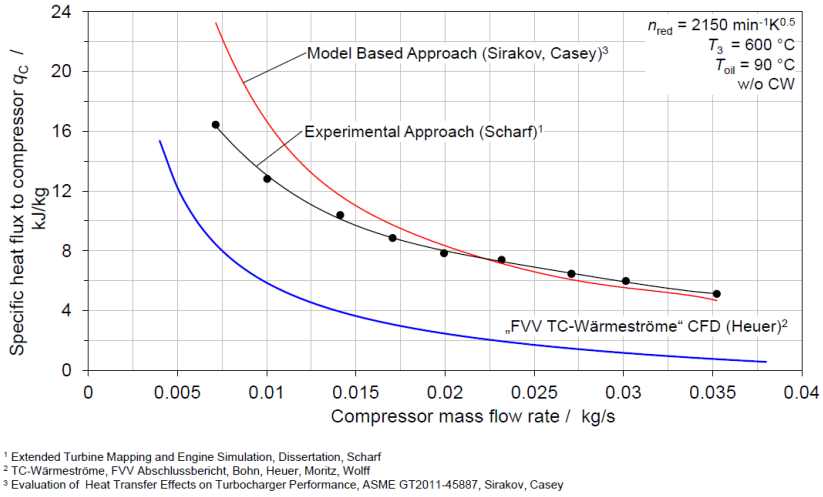

[1] Extended Turbine Mapping and Engine Simulation, Dissertation, Scharf
[2] TC-Wärmeströme, FVV Abschlussbericht, Bohn, Heuer, Moritz, Wolff
[3] Evaluation of Heat Transfer Effects on Turbocharger Performance, ASME GT2011-45887, Sirakov, Casey

Figure 2. 15: Comparison of calculated heat flux to compressor for different approaches [61]

As visible in figure 2.15, the research at RWTH showed that the heat flux to compressor decreased when mass flow in the compressor was increased [60, 61], accordingly to the two trends in the figure [40, 42]. The model based approach [42] over-predicts the specific heat flux to the compressor at low mass flows in comparison to the experimental approach. This could relate to the additional experimental data available in [60, 61] by the combination of hot gas-stand, turbine dynamometer and friction measurements. Moreover, the use of 3D computational

fluid-dynamics (CFD) techniques [40] could suggest a lower specific heat flux to compressor. However, it is important to consider the dependency that simulation tools would have on the treatment and definition of boundary conditions. Furthermore, the improvement in 1D simulations predictions depended also from an independent friction power model which was related to oil temperature and pressure [59]. In fact, the independent modelling of heat transfer and friction showed a significant improvement on non-adiabatic/on-engine efficiency of turbochargers compared to the use of efficiency multipliers [37, 60, 61]. The inclusion of these modelling approaches to two-stage turbocharging technologies should allow the prediction of temperature conditions upstream and downstream the system.

Specifically in two-stage systems, the HP compressor would have a higher inlet temperature than ambient conditions. This is because the charge temperature is previously incremented by the LP stage and no intercooler between the two compression stages is installed. Under these circumstances, the account for heat transfer upstream and downstream the HP compression stage could be beneficial. Burke et al. [62] showed that the amount of heat transmitted to the compressor was subjected to variation when the assumption of non-adiabatic conditions at pre-compression was imposed. This was particularly evident at high TIT combined to low mass air flow into the compressor. In the scenario of two-stage systems, it is important to notice that this assumption could be valid until the HP stage is engaged and not by-passed.

2.5 Installation and non-uniformity effects on compressor maps

Two-stage sequential systems consist of HP and LP compressors placed in sequence with the flow entering the HP stage after exiting the LP compressor. In automotive powertrains, bends between compressors are common system layout, in order to deal with packaging restrictions in vehicle engine compartments [22]. This can be cause of non-uniform distribution of flow velocity around the duct [63]. Moreover, flow swirl induced by the LP compressor can influence the performance of the HP compressor [64]. The effects of bends and pre-whirl at the HP compressor inlet could modify the compressor performance in terms of pressure ratio delivered and mass flow stable operating range.

Wallace et al. [64] showed that radial compressor operability was subjected to vary in terms of mass flow range, depending on the pre-whirl ratio. Variable inlet guide vanes were placed in front of the compressor impeller, in order to generate swirling flow. Positive pre-whirl enlarged the stability range of the compressor at lower mass air flow. However, this reduced the performance of the compressor at high flow rate [64]. In this scenario, a variable swirl generator device was installed at the compressor entrance, in order to modify the rate of pre-whirl [65]. In fact, at a speed of 98,000rpm, the pre-whirl intensity affected the constant speed line in the performance map of the compressor as visible in figure 2.16.

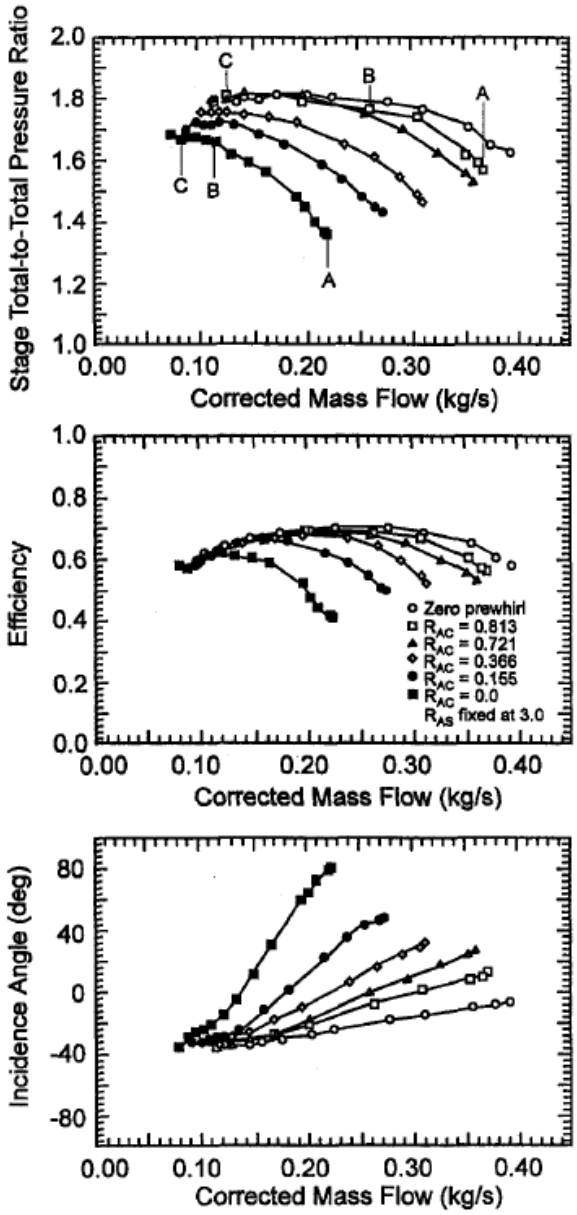

Figure 2. 16: Analysis of pressure ratio, efficiency and incident angle involving the compressor and the variable pre-whirl device [65]

The increase in vane angle led to a positive swirl at the compressor inlet, providing a reduction of efficiency and limitation in achieving pressure ratios at high mass air flow [66]. Improvements on compressor performance were achieved at low mass flow when high positive swirl was imposed to the flow. Under these conditions, the compressor operation stability was also extended to lower mass air flow [66]. Instead of inlet variable guide vanes, Galindo et al. [67] developed a swirl generating device which could be implemented in automotive powertrains. It was stated that negative swirl would be beneficial to extending the operating range at low mass air

flow. In fact, negative swirl (c_{1u}) could increase the velocity of flow at compressor entrance resulting in higher total velocity (w_1) as shown in figure 2.17.

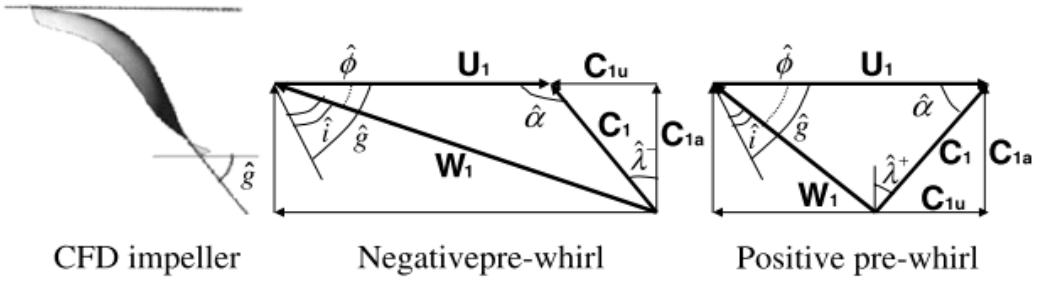

Figure 2. 17: Velocity triangles for negative and positive pre-whirl at the compressor entry [67]

In contrast to previous studies [65, 66], Galindo et al. [67] showed a better improvement in pressure ratio at lower mass air flow with negative pre-whirl. The stability enhanced at low flow was reduced with positive pre-whirl, as showed in figure 2.18. However, at the same time, pressure ratio and higher mass flow was reduced and choked conditions were anticipated.

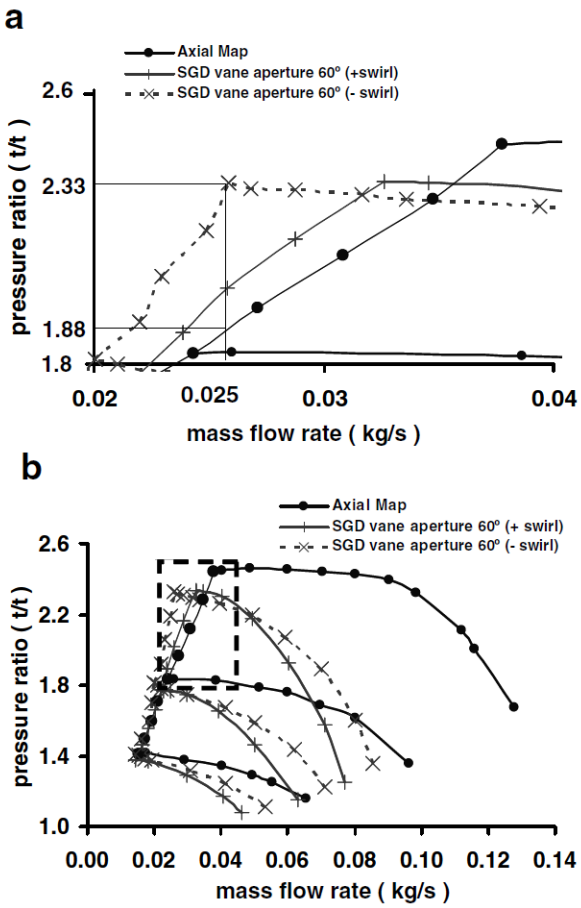

Figure 2. 18: Compressor performance maps for straight flow, negative and positive pre-whirl. A is a zoomed visual of the section in B [67]

It has been shown that the pipe geometry at the compressor inlet influenced the radial compressor performance [68]. Michigan State University investigated three turbocharger speeds and a reduction of total-to-total pressure ratio was observed, in the presence of a bend at the compressor inlet. An analysis of static-to-static pressure ratio showed no variations between the bend and straight inlet pipes. This could be explained with the limited influence of the secondary flow generated by the bend on the diffuser performance [68]. Moreover, strategies for the reduction of secondary flows were undertaken through 3D fluid-dynamics computations, advising on bend tuning [68, 69].

Due to vehicle packaging restrictions in the engine compartment, bends are often placed at the compressor inlet. In this way, the flow can be distorted, affecting the capacity of the compressor to convert the kinetic energy into enthalpy gain. An approach to reduce secondary flow and non-uniformity distribution of the flow

velocity could be represented by the insertion of vanes or grillage in the compressor inlet duct as shown in figure 2.19 [70].

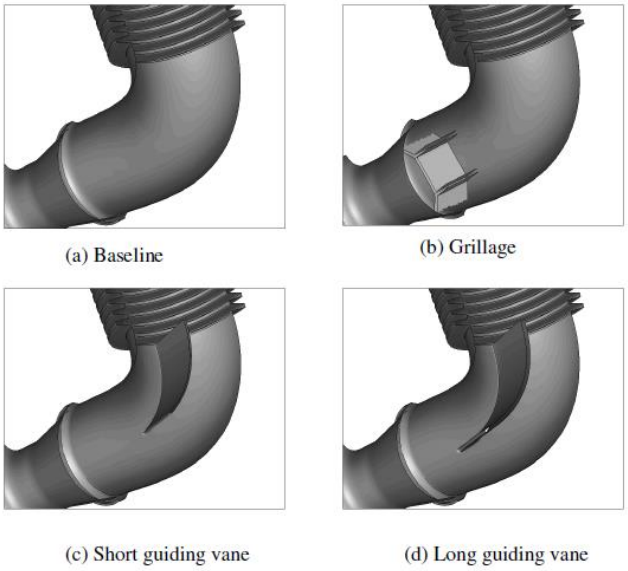

Figure 2. 19: Compressor inlet duct geometries [70]

Capon et al. [70] evaluated the different ducts geometries in a flow bench and subsequently in a turbocharged engine. The outcomes showed that incorporating a grillage in the duct could significantly affect the compressor outlet pressure, resulting in higher values at lower compressor tip speed. However, this was significantly lowered at compressor impeller speed higher than 460m/s. Figure 2.20 shows the compressor data that were collected from the engine experiments [70].

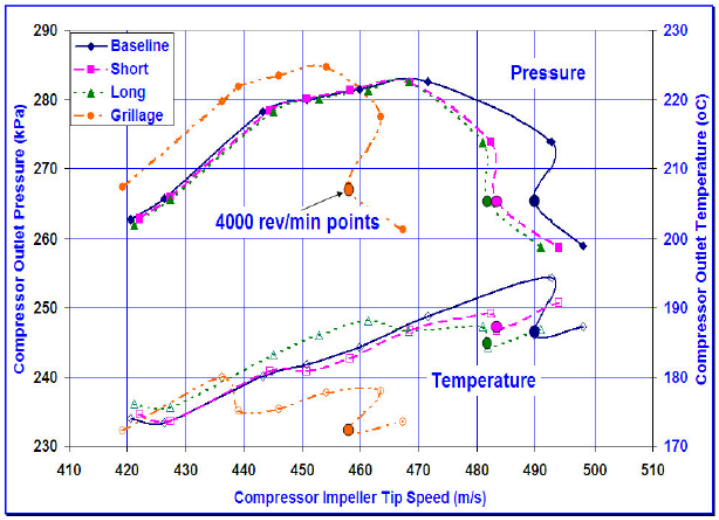

Figure 2. 20: Compressor outlet pressure and temperature for impeller tip speed and inlet duct geometries with condition at 4000rpm highlighted [70]

Noticeably, a reduction of outlet temperature was recorded, improving compressor performance. Perhaps, this outcome could be explained by the significant effect on flow disruption of the grillage on the non-uniformities, as also suggested by the elevated pressure drops recorded [70]. It is important to highlight that the variation of inlet duct design would cause measurable changes in compressor performance. These could not be beneficial for the turbomachinery as much as the introduction of ported shroud in the compressor casing [71]. In this way, the stability range of the compressor could be enhanced due to a reduction of recirculating flows at the compressor entry [72]. The orientation of the ported shroud in the casing could be adjusted in order to generate swirl at the compressor inlet as shown by Chen and Lei [71].

Mapping of turbochargers including vehicle packaging showed a significant influence of compressor performance, depending of the ducts and compressor geometries, as suggested by the findings in [60, 73]. In Capon and Morris [73], the compressor showed a reduced pressure ratio at higher flow and the map shifted towards lower mass air flow values when the clean-side duct is connected to the compressor. Furthermore, compressor adiabatic efficiency was reduced compared to standard straight pipe installation in gas-stand. For this reason, a flow modifier capable of generating more negative pre-whirl was installed in the clean-side duct which improved the compressor performance when compared to standard clean-side duct as visible in figure 2.21.

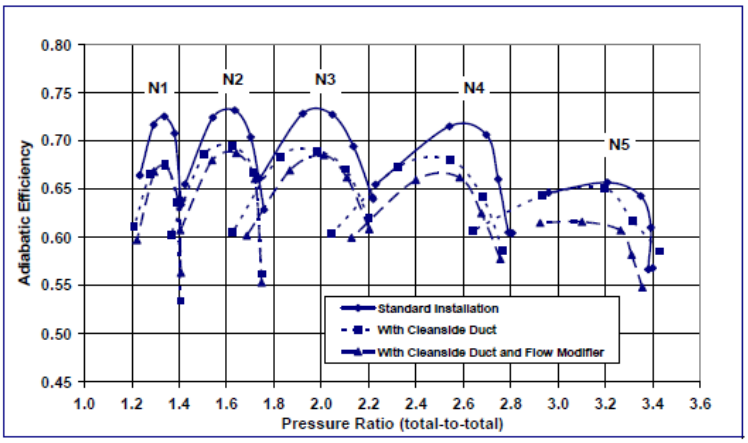

Figure 2. 21: Compressor adiabatic efficiency and pressure ratio for five rotating speeds at standard gas-stand installation, including the clean-side intake duct and the flow modifier [73]

In the research conducted by Scharf [60], the findings in compressor efficiency loss were in accordance to results from Capon and Morris [73]. However, the inclusion of the vehicle duct upstream the compressor reduced the flow capacity of the compressor at both high and low mass air flows. Specifically, the compressor resulted unstable, unable to match the pressure ratio at low mass air flow for the majority of the speed lines and better performances were recorded at high rotation speed, as shown in figure 2.22 [60].

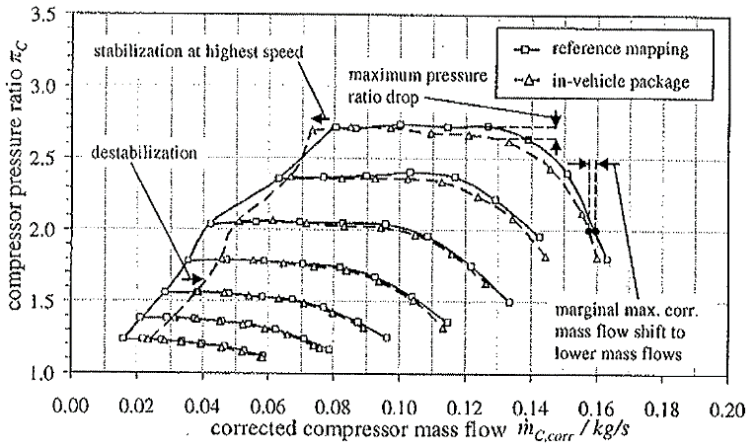

Figure 2. 22: Compressor performance maps measured in the gas stand for straight duct and in-vehicle clean side ducts [60]

Pipe geometries having different uniformity indexes and pressure drops were installed at the compressor inlet after been evaluated with computational fluid-dynamics simulations [74]. The uniformity index can be defined as the rate of

change in axial velocity along a reference section of the duct at the compressor inlet. In this scenario, low values of uniformity indexes result in extremely non-uniform flows. Furthermore, the evaluation of inlet ducts effects on compressor performance map was possible, due to an experimental analysis of the different bends on a turbocharger gas-stand in conjunction with 3D simulations. Figure 2.23 shows the results from the simulations of four bends (V1, V3, V9 and V10), having different uniformity indexes and pressure drops. It was clear that the geometry had an important role in the designation of the flow at the compressor entry [74].

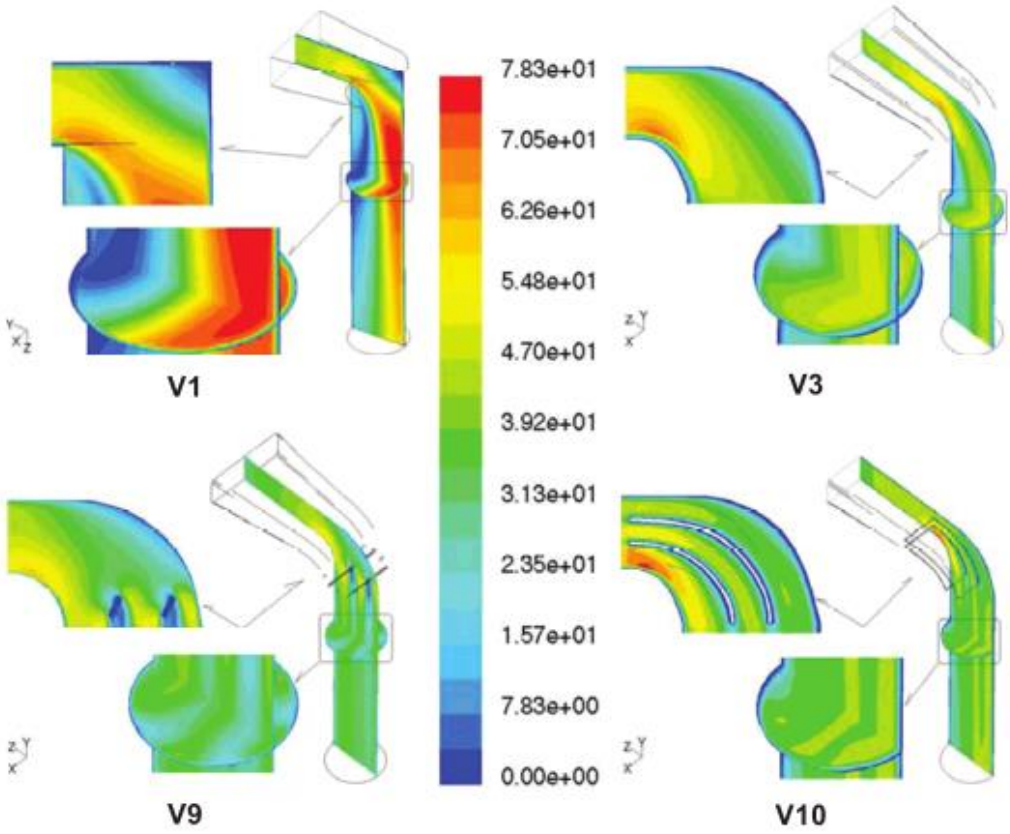

Figure 2. 23: Velocity distribution of four bends geometries (V1, V3, V9 and V10) under the same boundary conditions [74]

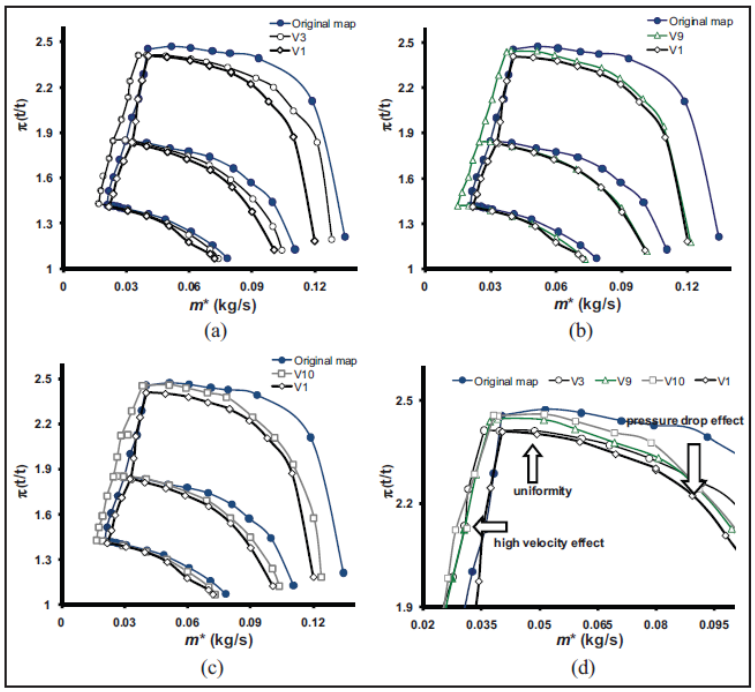

Figure 2. 24: Compressor performance maps measured in the gas stand for the four bends geometries under the same conditions [74]

Furthermore, velocity distribution and pressure drop affected the compressor map as shown in figure 2.24. It was clear that high velocity flow at the entry of the compressor impeller could improve stability in the low mass air flow region [74]. This could also be supported by the elongation of the flow axial velocity leading to higher total fluid velocity (please refer to figure 2.17). On the other side, pressure ratio was influenced positively by higher uniformity index at low mass air flow and negatively by high pressure ratio at higher mass flow. Moreover, it was important to notice that the detraction of duct pressure losses into compressor maps would leave the compression ratio mostly unchanged as visible in figure 2.25.

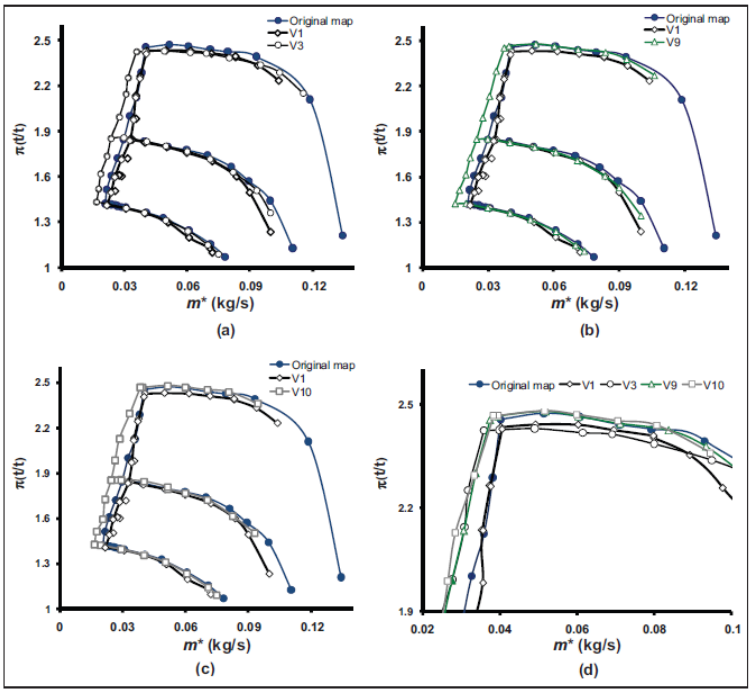

Figure 2. 25: Compressor performance maps measured in the gas stand for the four bends geometries under the same conditions without pressure drops in the bends [74]

Efficiency at various speed was also remained similar to original map when pressure losses in the ducts were subtracted. More importantly, the compressor stability at low mass air flow remained dependant on the inlet duct geometry and the flow velocity generated.

2.6 Proposed characterization of two-stage systems for 1D models

Two-stage systems could lead to a different behaviour of the single turbochargers in comparison to their stand-alone configurations, as previously tested in gas-stands [32]. This variation is due to the presence of bends and turbo-components in the sequential layout. As shown in previous section, due to bends and swirling flows, non-uniformities could affect the map measured in the gas-stand. Moreover, the temperature drop around turbines and compressors might be different under non-adiabatic conditions in comparison to fully adiabatic conditions. The presence of heat transfer could be source another source of error in 1D models, due to temperature variation in the efficiency maps.

Figure 2.26 shows a two-stage turbocharging system coupled to an internal combustion engine. As shown in the figure, the boosting system integrates external compressor and turbine by-pass (CBP and TBP) valves for the high pressure stage and an internal turbine wastegate (TWG) at the LP stage. Fresh air would be compressed sequentially by LP and HP compressors in order to increase air density at the engine intake. In addition, an intercooler would be reducing the temperature of the warm compressed air in order to improve air ingestion by the engine. Furthermore, following the combustion process in the engine, exhaust gasses would be expanding the series of HP and LP turbines to power the turbochargers. However, the wide operating range of the internal combustion engine in terms of flow and pressure demands requires a regulated operation of the two different sized turbomachine. Therefore, regulating valves in the system, such as CBP, TBP and TWG, can define an efficient operation of the turbochargers.

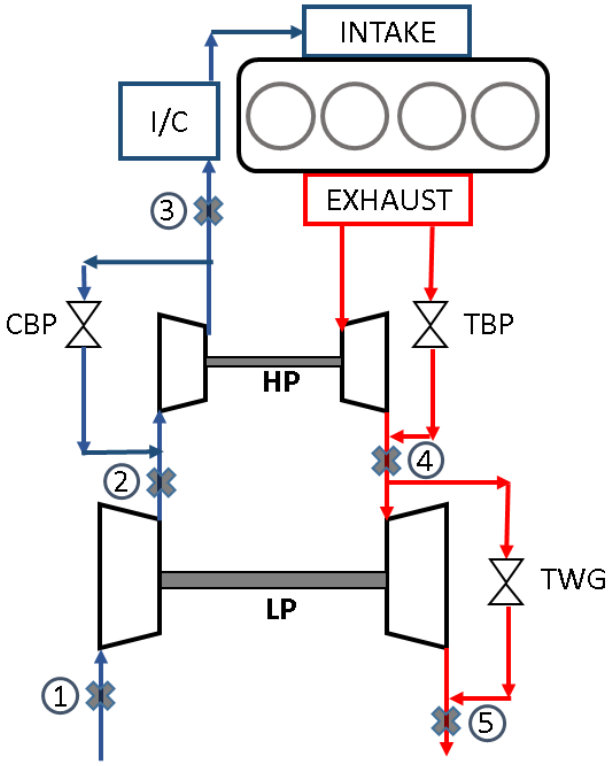

Figure 2. 26: Diagram of two stage turbocharging system and model inaccuracies introduced in the model are represented as number crosses from one to five

In conjunction with figure 2.26, the numbered crosses represent the input for map inaccuracies into 1D models when HP and LP turbochargers map are generated in gas-stands, following the SAE standard [24]. Due to vehicle packaging restrictions, the presence of bends and variation of diameters at the intake of the LP compressor could alter the stability range of the radial turbo-machine, due to non-uniform flow entering the compressor (point one). This layout is usually adopted, because of limited space available for positioning straight ducts at the compressor inlet under the vehicle bonnet. At point two of figure 2.26, the non-uniformity caused by the bends and the swirl motion induced by the LP compressor would compromise the ideal velocity triangle at the HP compressor entry. Moreover, the difference in temperature between the hot exhaust gas flowing through the turbine and the relatively colder air at the compressors could be source of heat transfer. This would result in a change of energy being transferred at the two stages due to different temperatures at inlet and outlet of the turbochargers. Therefore, this scenario could lead to an increase in temperatures at the compressor side (points two and three) and a further decrease at the points four and five. In addition, the swirl caused by

the HP turbine could influence the performance of the LP turbine, as suggested by the simulations [75].

Furthermore, it is important that appropriate maps of the two stage system are included into 1D models. It is clear that the current gas stand mapping procedure is not sufficient in representing the actual performance of the turbochargers in two-stage sequential systems. A different mapping approach, including the variation of turbocharges performance induced by flow non-uniformity, could address the issue. In fact, a full system map including LP and HP stages could account for changes in LP turbine and HP compressor behaviours. Moreover, the inclusion of air ducts, reflecting the application, could be considered, in order to represent the flow structure at the compressor inlet. In addition, a method accounting for efficiency changes, due to heat transfer needs to be included in the model, as part of the efficiency maps.

Information about rotating speed will need to be provided under conditions of equivalent formulations. The full system map might incorporate the operation of the turbocharging system under by-pass and wastegate openings which would also reduce the simulation complexity of 1D models. The behaviour of the CBP could be included in the two-dimensional (2D) compressor map when passively controlled. Moreover, an additional dimension could be added to the map, consisting of the percentage of opening position for the TBP valve. This would represent the system behaviour under several operating conditions. Conclusively, the LP turbine wastegate could be modelled using an external controller for the model. The equivalent map could be adopted for both 1D simulations and calibration strategies in engine control units (ECU).

2.7 Overview of existing key research

In order to provide an overview of the existing research analysed in this chapter, a summary of the main characteristics for each source has been included in table 2.3. The several sources have been categorised for two-stage turbocharging systems, heat transfer in turbochargers and flow effects on turbomachine performance, depending on the topic. Furthermore, difference is provided between experimental tests and modelling/simulation approaches in either gas-stand or engine.

Table 2. 3: Overview of literature review

Source	Two-stage	Heat Transfer	Flow Effects	Tests	Models / Simulations	Gas-stand	Engine
Amann, M., and Ouwenga, D., 2014 [30]							
Codan, E. and Christen, C., 2014 [22]							
Codan, E., and Huber, T., 2012 [24]							
Galindo, J., et al., 2010 [29]							
Lee, B., et al., 2009 [28]							
Marsiglia, R. F. and Bassetti, F. B., 2012 [19]					×		
Millo, F., Mallamo, F. and Ganio Mego, G., 2005 [20]	×						×
Saulnier, S. and Guilan, S., 2004 [17]							
Zhang, Q., et al., 2013 [26]							
Schernus, C., et al., 2011 [14]							
Weber, O., et al., 2012 [27]							
Choi, C., Kwon, S. and Cho, S., 2006 [18]				×			
Kang, J., et al., 2012 [16]							
Pflueger, F., 1998 [15]							

Source	Two-stage	Heat Transfer	Flow Effects	Tests	Models / Simulations	Gas-stand	Engine
Sauerstein, R., et al., 2010 [23]							✕
Turner, J.W.G., et al., 2014 [13]							
Fitzky, G., et al., 2010 [33]						✕	
Westin, F., and Burenius, R., 2010 [31]				✕			
Westin, F., and Burenius, R., 2010 [32]	✕						
Wik, C. and Hallbaeck, B., 2008 [21]					✕		✕
Grabowska, D., Palfreyman, D., and Reynolds, B., 2010 [55]			✕			✕	
Aghaali, H., and Angstrom, H.-E., 2012 [50]							✕
Burke, R. D., 2014 [59]							
Burke, R. D., et al., 2014 [52]							
Burke, R. D., et al., 2015 [63]							
Baines, N., Wygant, K. D., and Dris, A., 2010 [47]		✕		✕			
Lueddecke, B., Filsinger, D., and Bargende, M., 2014 [40]						✕	
Serrano, J. R., et al., 2007 [34]							
Shaaban, S., and Seume, J., 2006 [35]							
Bohn, D., Heuer, T., and Kusterer, K., 2005 [41]					✕		

Source	Two-stage	Heat Transfer	Flow Effects	Tests	Models / Simulations	Gas-stand	Engine
Casey, M. V., and Fesich, T. M., 2010 [37]							
Cormerais, M., Chesse, P., and Hetet, J. F., 2009 [46]							
Cormerais, M., et al., 2006 [44]							
Grigoriadis, P., et al., 2013 [38]						×	
Serrano, J. R., et al., 2010 [48]							
Serrano, J. R., et al., 2013 [49]							
Serrano, J. R., et al., 2014 [53]		×			×		
Sirakov, B., and Casey, M., 2013 [43]							
De Vos, S., et al., 2014 [57]				×			
Haehndel, K., et al., 2013 [56]							
Romagnoli, A., and Martinez-Botas, R., 2012 [58]							×
Lueckmann, D., et al., 2012 [62]							
Payri, F., et al., 2014 [51]							
Scharf, J., et al., 2012 [60]							
Scharf, J. S., 2010 [61]							
Anwer, M., and So, R. M. C., 1993 [64]						×	
Whitfield, A., and Abdullah, A. H., 1998 [66]			×				
Capon, G., and Morris, T., 2010 [74]							

Source	Two-stage	Heat Transfer	Flow Effects	Tests	Models / Simulations	Gas-stand	Engine
Capon, G., Leong, A., and Morris, T., 2006 [71]							×
Cavalcanti de Souza, R., and Krieger Filho, G. C., 2011 [54]					×		
Engeda, A., et al., 2003 [70]				×			
Galindo, J., et al., 2007 [68]							
Kim, Y., et al., 2001 [69]							
Serrano, J. R., et al., 2013 [75]			×			×	
Wallace, F. J., Whitfield, A., and Atkey, R. C., 1975 [65]					×		
Chen, H., and Lei, V.-M., 2013 [72]							
Harley, P. X. L., et al., 2014 [73]							
Liu, Y., et al., 2013 [76]							
Mohtar, H., et al., 2008 [67]							

2.8 Chapter summary and conclusions

In this chapter, the analysis of existing literature has developed the vision for a research gap in the characterisation of two-stage turbocharging systems for steady and pulsating flows. The absence of a specific mapping methodology for regulated two-stage turbocharging system results in the implementation of multiple turbochargers maps, representing the two turbomachines in 1D powertrain simulations. At this current stage, the influence of inter-stage effects on compressor and turbine performance as well as the effect of turbochargers heat transfer of temperature and efficiency estimations could influence the performance of the turbocharging system, without being accounted for in 1D simulations.

The aim of this research thesis would be to investigate and develop a novel and reliable methodology to represent performance of two-stage turbocharging systems. Additionally, the equivalent two-stage maps will be able to incorporate inter-stage flow effects of turbocharging systems, without incurring in prediction errors in the air-path for 1D powertrain simulations.

Moreover, this literature review chapter has reported mapping and modelling inaccuracies of two-stage turbocharging systems, resulting in the drawing of the following conclusions:

- It has been shown that 1D modelling approaches are able to investigate the interaction between engine and turbocharger in powertrains. However, the current turbochargers mapping and 1D models are not able to capture heat transfer and 3D flow effects which can influence two-stage systems operations.

- An appropriate consideration of heat transfer has to be made, also, accounting for the difference in thermal boundaries between HP and LP stages. In this scenario, heat flux could be considered upstream and downstream compression and expansion processes for each turbocharger.

- Single turbocharger mapping techniques show limitations in capturing flow effects at the inter-stage, affecting the performance of turbomachine in the

sequence. Therefore, the mapping of the full two-stage system in the gas-stand could be considered a solution which would account for the interaction effects, such as, flow non-uniformities and pressure drops of the system.

- The proposed characterization of two-stage systems could be a successful method to account for behaviours of the turbochargers in two-stage systems, representing the input of boosting system performance into 1D models. Moreover, this would add information on the system and the interaction with the regulative apparatus.

Chapter 3 – Development of an engine gas-stand for measuring performance of turbochargers

In this chapter, the development of an engine gas-stand facility is reported. Firstly, the chapter focuses on the requirements of an engine gas-stand to investigate performance of turbochargers. In particular, measurement and control systems employed in the facility are described. Secondly, mapping approaches of compressor and turbine in a newly developed engine gas-stand are explicated for a VGT turbocharger. In this scenario, controllable system variables are analysed across turbocharger operations. Lastly, the influence of sampling rate on the monitoring of turbine performance under pulsating flows is analysed.

Furthermore, details on the engine gas-stand control for mapping turbocharger have been presented in a paper at the ASME 2016 Turbo EXPO [76].

3.1 Requirements for an engine gas-stand

In order to evaluate performance of automotive turbochargers, several steady state operations are evaluated in gas-stand facilities. In this scenario, pressure, mass flow and temperature are monitored for each operating condition at the flow boundaries of the turbocharger, consisting of inlet and outlet of compressor and turbine. Both turbine and compressor performance are measured for certain values of constant rotating speed lines of the turbocharger shaft. In order to measure turbomachine performance under stable flow conditions, gas-stands are designed with the aim of reducing flow unsteadiness [24]. In addition, an accurate control of flow temperature at turbine and compressor can be obtained, quantifying adiabatic performance for the turbocharger [34]. In fact, turbochargers can perform adiabatic compressions and expansions at temperature equilibrium across the turbocharger, avoiding heat transfer from turbine to compressor. Therefore, TIT, compressor outlet temperature (COT) and temperature of the bearing housing should remain similar, avoiding heat transfer across the unit. The increase of TIT destabilises the ideal conditions and heat transfer from turbine to compressor would have an effect on the measured efficiency [40].

Non-adiabatic behaviour of turbocharger units is typical of boosted engines where exhaust energy is recovered and used to increase volumetric efficiency. In order to predict powertrain performance, system model simulations would have to integrate an accurate estimate of heat transfer from turbine and compressor, in order to represent the right turbocharger power [77] and air-path temperatures. Lumped capacitance [78] and parametric models [42] have been developed to estimate heat transfer in turbochargers. In this way, the real turbine and compressor efficiency can be estimated and disconnected from the heat transfer terms. In addition, the variation of oil temperature and pressure during the entire engine operating range would have an effect on turbocharger heat transfer balance [51]. The bearing housing conditions would also have an effect on friction and usable power [61, 79].

In conjunction with these effects, when linked to a reciprocating engine, turbochargers are subjected to unsteady flow due to the pulses generated from intake and exhaust valves motion. In more detail, measurements of instantaneous turbocharger torque at the shaft suggest that turbine extraction power follows the trend of expansion ratio [39]. Mass flow, turbine inlet pressure and turbocharger

speed are subjected to periodic pulses during a steady state operating point of the engine. In fact, the pulses are going to be repeatable for consecutive engine cycles as well as the turbocharger performance. Furthermore, flow temperature at the turbine inlet would be subjected to oscillations due to the unsteady conditions during an engine cycle. In order to study turbochargers behaviours under pulsating flows, a pulse generator would have to be developed to modify the flow in an engine gas-stand [80]. In this current case, an internal combustion engine is used to drive a turbocharger under unsteady flow conditions. At the same time, this system can be permutated into a steady gas-stand by placing a settling tank at the turbine inlet, damping the pressure fluctuations [81].

3.2 Engine gas-stand facility

In order to study turbochargers performance in engine-like conditions, an engine gas-stand has been developed [76]. This consists of a 2.2L Diesel engine, being externally supercharged through means of a boost rig. Figure 3.1 shows a caption of the test cell including boost rig (left side of the figure), Diesel engine (right side of the figure), instrumentation and control features. Moreover, in figure 3.2, the instrumented Diesel engine is positioned on the test bed and connected to the dynamometer, serving for power absorber/generator and engine speed controller.

Figure 3. 1: Engine test cell containing the engine gas-stand

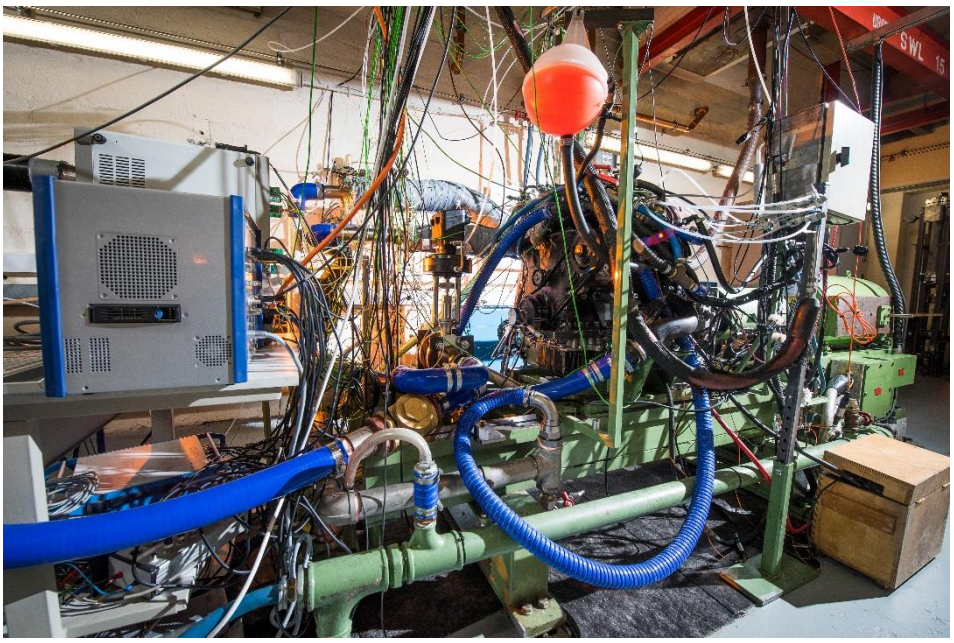

Figure 3. 2: Instrumented 2.2L Diesel engine gas-stand

In order to understand clearly the layout of the engine gas-stand, figure 3.3 shows a complete diagram of the system including the turbocharger. The boost rig is represented as a set of valves and ducts, controlling temperature, pressure and mass flow of air at the engine intake. In fact, hot and cold pressurized air up to 5barA is mixed by the hot valve in order to control temperature at the intake. Furthermore, main and dump valves regulate mass flow and pressure, respectively, at the engine intake to lower levels, as specified in table 3.1. It is important to notice that, although, the engine employs an exhaust gas recirculation (EGR) circuit for mitigating NO_x emissions, the recirculation valve is kept closed when focusing on turbine maps. In fact, exhaust gasses of a four-cylinder 2.2-litre Diesel engine provide power to the VGT, leading to rotation of the turbocharger. As shown in figure 3.3, an external back-pressure (CB) valve is generating load on the compressor, operating under steady flow. As in table 3.1, turbine VGT and CB valve allow for control of turbine and compressor pressure ratio (PR), respectively. Furthermore, in order to obtain a precise control of the turbine, engine intake conditions and fuel flow rate allow variation of the exhaust conditions. In fact, the position of the main throttle actuator is linked to fuel injection in the engine ECU, being responsible for the AFR control.

Table 3. 1: List of engine gas-stand inputs

INPUT	VARIABLE	RANGE
Hot valve	Boost Temperature	25 to 70 degC
Dump valve	Boost Pressure	0 to 3 barG
Main valve	Boost MAF	0 to 800 Kg/h
Main throttle	Engine AFR	14.6 to ∞
Dyno speed	Engine speed	0 to 4500 rpm
Turbine VGT	Turbine PR	0 to 100 %shut
CB valve	Compressor PR	0 to 100 %shut

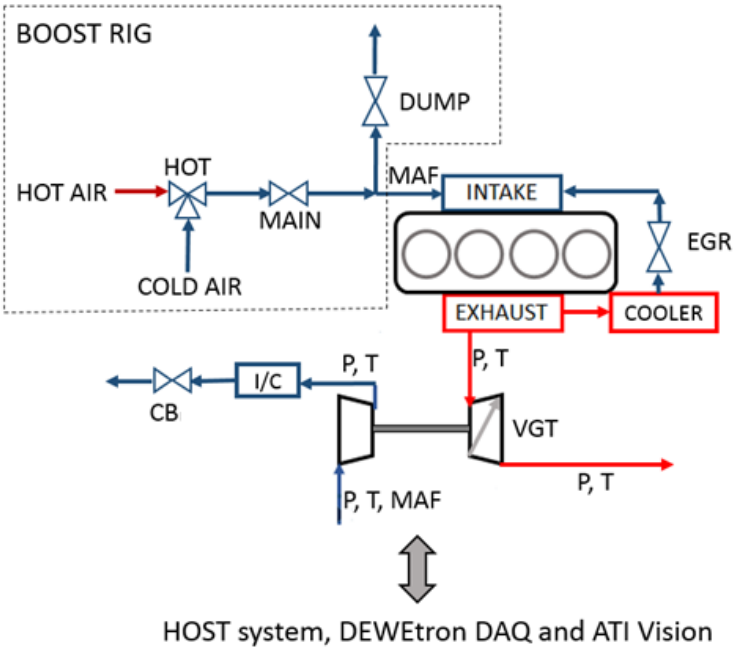

Figure 3. 3: Layout of the engine gas-stand

Furthermore, the operation of the engine gas-stand can be controlled, from the control room of figure 3.4, via external actuators, maintaining the engine gas-stand at constant operation and allowing transient variations of performance. In conjunction with figure 3.3, sensors and actuators communicate to the host system, DEWEtron DAQ and ATI Vision. Specifically, the host system allows for control and monitor of variables of most of the variables in table 3.1. In fact, main throttle and engine speed are varied by actuating controllers on the HOST system. Moreover, additional controllers are set for hot, dump and main valves which allow to target for pressure, temperature and mass flow at the engine intake. In the boost rig, proportional, integral and derivative (PID) gain controllers have been set which operate to set the positions of the valves. In addition, engine parameters can be controlled and monitored through the ATI Vision software by connecting to the ECU.

In this scenario, the VGT position is controlled by ATI Vision monitoring and setting operations via controller area network (CAN) messaging. In the case of a different turbocharger installed in the engine gas-stand for mapping, the position of the VGT could not be controlled through ATI Vision and the engine ECU, due to a different type of the VGT actuator/signal. Furthermore, the acquisition system DEWEtron DAQ is able to monitor variables such as in-cylinder pressure, exhaust pressure and turbocharger speed at frequencies as high as 500KHz.

Figure 3. 4: Control room of the engine gas-stand

3.2.1 Instrumentation and data acquisition

In figure 3.5, a turbocharger on the engine gas-stand is visible, including the thermally insulated measuring sections. In fact, in order to reduce the heat transfer between the flow and the test cell ambient, thermal insulation is applied along the ducts between the turbocharger and the measuring point for maintaining temperature and pressure. In this way, preservation of thermodynamic conditions of the flow entering and leaving the turbocharger compressor and turbine could be measured with absence of heat transfer terms.

Figure 3. 5: Turbocharger in the engine gas-stand

Pressures and temperatures have been measured at inlet and outlet of compressor and turbine. For this reason, appropriate measuring sections have been created for compressor inlet and outlet allowing for detection of static pressure and temperature. The adoption of a measuring section is suggested by SAE [24, 82] and ASME standards [83]. Although, a measuring section has been inserted at the outlet of turbine, turbine inlet conditions have been measured on the exhaust manifold with a single thermocouple having the tip placed at the centre of the flow. In fact, due to the highly pulsating flow induced by the engine exhaust valves, the use of several low response thermocouples would be inadequate and insufficient to provide useful information. In relation to the measuring sections at the compressor side, pressure rings to avoid possible radial pressure inhomogeneity are placed at inlet and outlet of the compressor, as in figure 3.6a. Due to temperatures below 493K within the compressor, platinum resistance thermometers (PRTs) are placed in the measuring sections before and after the compressor. In figure 3.6b, four PRTs in a radial section of the measuring section at the compressor outlet are shown. In this case, sensors tips are placed at different depths (one-half, one-third and one-quarter) of the duct diameter, accordingly to SAE standard [82]. At the compressor inlet, only two PRTs are placed in opposite radial locations at depths equal to one-third of the

duct diameter. Less accurate temperature sensors have been placed at turbine inlet and outlet, in order to monitor flow condition at higher temperatures. In this scenario, a single 3mm thick thermocouple (TC) has been placed at the turbine inlet, in order to reduce the possibility of sensor damage, possibly impacting the turbine wheel. Whereas, 1.5mm thick TCs have been placed in the measuring section at the turbine outlet as shown in figures 3.7 and 3.8. Specifically, eight thermocouples at different depths are placed in a straight insulated duct in order to better capture the temperature profile, despite the swirling flows [76].

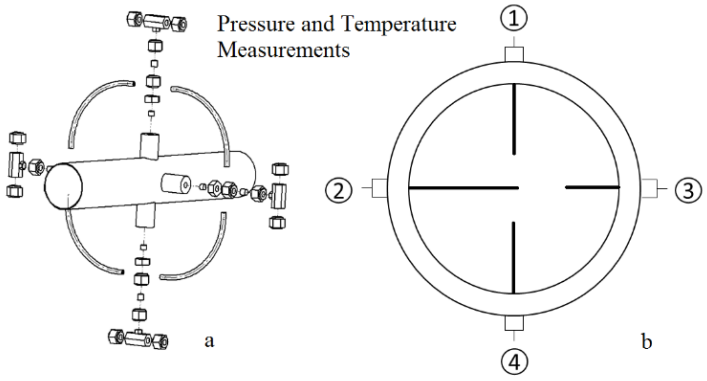

Figure 3. 6: Pressure (a) and 3mm PRTs (b) sensors adopted in the engine gas-stand to measure compressor performance

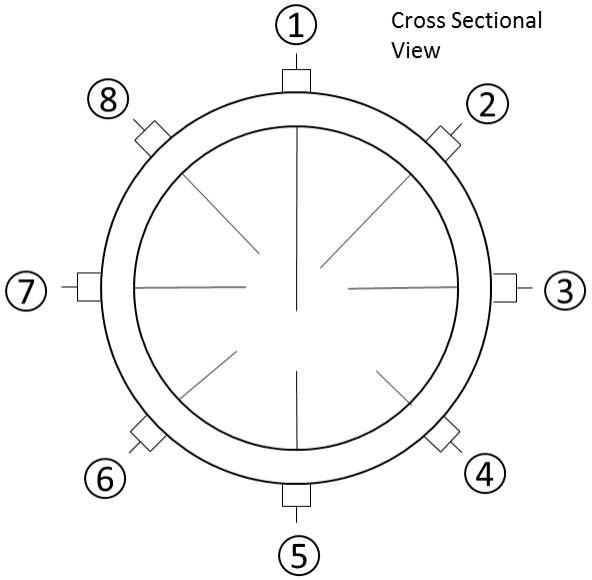

Figure 3. 7: 1.5mm K-type TCs in measuring section at turbine outlet

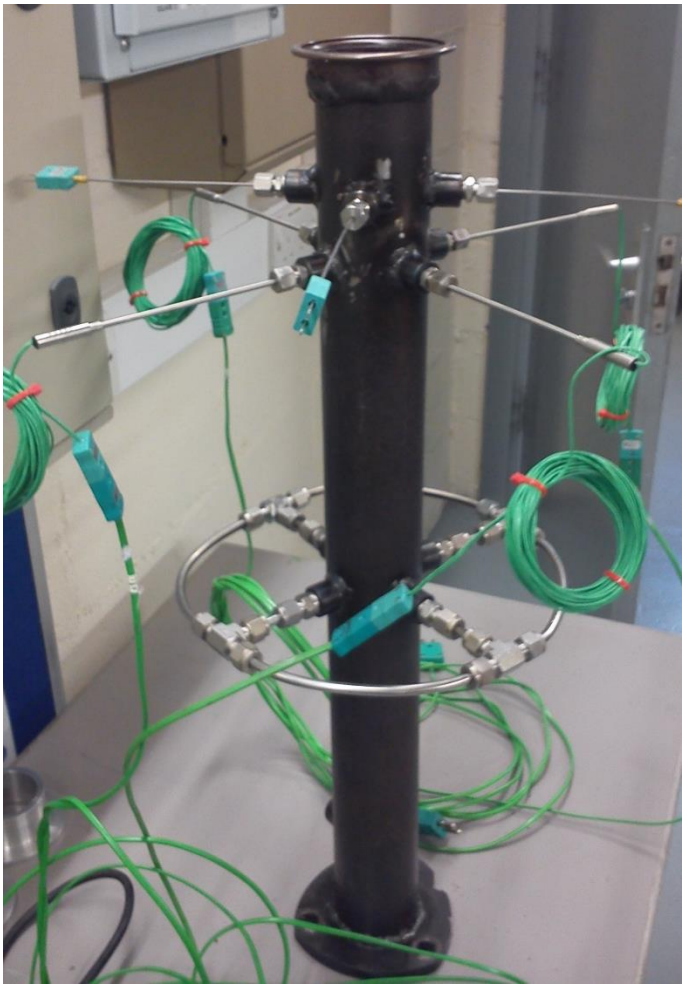

Figure 3. 8: Measuring section at the turbine outlet

Due to lubrication requirements, temperature of the oil entering the turbocharger bearing housing has been measured by a 1.5mm k-type thermocouple with the tip placed on the oil flow feeding the turbocharger. In case of extreme heat fluxes in the turbocharger, water cooling passages could be present in the turbocharger casing. In this case, temperature of the coolant entering and exiting the turbocharger can be monitored by 3mm k-type thermocouples, in the coolant pipes at the proximity of the turbomachine. In addition, the mass air flow (MAF) is monitored at the intake of engine and compressor with high accuracy of 1%, as visible in table 3.2. Due to the nature of steady flow within the compressor, high acquisition frequency is not required. Moreover, in order to quantify mass flow through the turbine, measurements from mass flow sensor at the engine intake and fuel mass flow meter in the engine test cell are combined. Due to the slow response of fuel flow gravimetric system, the turbine mass flow is monitored at a frequency of 1Hz. In the engine gas-stand layout, blow-by flow through the piston rings cannot be reverted

through the engine intake, as I conventional turbocharged powertrains. Furthermore, in order to avoid the introduction of errors in the mass flow measurements, the EGR valve of the engine air-path is completely closed. Water-cooled pressure transducers sampling at one decimal of an engine crank angle degrees (CAD) up to 500 KHz are positioned at the turbine connections to the exhaust manifold and at the turbine outlet, due to pulsating flows generated by the reciprocating engine. Once pressure, temperature and mass flow around the engine gas-stand can be monitored, the system can be used to map turbochargers in conjunction with an eddy-current turbocharger speed sensor placed at the compressor housing. Due to the high frequency nature of the compressor blades passing by the speed sensor, a high acquisition frequency has been adopted through the DEWEtron DAQ system.

Table 3. 2: List of sensors adopted in the engine gas-stand, including range, accuracy, response and sampling frequency of sensors and acquisition system

SENSOR	RANGE	ACCURACY	RESPONSE	ACQUISITION
PRT	-50 to 200degC	±0.3 + 0.005*T	0.04 Hz in air 1.66 Hz in water	1 Hz
K type TC	-200 to 1260degC	0.0075*T	1.66 Hz in water for 3mm 3.33 Hz in water for 1.5mm	
MAF	0 to 1200 Kg/h	1%	82 Hz	
Fuel flow	0 to 200 Kg/h	±0.05%	1 Hz	
Slow-sample Pressure	0 barA to 6 barA	0.25%	100 Hz	
Fast-sample Pressure	0 barA to 5 barA	0.3%	500 KHz	0.1 Crank Angle Degree (CAD)
Turbo speed	0 to 400,000 rpm	0.1%	100 KHz	

3.2.2 Temperature and pressure correction

In order to remove the dependency of measured turbine and compressor performance from intake conditions, mass flow ($\dot{m}$) and speed (N) are corrected in $\dot{m}_{corr}$ and N_{corr}, respectively, as visible in equations 3.1 and 3.2.

$$\dot{m}_{corr} = \dot{m} \frac{\sqrt{T_{t,in} / T_{ref}}}{P_{t,in} / P_{ref}} \tag{3.1}$$

$$N_{corr} = N * \sqrt{\frac{T_{ref}}{T_{t,in}}} \quad (3.2)$$

In order to remove inlet conditions dependency for mass flow measurements of compressor and turbine, total inlet temperature ($T_{t,in}$) and pressure ($P_{t,in}$) are normalised to reference values of temperature (T_{ref}) and pressure (P_{ref}), respectively. In equation 3.2, the rotational speed is only corrected for temperature. In the case of turbine maps, the reference values consist of 1atm and 288K. Meanwhile, the compressor performance map is corrected for 1bar and 298K. These reference values are referring to the corrections adopted by the turbocharger manufacturer.

3.2.3 Total-to-total and total-to static pressure ratios

In order to evaluate compressor and turbine pressure ratios, total pressure (P_t) would have to be identified, as in equation 3.3. The dynamic component of pressure would have to be evaluated, as depending on the ratio of specific heats (γ), the Mach number (Ma) and the static pressure (P_s). The same relation between static and total pressure could be extended to temperature, as reported in equation 3.4. Moreover, the ratio between speeds of fluid and sound is defined as the Mach number in equation 3.5. The speed of sound can depend on the ratio of specific heats, the constant of gas (R) and the temperature of the fluid.

$$P_t = P_s \left(1 + \frac{\gamma - 1}{2} Ma^2\right)^{\frac{\gamma}{\gamma - 1}} \quad (3.3)$$

$$T_t = T_s \left(1 + \frac{\gamma - 1}{2} Ma^2\right)^{\frac{\gamma}{\gamma - 1}} \quad (3.4)$$

$$Ma = \frac{V}{\sqrt{\gamma R T}} \quad (3.5)$$

Therefore, in equation 3.6, the total-to-total pressure ratio for the compressor could be defined as the ratio between total outlet ($P_{t,out}$) and total inlet ($P_{t,in}$) pressures.

Meanwhile, in equation 3.7, the total-to-static pressure ratio for the turbine could be expressed as the ratio between total inlet ($P_{t,in}$) and static ($P_{s,out}$) outlet pressures.

$$PR_{c,t-t} = P_{t,out}/P_{t,in} \tag{3.6}$$

$$PR_{T,t-s} = P_{t,in}/P_{s,out} \tag{3.7}$$

3.2.4 Total-to-total and total-to-static efficiencies

In order to evaluate the performance of turbine and compressor, thermodynamic properties at inlet and outlet of turbomachine are monitored. In equation3.8, total-to-total compressor efficiency ($\eta_{c,t-t}$) is equal to the ratio between isentropic ($Power_{c,is}$) and adiabatic ($Power_c$) compressor powers. Regarding the turbine, equation 3.9 shows the total-to-static turbine efficiency ($\eta_{T,t-s}$). This is defined as the ratio between adiabatic ($Power_T$) and isentropic ($Power_{T,is}$) turbine powers. Moreover, due to the difficulty that swirling flows can cause in the attempt to measure reliably turbine outlet temperature, thermomechanical/net ($\eta_{T,net}$) efficiency of the turbine could be preferred. In fact, as visible in equation 3.11, the net turbine efficiency is independent of the adiabatic turbine power. Furthermore, the net turbine efficiency is defined as the product of mechanical turbocharger (η_m) and total-to-static turbine efficiencies. Furthermore, in equation 3.10, the mechanical efficiency is highlighted as the ratio between compressor and turbine adiabatic powers.

$$\eta_{c,t-t} = \frac{Power_{c,is}}{Power_c} = \frac{T_{t,in} * \left(PR_{t-t}^{\gamma-1/\gamma}\right)}{T_{t,out}/T_{t,in}} \tag{3.8}$$

$$\eta_{T,t-s} = \frac{Power_T}{Power_{T,is}} = \frac{T_{t,in}/T_{s,out}}{T_{t,in} * \left(1/PR_{t-t}^{\gamma-1/\gamma}\right)} \tag{3.9}$$

$$\eta_m = \frac{Power_c}{Power_T} \tag{3.10}$$

$$\eta_{T,net} = \eta_m * \eta_{T,t-s} = \frac{Power_c}{Power_{T,is}} \tag{3.11}$$

3.3 Turbocharger mapping on engine gas-stand

3.3.1 Setting and measuring compressor performance

In the engine gas-stand of figure 3.3, performance of a turbocharger have been tested. In particular, for a standard single stage VGT turbocharger with compressor and turbine diameters of 49mm and 41mm, respectively, the mapping technique has been developed, in order to exploit compressor performance in a controllable environment. Once engine speed and turbine inlet temperature relating to a certain air-to-fuel ratio value have been fixed, CB valve is open, while, the VGT actuator is maintained in the close position. Referring to figure 3.9, the operating condition of the compressor at a certain rotating speed are recorded for point A. Additionally, the CB valve is slightly closed inducing an increase of pressure ratio and reduction of mass flow. In order to maintain turbocharger speed, engine load is increased, by adding boost at the engine intake. Fuel flow is slightly tuned, in order to achieve a constant turbine inlet temperature at point B. However, the variation of CB valve, boost demand at engine intake and engine fuel flow could result in a higher compressor speed at point B, in comparison to point A. Therefore, in order to re-establish the compressor speed as in point A, VGT position is widened slightly causing a deceleration of the turbocharger. In fact, the air mass flow at point C results in a lower value than both points A and B.

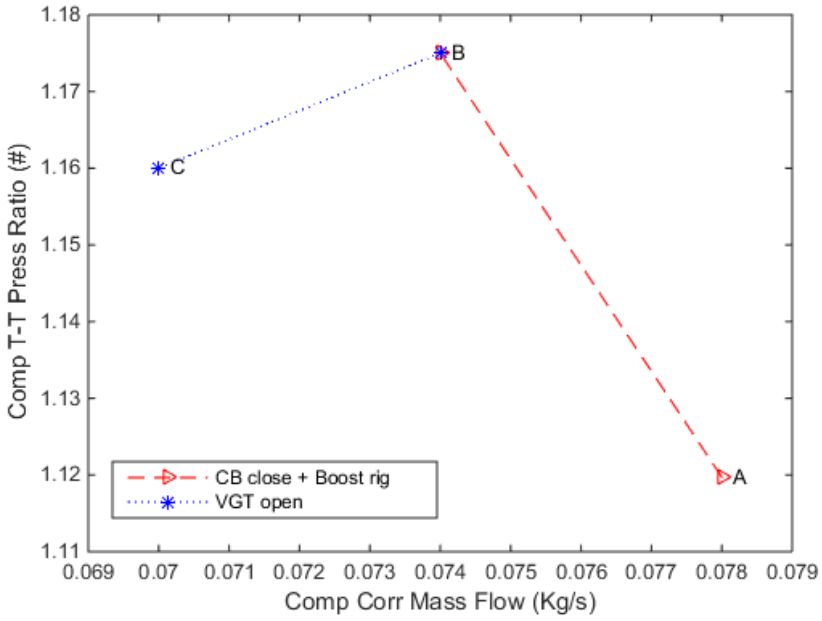

Figure 3. 9: Compressor T-T pressure ratio and corrected mass air flow for conditions A, B and C of the engine gas-stand

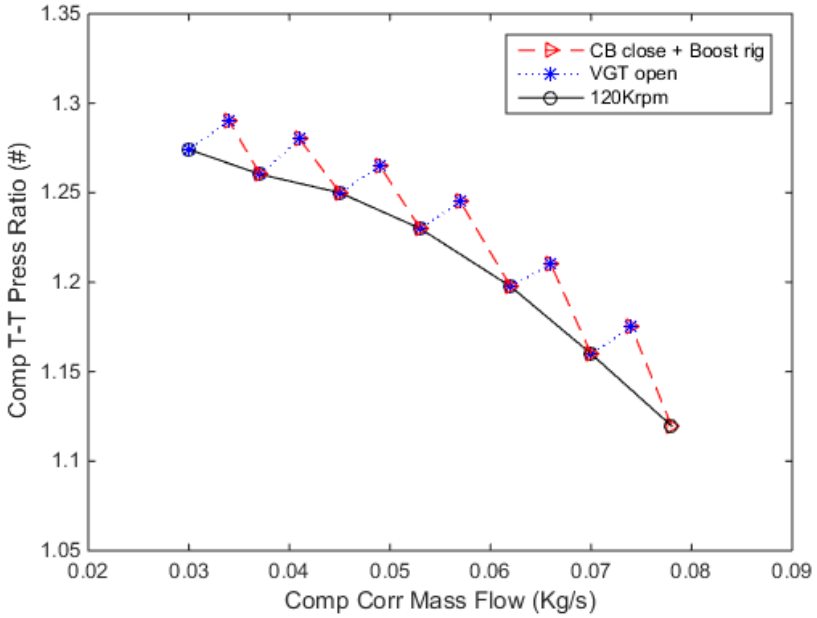

Figure 3. 10: Compressor T-T pressure ratio and corrected mass air flow for a constant corrected speed line

In the case where the process is repeated for reducing mass flow through the compressor and for different CB valve position, the surge region is reached at a certain mass flow value, by monitoring pressure oscillation in the compressor downstream duct. This process is shown in figure 3.10 for a constant speed line of the compressor. It is important to notice that in a fixed geometry turbine, the VGT is not present and, thus, this process could not be adopted as an input for mapping the compressor. Therefore, a reduction of boost pressure and injected fuel would be required to shift the operating conditions from point B to C (figure 3.9). Most importantly, the TIT would have to be kept constant.

The different speed lines that have been tested for the compressor at TIT of 600K and 830K of the VGT turbine are shown in figure 3.11. The engine speed has been kept constant at 2500rpm and boost pressure, fuel injected, VGT and CB valve position varied in order to achieve the correct operating points of the compressor. It is important to notice that the engine gas-stand would have to set some compressor mapping constraints. At 2500 engine rpm, the engine gas-stand operating at full boost would be able to explore the compressor speed line of 140Krpm, achieving turbine inlet temperatures of 600K. In order to maintain the low temperature at the

exhaust, the maximum amount of boost would be required, reducing the injected fuel amount. This would result in extremely lean combustion operations of the engine. On the low end of the compressor map, engine speed would have to be reduced from 2500rpm down to 1800rpm in order to maintain the compressor at 60Krpm and 830K of TIT. This would lead to zero boost at the engine intake and extremely fuel-rich combustion, being limited by the minimum allowed engine lambda (1.2) at the engine gas-stand exhaust.

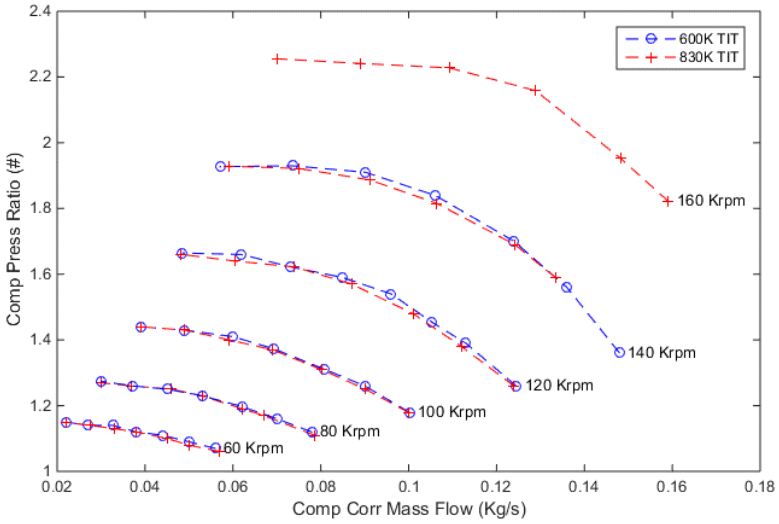

Figure 3. 11: Compressor T-T pressure ratio and corrected mass flow for 600K and 830K of TIT

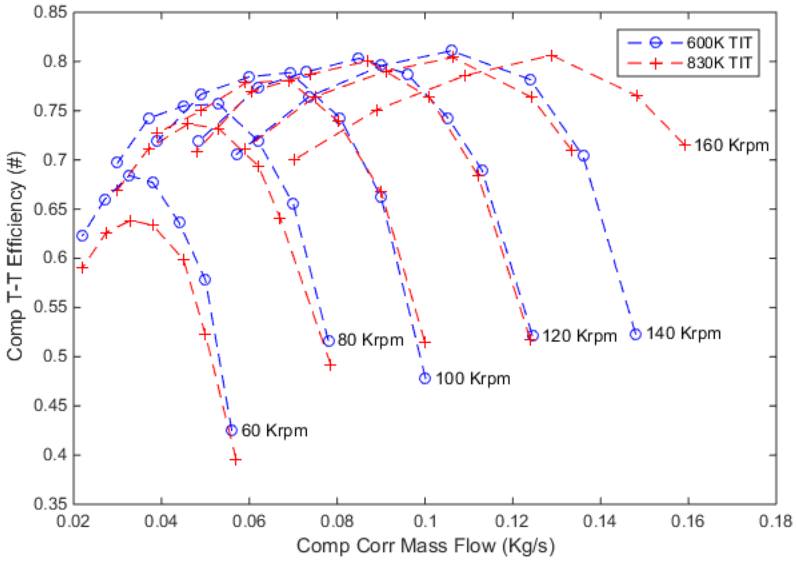

Figure 3. 12: Compressor T-T efficiency for 600K and 830K of TIT

As well as the pressure ratio, the compressor efficiency has been measured as the ratio between isentropic and adiabatic work. In figure 3.12, compressor total-to-total (T-T) efficiency is presented for two different turbine inlet temperature values. In particular, a reduction of best achievable efficiency can be visualized for the corrected compressor speeds of 60Krpm and 80Krpm. This gap is minimal for any other speed line. It is expected that for the case with higher turbine inlet temperature, the measured compressor efficiency is worsened. This is due to the prominence of heat transfer over the compression work. Moreover, the maximum efficiency achieved from the compressor results are higher than expected with peak values of 80%. This could be explained by an insufficient insulation at the measuring sections causing a reduction of the post compressor flow temperature. Therefore, additional layers of external insulations have been installed to reduce the heat flux from measuring sections to ambient. Moreover, the efficiency difference at low turbocharger speed recorded in figure 3.12 could be caused by the heat transfer to the compressor on the on-engine installation. It is important to state that a water cooled housing is present on the turbocharger as well as an oil lubricated bearing housing.

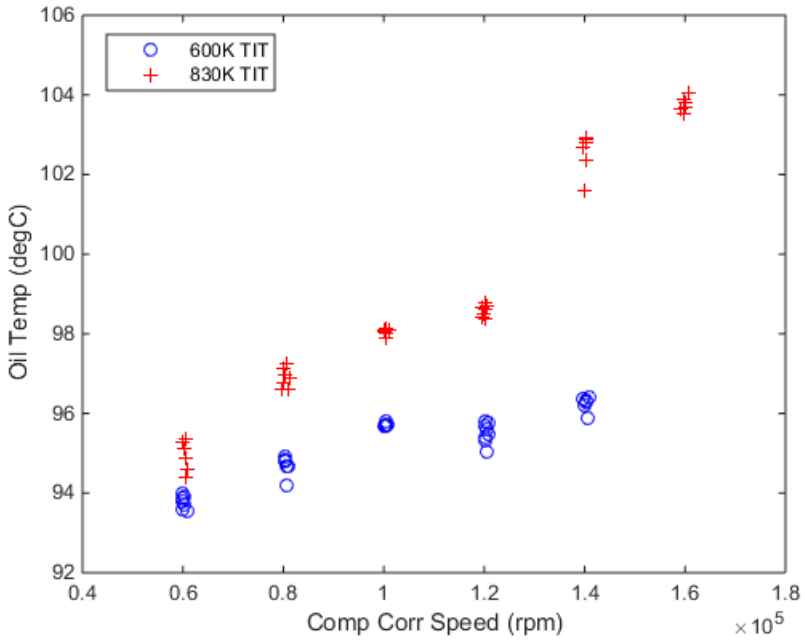

Figure 3. 13: Oil temperature at the engine sump and compressor mass flow for 600K and 830K of TIT

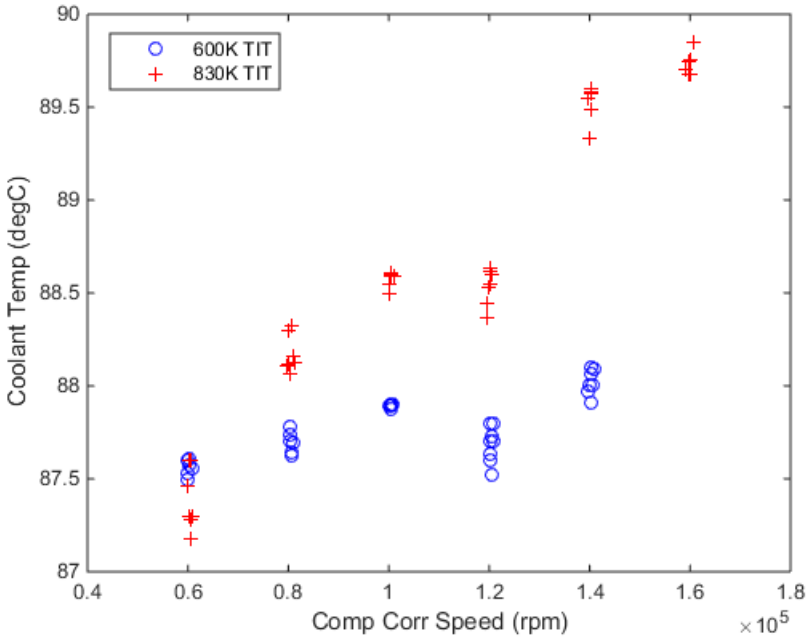

Figure 3. 14: Coolant temperature entering the turbocharger and compressor mass flow for 600K and 830K of TIT

Furthermore, oil temperature is higher for TIT of 830K as visible in figure 3.13. This suggests the presence of a slightly higher heat extraction rate in the bearing housing for 830K of TIT. In figure 3.14, coolant temperature differs slightly between the turbocharger conditions at 600K and 830K of TIT. In both figures 3.13 and 3.14, oil and coolant temperatures increase directly with compressor corrected speed. Due to coolant and oil being shared between the engine and the turbocharger, the temperature and the flow have been regulated in relation to the engine requirements.

3.3.2 Comparison with manufacturer data

The total-to-total pressure ratios and efficiencies generated for a different turbocharger compressor in the engine gas-stand have been compared to steady gas-stand data available from the manufacturer's map. In figures 3.15 and 3.16, two speed lines N1 (120Krpm) and N2 (140Krpm) generated at the engine gas-stand (EGS) and gas-stand (GS) have been compared for the same compressor. As shown by the two figures, the performance measured in the engine gas-stand have matched pressure ratios and efficiency numbers, by resulting in a maximum over-

estimation of approximately 2%. Moreover, the TIT is maintained at 830K for the EGS, comparing to the GS information.

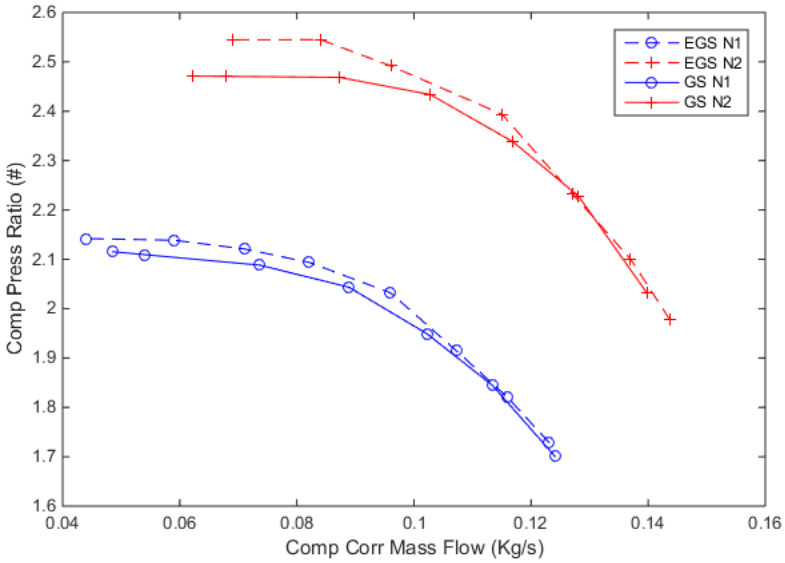

Figure 3. 15: T-T pressure ratio for two medium-high speed corrected compressor lines in engine gas-stand (EGS) and manufacturer's gas-stand (GS)

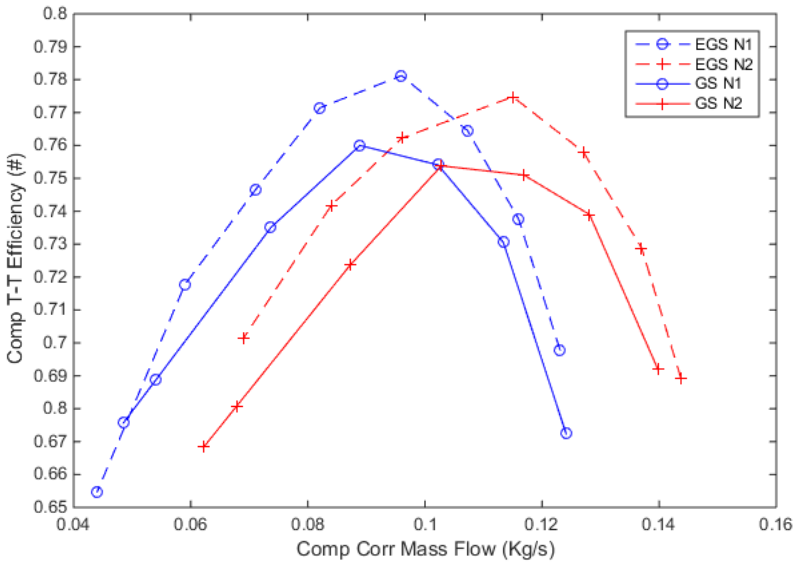

Figure 3. 16: T-T efficiency for two medium-high speed corrected compressor lines in engine gas-stand (EGS) and manufacturer's gas-stand (GS)

3.3.3 Monitoring of turbine performance

In order to perform turbine performance maps, the VGT is maintained in the same position for the different turbine corrected speed lines. Referring to figure 3.17, a turbine constant speed line is represented for a fixed position of the VGT actuator.

In order to measure turbine performance in the engine gas-stand facility, the real turbine mass flow has been calculated as the sum of air flow entering the engine intake and fuel flow entering the engine combustion chamber. Due to the low sampling frequency (1Hz) of the fuel mass flow meter, the turbine mass flow would be captured at low resolution. In addition, the low response rate of 3mm k-type thermocouples at the turbine inlet induces the imposition of an average value of the turbine inlet temperature in the turbine corrected mass flow formula (equation 3.1). In addition, total-to-static pressure ratio is generated by measured instantaneous pressure data at inlet and outlet. In order to generate the map of figure 3.17, the instantaneous pressure ratio is averaged for an entire engine cycle (720 crank angle degrees), as in equation 3.12. In fact, the sum of instantaneous pressure ratios (PR_{inst}) is divided by the number of samples in an engine cycle (*n*).

$$PR_{ave} = \frac{\sum PR_{inst}}{n} \tag{3.12}$$

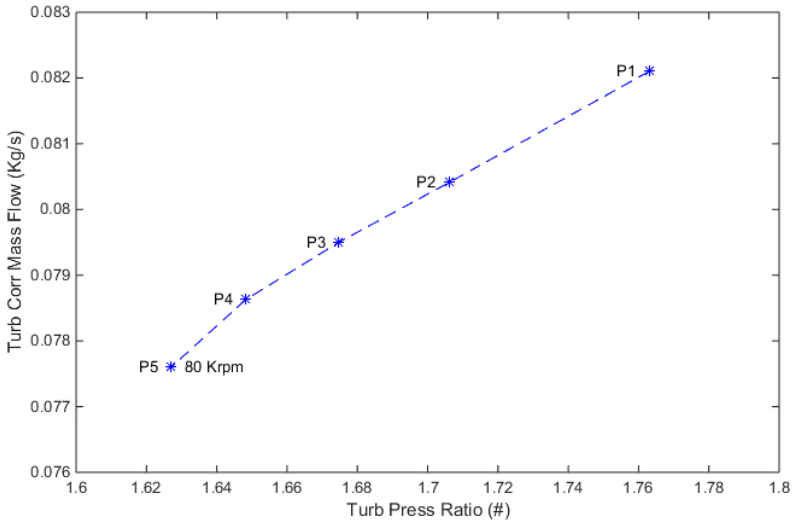

Figure 3. 17: Turbine pressure ratio and corrected mass flow for 5 points at 80Krpm corrected turbine speed

In order to move from P1 to P2, boost and fuel quantities are reduced by keeping the turbine inlet pressure constant. This would reduce mass flow and speed of the turbine. Therefore, the CB valve is closed, in order to achieve turbine corrected speed value as in point P1. If the process is repeated for few different points, a

turbine speed line is generated. The points in figure 3.17 maintain the same frequency of pulsation due to constant engine speed being maintained. On the other side, the amplitude of pulsation is varied between the five points as shown by the pressure traces in figure 3.18. Specifically, a difference in peak pressure and amplitude is visible between P1 and P5. Most importantly, figure 3.18 shows that the frequency of pulsation remains the same. This is due to the absence of variable cam timing and the constant engine speed being kept for all the turbine operating points. Moreover, the turbine outlet pressure remains constant through the five operations of figure 3.17.

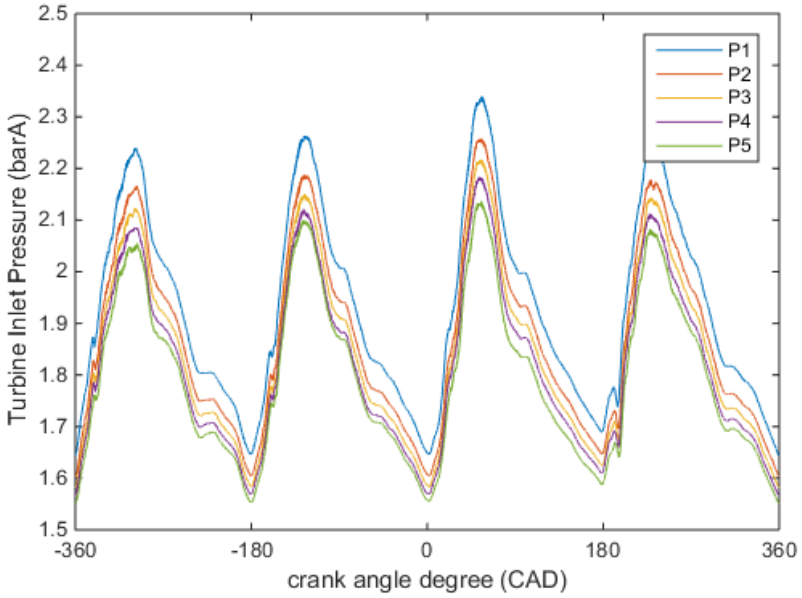

Figure 3. 18: Turbine inlet pressure sampled every 0.1CAD of the engine rotation (120KHz at 2000rpm)

3.3.4 Influence of sampling rates on measurements

As well as the compressor, turbine performance can be monitored in the engine gas-stand. In order to measure turbine performance for an automotive turbocharger, data available from the experimental test rig are exploited. Due to the presence of unsteady flow in the exhaust, the sampling frequency of pressure, temperature and mass flow sensors has a significant importance. In fact, in the case with two different acquisition rates, the measurements to define swallowing capacity of the turbine could differ. In this study, two acquisition frequencies for pressure transducers have been adopted, as low as 1Hz for the ‘slow’ sampling case (minimum sampling frequency for fuel metering system) and 120KHz at ‘fast’ sampling conditions

(maximum sampling frequency achievable at engine speed of 2000rpm), depending on engine speed. Temperature and mass flow measurements have only been monitored at 1Hz under 'slow' and 'fast' sampling rates. In addition, turbine swallowing capacity has been investigated at 0.5 VGT position with pulsating flows at the turbine inlet at a frequency of 66.67Hz. It could be suggested that the acquisition rates would not be adequate to capture the effects of oscillating flows on temperature, mass rates and pressure, in the case of 'slow' sampling speed. In fact, it is suggested that aliasing distortion [84] could be encountered in the experimental data, apart from 'fast' sampled pressure.

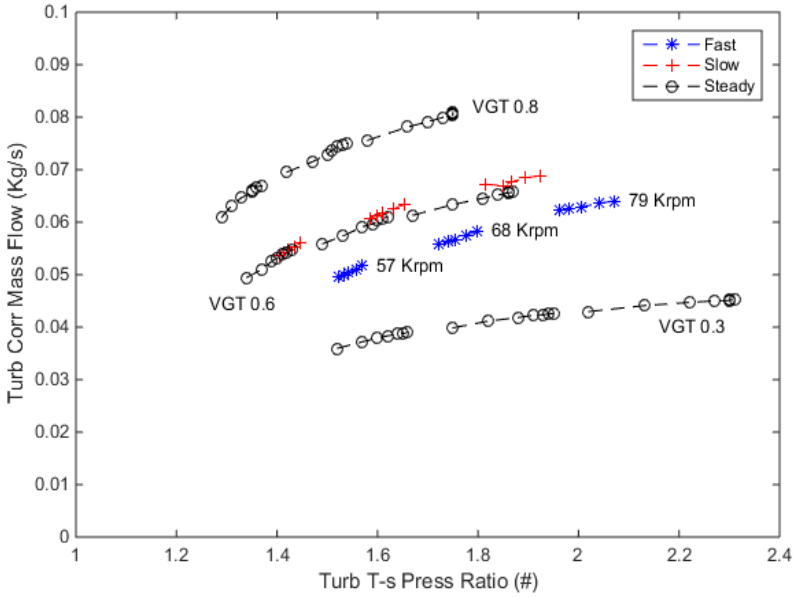

Figure 3. 19: Experimental 0.5 VGT turbine performance data acquired at 'slow' (1Hz) and 'fast' (120KHz) sampling speeds and compared to steady turbocharger manufacturer's data available at 0.3, 0.6 and 0.8 VGT opening positions. 'Fast' sampled data are cycle averaged. 'Slow' sampled data are averaged for 60sec. VGT has a travel of about 50mm between positions 0 and 1.

In figure 3.19, points from the steady manufacturer's map at 0.3, 0.6 and 0.8 opening positions of the variable geometry turbine (VGT) are shown. These data are compared to turbine performance measured in the engine gas-stand using 'fast' and 'slow' acquisition speeds. Although, the difference in the VGT opening position, 'slow' measured turbine swallowing capacities for three corrected speed lines at 57, 68 and 79 Krpm (actual turbocharger speeds of 99, 118 and 138Krpm) are similar to steady performance map data at 0.6 VGT. This similarity is certainly dismissed once pressure events on a higher frequency spectrum are analysed in the 'fast'

acquisition case. In fact, ‘slow’ acquisitions at 1Hz are only able to measure once per second with the pressure recorded being anywhere between minimum and maximum values of peaks in the 66.67 Hz oscillating trace. In conjunction with figure 3.19, this results in an underestimation of turbine pressure ratio and overestimation of corrected turbine mass flow, depending also on turbine inlet pressure. However, in the engine gas-stand, the impossibility to improve sampling rates of temperature and mass flow thus omits the dynamic effects of the exhaust process, occurring at 66.67 Hz in the experimental setting. It is clear that a lower acquisition rate of pressures at the turbine would not be adequate enough in the representation of the real performance. In fact, the averaging of pressure measurements at elevated sampling frequency shows a different pressure ratio.

3.4 Chapter summary and conclusions

In this chapter, the development of the engine gas-stand facility is presented and the following conclusions can be drawn:

- It has been shown that turbocharger performance can be explored in the engine gas-stand, emulating powertrain operating conditions of the turbomachine. Compressor and turbine performance variables can be monitored in the control room through acquisition and host systems implemented in the facility.

- In order to perform a compressor map under steady flow conditions, a mapping methodology has been developed and presented. Moreover, the effects of turbine inlet temperature on the apparent compressor efficiency are investigated. In fact, the engine gas-stand facility allows efficient control of turbine and exhaust temperature.

- The presence of pulsating flows at the turbine due to the alternating motion of the engine exhaust valves sets the requirement for fast response sensors and acquisition systems. In fact, the adoption of 500KHz pressure transducers, combined with an engine crank angle based acquisition system, allow for adequate monitoring of the pulses, influencing the resulting performance map of the turbine.

- Furthermore, limits on instantaneous mass flow and temperature measurements at the turbine have been highlighted, due to slow reaction of flow meter and k-type thermocouple. In fact, exhaust valve would induce a pressure fluctuation of 66.67Hz at 2000rpm of the engine, while reactions on the order of 1Hz would be recorded by mass flow and temperature sensors.

- Therefore, the absence of reliable temperature and mass flow measurements at the turbine would neglect the possibility to measure complete turbine performance parameters, generating turbine maps.

Chapter 4 – Attempt to correlate simulations and measurements of turbine under pulsating flows

In this chapter, a turbine model to improve correlation with experimental measurements in the engine gas-stand has been presented. A hybrid unsteady/quasi-steady model of the turbine is developed in order to predict turbocharger turbine performance under unsteady flows in 1D models. In order to evaluate isentropic turbine efficiency and reduce heat transfer effects [57], inlet temperature at the turbine rotor has been experimentally measured and compared to measurements at the exhaust manifold. In the proposed turbine model, tuning of the geometry is not necessary due to geometrical representation of turbine tongue and diffuser through tapered ducts, accounting for the turbine mass storage and pressure wave dynamics. Furthermore, virtual sensors and thermocouples have been implemented into the 1D model to correlate experimental time-averaged temperature measurements. The correlation attempt is performed on a single stage turbocharger with the intention to expand the application to two-stage turbochargers, owing to the presence of high flow motion at the inter-stage.

The proposed turbine model and investigation in the chapter have been developed under the Future Research Leader Incubator Scheme from the University of Bath at the Nanyang Technological University.

4.1 Turbine under pulsating flows

The use of turbochargers in conjunction with reciprocating internal combustion engines are able to provide benefits to the system for constant and transient conditions [85] and to the release of harmful pollutants into the environment through the engine tailpipe [86]. The perfect matching of turbochargers to the engine for satisfying the breathing characteristics is possible though an accurate preliminary analysis of turbocharger performance [35]. In a turbocharger, compressor and turbine performance are evaluated in test gas-stands working under steady flows [83]. In the case of a turbine, swallowing capacity and efficiency maps are generated at constant turbine speed lines linking pressure, temperature and mass flow measurements. In this scenario, steady performance maps are considered for an engine system analysis and an initial performance evaluation of automotive powertrains [87, 88]. The presence of pulsating flows at the turbine inlet can vary the operating conditions of the turbine from quasi-steady to fully unsteady, reducing the relevance of steady performance maps [89]. In engine gas-stands, pulsating flows at the turbine inlet of automotive turbochargers can be applied, allowing the analysis of performance and the change in quasi-steady conditions [90].

In the presence of unsteady flows in turbocharger turbine, performance measurements through the use of external instrumentation are significantly dependant on the positioning [76, 91]. Furthermore, deviation from steady efficiency is significant due to the presence of oscillating flow parameters in relation to operating pulsation amplitude and frequency [92, 93]. Accordingly to the definition of total-to-static turbine efficiency, turbine adiabatic power is correlated to inlet and outlet temperature measurements [35]. Owing to the effect of fluctuating flows [94], standard thermocouples have difficulties in monitoring instantaneous temperature, solely allowing the availability of time-averaged data. In this case, taking into account the compressor power in the turbocharger can remove the uncertainty of turbine outlet temperature from the turbine efficiency equation [95]. Therefore, the development of monitoring equipment for measuring instantaneous temperature [96] and the adoption of instantaneous torque meters on turbocharger shaft [39] can be considered valuable attempts for capturing unsteady turbine efficiency experimentally. In conjunction with temperature measurements of unsteady flows, increased difficulty is added for instantaneous mass flow measurement at hot turbine conditions [97]. In fact, investigations have been performed in turbocharger

gas-stands incorporating pulsating devices at the turbine inlet [98]. In these cases, instantaneous mass flow measurements have shown differences on turbine hysteresis loops and average performance between straight ducts and bends at the turbine inlet, emulating the effect of an engine exhaust manifold [99].

The oscillation of pressure at turbine inlet affects the turbine behaviour and attempts in modelling the expansion process have been performed, monitoring instantaneous turbine torque at the shaft [91]. Wave actions and filling and emptying models to account for pulsating turbines have been developed, obtaining agreement between predictions and experimental data available. Models presented in Serrano et al. [100], Piscaglia et al. [101] and Chiong et al. [102] can be implemented in 1D codes and are able to account for flow pulsations generated by internal combustion engines. However, in order to obtain useful agreements, the coupling between turbine rotor, stator and diffuser has to be accurately tuned against turbine experimental [103] and geometrical data [104]. On the other hand, the exclusion of steady turbine map from turbine model could be a lengthy process to obtain significant benefits in unsteady performance definitions of turbocharger turbine [60]. In addition, the degree of complexity is increased in fully unsteady turbine models and performance could be poorly predicted under unequal flow admissions for twin and double entry turbocharger turbines [105].

4.2 Effect of turbine inlet temperature

The obtained improvement in increasing sampling frequencies has led to calculation of T-s turbine efficiency considering values for the 'fast' acquisition, due to improvement over aliasing distortion of measurements [84]. Due to temperature dependency of turbine performance, measurements have been monitored through 3mm k-type thermocouple at turbine inlet and 1.5mm k-type thermocouple at turbine outlet. Unfortunately, the thermocouples adopted in the engine gas-stand are characterised by a significantly low response rate and a possible increment over the 1Hz sampling rate would not have been beneficial. Although, inaccuracy of temperature measurements owing to the presence of oscillating flows, further errors could be introduced because of the thermocouple position since only average temperatures could be obtained experimentally. For this reason, two identical thermocouples have been placed at different locations in the exhaust and turbine inlet sections, shown in figure 4.1, and turbine measurements have been performed for operating conditions shown in figure 4.2.

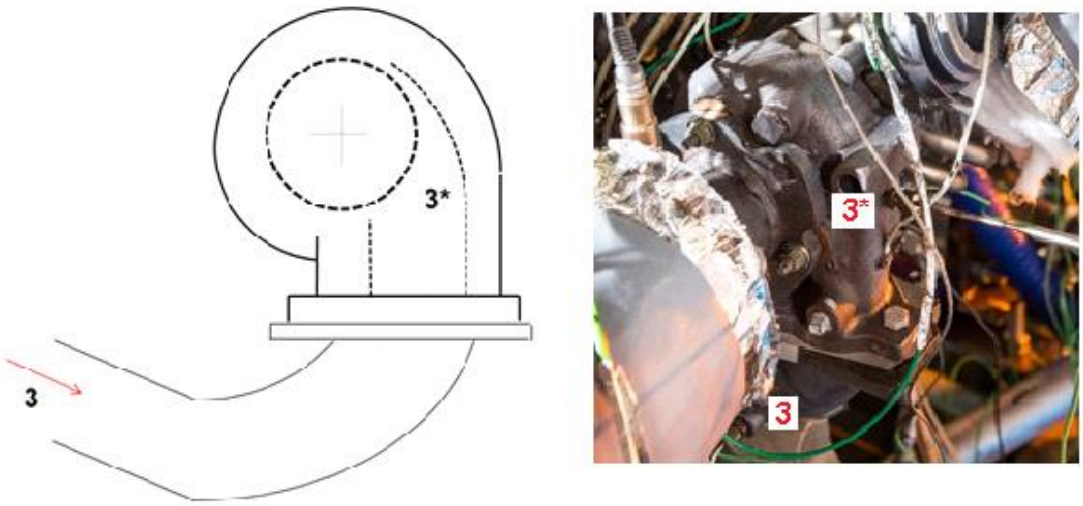

Figure 4. 1: Schematic of the two thermocouple at 3 and 3* for the evaluation of TIT

In figure 4.1, flow temperature has been monitored at the exhaust manifold exit (i.e. inlet to the turbine) (3) and at the proximity of the turbine tongue (3*). The outlet temperature at 4 has been considered as a unique average value of the thermocouples as plotted in figure 4.2. Therefore, T-s turbine efficiency could be calculated for the two different turbine inlet temperatures indicated. It could be expected that the flow temperature in the proximity of the turbine would be lower

due to heat transfer in the exhaust section. However, the analysis highlights that higher efficiency could be measured, referencing 3* as turbine inlet temperatures. In this scenario, measurements suggest that conditions at 3* are hotter than the thermocouple in 3.

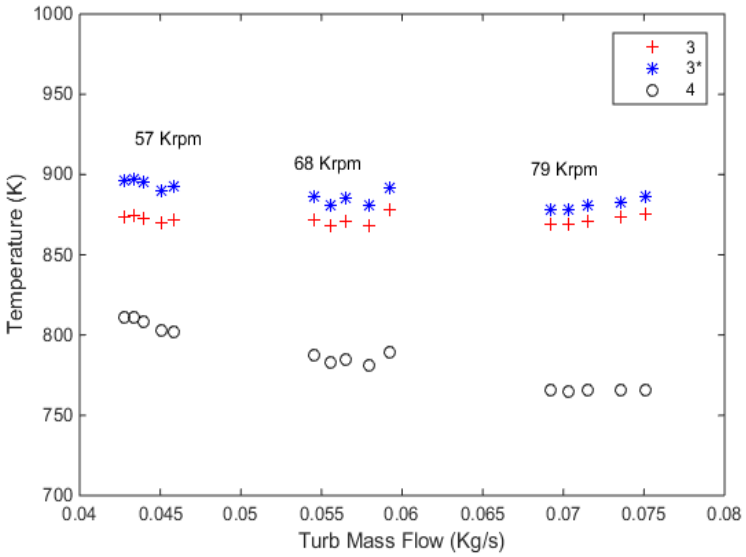

Figure 4. 2: Turbine mass flow and experimental temperatures measured in the engine gas-stand at the positions 3 (turbine inlet temperature), 3* (turbine inlet temperature in the turbine tongue and in the proximity of the turbine rotor) and 4 (turbine outlet temperature averaged across eight thermocouples) for the three corrected speed lines at 57, 68 and 79 Krpm

The cause for higher time-average temperature at the proximity of the turbine rotor could be given by the possibility of exhaust gasses to converge towards the turbine rotor. The thermocouple closer to the turbine tongue (3*) would be measuring temperature under different conditions of the thermocouple positioned at 3. In fact, it would seem that the thermocouple positioned at the exhaust manifold (position 3) is affected by 3D temperature distribution, due to the close proximity of multiple Y-junctions and bends in the exhaust manifold. In this scenario, the temperature at the tip of the thermocouple 3* would be similar to a 1D flow domain. However, a 3D flow analysis would be required to improve the understanding, as investigated in [99]. Furthermore, the reduction of diameter at the turbine inlet towards the turbine tongue and volute would accelerate the flow velocity. Accordingly to the definitions of Strouhal number and reduced frequency, it would result in a reduction of the flow unsteadiness.

4.3 Hybrid unsteady/quasi-steady turbine model

4.3.1 Modelling approaches

In order to represent turbochargers performance in 1D powertrain models, steady performance maps for compressor and turbine are adopted, assuming that the turbocharger behaves quasi-steadily. In the case of a turbine, boundaries at inlet and outlet of the turbomachine are coupled to the performance maps, replacing internal volumes from tongue to diffuser. Additionally, in internal combustion engine applications, turbine inlet temperature and turbine outlet temperature (TOT) are measured at exhaust manifold exit and at the exhaust duct preceding after-treatment systems, respectively. In 1D powertrain model simulations, average temperature is monitored via virtual sensors for the considered radial section of the duct. In this research study, virtual temperature sensors (VTS) and thermocouple (VTC) models have been positioned at the same positions at in the experiments (3, 3* and 4) to evaluate TIT and TOT and account for the predicted turbine performance. Moreover, two turbine models have been implemented and temperature measurements through virtual sensors and thermocouples have been evaluated, in order to improve efficiency and TOT representation. In particular, five modelling approaches have been developed as shown in table 4.1, specifying turbine and temperature models.

Table 4. 1: Modelling approaches of turbine in an automotive turbocharger

APPROACH	TURBINE MODEL	TIT	TOT
Virtual T3	Steady Map	VTS 3	VTS 4
Virtual TC3	Steady Map	VTC 3	VTC 4
Virtual T3*	Hybrid unsteady/quasi-steady	VTS 3*	VTS 4
Virtual TC3*	Hybrid unsteady/quasi-steady	VTC 3*	VTC 4
Virtual TC3*-T4	Hybrid unsteady/quasi-steady	VTC 3*	VTS 4

In the case of virtual T3 and TC3, steady maps for the entire turbine have been considered. In order to account for the temperature at 3*, the hybrid unsteady/quasi-steady turbine model has been developed. The model differs from the approach adopted by Piscaglia et al. [101], because of the adoption of tapered ducts at the turbine inlet and diffuser, instead of volumes for mass storage behaviours. In addition, in the hybrid unsteady/quasi-steady turbine model, turbine volute is modelled in the steady turbine map, in order to account for part of the expansion

process taking place upstream the turbine rotor. On the other side, both models from Piscaglia et al. [101] and Chiong et al. [102] are modelling turbine volute in volumes and ducts, respectively. As suggested by Yang et al. [106], in the duct between the turbine inlet and the tongue (inlet of the volute), the phase shift in pressure and temperature is significantly noticeable. In addition, this phase shift is highly reduced along the volute, due to the increased bulk flow velocity. In fact, the increase in flow velocity can be supported by the reduction of the cross sectional area. It is important to notice that the increase of flow velocity is inversely proportional to the flow unsteadiness, as supported by the Strouhal number [107] and the reduced frequency [108].

In the hybrid unsteady/quasi-steady turbine model, turbine tongue and diffuser are treated as unsteady, being modelled though tapered ducts, while the unscaled turbine steady performance map represents the expansion process in the rotor. Unlikely, in the hybrid unsteady/quasi-steady turbine model, frequency tuning is not necessary as the steady turbine map is adopted for the expansion process, considering volute and rotor operating under quasi-steady conditions. This representation can be valid for small volutes and steady turbine maps can be adopted for the quasi-steady expansion process, allowing simultaneously the monitoring of TIT closer to the turbine rotor. The proposed hybrid unsteady/quasi-steady turbine model would be able to represent the unsteady flow operations of turbine inlet (up to the turbine tongue) and turbine diffuser. Due to the difficulty in obtaining geometrical data from turbochargers, the turbine model has based the dimensions of added unsteady flow sections to the model from simple real geometrical measurements. In addition, no further tuning to represent steady and unsteady flow conditions has been applied. Furthermore, non-intrusive measurements can be performed without dismantling the turbomachine to evaluate turbine tongue and diffuser dimensions. A diagram of the 1D hybrid unsteady/quasi-steady turbine model can be visualised in figure 4.3. The turbine inlet to the tongue is modelled as a 78.65mm tapered duct, with diameters of 34mm at the inlet and 25mm (turbine tongue side) at the outlet. Meanwhile, the turbine outlet is modelled as a 40mm tapered duct, with diameters at the inlet of 44mm (turbine wheel side) and 60mm at the outlet.

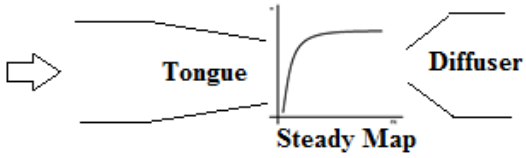

Figure 4. 3: Hybrid unsteady/quasi-steady turbine model

Referring to table 4.1, the hybrid unsteady/quasi-steady turbine model is adopted in three simulation approaches, as virtual T3*, virtual TC3* and virtual TC3*-T4. In these 1D models, TIT is correlated to thermocouple measurements at the turbine tongue in the experimental engine gas-stand. As is clear, TIT and TOT are modelled through virtual temperature sensors (VTS), evaluating the temperature at a section of the duct, and virtual thermocouples (VTC), considering the thermal characteristics of the mineral insulated k-type thermocouple. In the latter case, a grounded thermocouple with wires diameter of 0.3mm has been defined, solving the governing heat transfer equations 4.1 and 4.2. The 3mm 304 stainless steel sheath is modelled with a thickness of 0.5mm, as shown in figure 4.5. In addition, the thermocouple tip is position within the turbine tongue flow, approximately, at the centre of the duct.

The thermocouple model adopted in the Ricardo WAVE® 1D powertrain model considers heat transfer from the flow to the sensing elements. Due to the presence of an insulating heat sheath in the thermocouple, equations for conduction, convection and radiation are solved, in order to calculate the temperature sensed by the thermocouple bulb and wire. According to the plot in figure 4.4, heat is transferred through convection from the hot gas flow to the thermocouple sheath. In the case of an insulated and grounded thermocouple, the heat is radiated and conducted to the surrounding walls. Meanwhile, the remaining heat is sensed by the thermocouple through the bulb. Therefore, it is clear that part of the heat contained in the gas flow is not being sensed by the thermocouple bulb.

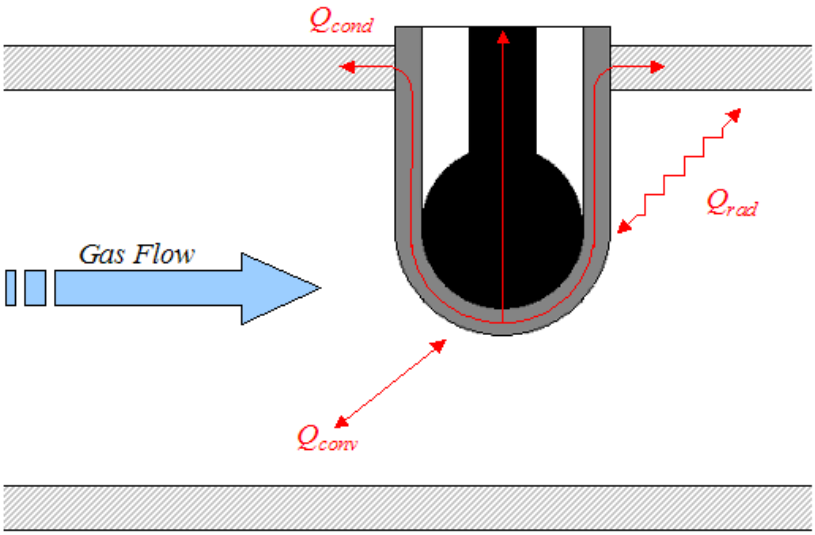

Figure 4. 4: Thermocouple model as represented in the 1D model developed in Ricardo WAVE® [109]

Specifically, equation for heat exchanged through convection (Q_{conv}) and radiation (Q_{rad}) are solved as in equations 4.1 and 4.2. in relation to the convection formula, h refers to the convective heat transfer coefficient and A_{tip} represents the area of thermocouple tip. Moreover, ε considers the emissivity of the material at the value of 0.8, σ is the Stefan-Boltzman constant and F represents the radiation view factor to walls at the value of 1.

$$Q_{conv} = hA_{tip}(T_{gas} - T_{tip}) \tag{4.1}$$

$$Q_{rad} = \varepsilon\sigma F A_{tip}(T_{wall}^4 - T_{tip}^4) \tag{4.2}$$

In this case, temperature of the gas (T_{gas}), thermocouple tip (T_{tip}) and duct wall (T_{wall}) are required in order to estimate the heat being captured by the sensing element of the thermocouple. Furthermore, it is important to consider the convective heat transfer coefficient (h) of the various thermocouple elements, such as the sheath, the bulb and the wire.

Specifically, in the hybrid unsteady/quasi-steady turbine model, the turbine inlet to the tongue has the dimension of a tapered duct with inlet and outlet diameters of 34mm and 25mm, respectively. The total length of the tongue consists of 78.6mm

which has been externally measured from the experimental turbocharger turbine tested in the engine gas-stand. The VTC is positioned 74.5mm away from the inlet of the turbine tongue. The turbine diffuser is represented as a 40mm long tapered duct with inlet and outlet diameters of 44mm and 60mm, respectively.

4.3.2 Models calibration procedure

In the engine gas-stand, the compressor outlet is not connected to engine intake and there is not direct influence. In order to calibrate the 1D powertrain model, the intake and exhaust conditions have to correspond to the experimental data. Therefore, engine inlet conditions can be targeted defining the correct boundaries as provided by the boost rig. In order to correlate exhaust and turbine operations, the VGT position has been imposed at 50%, to match with the experiments. Moreover, mass flow through the system is achieved by targeting air and fuel flows. A correlation of modelled combustion events with experiments would generate correct exhaust flow temperature. In this scenario, heat transfer characteristics of exhaust manifolds and ducts have been defined in connection with the materials.

In order to reduce the gap between experimental and modelled temperature estimates, heat transfer multipliers for exhaust ducts, including turbine tongue and diffuser for the hybrid unsteady/quasi-steady model, have been increased. Under these circumstances, an absolute error in TIT prediction of 10K has been targeted using a unique heat transfer multiplier for each of the three corrected turbine speed lines (57, 68 and 79 Krpm). On the other side, a heat transfer multiplier for turbine diffuser has been defined equal to turbine inlet and exhaust manifold settings. Furthermore, it is important to consider that the turbocharger has been subjected to acceleration/deceleration in relation to the measured inertia of the shaft, accounting for variation turbine power.

4.4 Interpretation of models

4.4.1 Average data correlation

In order to quantify possible benefits from the adoption of the novel unsteady/quasi-steady turbine model into the 1D engine gas-stand simulation, performance parameters related to the turbine have been investigated for the 15 operating conditions tested in the engine gas-stand facility. Therefore, turbocharger speed, turbine mass flow, turbine inlet and outlet pressures and TOT are evaluated for correlation between experiments and simulation results. Specifically, in this section, time-average values are compared and analysed in relation to the 1D predictions presented. It is important to notice that 1D modelled time-average terms are matched for sampling frequency to the experimental acquisition equipment in the experimental engine gas-stand facility. In particular, in order to assess the correlation between predicted and measured conditions of the air-path and turbine operations, time-average simulation results have been investigated at 1Hz for TOT and turbine mass flow. Due to the higher sampling rate in the experimental facility, turbocharger speed and turbine inlet and outlet pressures have been analysed at intervals of 0.1CAD, resulting in 120KHz at an engine speed of 2000rpm. From figure 4.5 to 4.9, prediction differences relative to the experimental measurements are presented. Steady turbine map (T3 and TC3) and hybrid unsteady/quasi-steady (T3*, TC3* and TC3*-T4) turbine models are compared for several turbocharger operating conditions.

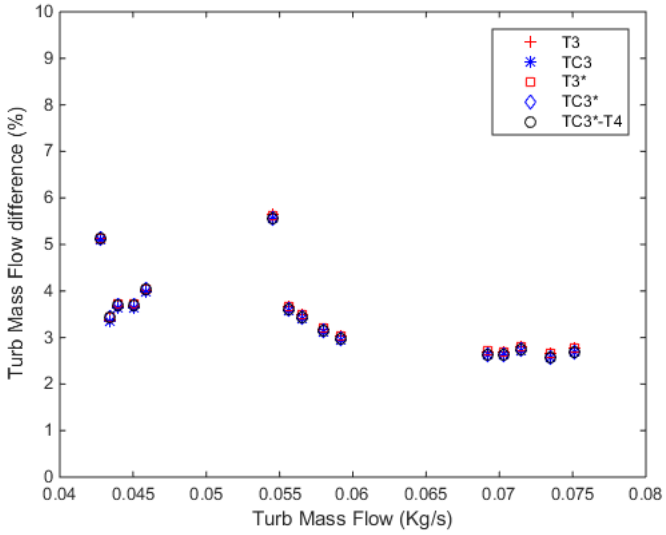

Figure 4. 5: Difference between predicted turbine mass flow and experimental turbine mass flow measured in the engine gas-stand

In figure 4.5, the maximum difference in predicted turbine mass flow consists of about 6%. It is important to notice that the differences remain similar for the several turbine modelling approaches under the same operating condition. Although, in the hybrid unsteady/quasi-steady turbine model, turbine inlet until the tongue and diffuser are modelled as converging and diverging ducts, respectively, this seems to have a reduced effect on the engine back-pressure. However, the predicted turbine mass flow remains unaffected from the variation in turbine modelling approaches. Moreover, slightly different results have been recorded in the turbocharger speed prediction, shown in figure 4.6. Turbocharger speed differences in the modelling approaches are visualised against turbine mass flow, instead of absolute turbocharger speeds, in order to identify a possible mass flow dependency. In this figure, the highest difference value of about 10% is found at the largest turbine mass flow for the TC3*-T4 and TC3* models. In both these scenarios, the hybrid unsteady/quasi-steady turbine model is implemented, suggesting an over-prediction of turbine expansion ratio. Therefore, the novel turbine model suggests that a slightly higher back-pressure can be caused due to the increasing predicted turbocharger speed compared to steady turbine map alone. The slight rise of difference in turbocharger speed prediction at high turbine mass flow could be supported, due to the limited number of experimental data points populating the steady turbine map at 79Krpm, meaning that turbine performance are based on extrapolated data points.

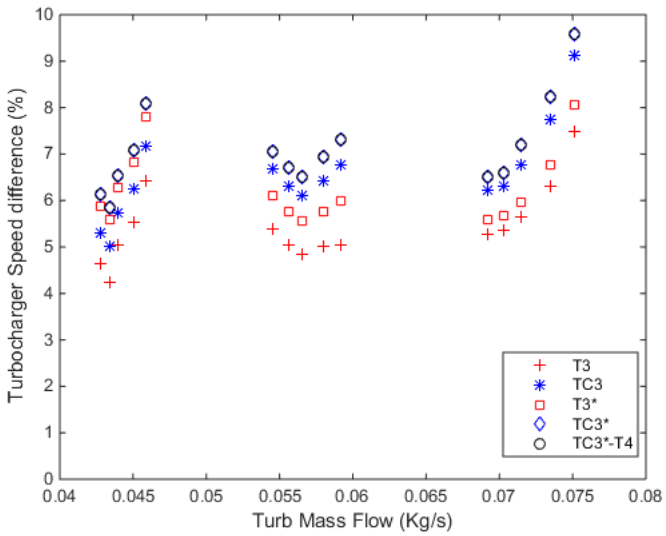

Figure 4. 6: Difference between predicted turbocharger speed and experimental turbine mass flow

Figures 4.7 and 4.8 confirm the increase of back-pressure through the implementation of the hybrid unsteady/quasi-steady turbine model. Although, the maximum difference is of about 12% and 10% for inlet and outlet pressures, respectively, gap between experimental and simulated values is maintained similar at inlet and outlet of the turbine. It is important to state that the pressure measurements in the engine gas-stand are able to consider the different pressure peaks, in correlation to the exhaust discharge events of every cylinder. In addition, the measurement of static pressure in the exhaust manifold is able to capture the 3D pressure distribution inside the exhaust manifold. These phenomena are not represented into the 1D model simulation and a possible difference of predicted turbine inlet and outlet pressures from the experimental data can occur. In figures 4.7 and 4.8, differences in predicted turbine inlet and outlet pressures are displayed against the absolute experimental pressure values, respectively. Additionally, in T3*, TC3* and TC3*-T4 modelling approaches, the positive error recorded in figure 4.7 is resembled at the turbine outlet pressure of figure 4.8. In this way, the novel turbine model would be able to maintain the prediction over turbine pressure ratio. However, a scaling of turbine diameter might be required due to the restricted dimension across the turbine rotor. Overall, differences for predicted turbine inlet and outlet pressures in steady turbine maps show a maximum difference of about 5% between predicted and experimental values in figures 4.7 and 4.8.

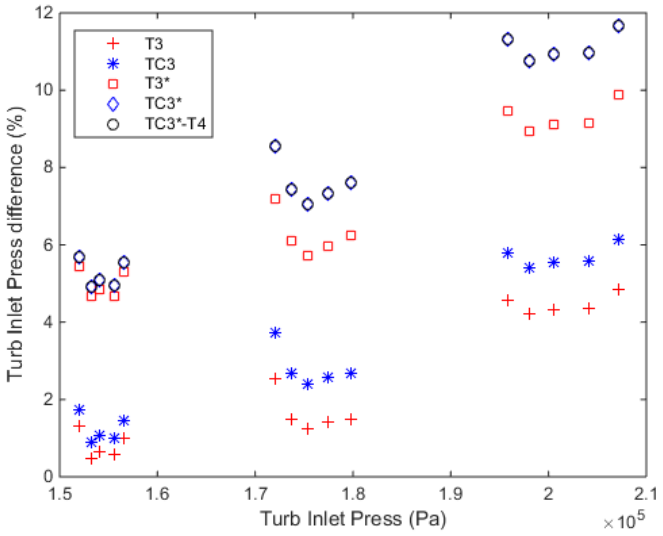

Figure 4. 7: Difference between predicted turbine inlet pressure and experimental turbine inlet pressure

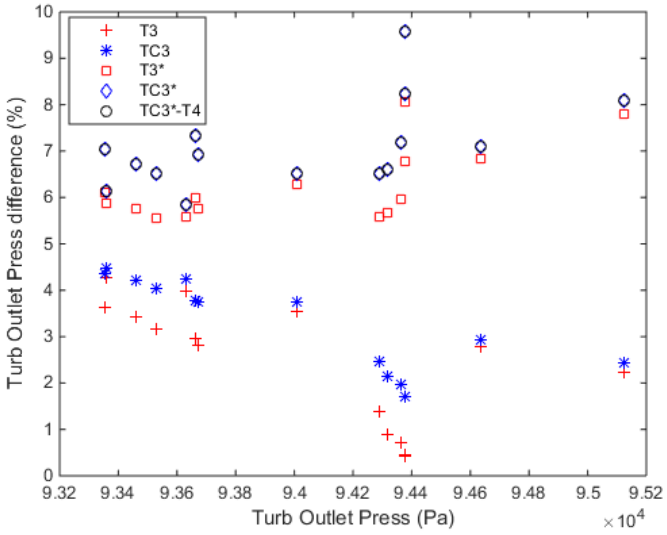

Figure 4. 8: Difference between predicted turbine outlet pressure and experimental turbine outlet pressure

The investigation of estimated average outlet temperature correlates to the experimental values with different precision, accordingly to the turbine modelling method. Steady turbine maps cause an over-prediction of turbine outlet temperature as a minimum of 20K, as supported by figure 4.9. The implementation of the hybrid turbine model is able to reduce the gap between experimental and modelled TOT, for virtual sensors included at inlet and outlet turbine flows. However, the assumption of equivalency between the average TIT across a radial section of the modelled duct and the temperature measured through a thermocouple in the engine gas-stand is not recommended. Therefore, the use of virtual thermocouple at 3* and virtual sensor at 4 would refer to the type of instrumentation adopted in the experimental rig, as best represented by a maximum difference of about 25K in TOT prediction through the TC3*-T4 model of figure 4.9. It is important to highlight that sampling frequency of predicted and measured temperatures have been matched for comparison. In fact, a frequency of 1Hz has been chosen, due to the limits in reaction time of real thermocouples in the engine gas-stand.

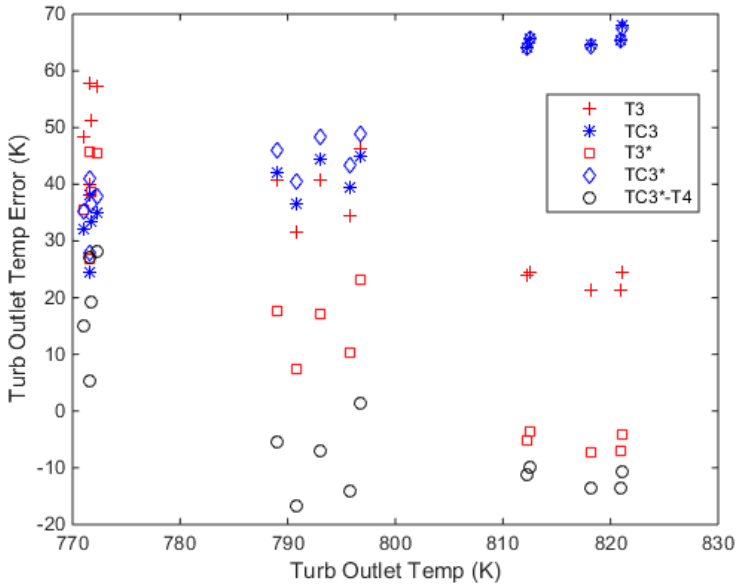

Figure 4. 9: Temperature difference between experimental and predicted TOT against experimental TOT values

4.4.2 Instantaneous turbine performance correlation

From the experimental data available in figure 4.2, the modelling approaches of table 4.1 have been applied to the operating conditions of the turbine, including the steady-state map and hybrid unsteady/quasi-steady turbine representations. As well as evaluating the proposed turbine model under time-averaging at fixed sampling frequencies, instantaneous measurements would be able to provide additional details, focussing on the improvement of turbine performance representation. In fact, through an accurate analysis, instantaneous temperature and pressure correlations between experiments and simulations can be investigated. In this scenario, in order to quantify qualities of the proposed turbine modelling method, one operating condition of the turbocharger turbines has been investigated for instantaneous performance evaluation. According to time-average data, attention has been focused on pressure ratio, turbine total-to-static efficiency and turbine inlet and outlet temperatures.

Therefore, turbine performance for one operating condition at corrected turbine speed of 79 Krpm are exploited to evaluate the improvements in the representation of turbine performance in the 1D model. This operating speed has been considered due to the maximum discrepancy recorded between predicted and measured turbine inlet and outlet pressures, shown in figures 4.10 and 4.11. In fact, although,

the magnitude of difference refer to average pressure values, the highest change in turbine performance between prediction and experiments is expected. Additionally, the total-to-static turbine efficiency has been calculated using virtual thermocouples, reflecting the thermal behaviour of the sensing material, and virtual temperature sensors, evaluating the temperature of the flow for a section of the duct.

Table 4. 2: Correlation of turbine performance for steady map approaches

APPROACH	PR	MASS FLOW	SPEED	$\eta_{T\text{-}s}$
Experimental 3	2.08	0.0692 Kg/s	79 Krpm	0.68
Virtual T3	-0.5%	+2.6%	+5.3%	-8.8%
Virtual TC3	+0.5%	+2.6%	+6.2%	+19.1%

Table 4. 3: Correlation of turbine performance for hybrid unsteady/quasi-steady approaches

APPROACH	PR	MASS FLOW	SPEED	$\eta_{T\text{-}s}$
Experimental 3*	2.08	0.0692 Kg/s	79 Krpm	0.73
Virtual T3*	0%	+2.6%	+5.6%	-9.6%
Virtual TC3*	+1%	+2.6%	+6.5%	+24.6%
Virtual TC3*-T4	+1%	+2.6%	+6.5%	-20.5%

In tables 4.2 and 4.3, pressure ratio (PR), turbine mass flow, turbocharger speed and T-s turbine efficiency ($\eta_{T\text{-}s}$) related to experiments and simulations are reported. It is important to consider that the average efficiency is dependant of instantaneous pressure and temperature trends. The predictions from tables 4.2 and 4.3 refer to engine cycle-averaged calculations considering the sampling frequency for each of the variables monitored in the experiments. The efficiency calculated in the experimental gas-stand has been calculated from instantaneous pressure and temperature. Although, the former could be directly measured in the engine gas-stand, the latter has been generated by the implementation of equation 4.3. Therefore, a polytropic process has been assumed in the engine exhaust, where ratio of specific heats (γ) are depending on the engine AFR and the combustion products, i.e. CO_2, water vapour, nitrogen and oxygen in excess. Moreover, the cycle-averaged efficiency could be calculated, using the obtained instantaneous parameters and applying equation 3.12. In relation to the experimental values, instantaneous temperatures (T_{inst}) have been computed through instantaneous (P_{inst}) and average (P_{ave}) pressure and temperature (T_{ave}) information in equation 4.3, in conjunction with the ratio of specific heats (γ) of the polytropic process [107].

$$T_{inst} = T_{ave} * \left(\frac{P_{inst}}{P_{ave}}\right)^{\frac{\gamma-1}{\gamma}} \quad (4.3)$$

In addition, the predicted turbine efficiency in the models has been generated in a similar way to the experimental calculated efficiency. Due to the possibility to monitor instantaneous temperatures in the1D model, equation 4.3 has not been applied to the predicted temperatures in models. In this way, the comparison between simulations and experiments could be maintained reasonable. Analysing the average data information in tables 4.2 and 4.3, it seems that the virtual T3 model, adopting the turbine steady map approach and virtual sensors for temperature estimation would be able to represent engine gas-stand performance better than other approaches. Although, the matching of average turbine performance is important to state the validity of the model, investigation of instantaneous sensors data would show a change in prediction. In figure 4.10, the experimental pressure ratio from the engine gas-stand is compared with the simulations. However, in figure, discrepancies could be noticed in the peaks, reaching about 12% of differences in the prediction of pressure ratio. Moreover, the structure of the experimental rig allowed positioning of pressure transducers in the proximity of position 3 and 4.

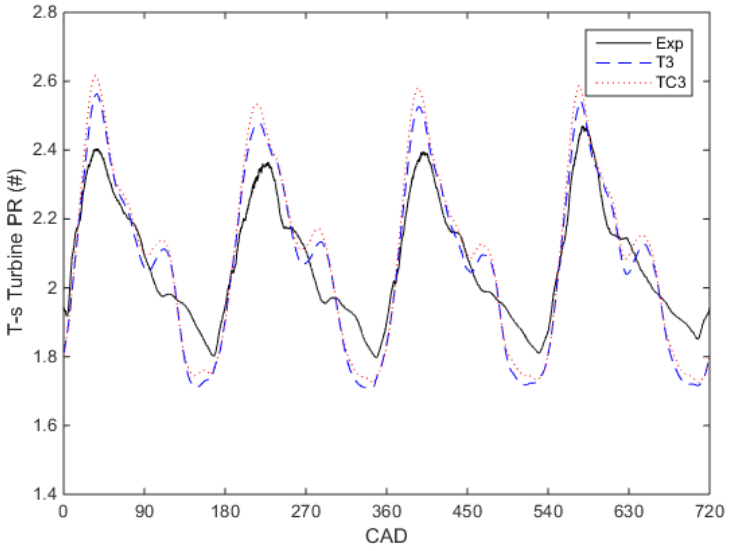

Figure 4. 10: Instantaneous PR from experimental (3) and modelled (T3 and TC3) analyses of the same turbine operating condition

Most importantly, the TIT has been analysed in figure 4.11, showing that T3, TC3, T3* and TC3* in comparison to instantaneous data of experimental temperatures, assuming a polytropic process, at 3 and 3*. In equation 4.3, experimental temperature at 3* includes instantaneous pressure solely at position 3, as the available pressure transducer at turbine inlet. It seems than the hybrid model of the turbine can allow an improvement, correlating experimental and modelled TIT. In fact, it is important to notice that thermocouples for turbine inlet flow measurements are able to capture average temperature, due to low rate of response. The adoption of the virtual thermocouple is not able to show a particular difference towards virtual sensors, apart from slower response to temperature reductions. Moreover, experimental T-s turbine efficiency has lower rate of oscillation compared to simulated approaches as shown in figure 4.12. This scenario can be explained by significant difference between experimental and modelled instantaneous TIT. In fact, a lower amplitude of fluctuation is recorded in the experimental temperatures of figure 4.11. In relation to the virtual temperatures, it appears that T3 and TC3 approaches recorded significantly higher fluctuations compared to T3* and TC3*. Therefore, the adoption of 1D hybrid unsteady/quasi-steady turbine model can reduce the gap with experiments, on the basis of the obtained instantaneous temperatures obtained by equation 4.3.

Furthermore, it is important to notice that the resulting pressure and temperature predictions are related to the discretisation length adopted. In the 1D models, suggested discretisation length of 30mm is adopted. Moreover, heat capacities representing the exhaust manifold mass are neglected, although these are expected to have a significant role towards the modelling of the flow temperature. Therefore, a reduction of the temperature slope would be achieved with the inclusion of heat capacities.

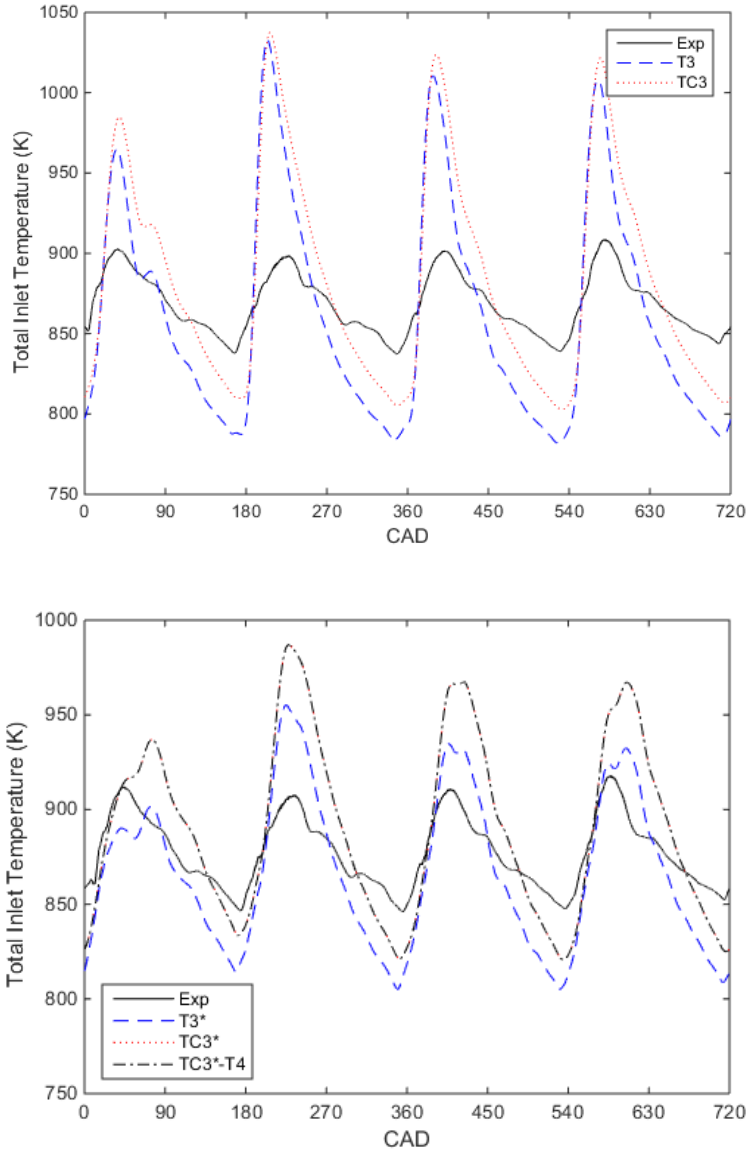

Figure 4. 11: Instantaneous total TIT from experimental (3 and 3*) and modelled (T3, TC3, T3* and TC3*) analyses of the same turbine operating condition. Experimental values of temperatures are calculated using equation 4.3

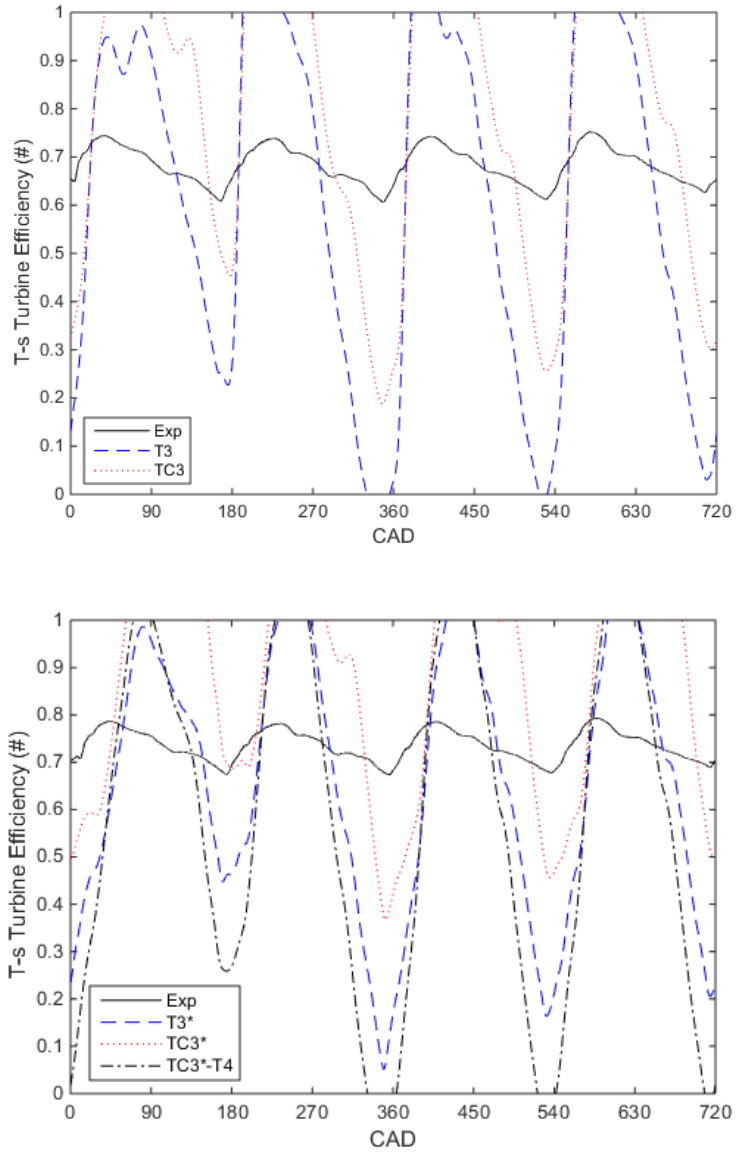

Figure 4. 12: Instantaneous T-s turbine efficiency from experimental (3 and 3*) and modelled (T3, TC3, T3* and TC3*) analyses of the same turbine operating condition. Experimental values of temperatures are calculated using equation 4.3

In addition, a similar trend is present once the instantaneous measurements are included for the calculation of total-to-static turbine efficiency, as plotted in figure 4.12. It is important to understand that the modelled efficiencies of figure 4.12 are evaluated by the implementation of predicted instantaneous temperature in the total-to-static efficiency formula (equation3.9). In fact, due to the larger predicted temperature fluctuations of figure 4.11, impossible efficiencies higher than 100% are recorded. Moreover, it is important to understand that the heat transfer in ducts between temperature measurements and turbine rotor are modelled, in order to resemble the experimental setting. In order to evaluate the prediction, the maximum

amplitude of oscillation in the efficiencies of figure 4.12 is reported in tables 4.4 and 4.5. As suggested, a reduced fluctuation is predicted through the virtual TC3* approach resulting in an efficiency amplitude of 0.97. Comparing approaches, it is evident that lower fluctuations are achieved with virtual thermocouple models due to representation of the physical element and the additional thermal masses of a mineral insulated k-type thermocouple. However, in the case of virtual thermocouples at turbine inlet and virtual temperature sensor at turbine outlet, in TC3*-T4, an elevated oscillation in turbine efficiency is recorded compared to the experimental conditions.

Table 4. 4: Efficiency amplitude for steady map approaches

APPROACH	EFFICIENCY AMPLITUDE
Experimental 3	0.14
Virtual T3	1.39
Virtual TC3	1.07

Table 4. 5: Efficiency amplitude for hybrid unsteady/quasi-steady approaches

APPROACH	EFFICIENCY AMPLITUDE
Experimental 3*	0.11
Virtual T3*	1.02
Virtual TC3*	0.97
Virtual TC3*-T4	1.27

As well as TIT, the analysis of TOT would be able to validate the turbine models in the prediction of turbine efficiency. Total outlet temperatures are significantly reduced through the turbine, as visible in figure 4.13. However, the experiments suggest that the instantaneous temperature is stable across the engine cycle, due to steady turbine outlet pressure. Furthermore, it is important to notice that thermocouples have been adopted for capturing exhaust flow temperature in the TC3 and TC3* simulations. These have resulted in a slightly lower temperature than measurements through virtual sensors as supported by figure 4.13. In addition, several thermocouples have been used in the experimental engine gas-stand facility, due to marked flow motion at the turbine outlet. In order to evaluate the instantaneous temperature using equation 4.3, the average temperature of the multiple thermocouples at the exhaust has been introduced into the equation as T_{ave}. In this scenario, a virtual sensor averaging the temperature across a radial section of the duct would be able to reflect the experimental values.

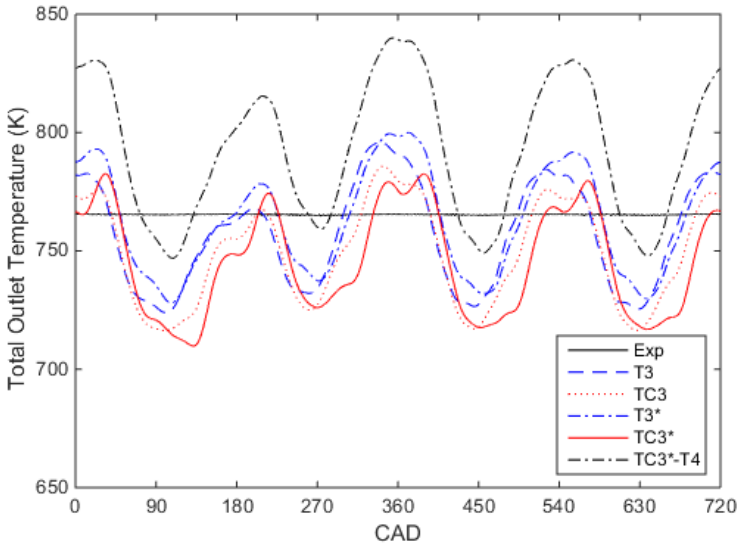

Figure 4. 13: Instantaneous TOT from experimental (T4) and modelled (T3, TC3, T3* and TC3*) analyses of the same turbine operating condition. Experimental values of temperatures are calculated using equation 4.3

4.5 Chapter summary and conclusions

In this chapter, the development of a turbine model to account for unsteady conditions in the engine gas-stand is presented. The main conclusions can be listed below:

- Modelling of turbine tongue for 1D flow simulations have shown that a closer matching between the time-average experimental turbine inlet temperature and the virtual temperature is possible. In fact, the converging dimensions at 3* cause a reduction of temperature oscillation, as supported by simulations, increasing fidelity in TIT correlation.

- Moreover, the use of virtual temperature sensors in T3* model is beneficial in the representation of TIT at 3*, as supported by the temperature gap for the average TOT. However, this is valid when TOT is correlated with virtual temperature sensors which could represent the measured temperature across a radial section of the exhaust duct.

- The hybrid unsteady/quasi-steady turbine modelling approach has not been combined with heat transfer correction factors, limiting the adoption of the model to medium/high turbocharger speeds where heat transfer has reduced impact on the turbine gas flow temperature.

- Furthermore, the adoption of experimental steady turbine performance maps marks the dependency of the model accuracy on the number of data points available. In fact, a significant difference increase regarding predicted turbocharger speed could be recorded as at high mass flow values in figure 4.6.

- The proposed turbine model has showed an attempt to include the unsteady flow behaviour, although, higher degree of information would be required, in order to optimise the approach, such as the VGT internal opening areas. However, the use of 3* temperature could be applied as a reference for two-stage turbocharging systems, reducing the effect of heat transfer in ducts.

Chapter 5 – Compressor surge definition at steady and unsteady flow conditions

In this chapter, the compressor surge behaviour of an automotive turbocharger has been investigated. In two-stage turbocharging systems, inter-stage flow effects, such as swirling flows, can influence performance of compressors. Therefore, advanced studies on surge onset for turbocharger compressors would be necessary for the following studies. In the engine gas-stand layout, steady compressor performance can be monitored due to the absence of pulsating flows. Therefore, surge has been analysed as variation of pressure and mass flow. In addition, the air injection technique [110, 111] has been implemented for exploring compressor surge for a fully pulsating turbocharger (compressor and turbine), as in a parallel two-stage turbocharging system [112]. This method is able to take into consideration real engine applications, as the change in compressor downstream volume during the engine intake process. Accordingly to studies in literature [113, 114], frequencies of oscillations caused by surge are analysed through the implementation of FFT. Furthermore, in order to characterise surge onset at steady and unsteady flow conditions, amplitude and coefficient of variation (CoV) for the magnitude of FFT in the low frequency region are monitored.

Conclusively, part of the findings in this chapter have been presented and published at the 2017 Global Power and Propulsion Forum [115].

5.1 Requirements for surge definition

The demand for small and efficient powertrain architectures to power transportation vehicles has required the increase of power output from naturally aspirated internal combustion engines [12]. The inclusion of compressors to maximise deliverable engine torque and turbines to recover exhaust energy is a significant strategy towards fuel economy improvements of powertrains [35]. Due to the flexible operations of an internal combustion engine, turbochargers are requested to deliver high pressure ratios at changing air flow conditions using variable turbine and two stage technologies [116, 117]. Therefore, turbochargers selection is fundamental for power and efficiency optimisation.

In relation to the compressor characteristics, an extreme pressure ratio could be demanded at low mass flow, pushing the compressor to operate over an instable region where the compressor is not able to convert energy with adequate efficiency. This is represented by the surge limiting area of the compressor map, which causes the flow to recirculate at the compressor inlet [72]. In axial [118, 119] and radial [120] compressors, surge process has been modelled and analysed against experimental data [121], resulting in a system dependency process, inversely proportional to the Helmholtz resonator frequency [108]. The model has been implemented in steady [122] and unsteady [123] flow conditions and the importance of experimental data is necessary to define and represent the compressor surge behaviour.

The volume and size of downstream compressor influence the surge dynamics in relation to the operating mass flow [124]. The reduction of volume at the compressor outlet allows the measurement of close to zero mass flow conditions in the compressor performance map [125]. In addition, 1D compressor models have been able to simulate surge dynamics once specific characteristic factors of the system and compressor time delay are included [113]. The oscillation of mass flow and pressure ratio during compressor surge can be recorded in rising values of standard deviation from the mean value under steady flow conditions [126]. However, Fast Fourier Transform (FFT) of pressure signals are not suggested for pulsating flow application due to possible engine frequency interactions [126].

Furthermore, Galindo et al. [127] proved that pressure oscillation at the outlet of the compressor could extend the surge line towards lower mass flow conditions when compared to steady gas-stand measurements. Moreover, a similar approach has

been adopted by Marelli et al. [128]. In this study, the stability range of the compressor differed between the steady map and the pulsating rig. However, no significant variation could be detected for the averaged surge line generated in the same rig when pulsation are introduced and the highest sampling frequency of 80Hz was adopted [128].

Although, surge in compressors can be measured and quantified in turbocharger gas-stands, experimental test rigs would have to be purposively developed in order to introduce pulsating flows at the compressor outlet. The use of rotating valves in the ducting system at the compressor outlet would be able to introduce pulses and unsteadiness in the flow [127]. The introduction of pulsations in the frequency range of 40-67Hz provides an improvement in surge margin of about 15%, while maintaining the volumes of the steady turbocharger gas-stand [127]. Furthermore, it has been proven that pulsation frequencies have reduced effects on surge margin in comparison to amplitude of pulsations. This statement can be supported by the variation of volume between the compressor and the rotating valve, causing a reduction of pressure amplitude and a reduced effect on surge margin [129]. Therefore, the investigation of compressor surge in systems closer to the final application could reduce the uncertainty on the estimation of the surge margin. Specifically, in relation to automotive powertrain applications, on-engine measurements would be able to provide the required conditions [110], including the variation of compressor downstream volume during the engine intake process.

5.2 Unsteady compressor facility

In this specific layout, an external boost rig supply is connected in parallel to the turbocharger compressor with the inclusion of a non-return valve. The unsteady compressor facility introduces pulsations at both compressor and turbine, due to pulsating flows generated by the internal combustion engine. In this scenario, compressor surge onset in the presence of pulsating flows will be influenced by the alternating opening and closing motion of intake valves of the engine. In the current configuration of figure 5.1, the turbocharger is powered by the energy of the engine exhaust gases with temperature and mass flow controlled by the AFR and engine speed, respectively. Engine speed is maintained at constant rotation of 2000rpm, to maintain the frequency of pulsation. Finally, the VGT is operated to control the turbocharger speed. In order to limit the amount of boost being delivered to the engine intake, a compressor restricting flow (CRF) valve is installed upstream the compressor, reducing the pressure. More importantly, the volume of the ducting at compressor outlet remains constant between the engine gas-stand, inducing steady flow at the compressor, and the unsteady facility of figure 5.1 for a total of about 0.48m^3, including the intercooler. This refers to ducting from compressor outlet to CB valve of the engine gas-stand and to three-way junction in figure 5.1. In particular, 51mm ducts have been adopted at compressor inlet and outlet. Moreover, engine intake flow is maintained at a temperature value of 313K through the controlled boost rig, inter-cooler (I/C) at the compressor outlet and the obstruction of the EGR valve.

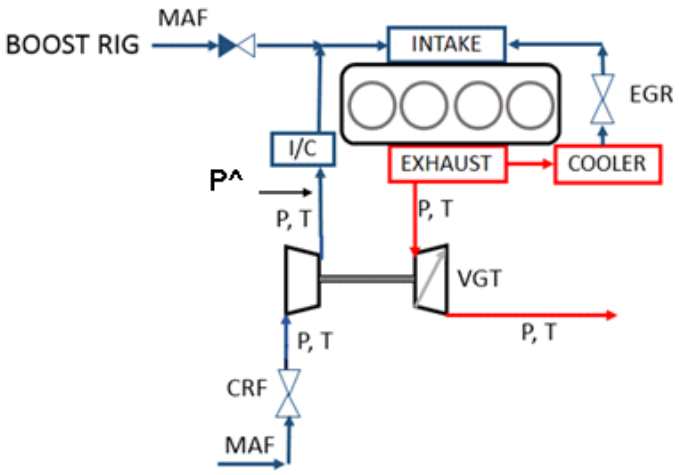

Figure 5. 1: Unsteady turbocharger gas-stand for testing automotive turbochargers. Unsteadiness is generated by the intake valves motion of the 2.2L Diesel engine. A piezo-resistive pressure transducer, identified as P^, is positioned on the side of the 2.5" compressor outlet duct at a distance of 1200mm from the compressor

Pressure and temperature across the compressor is captured through averaging pressure rings and platinum resistance temperature (PRT) sensors, respectively. The positioning of the measuring points reflects the instructions given by ASME [83] and SAE [82] standards. In addition, the measuring system has been maintained from the engine gas-stand facility, including measuring sections for monitoring pressure at compressor inlet and outlet, as well as the turbine boundary conditions. Furthermore, due to the presence of highly pulsating flows, imposed by the engine intake valves motion, a fast sampling pressure transducer has been placed between the compressor and the inter-cooler (*P^* in figure 5.1). In fact, a pressure signal is monitored through a transducer with a response of 500KHz. Therefore, DEWEtron DAQ, acquisition system, is adopted to monitor this pressure values every decimal of crank angle degree of the engine (i.e. 120KHz at 2000 engine rpm).

5.2.1 Experimental analysis

In both the engine gas-stand layout of chapter 3 and the unsteady turbocharger gas-stand, mass flow and pressure outlet signals are monitored to control surge onset and the elevated instabilities for the compressor. The maximum sampling frequency for the compressor mass flow sensor is 80 Hz, while the pressure sensor has a capability of 500 KHz. In addition, the acquisition system represents the real limit due to a resolution of decimal crank angle degree (CAD), reducing the maximum sampling frequency for the pressure signal. In equations 1, 2 and 3, standard deviation (*SD)*, coefficient of variation c_v and maximum amplitude θ are shown and adopted for the investigation of the compressor surge dynamics.

$$SD = \sqrt{\frac{1}{n}\sum_{i=1}^{n}(x_i - \psi)^2} \tag{5.1}$$

$$c_v = \frac{\sigma}{\psi} \tag{5.2}$$

$$\theta = (M - m) \tag{5.3}$$

In relation to equation 5.1, n is the total number of x_i samples, ψ is the mean value, higher and lower values of the samples are indicated as M and m, respectively. Furthermore, the FFT of compressor outlet pressure and mass flow are analysed. In particular, the FFT of compressor mass are limited to 40Hz due to possible aliasing distortion of the signal into frequency components [84]. In order to monitor the dynamics of surge in automotive turbochargers, experimental investigations on a VGT turbocharger in the engine gas-stand and the unsteady layout are performed. A 2.2L Diesel engine with impeller diameters of 49mm has been test regarding the surge onset. Moreover, surge onset has been investigated in both steady and unsteady flows of the compressor.

5.3 Compressor surge at the engine gas-stand

The compressor map has been generated under steady flow conditions in the engine gas-stand facility and is visible in figure 5.2. Circle points represent stable operations at several corrected compressor speeds and surge points at three compressor speeds are also plotted. Therefore, operating the compressor at low mass flow causes recirculating flows at the inlet, resulting in instabilities as the surge loops of figure 5.2.

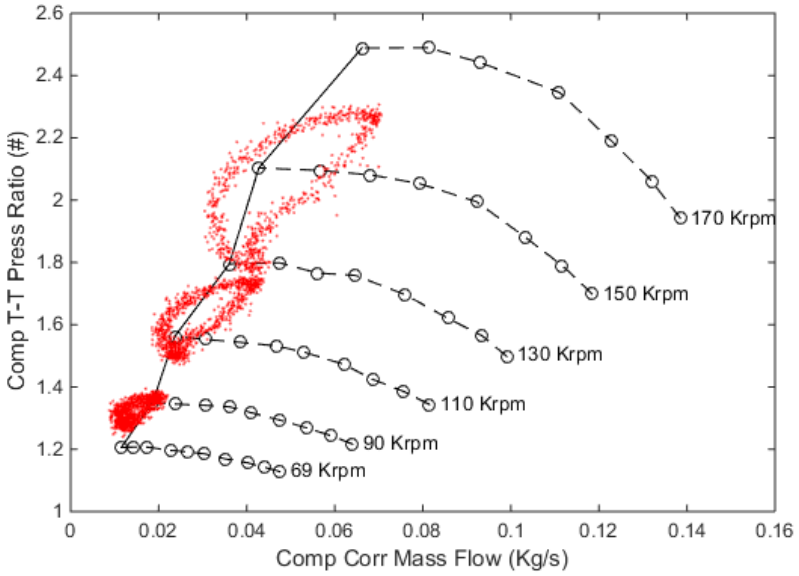

Figure 5. 2: Compressor map and surge points for steady compressor flow

Surge loops at 69, 110 and 150Krpm are shown, resulting in wide pressure ratio and mass flow oscillations. It is clear that the magnitude of oscillation increases directly with compressor speed for the pressure ratio and the corrected mass flow. The data points considered have a sampling frequency of 80Hz due to limits on mass flow measurements. The average total-to-total pressure ratio and corrected mass flow are plotted in figure 5.3 as a result of 10Hz, 80Hz and the maximum allowable frequencies for sampling the pressure data. In particular, the highest sampling frequency would refer to decimals of crank angle degrees of engine revolutions. Moreover, the frequencies would vary between 75KHz (1250rpm of the engine) and 120KHz (2000rpm of the engine).In conjunction with figure 5.3, it is evident that the variation of frequency has small impact on the location of the surging conditions, suggesting that 10Hz sampling frequency would be adequate for

capturing flow and pressure oscillations. Therefore, a more accurate analysis of the experimental measurements is required to have a clear vision of the surge onset.

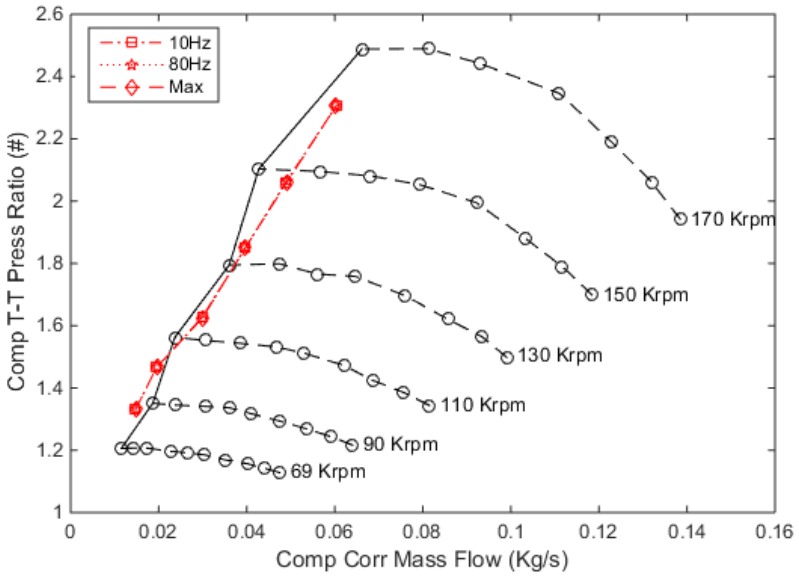

Figure 5. 3: Influence of sampling frequency on the compressor surge points for steady compressor flow

In figure 5.3, it is important to notice that average measurements of pressure ratio and compressor mass flow is performed for 150 engine rotations. Moreover, the red lines represent average values for unstable surging operations of the compressor in the engine gas-stand. Meanwhile, the black line of the compressor map represents last stable operations of the compressor, limiting the surge area. In addition, it is possible to state that the shift of average operating points of high speed surge towards the stable compressor map region could be caused by an increase of the flow recirculation and temperature at the compressor inlet.

5.3.1 Pressure data investigation

As the acquisition system is dependant of the engine speed, surge at 69, 110 and 150Krpm is captured at 75, 90 and 120KHz, respectively. In table 5.1, standard deviation, coefficient of variation and maximum amplitude for compressor outlet pressure are considered at the last stable point before surge onset and at surge conditions. The point before surge is limited to the engine gas-stand operability. It can be noted that c_v values of about 0.6% are common for stable operations and a

minimum of 2.6% for surging conditions. The trend of parameters at the three compressor speeds for the last stable point and the instable operation is similar. Therefore, monitoring the pressure signal at the compressor outlet could provide significant information on surge onset.

Table 5. 1: Standard variation, coefficient of variation and amplitude of compressor outlet pressure for steady compressor flow

75-90-120 KHz	*SD*	c_v	*θ*
Pre Surge 69krpm	0.84 KPa	0.64%	19.2 KPa
Surge 69krpm	3.43 KPa	2.63%	26.4 KPa
Pre Surge 110krpm	1.04 KPa	0.62%	21.94 KPa
Surge 110krpm	8.6 KPa	5.44%	46.47 KPa
Pre Surge 150krpm	1.21 KPa	0.56%	23.42 KPa
Surge 150krpm	17.04 KPa	8.59%	68.16 KPa

As demonstrated by the FFT analysis of the pressure signal, pressure oscillations at around 10Hz are present for surging conditions, as shown in figure 5.4. The last stable point recorded before surge shows a small increase of pressure fluctuation in the frequency of about 10Hz. In fact, while moving towards compressor surge conditions, amplitude of pressure oscillations at 10Hz increases until the instability of the compressor is reached. Moreover, it is important to notice that, although, the turbine is subjected to pulsating flows, the FFT signals of figure 5.4 present insignificant peaks at 41.67, 50 and 66.67Hz. These frequencies correspond to the motion of engine exhaust valves at the three different compressor speeds analysed in figure 5.4.

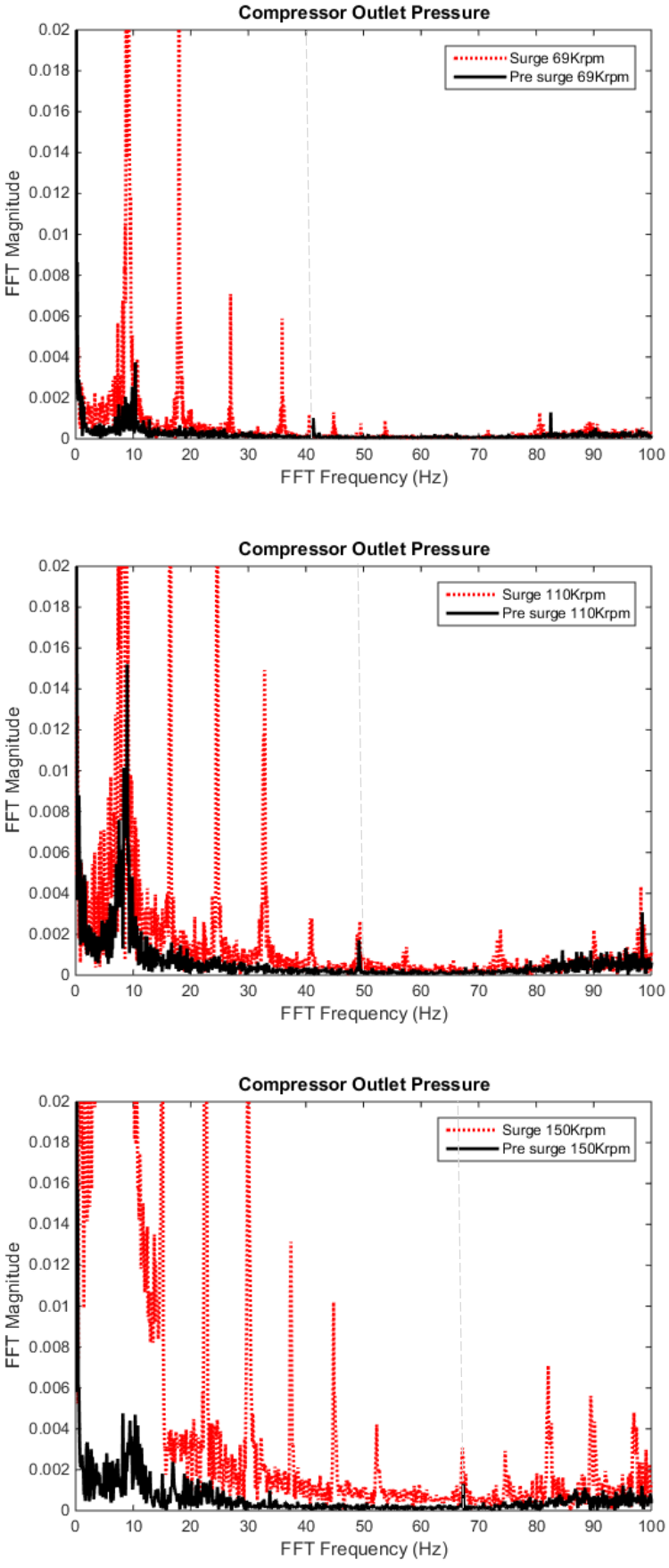

Figure 5. 4: FFT of compressor outlet pressure for surge and pre surge at 69, 110 and 150Krpm for steady compressor flow

5.3.2 Mass flow data investigation

The mass flow sensor at the inlet of the compressor has been considered for the definition of instabilities and surge onset. In fact, data in table 5.2 show variations higher than 20% in mass flow measurements at every compressor speed considered at instable conditions. Due to the maximum sampling frequency of 80Hz, FFT magnitudes have been considered acceptable up to 40Hz, in conjunction with the Nyquist-Shannon sampling theorem, avoiding errors in the representation of the signal into frequency components [84]. In figure 5.5, the pre surge conditions are not able to capture significant peaks of FFT. This could be due to the wide distance between the mass flow sensor and the compressor wheel. Moreover, harmonics of the surging frequency event are recognisable in figure 5.5.

Table 5. 2: Standard variation, coefficient of variation and amplitude of compressor mass flow for steady compressor flow

80 Hz	*SD*	c_v	θ
Pre Surge 69krpm	0.001 Kg/s	9.18%	0.006 Kg/s
Surge 69krpm	0.0032 Kg/s	21.61%	0.0132 Kg/s
Pre Surge 110krpm	0.0011 Kg/s	4.9%	0.0091 Kg/s
Surge 110krpm	0.0072 Kg/s	24.55%	0.0255 Kg/s
Pre Surge 150krpm	0.0011 Kg/s	2.55%	0.0052 Kg/s
Surge 150krpm	0.0116 Kg/s	24.56%	0.0398 Kg/s

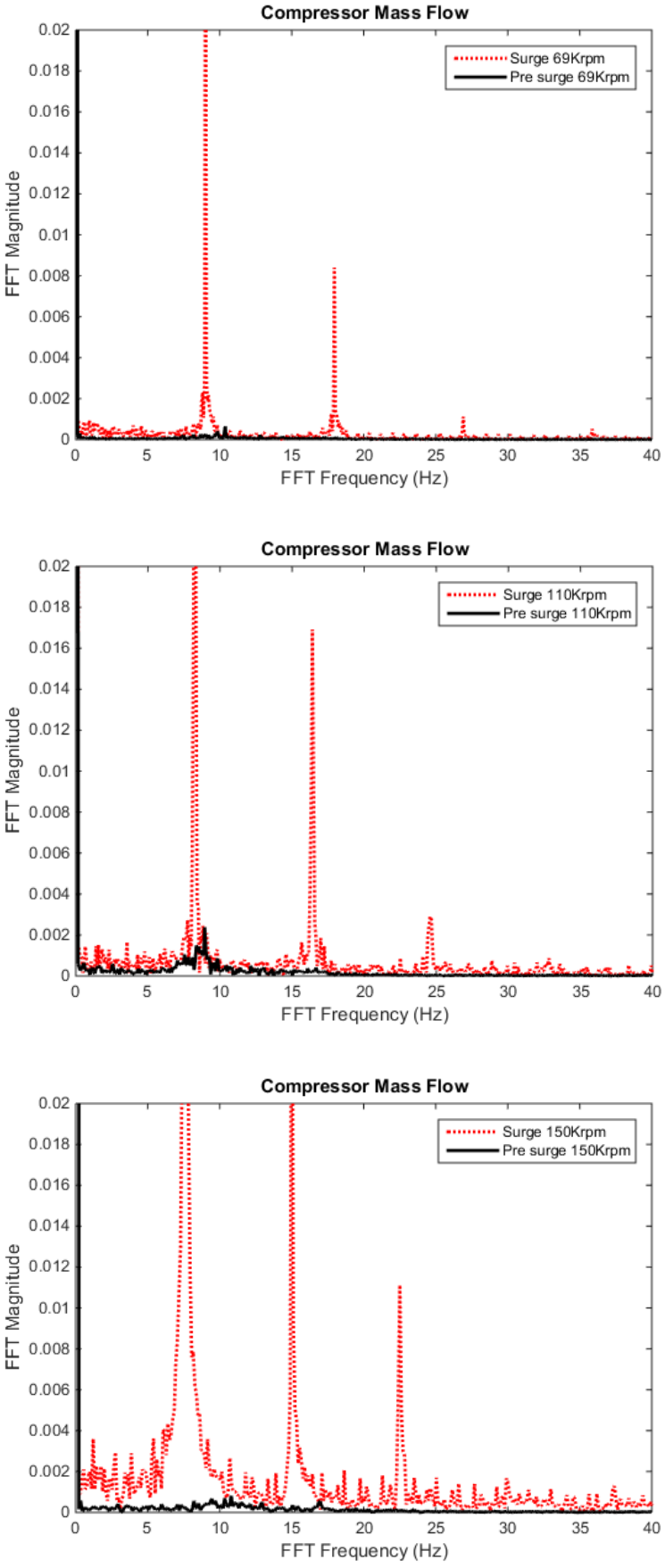

Figure 5. 5: FFT of compressor mass flow for surge and pre surge at 69, 110 and 150Krpm for steady compressor flow

5.4 Compressor surge in the unsteady turbocharger gas-stand

In order to study the characteristics of compressor surge for unsteady compressor flows in turbochargers, pressure pulsations at compressor outlet and turbine inlet have been generated. The engine gas-stand has been reconfigured, in order to generate flow pulsations at the compressor outlet, owing to the motion of engine intake valves. Therefore, in the layout of figure 5.1, the boost rig has been adopted to control load on turbocharger and engine intake pressure. In this scenario, a small operating area of the compressor in the proximity of surge has been investigated. It is important to notice that the black line, connecting the various speed lines, limits stable compressor operations from the surge area. In fact, the last operating point could be identified in the compressor, before inducing the compressor into surge as visible with the red dots in figure 5.6.

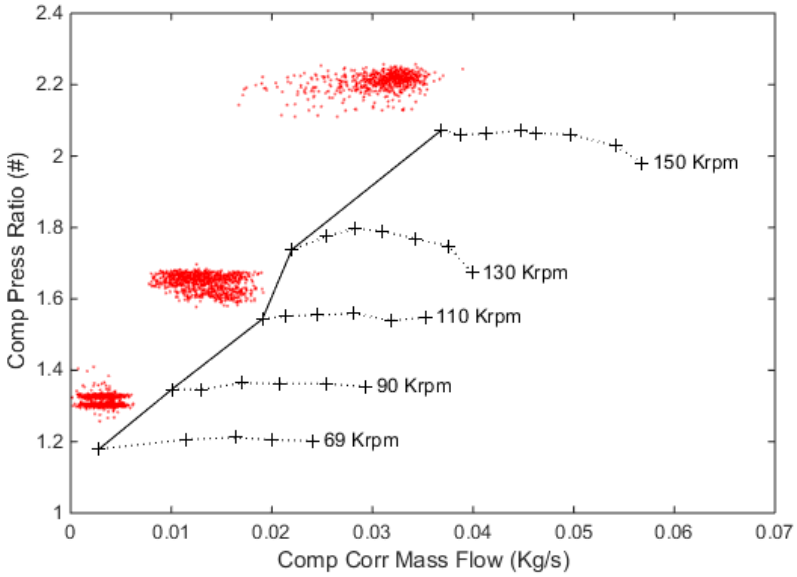

Figure 5. 6: Compressor map and surge points for pulsating compressor flow

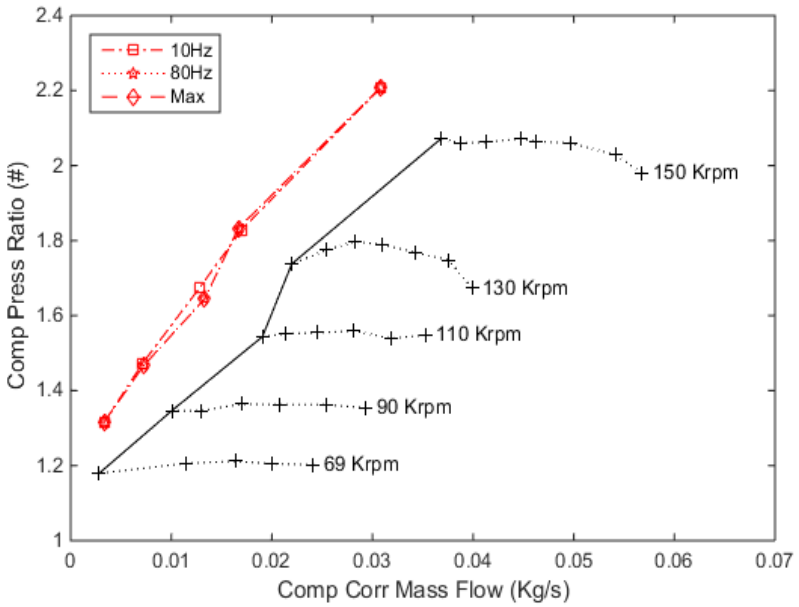

Figure 5. 7: Influence of sampling frequency on the compressor surge points for unsteady compressor flow

In figure 5.7, crosses show the time averaged stable operations of the compressor and the cyclic surge data points at 69, 110 and 150Krpm, laying outside the operating map. Experimental data of figure 5.6 and 5.7 are collected at different engine speeds in order to keep constant TIT. The intake valve motion causes pulsations at 41.67, 50 and 66.67Hz for compressor speeds of 69, 110 and 150Krpm, respectively. In addition, the sensitivity study on sampling frequency shows a small influence on the averaged surge points of the compressor map. In particular, it seems that an acquisition frequency of 10Hz is less adequate to represent surge points under pulsating conditions, in according to figure 5.7, due to the variation at 110Krpm.

5.4.1 Pressure data investigation

The identification of surge is extremely important in order to limit the compressor operations when connected to an internal combustion engine to avoid power and efficiency losses. Therefore, pressure oscillations at the compressor outlet have been controlled at surging and stable pre-surging conditions. Unlike, in the presence of steady flow conditions at the compressor, c_v values of table 5.3 have resulted lower at surging conditions than in table 5.1. Moreover, it has resulted that surge

onset would be difficult to capture at the compressor speed of 69Krpm for the unsteady compressor case. In conjunction with the information provided by table 5.3, this is suggested by the FFT analysis of figure 5.8.

At 110 and 150Krpm, surge frequencies have resulted slightly higher than under steady compressor operations in the FFTs. This can be correlated to the variation of compressor outlet ducts and volumes due to the presence of the boost rig. As well as at steady compressor flow conditions, the low frequency peaks increase while deteriorating the compressor stability for unsteady flow conditions in the turbocharger. Furthermore, engine intake valves motion causes significant pulsations of the compressor outlet pressure in the unsteady gas-stand configuration. According to figure 5.8, these pulsations and surging flow have disparate frequencies.

Table 5. 3: Standard variation, coefficient of variation and amplitude of compressor outlet pressure for unsteady compressor flow

75-90-120 KHz	*SD*	c_v	θ
Pre Surge 69krpm	2.21 KPa	1.73%	28.29 KPa
Surge 69krpm	2.28 KPa	1.78%	27.97 KPa
Pre Surge 110krpm	1.3 KPa	0.86%	22.78 KPa
Surge 110krpm	2.14 KPa	1.41%	25.21 KPa
Pre Surge 150krpm	0.96 KPa	0.5%	14.71 KPa
Surge 150krpm	2.1 KPa	1.09%	21.32 KPa

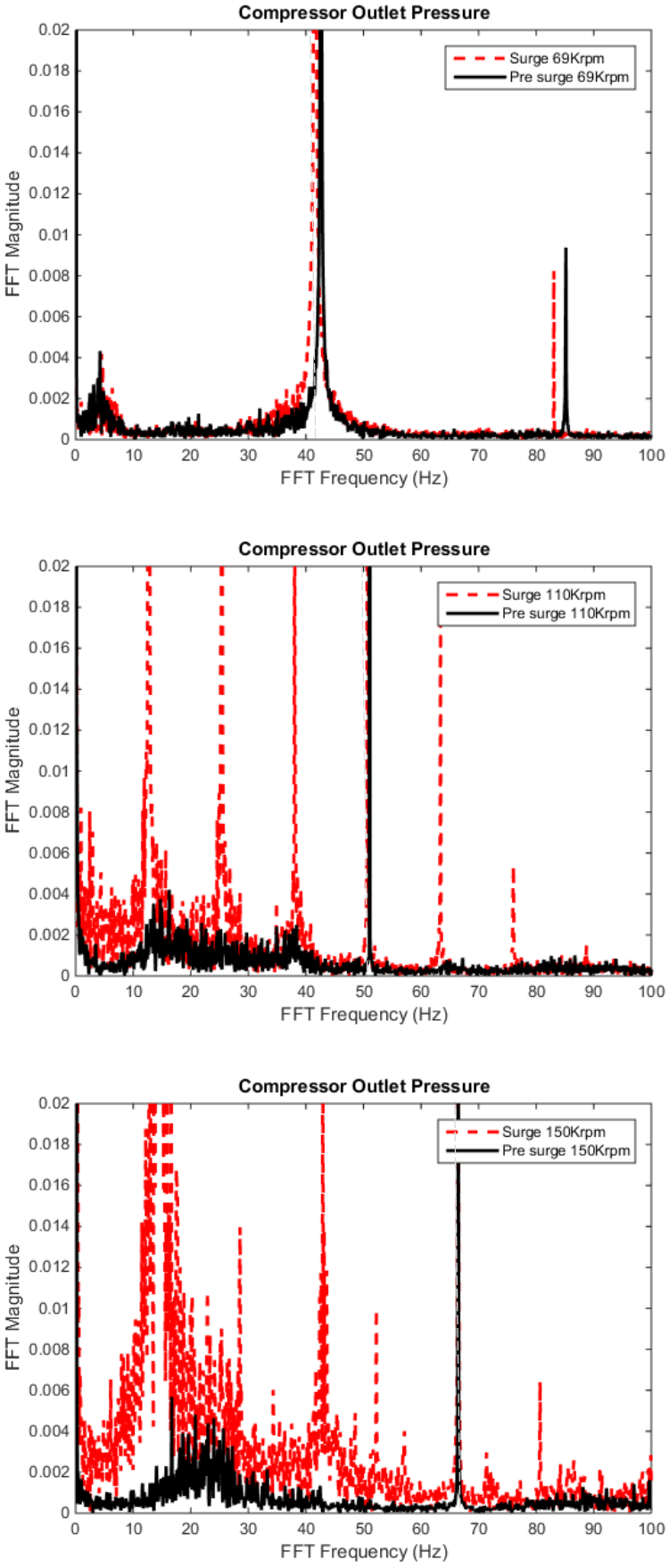

Figure 5. 8: FFT of compressor outlet pressure for surge and pre surge at 69, 110 and 150Krpm for unsteady compressor flow

5.4.2 Mass flow data investigation

Dissimilarly to pressure data in table 5.3, compressor mass flow variations of table 5.4 are more severe at 110 and 150Krpm when compressor is under surge. In addition, a clearer distinction between stable and unstable conditions could be made. Additionally, a difficult indication of surge is existent for the lower compressor speed analysed. Due to the 80Hz sampling rate of the mass flow sensor, FFTs of compressor mass flow are interested to possible aliasing distortion for flow variation due to engine intake. For the expressed reason, the analysis has not been found of high relevance.

Table 5. 4: Standard variation, coefficient of variation and amplitude of compressor mass flow for unsteady compressor flow

80Hz	*SD*	c_v	θ
Pre Surge 69krpm	0.001 Kg/s	31.33%	0.0064 Kg/s
Surge 69krpm	0.001 Kg/s	68.74%	0.0056 Kg/s
Pre Surge 110krpm	0.001 Kg/s	6.03%	0.0057 Kg/s
Surge 110krpm	0.0023 Kg/s	18.33%	0.011 Kg/s
Pre Surge 150krpm	0.001 Kg/s	3.34%	0.0064 Kg/s
Surge 150krpm	0.0028 Kg/s	10.54%	0.0184 Kg/s

5.5 Effect of pulsations on compressor surge

The FFT analysis of compressor outlet pressure data has been shown to be very useful for the distinction between stable and unstable conditions. This statement has had significant validity for both tested flow conditions in the engine gas-stand and the unsteady turbocharger gas-stand. Specifically, in the former layout, the turbine is subjected to pulsating flows, while, the compressor is not affected. In the latter layout, both turbine and compressor are subjected to pulsating flows of intake and exhaust engine processes. In fact, this is highlighted by the fact that surging frequencies appear at different rates compared to engine generated events, as the motion of intake valves. In this way, it is possible to monitor the surge onset and recirculating flows at the compressor inlet. Due to the better controllability of the system of figure 5.1, it has been possible to reduce compressor mass flow intervals between fixed operating points of the unsteady turbocharger. In addition, the presence of pulsations at compressor outlet has varied the stability range of the compressor before surge, as shown in figure 5.9.

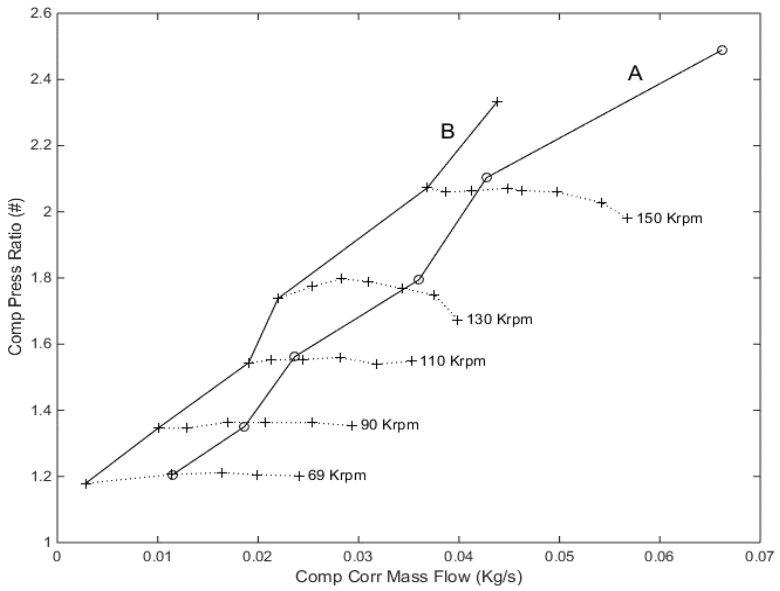

Figure 5. 9: Last stable points before compressor surge for steady (A) and pulsating (B) compressor

5.5.1 Inlet temperature analysis

In order to support the identification of surge and the proximity to instable operations, a temperature rise investigation on the compressor inlet temperature has been performed. A 1.5mm thick k-type thermocouple placed 25mm away from the compressor wheel is measuring the flow temperature at a depth of half the compressor blades. The temperature measured at the compressor inlet is compared to the ambient intake temperature conditions. Although, the thermocouple is kept at the same position for steady and unsteady compressor flow conditions in the turbocharger, temperature rise has been higher with the presence of pulsating flows at the compressor outlet, as it can be noted in figures 5.10 and 5.11.

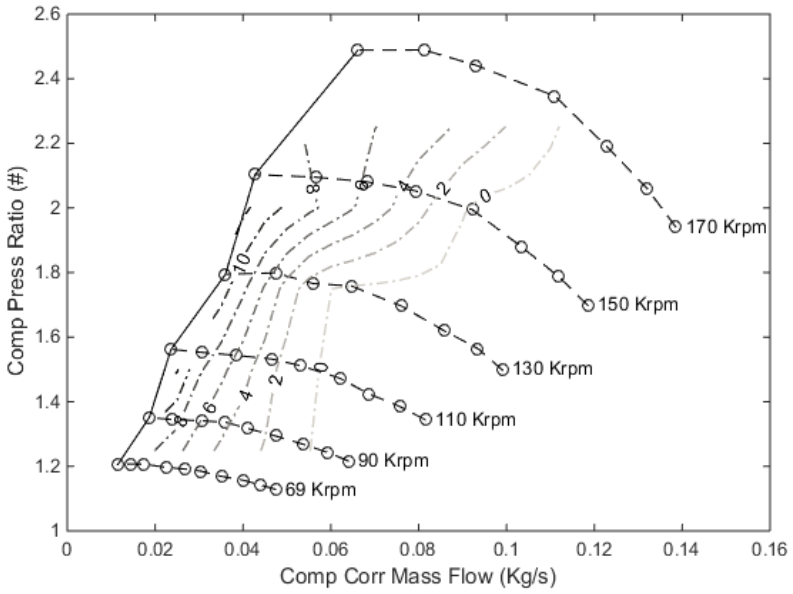

Figure 5. 10: Contour of temperature rise (degC) at 25mm from compressor wheel to main intake conditions for steady compressor flows

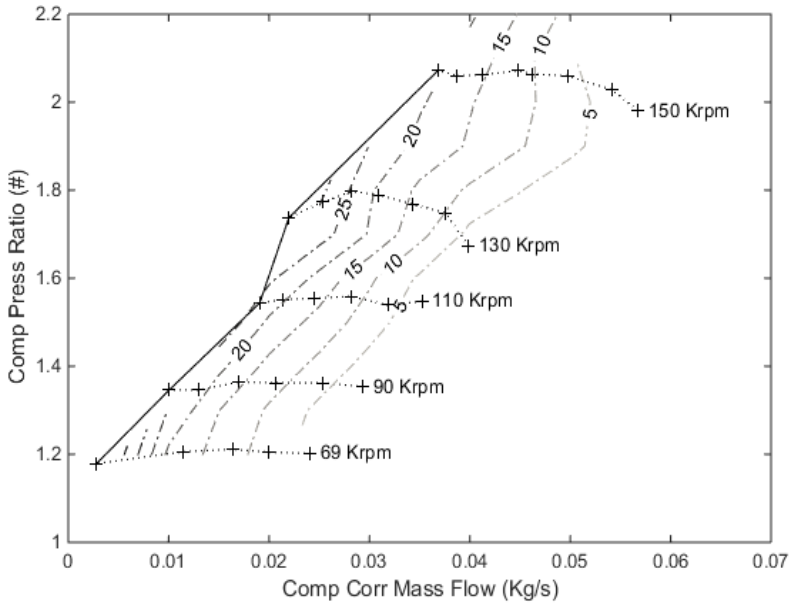

Figure 5. 11: Contour of temperature rise (degC) at 25mm from compressor wheel to main intake conditions for unsteady compressor flows

In figure 5.11, the higher temperature rise recorded at the compressor inlet could suggest that a larger flow recirculation is allowed in the presence of flow fluctuations at both turbine and compressor of the turbocharger. In fact, the presence of steady flows at the compressor seems to restrict the stability range at low corrected mass flow values. Furthermore, it is important to consider that the compressor outlet volume has been slightly increased, in order to accommodate the boost rig supply and perform experiments, referring to figure 5.11. According to Hansen et al. [120], this should have worsen the compressor surge tolerance in comparison to the steady compressor flow, due to larger volumes at the compressor outlet for the unsteady turbocharger setting. Therefore, it seems that the effect of pulsating flows has a significant benefit in improving tolerance to compressor surge.

5.6 Steady gas-stand facility for in-depth instabilities analysis

The development of surging flows in turbocharger compressors for automotive powertrains is investigated in specifically equipped steady turbocharger gas-stand. In this experimental facility, shown in figure 5.12, steady flows are ingested by compressor (item 12) and turbine (item 10) of the automotive turbocharger. Two separate ducting systems for turbine and compressor of the turbocharger are installed. Turbine is powered through hot pressurised air and compressor is loaded via an externally controlled back-pressure valve (item 13). Specifically, the air flow at the turbine is modulated from ambient conditions to 7bar absolute via a pressure regulator (item 1) and turbine inlet temperature is increased via two 44KW electric heaters (item 9). Due to lubrication requirements of automotive turbochargers, an oil conditioning unit (item 15) is installed in the turbocharger gas-stand. The oil temperature in controlled at 90degC downstream the bearing housing and in the conditioning unit. The temperature control is defined to resemble warm engine conditions for automotive powertrain operations. In order to measure the oil flow during operations, a volumetric flow meter is installed upstream the bearing housing. In this way, the oil flow range during turbocharger operations is in the range of 1.2L/min and 2.2L/min. In addition, a cooling unit (item 16) could be adopted for the water-cooling loop of compressor and bearing housings, if required.

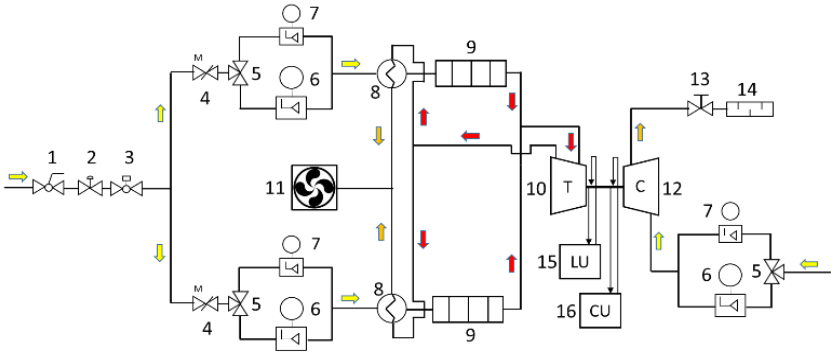

Number	Turbocharger gas stand equipment
1	Manual ball type shut off valve
2	SMC pneumatic pressure regulator
3	Ball type valve with Kinetrol electro-pneumatic positioner
4	Sierra CP motorized butterfly valve
5	Fiesto 3-way ball type valve
6	3" McCrometer V-cone mass flow meter with Siemens DSIII differential pressure transmitter
7	2" McCrometer V-cone mass flow meter with Siemens DSIII differential pressure transmitter
8	Bowman gas-to-gas heat exchanger
9	Axes Design variable power electric heater
10	Turbocharger turbine
11	Electrically controlled roof extraction fan
12	Turbocharger compressor
13	Motorized backpressure valve
14	In-line type performance silencer
15	Turbocharger lubrication unit c/w variable speed pump, electric heater, gas-to-water heat exchanger, pressure & temperature sensors
16	Turbocharger bearing housing cooling unit c/w electric heater, water-to-water heat exchanger, temperature sensors

Figure 5. 12: Steady turbocharger gas-stand for testing automotive turbochargers

In order to monitor turbocharger operations, thermodynamic performance parameters would have to be monitored through mass flow, pressure, temperature and turbocharger speed sensors. Most importantly, the turbocharger gas-stand of figure 5.12 considers ASME [83] and SAE [24, 82] standards for evaluating compressor and turbine performance maps. Specifically, similarly to engine gas-stand of chapter 2, pressure rings are placed at inlet and outlet of the turbomachine flow ports, evaluating static pressure along a section of the gas-stand measuring duct. Moreover, temperature is measured at the compressor with two platinum resistance thermometers (PRT) at depth of one-third of the measuring section diameter at inlet and four PRTs at depths of one-fourth, one-third and half of the measuring section diameter. In particular, at compressor outlet, the PRTs positioned at depths of one-third of the diameter are placed at 0 and 180degrees. Furthermore, at inlet and outlet of the turbocharger turbine, four 1.5mm K-type thermocouples are positioned radially along a measuring section as at the compressor outlet. In conclusion, mass flow at compressor and turbine inlets is measured by V-cone mass

flow meters (items 6 and 7 in figure 5.12), while, turbocharger speed is monitored through an eddy-current speed sensor mounted at the compressor housing, capturing the speed of the passing blades.

Table 5. 5: List of sensors adopted in the steady turbocharger gas-stand. P^ is sampled at 100Hz, while, remaining sensors are sampled at 10Hz

SENSOR	RANGE	ACCURACY
PRT	-50 to +200 degC	±0.3 + 0.005*T
1.5mm K type TC	-200 to 1260 degC	0.0075*T
V-cone mass flow	0 to 1200 Kg/h	±0.5%
Pressure	0 barA to 6 barA	0.08%
Turbo speed	0 to 400,000 rpm	0.1%

In table 5.5, range and accuracy of the sensors installed in the turbocharger gas-stand is provided. The adoption of low sampling rates and response times of sensors is possible owing to the presence of steady flows at turbine and compressor. As the investigation of surge onset on the basis of instabilities at the compressor outlet is the focus of the research, sampling rate of pressure transducer *P^* is increased in order to overtake the sensor response rate of 1KHz. In figure 5.13, the location of the sensor is shown at a distance from the compressor outlet port of 490mm. In this case, pressure rings are absent and the pressure transducer is directly flash mounted on the side of the 3" duct. Fixed diameter measuring sections at both inlet and outlet of the compressor are installed, while a reduction in the duct section is introduced in order to connect to inlet and outlet of the turbocharger compressor.

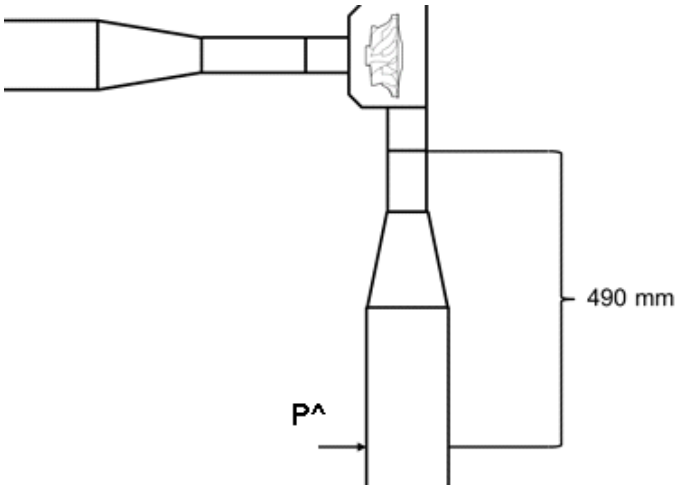

Figure 5. 13: Layout of ducting around the compressor. A pressure transducer, identified as P^, is positioned on the side of the 3" compressor outlet duct at a distance of 490mm

5.7 Compressor surge at steady and unsteady turbocharger gas-stands

As well as investigating behaviour and onset of surge under steady flow conditions in the turbocharger gas-stand, the analysis has been extended to unsteady flow conditions. Experiments on the compressor have been performed in the unsteady turbocharger gas-stand, with the presence of pressure and flow oscillations due to the motion of engine intake valves. In this layout, the compressor load is controlled through the external boost rig supply by restricting the flow. Therefore, the compressor could be subjected to surge while unsteadiness of flow is generated at 66.67Hz from the engine intake valves. In figure 5.14, the performance maps for the compressor at steady and unsteady flow conditions are shown. Additionally, it is important to consider that ducts at compressor inlet and outlet have sizes of 2.5", differing from the 3" ducts in the steady turbocharger gas-stand.

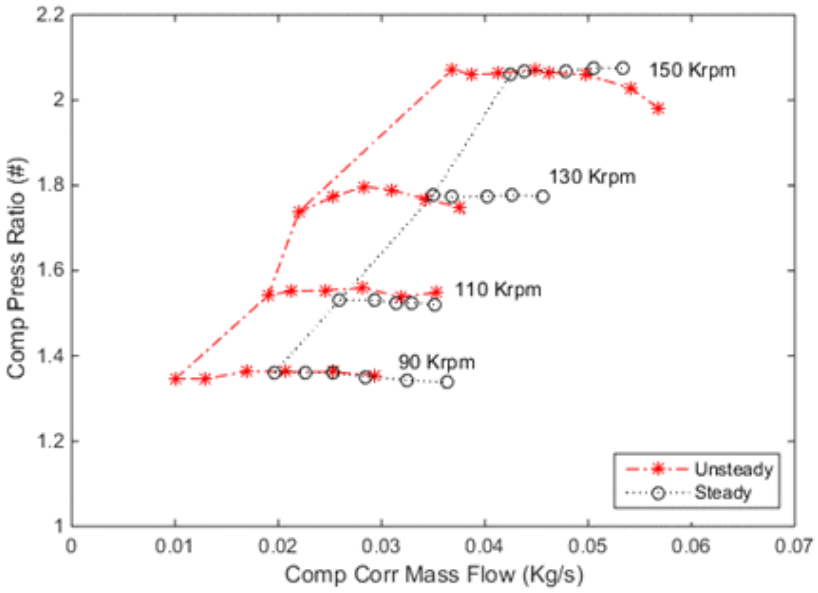

Figure 5. 14: Steady and unsteady performance maps for compressor

The graph in figure 5.14 highlights the change in compressor mass flow operations between unsteady and steady operations. In particular, the presence of pulsating flows at the compressor outlet allow for stable operation of the compressor at lower minimum mass flow rates. In addition, although, ducts and volumes around the compressor in steady and unsteady turbocharger gas-stands are different, leading to a variation of the compressor reference map [60], the focus of the study is on the

development and the traceability of compressor surge at steady and unsteady flow conditions. It is important to note that the experiments on the unsteady gas-stand, recreating steady flow conditions on the compressor in the engine gas-stand, has shown a similar position of surge to the steady map of figure 5.14 [115].

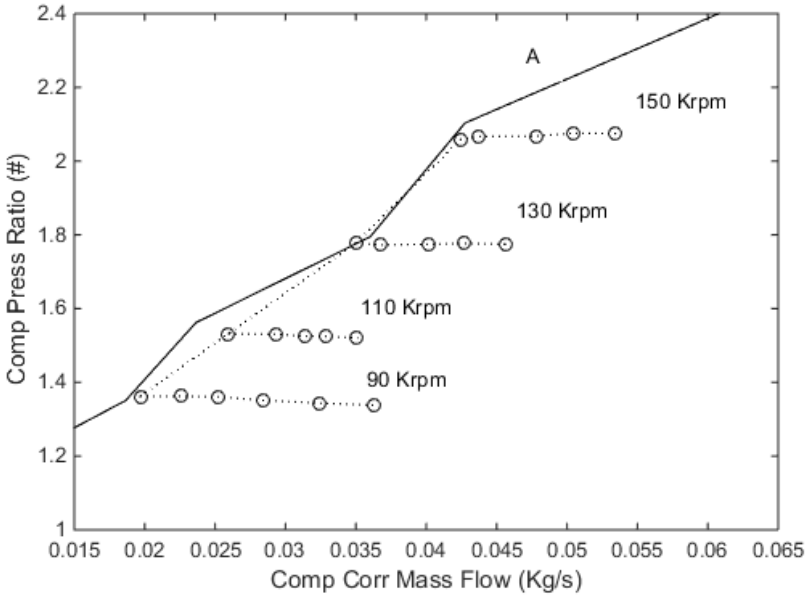

Figure 5. 15: Steady performance map for compressor in turbocharger gas-stand and surge line A obtained in the engine gas-stand (figure 5.9)

In figure 5.15, the comparison between the compressor map generated in the turbocharger (line A) and the engine gas-stands is shown. As visible, the two surge lines are at a similar position, although, the steady-state map generated in the turbocharger gas stand is slightly shifted to higher corrected mass flow rates. In addition, the maximum different in stable operating ranges is obtained at 110Krpm, with surge line A (pulsating flows at turbine) being positioned at significantly lower compressor mass flow values. The results shown in figure 5.15 highlight a really important outcome of this chapter, suggesting that the small pulsations at the turbine for the case of the surge line A have a small influence on the position of the compressor surge line.

5.7.1 FFT analysis of compressor downstream pressure

Therefore, the analysis of FFT for the compressor outlet pressure *P^* signal is conducted. In fact, peaks of FFT magnitude at low frequency (up to 100Hz) and

frequency of oscillation are investigated, in figure 5.16. Importantly, the peak of FFT at 66.67Hz has been excluded owing to the motion of engine intake valves.

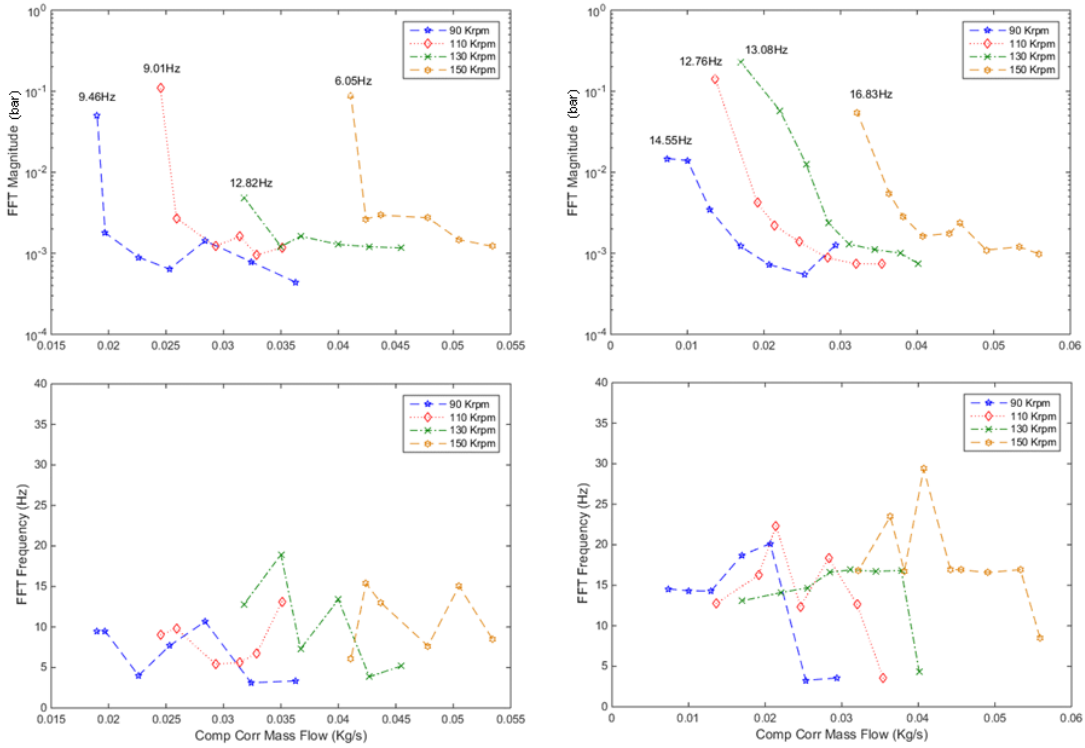

Figure 5. 16: At the left hand-side, magnitude in bar and corresponding frequency of FFT for *P^* pressure signal of compressor at steady flow conditions. At the right hand-side, magnitude in bar and corresponding frequency of FFT for *P^* pressure signal of compressor at unsteady flow conditions. Operations in proximity of surge and surging condition at the lowest mass flow are investigated

Operations in proximity of surge are monitored, showing different surge onset between steady and unsteady flows at compressor outlet. In particular, the instantaneous transition from stable to instable operations noticed in the steady turbocharger gas-stand, figure 5.16 highlights a progressing transition to surge accordingly to the peak of FFT magnitude. The frequency of oscillation shows a difference between steady and unsteady layouts with ranges of 6-12.82Hz and 13-16.83Hz, respectively. In figure 5.16, comparing behaviour of compressor at different rotating speeds confirms the smooth growth of instabilities in the presence of flow unsteadiness. In fact, instead of stability resembled at mass flow rate of 105% of surge in absence of pulsations, the constant increase of FFT magnitude could become a warning signal for surge. However, the variation of FFT magnitude across the compressor speeds analysed under unsteady conditions would cause difficulties in defining a limit for the compressor safe operations.

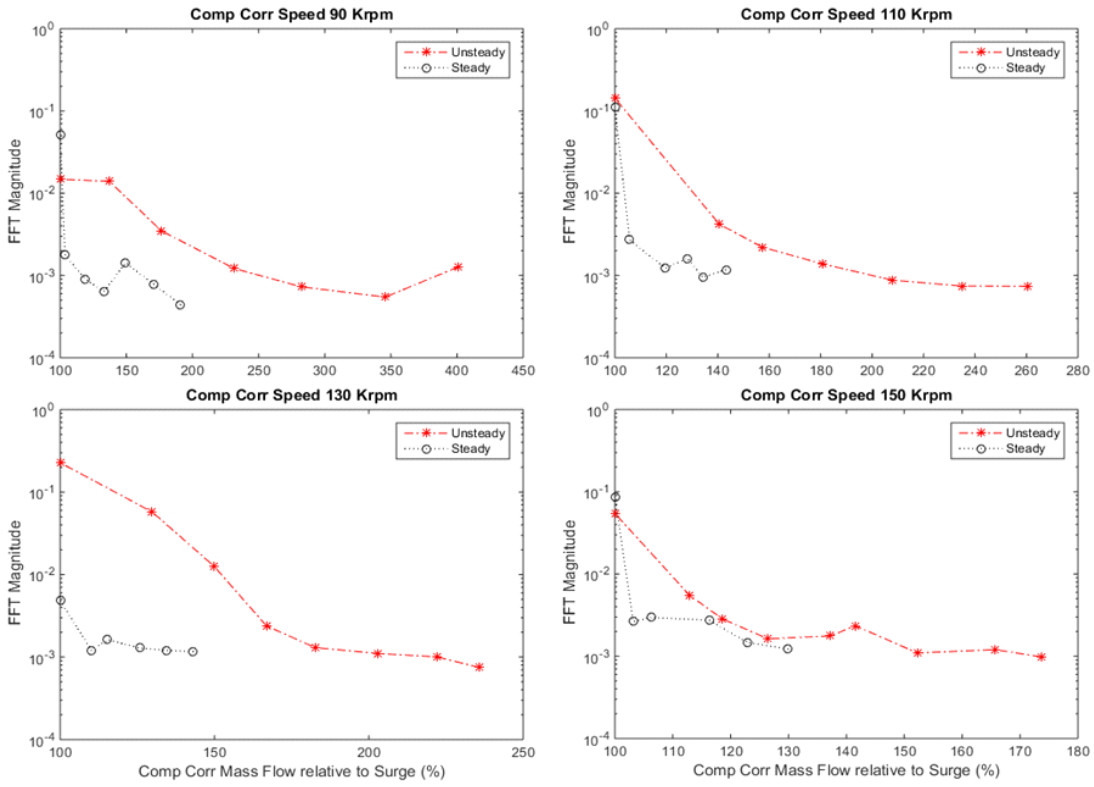

Figure 5. 17: Magnitude in bar of FFT for *P^* pressure signal of compressor at steady and unsteady flows. Corrected mass flow is expressed in terms of percentage of surging mass flow value, equal to 100%.

Therefore, the extension of the analysis to average and CoV of the FFT magnitude has been necessary for detailed investigation of surge in the presence of pulsating flows at the compressor outlet. In this scenario, a frequency range of 3-20Hz is considered for both the flow conditions in compressor, in according to the data of figure 5.16. In this way, it has been possible to understand the surge onset. In according to figure 5.18, it can be stated that the average value of FFT is lower than 10^{-3}bar during fully stable operations. While moving into surge, the average value of FFT increases steadily across a constant speed line. Additionally, in figure 5.17, a constant rate of increase in average value of FFT magnitude could be defined for each of the compressor speed lines. More importantly, the rise in average FFT values starts at different percentages of mass flow rates in relation to surge, about 300% at 90Krpm and 130% at 150Krpm. In this case, a slightly conservative threshold could be defined for the compressor in relation to the average values of FFT magnitude. On the other side, the investigation of CoV is not able to generalise the surge onset across compressor speeds, due to the CoV obtaining similar values at stable and surging operations for the same speed line, such as 150Krpm.

Conclusively, in figures 5.17 and 5.18, the differences in the growth of instabilities due to surge have been analysed, with a progressing development of surge in the case of unsteady flows.

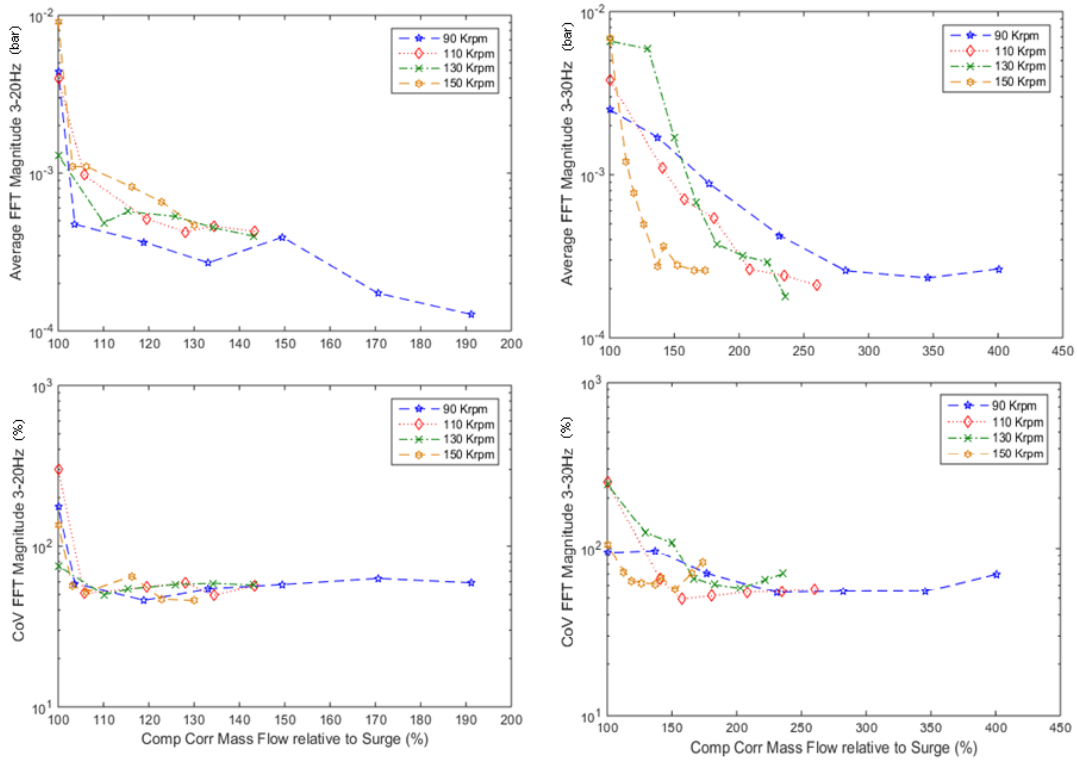

Figure 5. 18: At the left hand-side, average magnitude in bar and CoV of FFT in the range of 3-20Hz for *P*^ pressure signal of compressor at steady flow. At the right hand-side, average magnitude in bar and CoV of FFT in the range of 3-20Hz for *P*^ pressure signal of compressor at unsteady flow. Corrected mass flow is expressed in terms of percentage of surging mass flow value

5.8 Chapter summary and conclusions

In this chapter, a FFT investigation of the compressor outlet pressure has been conducted in the engine gas-stand, as well as the steady and unsteady turbocharger gas-stands. The investigation has allowed the characterisation of compressor surge which can be adopted in two-stage turbocharging systems. Furthermore, conclusions from this chapter can be drawn as below:

- The unsteady fluctuating flow conditions is able to incorporate real engine applications, including the variation of compressor downstream volumes during engine intake process. With flow pulsation, the compressor extends the operability area at lower mass flow

- In unsteady flow conditions, the FFT of pressure becomes extremely important for identifying surge onset. For the lowest compressor speed of 90Krpm, instabilities could be recorded at about 230% of the surging mass flow rate. In this way, a threshold level would be able to provide a safety factor to avoid surging conditions during compressor operations.

- In the comparison between surge lines at the steady gas-stand and the unsteady turbocharger gas-stand, it is clear that the presence of flow pulsations affects the stable operating range of the compressor. Specifically, pulsating flows at the compressor reduce the tendency of the compressor to surge, shifting the surge line towards lower corrected mass flows, as shown in figure 5.14.

- In the steady gas-stand, FFT magnitude increases at 105% of the surging mass flow rate. This occurrence has been recorded with CoV values of FFT magnitude spiking above 100%. Furthermore, FFT analysis has been limited to frequency ranges of 3-20Hz.

Chapter 6 – Equivalent performance of two-stage turbocharging systems

In this chapter, a novel mapping approach has been investigated for two-stage turbocharging systems. The equivalent maps for high and low pressures turbochargers are generated into a 1D simulation code, in order to explore the methodology. However, at this instance, effects of swirling flows on turbomachine performance are not considered as standard maps from the steady turbocharger gas-stand have been adopted. Firstly, performance of the two-stage turbocharging system on the Diesel engine are investigated, in order to explore the dynamics of the boosting device. Secondly, the equivalent two-stage system maps are generated into the 1D code for steady flow conditions at both turbines and compressors. In this scenario, an equivalent turbocharger speed has been defined, accounting for operating conditions of both HP and LP turbochargers. Lastly, equivalent performance maps of the two-stage turbocharging system are validated in a complete powertrain model.

The equivalent mapping methodology for two-stage turbocharging systems presented in this chapter has been published and presented at the ASME 2016 Internal Combustion Engine Fall Technical Conference [117].

6.1 Applications of two-stage systems

The increasing demand for cleaner internal combustion engines has defined a necessity to further develop efficient powertrain systems. One of the key technologies, contributing to the improvement of engine efficiency, is represented by two-stage sequential turbocharging systems, for small and large reciprocating engines [16, 23]. More importantly, the combination of advanced boosting systems and variable valve technologies, allowing extreme Miller cycles, are targeting emission reduction without penalisation of achievable power and torque [20]. In addition, two-stage turbocharging systems can improve vehicle acceleration for small downsized engines, being of comparable performance to bigger natural aspirated engines [27].

Since early powertrain applications, two-stage turbocharging operations have been regulated in order to comply with powertrain requirements in terms of mass flow by means of by-pass valves acting on turbines and compressors [14, 130]. When there is a necessity for maximum boost levels, the by-pass valves are closed and the maximum expansion rate can be captured by LP and HP turbines [14]. Due to the sequential layout of the turbocharging system, HP compressor and LP turbine are subjected to turbulent and swirling flow at the inlet which can change the operating performance and stable operable range of mass flow [64, 75]. In addition, the temperature increase at the HP compressor inlet may lead the heat transfer in the HP turbocharger to change together with the apparent efficiency [62]. In accordance to current standards for measuring turbocharger performance in gas-stands [24, 82], the effects influencing the turbochargers behaviour in two-stage systems are not being considered. Therefore, an appropriate map for two-stage turbocharging systems may be required in order to incorporate the effects, influencing turbocharger performance [11].

6.2 Two-stage system performance experimental analysis

In order to define a mapping approach for the two-stage turbocharging system, an experimental analysis of the boosting system is necessary. In fact, a powertrain system including a 2.2L Diesel engine with sequential turbochargers has been tested for optimal torque. Figure 6.1 shows the layout of the system experimented and simulated in this research. Conditions of the air-path have been evaluated for the powertrain system in order to obtain full representation of the turbochargers dynamics.

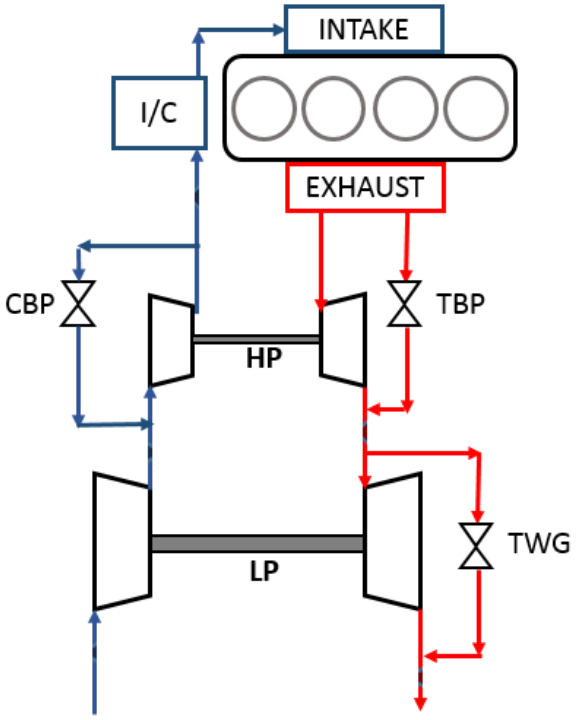

Figure 6. 1: Powertrain layout including two-stage sequential turbocharging system

Inlet and outlet conditions of LP and HP turbochargers have been monitored during the experiments in terms of pressure and temperature. In addition, the turbochargers speeds have been controlled by using eddy current sensors on the compressors. As shown in figure 6.1, TBP and TWG valves have been actively controlled and their position monitored. On the compressors side, the maximum pressure at the inlet of the HP stage is limited by a passive CBP valve whose position has been monitored through a linear displacement sensor. Steady state performance of the powertrain has been evaluated for several load conditions at speeds between 1000rpm and 2500rpm. Moreover, the total compressor pressure

ratio delivered by the two compressors to the engine intake during the experimental phase is shown in figure 6.2. In particular, it has been noticed that during the operation, the TWG valve has always been kept closed.

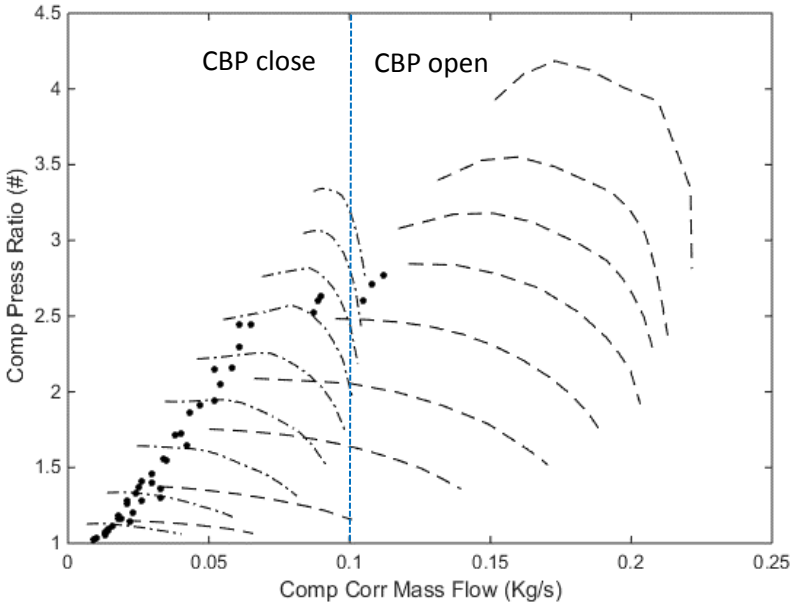

Figure 6. 2: Total pressure ratio across the two turbochargers in relation to LP and HP compressor maps including CBP valve operations

In figure 6.2, the majority of the operating points from the powertrain system lies within the mass flow range of each compressor. However, few points above 0.1kg/s stay outside the mass flow range of the HP compressor. Moreover, the CBP valve operates passively to reduce load and choking of the HP compressor. In order to understand the turbochargers behaviour across the engine operation, HP and LP turbochargers speed have been analysed in figure 6.3. It is clear that the HP turbocharger speed increases progressively along with the LP unit until 170Krpm is achieved on the smaller turbomachine. Once this speed is reached at the HP stage, the relationship between the two turbochargers speed becomes inversely proportional for increasing LP turbocharger speed. In fact, the rise of LP turbocharger speed from 100Krpm causes a deceleration of the HP stage.

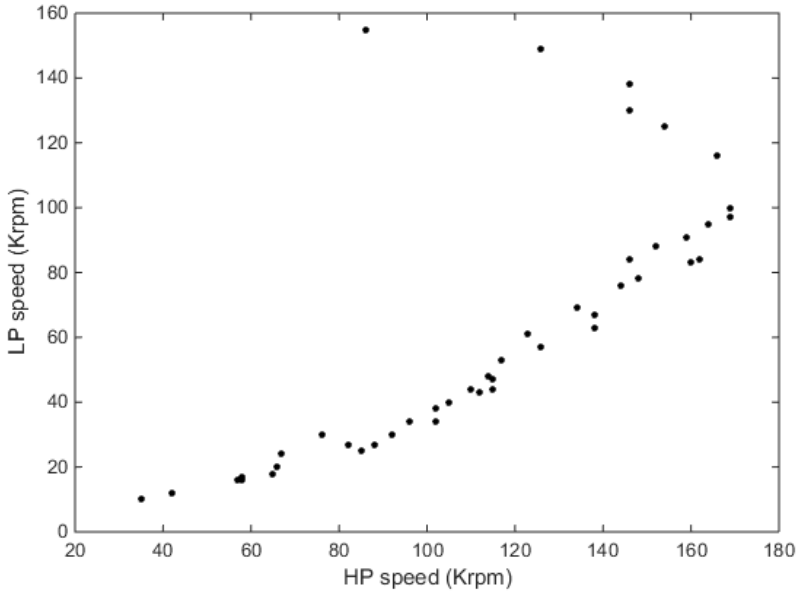

Figure 6. 3: Speed relationship between the LP and the HP turbochargers in the tested two-stage system

In order to better understand the dynamics of the turbocharging system and the two units, the pressure ratio delivered by the HP and LP turbochargers have been investigated and compared to the boosting system capability in figure 6.4 and 6.5. For both compressor and turbine, the HP load is subjected to a reduction once the pressure ratio of about 1.6 is achieved. Although, the pressure ratio on the HP stage decreases for mass flow higher than about 0.6 and 0.7kg/s for the compressor and turbine, respectively, the pressure ratio delivered by the total two-stage system keeps increasing. The main reason for improving the total pressure ratio can be explained by higher load reversed onto the LP turbocharger as suggested by figures 6.4 and 6.5. Furthermore, in order to correlate operations of turbochargers, the mass flow values in figures 6.4 and 6.5 refer to the entire system flow, without considering the split of flow between HP and LP stages during by-pass valve operations.

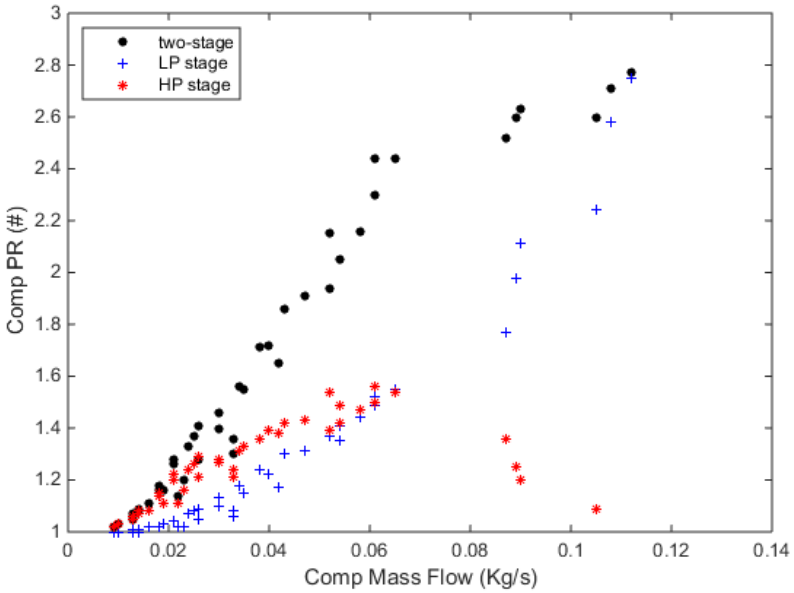

Figure 6. 4: Compressor pressure ratio for full two-stage system, LP and HP stages, and mass flow of full two-stage system

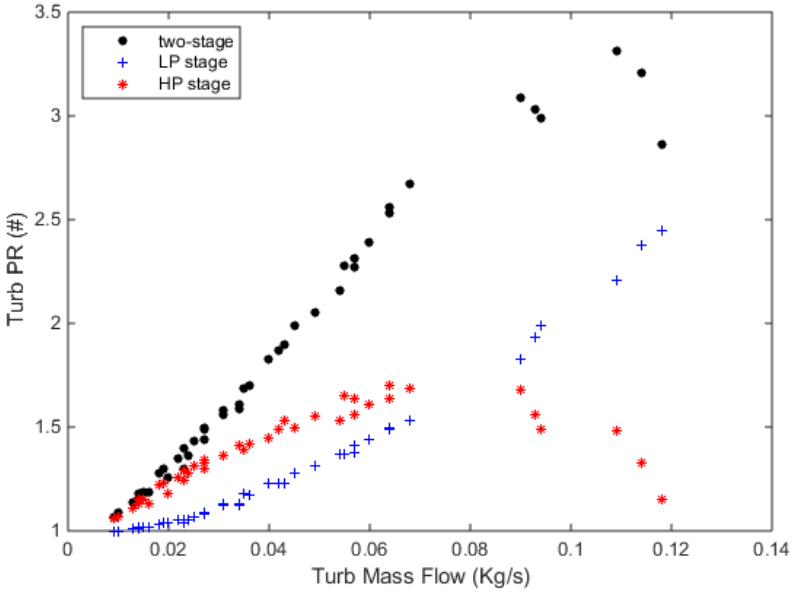

Figure 6. 5: Turbine pressure ratio for full two-stage system, LP and HP stages, and mass flow of full two-stage system

An accurate analysis of the by-pass valves dynamics has resulted in the TBP actuator at the HP stage to influence the boosting system behaviour. In fact, turbochargers speeds change once the turbine by-pass is opened causing a reduction of extraction capacity of the HP turbine. In addition, it is also important to

state that the experimented engine has fixed valve timing and lift at both intake and exhaust. Therefore, the change in turbocharger load is not caused by external parameters. Figure 6.6 shows the variation in both turbocharger speeds for different TBP valve positions.

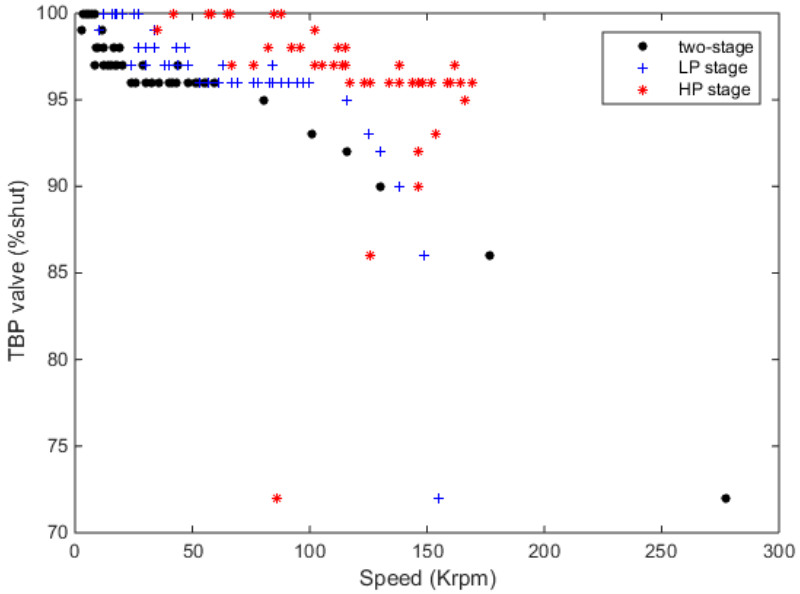

Figure 6. 6: TBP valve position and speed of equivalent two-stage, LP and HP turbochargers

As visible in figure 6.6, opening the by-pass valve reduces the HP turbocharger speed and, for constant load, allows the speed of LP turbocharger to increase. In order to account for the relationship between the two turbocharger speeds, an equivalent turbocharger speed (N_{eq}) has been defined as in equation 6.1. The power of the LP turbocharger speed (N_{LP}) over the HP turbocharger speed (N_{HP}) can account for deceleration of the HP turbocharger into the equivalent speed term.

$$N_{eq} = N_{LP} * \left(\frac{N_{LP}}{N_{HP}}\right) \tag{6.1}$$

The reason for developing a term to describe an equivalent two-stage speed relies on the necessity to create a performance map for the turbocharging system. As shown in figure 6.6, the equivalent two-stage speed increases when the TBP valve is progressively opened. Furthermore, under constant back-pressure values at compressors and turbines, figure 6.7 shows the directly proportional relationship

between the new speed term and the compressor mass flow, unlike the HP term once the TBP valve is open.

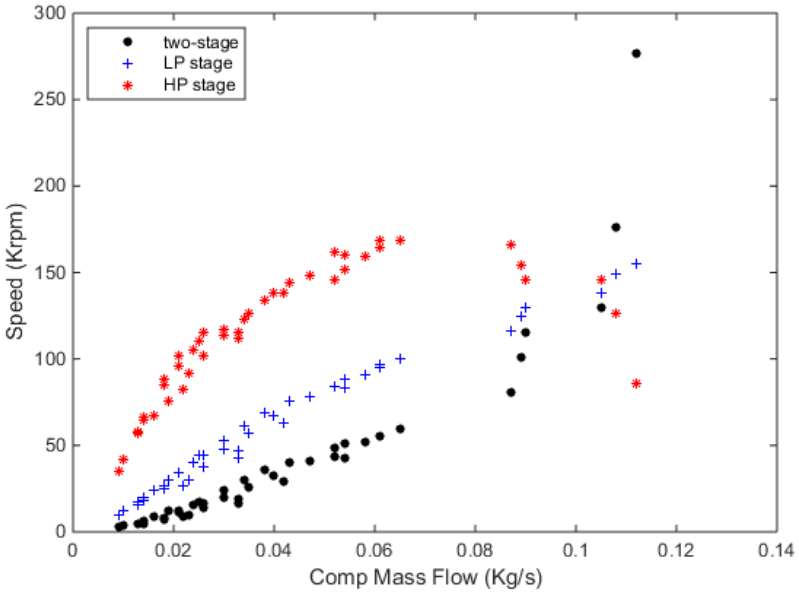

Figure 6. 7: Compressor speed of equivalent two-stage, LP and HP turbochargers, and mass flow of the full two-stage system

6.3 Simulating the equivalent mapping approach

In order to account for non-uniformity and swirling effects at the inlet of the HP compressor and LP turbine, a mapping strategy for the two-stage turbocharging system needs to be explored. In this circumstance, a 1D model of the turbocharging system has been developed including the performance maps of each stage as acquired from a steady turbocharger gas-stand in stand-alone configuration. Moreover, measuring sections have been placed around the boosting system in order to capture turbocharging performances without any heat losses. The measuring sections are 2” in diameter and have a length of 600mm at inlet and outlet of compressor and turbine systems. In order to avoid any change in measurements due to heat transfer, the measuring sections have been considered fully insulated.

In conjunction with figure 6.8, compressor maps along constant equivalent two-stage speed lines have been generated at different back-pressure conditions at point 2 and pressure values at point 3. As well as compressors, the equivalent turbine map has been generated by varying the pressure at point 3. In order to perform the simulations, measuring sections of the gas-stand have been included in the model. Specifically, these have been placed at inlet at outlet of the turbocharging system. Referring to figure 6.8, measuring sections are positions at points 1, 2, 3 and 4.

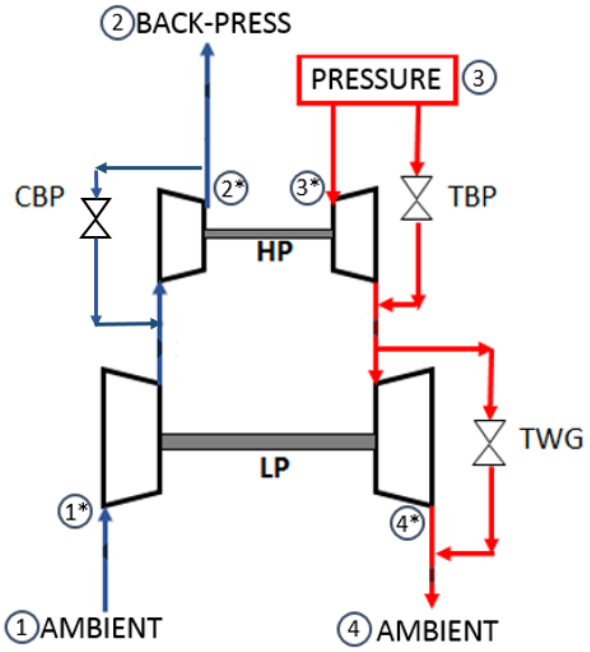

Figure 6. 8: Two-stage sequential turbocharging system as defined into the 1D code

In order to generate the equivalent performance map of the turbocharging system, governing laws on the valves have been set. Apart from having the TWG valve constantly shut, the CBP valve is regulated to open only at pressures of 2.25bar while TBP valve position is controlled during the mapping methodology. Moreover, in relation to the mapping method, the ambient condition has been defined as 1bar of pressure at 298K of temperature. Pressure level at point 3 has been varied from 1.5bar to 4bar when mapping the compressors and 1.25bar to 4.25bar when mapping the turbines. At this point, the temperature is kept constant at 873K. Furthermore, the back-pressure at point 2 has been generated by mean of an orifice which is varied during compressor maps and maintained fixed during turbine maps.

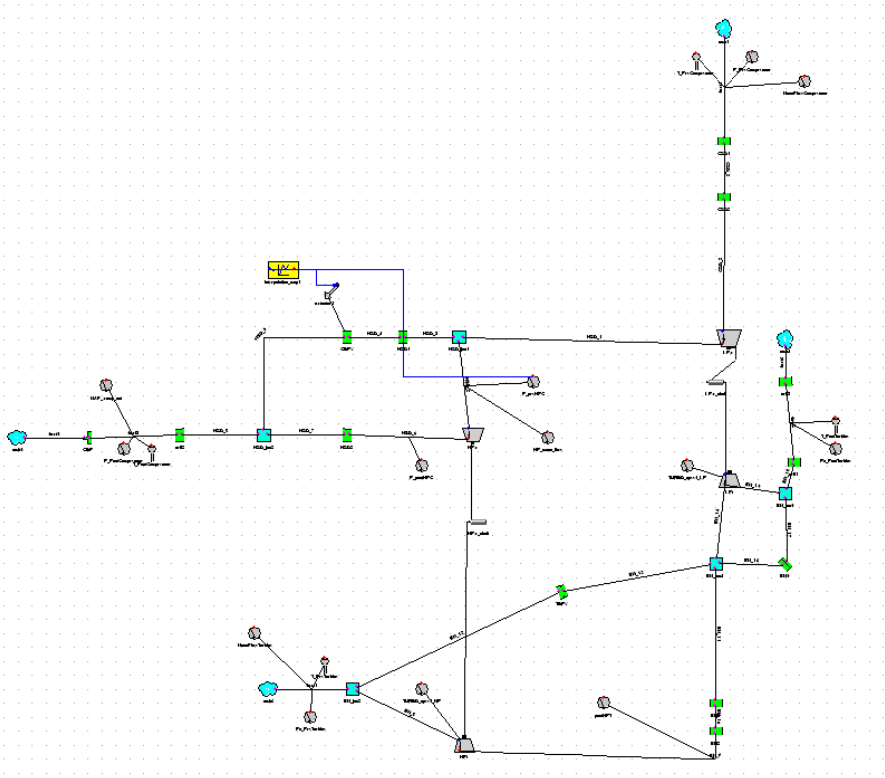

Figure 6. 9: Picture of the 1D model to simulate the two-stage mapping approach

In order to evaluate the effect of heat transfer at the inter-stage of the two compressors, material thickness of the duct has been included. The 1D simulation tool is able to capture the temperature soaking effect of the aluminium inter-stage duct. Furthermore, it is important to notice that the external heat transfer, such as convection and radiation are not considered. Therefore, internal convection and heat conduction along the duct is solved. In order to explicate the simulation of equivalent two-stage mapping, a picture of the 1D model in the software Ricardo WAVE ® is shown in figure 6.9. Both compressor and turbine stages are modelled, including by-pass regulating valves and ducts.

6.4 Equivalent two-stage turbocharging system performance maps

6.4.1 Compressor map

In this section, the simulation results are discussed and generated maps have been analysed. In figure 6.10, the equivalent two-stage map is shown for several equivalent speed lines. It is important to state that in all the maps generated to describe the two-stage system, surge and choke conditions are based on the instabilities achieved from each turbocharger. For equivalent speeds below 20krpm, the HP compressor would be responsible for the surge line of the equivalent map in figure 6.10. At higher equivalent speeds, the LP compressor is surging at higher mass flows, limiting the stability range of the two-stage turbocharging system at lower mass flows. In regards to choke, at equivalent speeds below 20krpm, the LP compressor would be limiting performance of the turbocharging system, due to negative pressure ratios and low rotating speeds of the LP machine. Moreover, at high equivalent speeds (above 30krpm), the HP compressor would be choking, limiting performance of the entire system at high flows.

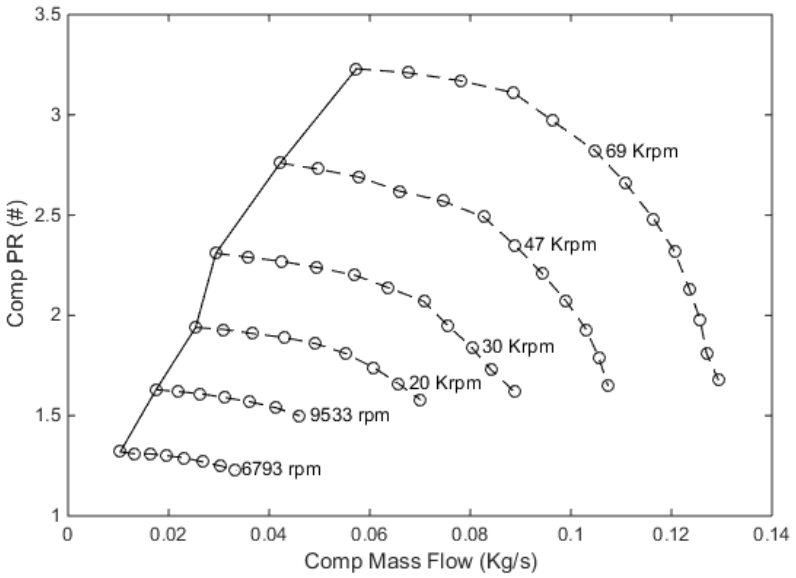

Figure 6. 10: Compressor equivalent two-stage performance map for constant equivalent speed lines

In more detail, the pressure ratio across the two compression stages is measured at points 1 and 2 from figure 6.8, representing the measuring sections. At these positions, total temperatures have been measured for producing the equivalent

compressor efficiencies. As shown in figure 6.11, high values of efficiencies have been measured, reaching unrealistic conditions. These can be explained by the heat transfer occurring in the inter-stage connecting ducts, as explained in 6.3. In fact, when adiabatic walls (no heat transfer between flow and ducts) have been set for the ducts between the two compression stages, equivalent compressor efficiency assumes reasonable values by only considering the pressure drop occurring in the ducts.

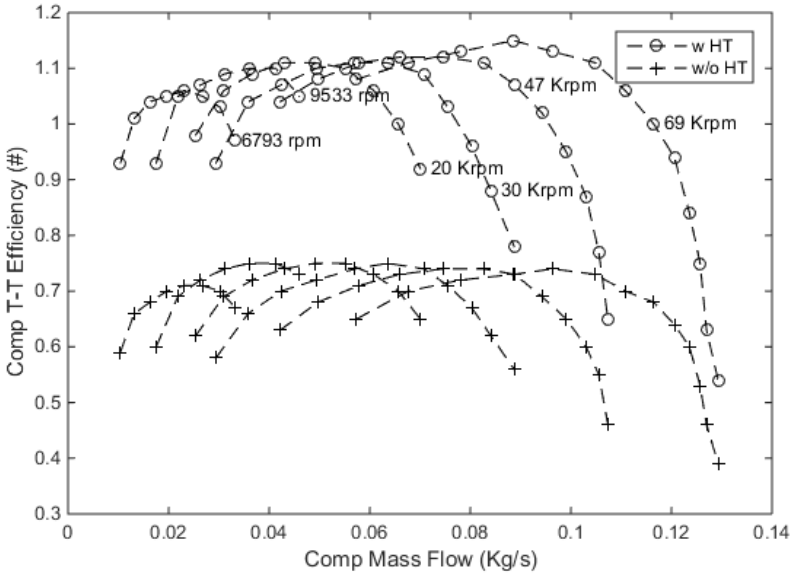

Figure 6. 11: Compressor equivalent two-stage efficiency maps for constant equivalent speed lines with and without heat transfer in the inter-stages ducts

Due to the absence of insulation in the ducts between HP and LP compressors, it is important to account for the heat transfer effects when representing the equivalent two-stage efficiency map. In fact, the total temperature values have been measured at the inlet of LP compressor and outlet of HP compressor, excluding the measuring section and the relative drops. In figure 6.12, the efficiency measured at points 1 and 2, as specified in the diagram in figure 6.8, is compared to values measured of temperatures recorded at 1* and 2* in the 1D simulations. It is clear from the graph that the compressor efficiency measured for the two-stage systems at points 1* and 2* has been considered the optimal solution to evaluate the mapping methodology through simulations.

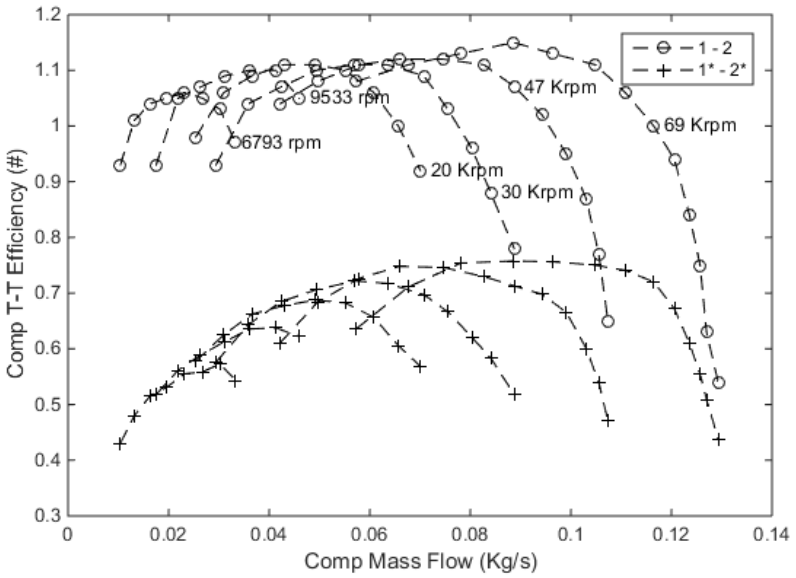

Figure 6. 12: Compressor equivalent two-stage efficiency maps for constant equivalent speed lines at points 1-2 and 1*-2*

6.4.2 Effect of turbine by-pass on compressor map

The compressor maps generated in the previous subsection have been referred to a position of the TBP valve being completely closed. In addition, it is wise to remember that the CBP valve is automatically controlling the maximum value of pressure at the inlet of the HP compressor while the TWG valve is always closed. In order to obtain the full performance of the system, it has been decided to vary the position of the TBP valve as it would usually happen in a VGT single stage turbocharger. However, for constant levels of HP turbine inlet and compressor back pressure in a two-stage system, varying the position of the TBP actuator causes a change in the speed of the two turbochargers. In addition, the stability range of the system varies according to the compressor equivalent map. In more detail, Figure 6.13 shows the shift of surge line towards higher values of mass flow when moving from 100% to 50% closed position of the TBP valve. As demonstrated, the opening of the TBP valve influences the operation of the two turbochargers, reducing power from the HP stage. It is important to notice that equivalent speed varies when the TBP valve is controlled. The speed lines in figure 6.13 are subjected to variation, as the relationship of speeds for the HP and the LP turbochargers changes. Specifically, table 6.1 reports the equivalent speed values for the different TBP positions, in order to reduce complexity in figure 6.13.

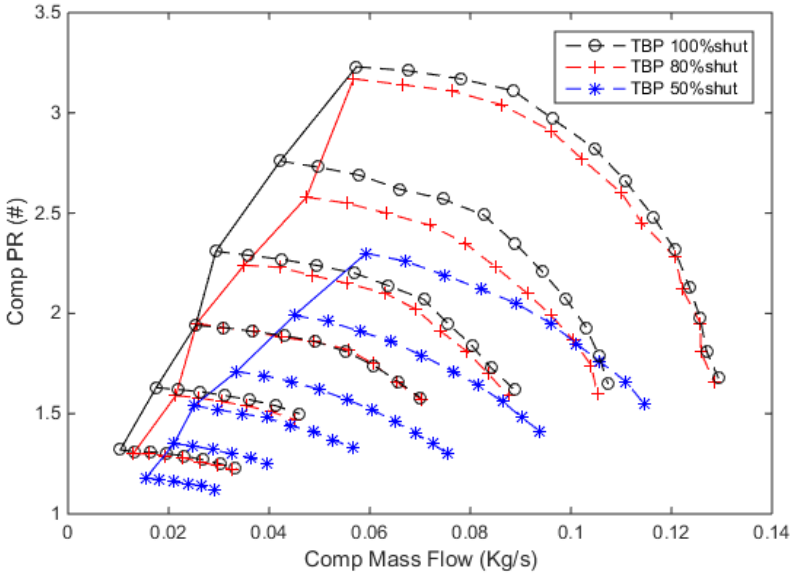

Figure 6. 13: Compressor equivalent two-stage performance map for equivalent speed lines and different position of the TBP valve

Table 6. 1: List of equivalent speed lines referring to figure 6.13

TBP	EQUIVALENT SPEED LINES (rpm)					
50%shut	9260	13240	28950	44545	72645	109010
80%shut	6940	9800	20230	30625	50625	71176
100%shut	6790	9530	20230	29880	47370	69540

The reduction of the boost delivered is noted, due to a reduction of the double compression obtained across the two stages. This is a valid statement as the map shown in figure 6.13 relates to different values of equivalent speed lines for three positions of the TBP valve. This is due to the definition of equivalent speed where the term increases considerably with the value of LP turbocharger speed. In order to represent equivalent maps from simulations, in figure 6.13, the relationship between HP and LP turbochargers relates to the opening of the TBP valve. In fact, contribution from the LP stage is directly correlated to the opening of the TBP valve. This is also a valid statement for the maps in figure 6.13. In this case, the LP turbocharger speed is fixed constant for each of the six speed lines represented in figure 6.13 at every position of the TBP valve. In the case of mapping the turbocharger for constant LP speed lines, a reduction of deliverable boost is obtained as in figure 6.13. However, the stability range for the TBP position of 50% is different between figures 6.13 and 6.14, due to different share of speed and power

for HP and LP compressors. Specifically, in figure 6.14 for TBP valve at 50%, the HP stage is operating at low speed, improving the surge margin of the complete two-stage system. Referring to figure 6.14, for all the TBP valve positions, the LP compressor speed lines are maintained constant, as 25, 35, 55, 70, 90 and 110Krpm.

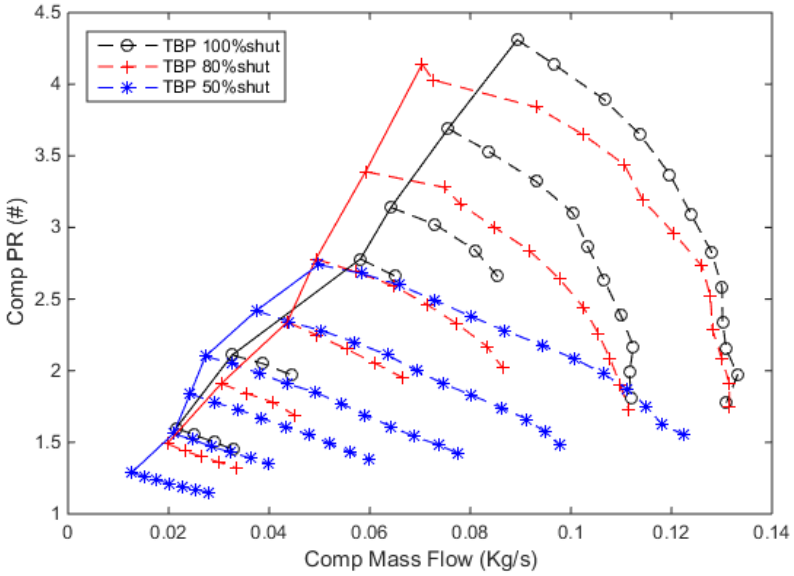

Figure 6. 14: Compressor equivalent two-stage performance map for LP speed lines of 25, 35, 55, 70, 90, 110Krpm and different position of the TBP valve

Furthermore, in figure 6.15, in the condition of constant HP turbocharger speed lines, the boost levels increase when the TBP valve is opened. This is due to high levels of rotational speed in the LP turbocharger and an increasing level of boost deliverable by the LP compressor. Referring to figure 6.15, the HP compressor is maintained at constant speed for each speed line in the several TBP opening positions. Specifically, the six speed lines refer to HP rotating speeds of 92, 128, 150, 164, 171 and 174Krpm.

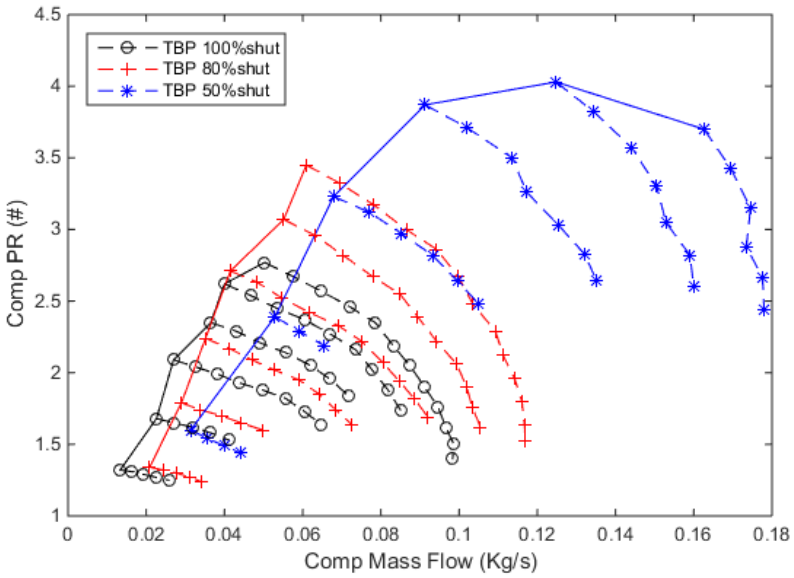

Figure 6. 15: Compressor equivalent two-stage performance map for HP speed lines of 92, 128, 150, 164, 171 and 174Krpm and different position of the TBP valve

6.4.3 Turbine performance map

As well as compressor equivalent two-stage maps, the performance of LP and HP turbines have been analysed for different positions of the TBP valve. In this scenario, the turbine equivalent map has been generated for the same values of equivalent constant speed lines by varying turbine inlet pressure. In figure 6.16, the equivalent turbine map is shown for the same equivalent turbocharger speeds of figure 6.14 and table 6.1. In order to reduce complexity, the speed labels have been omitted from figure 6.16, although, details on equivalent speed lines can be seen in table 6.1.

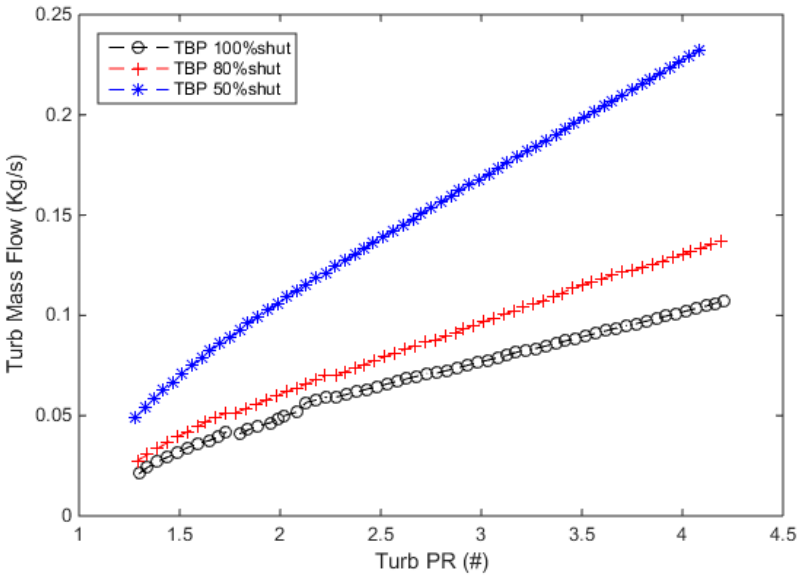

Figure 6. 16: Turbine equivalent two-stage performance map for equivalent speed lines (referring to table 6.1) and different position of the TBP valve

It is evident that TBP valve in open position requires higher levels of mass flow to obtain a certain value of pressure ratio when compared to fully shut position of the by-pass valve. In the case of turbine mapping, the measuring sections have been simulated into the 1D code as for the compressors. At the same time, the total-to-static expansion efficiency has been evaluated by measuring temperatures at the measuring sections (points 3 and 4 of figure 6.8) or just at the proximities of LP and HP turbines (points 3* and 4*of figure 6.8). Figure 6.17 shows the values of turbine equivalent efficiency calculated at points 3*-4* and 3-4. This resulted in extremely elevated efficiency values for temperatures measured in points 3 and 4 which can be seen in figure 6.8. The presence of diabatic measuring ducts at inlet and outlet of two-stage turbines system could reduce the temperature entering the HP turbine. In addition, the temperature sensed at point 4 would be lower than the temperature exiting the LP turbine. Therefore, the efficiency evaluation of the expansion process across the two turbines would be influenced by the heat transfer in the measuring sections. These could be explained by a significant variation of temperature before reaching the HP turbine and the measuring section at the outlet of the turbocharging system (point 4).

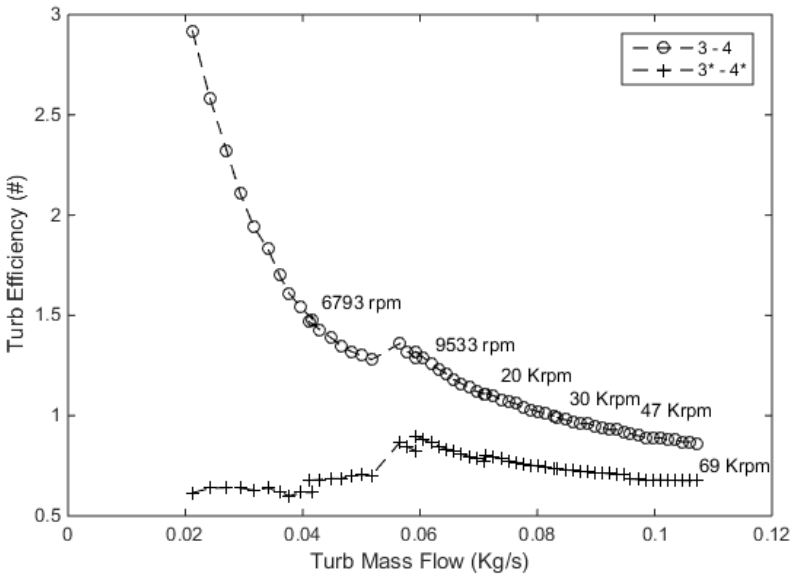

Figure 6. 17: Turbine equivalent two-stage efficiency maps for constant equivalent speed lines at points 3-4 and 3*-4*

Therefore, the same strategy for measuring temperature in the simulation has been adopted in conjunction with the compressors. In fact, the efficiency evaluated through points 3* (HP turbine inlet) and 4* (LP turbine outlet) has resulted in acceptable values of equivalent efficiency, excluding heat transfer at inlet and outlet of HP and LP turbines, respectively. It is important to notice that heat transfer has been set for stainless steel inter-stage ducts without variation of heat transfer multipliers for the data presented in figure 6.17.

6.5 Analysis of thermodynamic processes

An accurate analysis of the thermodynamic processes at the compressors and turbines may provide useful information of the full two-stage system compression and expansion. When the TBP valve is fully closed, the full amount of air flow is compressed and expanded by HP and LP stages. In relation to the compressors, the air enters the HP compressor at the P_1 pressure and exits at the inter-stage pressure $P_{in\text{-}st}$. Due to the inter-stage ducts and heat losses in the ducts, the conditions of HP_{in} and LP_{out} are not the same. In the end, the LP compression brings the air to the condition of HP_{out}. The two-stage compression process is shown in figure 7.18 for the relationship between entropy (*s*), the ability of the system to do thermodynamic work, and enthalpy (*h*), the energy in a thermodynamic system. In addition, the processes in figures 6.18 and 6.19 considers the absence of heat transfer along the turbochargers shafts.

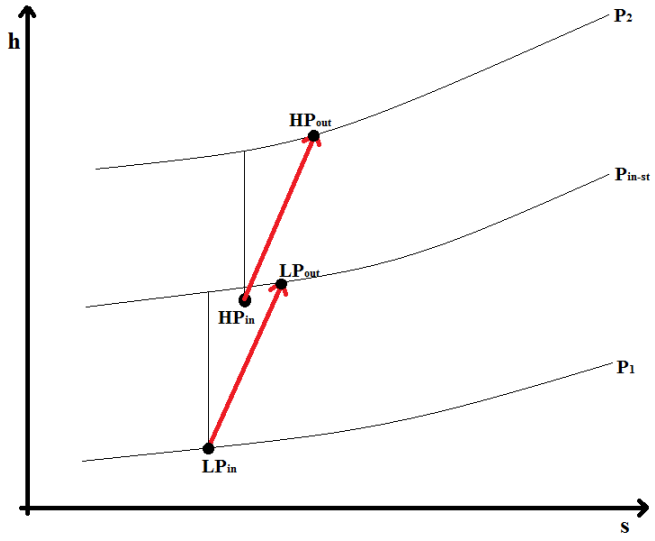

Figure 6. 18: Enthalpy and entropy diagram for the two-stage compression when TBP valve is fully closed

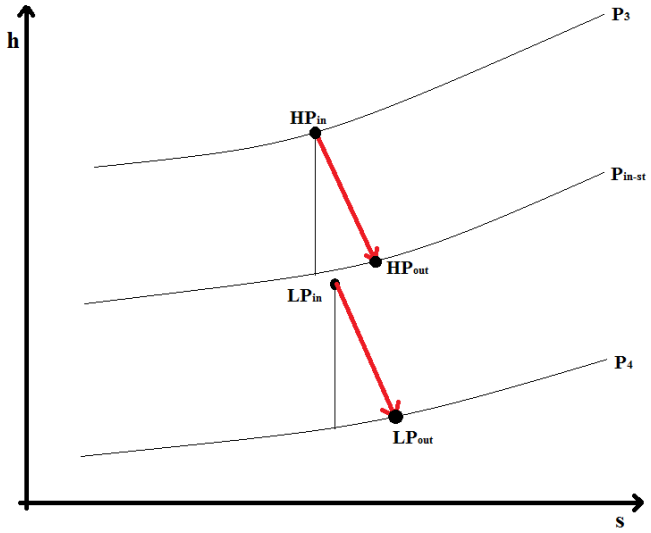

Figure 6. 19: Enthalpy and entropy diagram for the two-stage expansion when TBP valve is fully closed

In the case of expansion, figure 6.19 shows the equivalent process taking place in LP and HP turbines. In the same way, the losses at the inter-stage ducts cause the conditions to change between stages. Opening the TBP valve can cause a change in the expansion processes between the two stages considering that boundary conditions of flow at inlet and outlet of the turbocharging system remain the same in value. Referring to figure 6.18, as the TBP valve opens, $P_{in\text{-}st}$ rises closer to P_2 causing the LP compressor to provide more of the pressure ratio. Moreover, a reduced load on the HP turbine increases the pressure level at the inlet of the LP turbine by pushing $P_{in\text{-}st}$ closer to P_3 in figure 6.19.

6.6 Powertrain simulation

In order to validate the novel mapping methodology developed in the previous section, the 1D model of the 2.2L Diesel engine including the two-stage turbocharging system has been analysed. The engine has been simulated under full load condition at 1000rpm where the by-pass valves are kept completely closed. First of all, the boosting system has been modelled in the standard approach by having the two turbochargers as single units (maps) connected by ducts. Additionally, the equivalent two-stage speed has been calculated by the speed values of the two turbochargers and the equivalent map has been included in the simulation model. In this scenario, the turbocharging system has been modified into the 1D model as one single turbocharger map representing the two units and accounting for the entire processes as shown in figures 6.18 and 6.19. Importantly, the equivalent maps include the presence of heat transfer in the interconnecting ducts as in the standard representation of the two-stage turbocharging system.

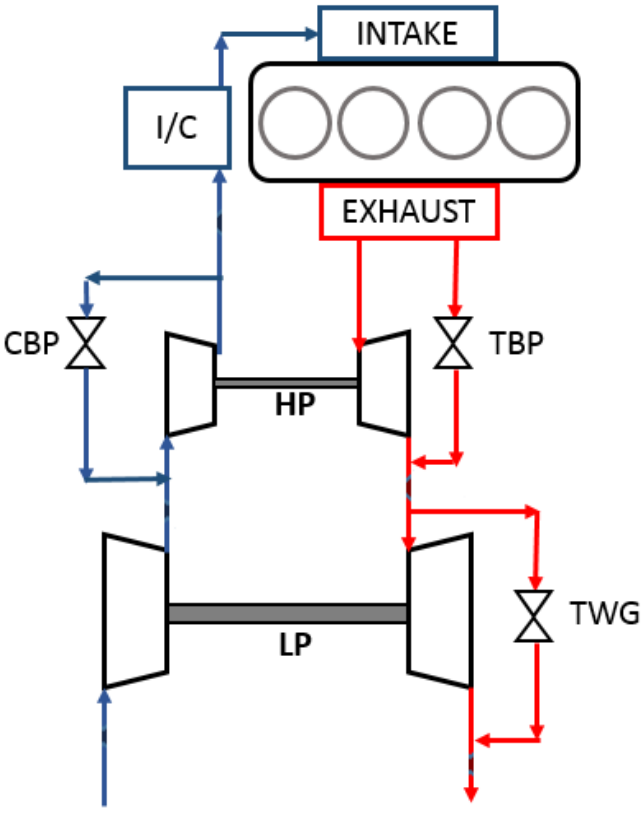

Figure 6. 20: Layout of the 1D engine model including the two turbochargers maps

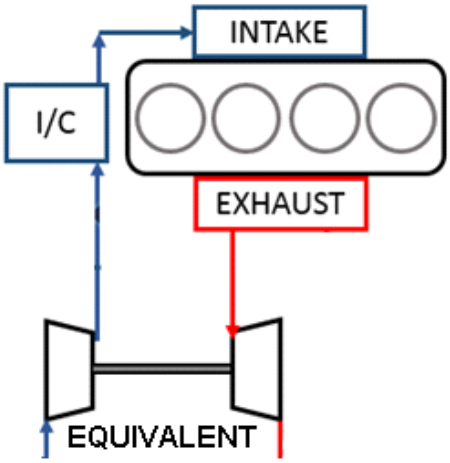

Figure 6. 21: Layout of the 1D model including the equivalent two-stage turbocharger maps

The modelling approaches considering two turbochargers maps and a single equivalent map for the turbocharging system can be seen in figures 6.20 and 6.21. As a result, the same power has been achieved in the two models including representations of standard and equivalent turbocharging systems. In fact, this has been possible owing to a PID controller acting on the amount of fuel injected in the combustion chambers. In order to quantify the benefits of the mapping approach, conditions of the engine air-path have been compared between standard and equivalent turbocharging system representations. The differences recorded are shown in table 6.2 where the maximum error is given by the exhaust temperature prediction. In this case, the standard mapping approach has been considered as the benchmark, referring to the use of independent maps for HP and LP turbomachines without corrections for heat transfer and friction. Although, a perfect match between standard and equivalent approaches would be expected, the variation in table 6.2 could be caused by the data interpolation of the maps in the 1D models [131]. In fact, it is expected that an experimental comparison could be able to provide a deeper outlook.

Table 6. 2: Estimation error for the equivalent mapping approach compared to standard approach

VALUE	ERROR	STANDARD	EQUIVALENT
I/C inlet temperature	+1.94%	422.9K	431.1K
I/C inlet pressure	+2.51%	283KPaA	290KPaA
Exhaust temperature	+5%	915.8K	961.6K
Intake mass flow	-0.47%	239.9Kg/h	238.8Kg/h
Exhaust mass flow	-0.14%	253.9Kg/h	253.5Kg/h

6.7 Chapter summary and conclusions

In this chapter, a mapping methodology to convey the inclusion of interaction effects between turbochargers in two-stage sequential systems has been proposed and analysed through 1D simulations. Additionally, the main conclusions can be drawn as follows:

- The equivalent speed term has been found capable of representing the two-stage turbocharging system. Neither LP nor HP constant turbocharger speed lines could be adopted for representing the performance of the system when the TBP valve is open.

- Moreover, into the 1D model, the temperatures in the measuring sections have not been able to provide useful information over the efficiency of the turbocharging system. This could be caused by the difficulties in tuning the 1D model for pressure and heat transfer in each single duct.

- Reduced errors can be achieved in the prediction of the air-path status with the adoption of the equivalent map when compared to the standard representation of two-stage turbocharging systems.

- Furthermore, the investigation suggests that mapping two-stage turbocharging systems as a full system into a steady turbocharger gas-stand can represent effectively the real performance of the boosting technology.

Chapter 7 – Mapping of two-stage turbocharging system in steady turbocharger gas-stand

In this chapter, the influence of mapping methodology on the performance map of a two-stage turbocharging system is described. In particular, the study researches the accuracy of equivalent two-stage maps in comparison to stand-alone turbochargers maps for HP and LP stages. The investigation focuses on the comparison of combined stand-alone measured performance maps and equivalent maps of the two-stage system. Initially, the chapter describes the experimental setting and campaign to perform the study in the steady turbocharger gas-stand. Moreover, stand-alone and equivalent maps of the turbocharging stages are measured under adiabatic and diabatic conditions. In addition, the procedure for combining stand-alone maps of the two turbochargers is described in the chapter. Lastly, the main outcome is reported in the analysis of equivalent and combined maps, as measured and heat corrected, in regards to the variation of system performance.

Furthermore, the investigation reported in this chapter has been published in the Journal of Energy [132].

7.1 Inter-stage phenomena in two-stage turbocharging systems

The increasing demand for environmental friendly automobiles is leading the efficiency improvement and reduction of harmful emissions in internal combustion engines, adopting key strategies, such as HP and LP EGR [133, 134], turbocharging [86] and waste heat recovery solutions [135]. Furthermore, the reduction of engine swept volume and number of cylinders is able to improve thermal efficiency of internal combustion engines, through the decimation of friction losses [12]. Therefore, the adoption of boosting technologies is a necessary action to restore rated power of downsized internal combustion engines at steady [136] and transient [85] operations. In this scenario, two-stage turbocharging systems are able to impact positively on the engine pumping losses [28] and powertrain system flexibility [137]. In fact, the choice of a two-stage system results in a wider flow range operation, generating high levels of boost at every engine speed, as the maximum pressure ratio is not delivered by a single turbocharger [138]. In this way, reduction of mechanical and thermal stresses on the single turbocharger is reduces [139]. However, two-stage turbocharging systems lead to a rise of system complexity in regards to powertrain control [140].

In these boosting technology, HP and LP turbochargers are connected sequentially and regulated via by-pass valves [35]. In fact, exhaust gases of the internal combustion engine are ingested by the HP turbine, incurring a first expansion phase, and the LP turbine, being subjected to the last expansion phase. As well as turbines, the air is compressed sequentially by LP (high mass flow and rotating inertia) and HP (low mass flow and rotating inertia) compressors. In conditions of elevated engine speed, the exhaust flow is diverted away from the HP turbine inlet via the TBP valve, in order to expand exhaust gasses in LP turbine and reduce engine back-pressure. The HP CBP valve is activated at high mass flows, to avoid choking of the HP compressor and performance disruption of the two-stage system. Furthermore, the sequence of HP and LP turbochargers can generate swirling motion of the flow, causing a variation of performance maps of two-stage systems [11].

Analysis of turbochargers performance in two-stage regulated systems has stated that performance changes in the HP compressor and LP turbine can occur [30]. Specifically, reduction of swallowing capacity and pressure ratio of LP turbine and

HP compressor, respectively, can be recorded in comparison to the stand-alone maps. Moreover, LP turbine and HP compressor also appear to deliver lower efficiencies in two-stage regulated systems [30]. In reference to this, it is important to focus on the cause of performance distortion of the turbomachine in sequential systems. In fact, the presence of complex ducting geometries at the inlet of the HP and LP compressors causes a variation of the performance map measured with straight ducts, as is typical in gas-stands [74, 141]. In the case of radial turbines, swirling flows generated at the HP turbine outlet cause vortexes at the LP turbine inlet, resulting in a variation of LP turbine efficiency [142]. As well as turbines, the presence of pre-whirl can distort pressure ratio and efficiency of compressors in two-stage systems [65]. Additionally, in diabatic operations of the two-stage system, heat transfer from turbines to compressors influences thermodynamic boundary conditions of the turbomachinery [57, 58].

7.2 Experimental setting

7.2.1 Full two-stage system and stand-alone turbochargers

In order to perform the study, a two-stage sequential turbocharging system with regulating valves has been experimentally investigated. In this system layout, HP and LP turbochargers are connected in series with CBP and TBP valves controlling the operation across a vast range of mass flows through compressors and turbines. In fact, the two turbochargers have different sizes in order to be able to generate elevated levels of boost at low and high mass flow rates. Specifically, as in table 7.1, HP and LP compressors have wheel diameters of 40cm and 60cm, respectively. Clearly, in figure 7.1, the pressure at point 3 is varied in order to control the expansion ratio in the turbine stages. Meanwhile, the load created by HP and LP compressors is generated though a back-pressure valve at point 2 in the turbocharger gas-stand.

Table 7. 1: Characteristics of HP and LP turbochargers, including compressor and turbine sizes, maximum rotating speed and VGT position

STAGE	COMPRESSOR SIZE	TURBINE SIZE	MAXIMUM SPEED	VGT POSITION
HP	40cm	36cm	260Krpm	50% shut
LP	60cm	47cm	186Krpm	50% shut

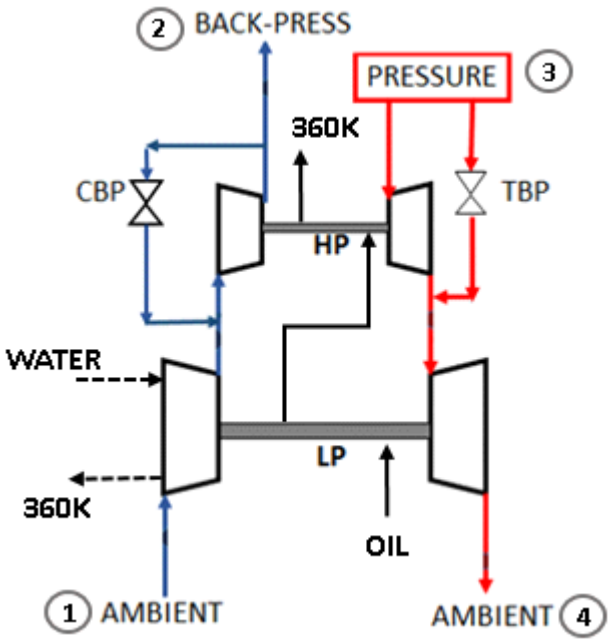

Figure 7. 1: Schematic of two-stage turbocharging system with regulating valves: TBP and CBP, as installed in the turbocharger gas-stand

In according to the definition of equivalent two-stage map [117], turbine and compressor equivalent maps are evaluated across the two stages, as in figure 7.1, using the definitions of pressure ratio (*PR*), mass flow rate ($\dot{m}$) and efficiency (η) for compressor and turbine in equations 8.1-6, respectively. In this scenario, the two-stage system is treated as a single turbocharger with compression and expansion processes. The equivalent mass flow rate of compressor and turbine are corrected for pressure (P_{ref}) and temperature (T_{ref}), being equivalent to 298K and 1bar for compressor and 288K and 1atm for turbine, similarly to the turbochargers manufacturer. In equation 8.1, the total-to-total (T-T) pressure ratio ($PR_{t\text{-}t}$) is defined for the compressor as the ratio between outlet (P_{t2}) and inlet (P_{t1}) total pressure. In regards to mass flow rate in the compressors ($\dot{m}_c$), correction from measured total temperature (T_{t1}) and pressure (P_{t1}) conditions to reference values is shown in equation 7.2. Furthermore, total-to-total compression efficiency ($\eta_{t\text{-}t}$) is shown in equation 7.3, relating isentropic and adiabatic compressions, including the ratio of specific heats (γ).

$$PR_{t-t} = P_{t2}/P_{t1} \tag{7.1}$$

$$\dot{m}_{c,corr} = \frac{\dot{m}_c\sqrt{T_{t1}/T_{ref}}}{P_{t1}/P_{ref}} \tag{7.2}$$

$$\eta_{t-t} = \frac{T_{t1} * \left(PR_{t-t}^{\gamma-1/\gamma}\right)}{T_{t2}/T_{t1}} \tag{7.3}$$

The definition of compressor performance, pressure ratio ($PR_{t\text{-}s}$), corrected mass flow ($\dot{m}_{t\_corr}$) and turbine net efficiency (η_{net}) are considered in equations 7.4-6. Similarly to the compressor, turbine pressure ratio is calculated between turbine inlet (P_{t3}) and outlet (P_{s4}) pressures. Additionally, mass flow is corrected by turbine inlet temperature (T_{t3}) and pressure, in conjunction with reference conditions. In particular, turbine net efficiency replaces the total-to-static expansion efficiency, due to the dependency on adiabatic turbine power, accounting for turbine outlet temperature. In fact, the presence of swirling flows at the turbine outlet could

introduce inaccuracy in the estimation of turbine total-to-static efficiency. In fact, turbine net efficiency of equation 7.6 considers the ratio between compressor power ($Power_c$) and turbine isentropic power ($Power_{T,is}$). This definition lumps the friction into the definition of turbine net efficiency.

$$PR_{t-s} = P_{t3}/P_{s4} \tag{7.4}$$

$$\dot{m}_{T,corr} = \frac{\dot{m}_T\sqrt{T_{t3}/T_{ref}}}{P_{t3}/P_{ref}} \tag{7.5}$$

$$\eta_{net} = \frac{Power_c}{Power_{T,is}} \tag{7.6}$$

Due to the dependency between the performance of the turbocharging system and the speeds of HP and LP stages, an equivalent two-stage system speed [117] has been defined in equation 7.7 and corrected for inlet total temperature ($T_{t,in}$) of turbine or compressor in equation 7.8. Accordingly to the definitions in equations 7.1-8, the equivalent two-stage system maps can be generated in the steady turbocharger gas-stand, treating the turbocharging system as a single turbocharger.

$$N_{eq} = N_{LP} * \left(\frac{N_{LP}}{N_{HP}}\right) \tag{7.7}$$

$$N_{eq,corr} = N_{eq}\sqrt{T_{ref}/T_{t,in}} \tag{7.8}$$

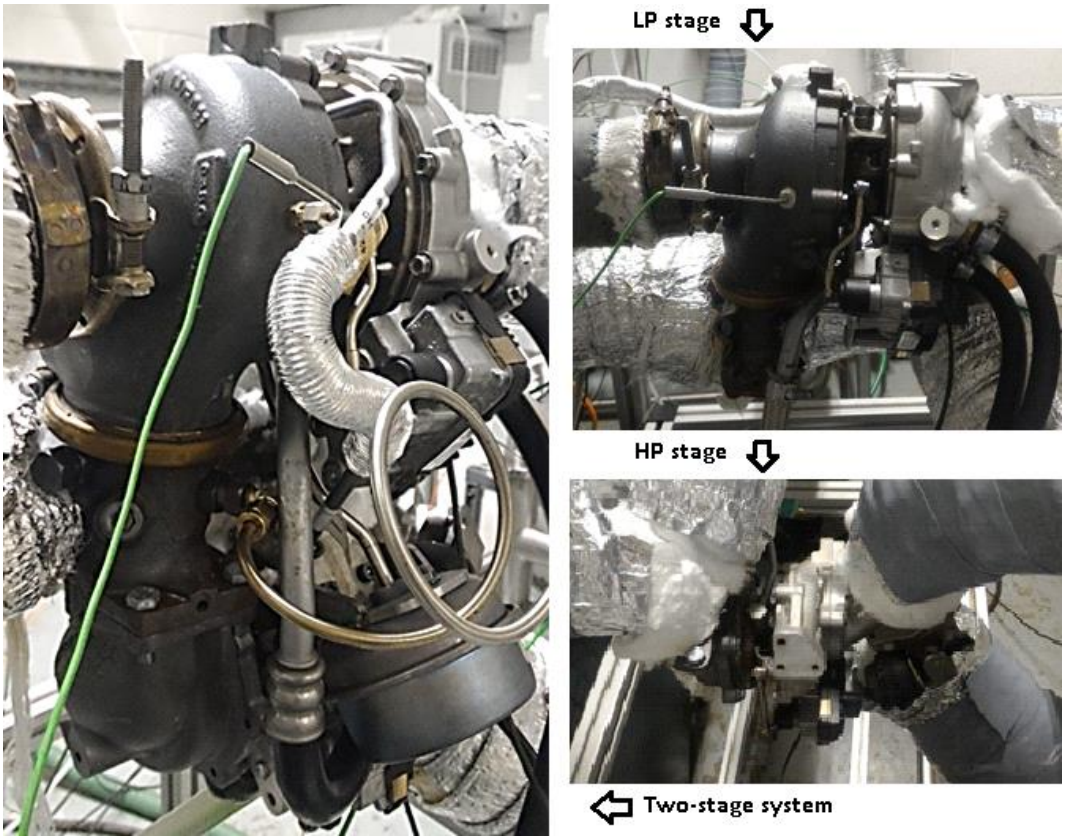

Figure 7. 2: On the left hand-side, the two-stage turbocharging system installed in the steady turbocharger gas-stand. The LP turbocharger is positioned on top, while, the HP turbocharger is connected at the bottom of the exhaust manifold. On the right hand-side, LP and HP stage in stand-alone configuration

In the proposed study, in order to focus on the effect of inter-stage phenomena on two-stage system performance prediction, the TBV valve is constrained to the fully closed position. In addition, the VGT of both HP and LP stages fixed at 50% between minimum and maximum allowable opening area. Due to the complexity of the turbocharging system design, difficulties persist in the estimation of the effect of VGT on the opening area of HP and LP turbines. Therefore, HP and LP turbochargers have been treated as fixed geometry turbines with a reduction of the operating range, reducing the VGT to 50%. In conjunction with the testing of the full two-stage system, stand-alone HP and LP turbochargers have been investigated in the steady turbocharger gas-stand, as shown in figure 7.2.

7.2.2 Experimental campaign

Both HP and LP turbochargers have been mapped under adiabatic and diabatic conditions in order to quantify the heat correction of the turbochargers. Due to the presence of a water-cooling housing in the LP compressor, tests w/ and w/o cooling effects have been performed in both the two-stage system and the LP turbochargers in stand-alone configurations. In case of adiabatic maps, compressor outlet and turbine inlet temperatures are matched, although the bearing housing is controlled at an SAE 5W-30 oil outlet temperature of 360K. Although, this condition may not represent complete adiabatic conditions of the turbocharger [143], the dependency of compressor and turbine power from friction changes between adiabatic and diabatic maps is reduced [79]. Furthermore, in case of diabatic maps, the TIT is maintained at 773K for both LP and HP turbochargers whilst lubricating oil temperature is controlled at 360K. In summary, the experimental campaign for the study is reported in the test matrix of table 7.2.

Table 7. 2: Test matrix for HP and LP turbochargers and the full two-stage system. The adiabatic test is performed matching compressor outlet and turbine inlet temperature

	ADIABATIC	DIABATIC AT 773K TIT w/o WATER-COOLING	DIABATIC AT 773K TIT w/ WATER-COOLING
HP stage	√	√	NA
LP stage	√	√	√
Two-stage	NA	√	√

7.3 Experimental results

7.3.1 Equivalent two-stage maps

In figure 7.3, equivalent two-stage maps for compressor and turbine are generated in the turbocharger gas-stand w/ and w/o water-cooling at the LP compressor. In the case of compressor cooling, the downstream compressor coolant temperature is maintained at 360K. It is important to notice that the corrected speed lines in figure 7.3 relates to the equivalent speed term of equation 7.8. As visible, the equivalent two-stage compressor and turbine maps have been limited to 46Krpm and 28.3Krpm, respectively, corresponding to 200Krpm and 100Krpm of HP and LP turbochargers, respectively.

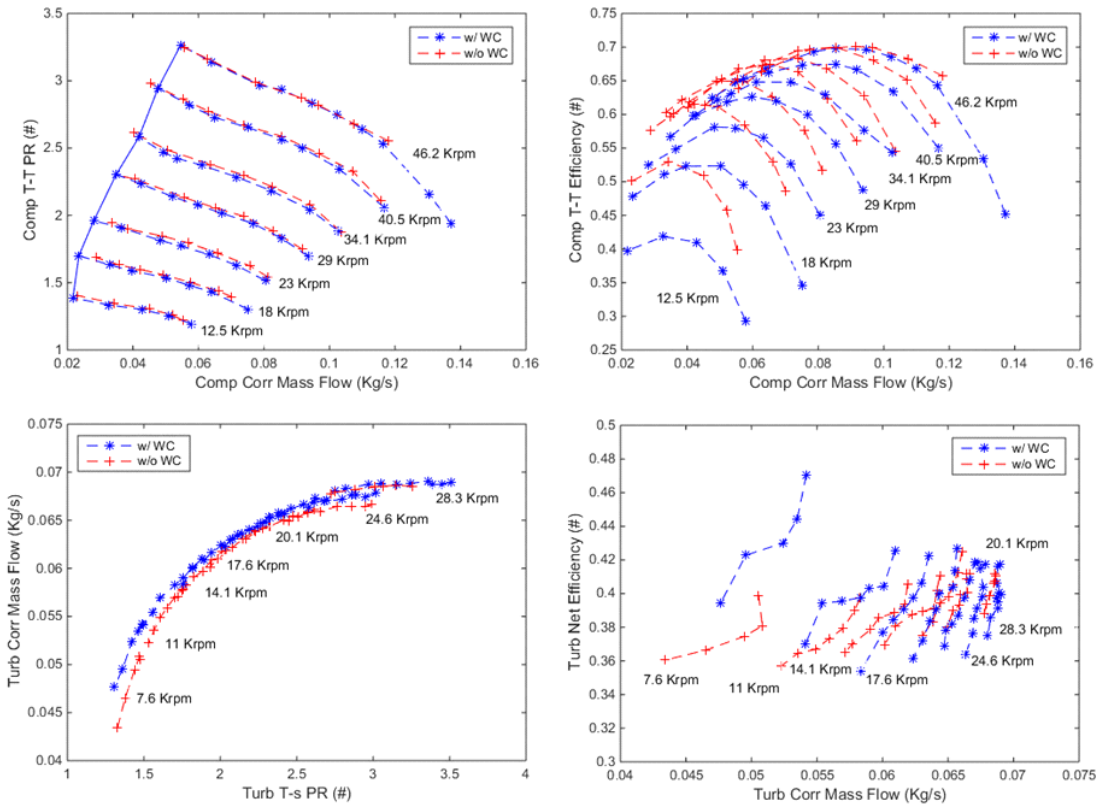

Figure 7. 3: At the top, equivalent performance map for the two-stage compressors. At the bottom, equivalent performance map for the two-stage turbines. Two cases w/ and w/o water-cooling at the LP compressor are considered

The adoption of a water-cooling system at the LP compressor has a negative effect on the equivalent compressor total-to-total (T-T) efficiency, due to the downstream compressor water temperature controlled at 360K. In this scenario, the water-cooling system can extract and introduce heat to the LP compressor flow due to the

constantly controlled temperature of 360K. However, as visible at the top right corner of figure 7.3, compressor efficiency is lower in the presence of water-cooling for the vast majority of speed lines. In addition, a small reduction of available pressure ratio in the two-stage system is obtained, in comparison to the case of the uncooled LP compressor. The increase in turbine net efficiency (η_{net}), for the case w/ water-cooling, could be supported by an increase in apparent compressor work, due to the lower compressor efficiency. Meanwhile, the effect of water-cooling LP compressor housing shows a small change in turbine swallowing capacity at low pressure ratios, perhaps, due to the variation of compressor power demand.

7.3.2 Stand-alone turbochargers maps

In order to analyse the influence of inter-stage effects on the prediction of two-stage system performance, stand-alone turbochargers maps would have to be measured, resembling operating conditions of the complete system. In conjunction with the equivalent two-stage maps generated in the turbocharger gas-stand at diabatic conditions, stand-alone maps for HP and LP turbochargers would have to be investigated at similar conditions of heat transfer. However, it is important to consider that temperature at inlet of HP compressor would be higher than ambient, while ,TIT of LP turbine could be lower than 773K [11].

The investigation of adiabatic and diabatic compressor maps is able to provide correct estimation of heat transfer and effective efficiencies at compressors and turbines [57]. For both LP and HP turbochargers, the quantification of the heat transfer term to the compressor is possible, assuming that the heat source is added to the flow following the adiabatic compression. Meanwhile, the heat transfer term is included at the turbine entry, due to the temperature dependency of the expansion processes on the turbine efficiency. In this way, heat corrected efficiencies for LP and HP compressors and turbines can be estimated, as shown in figures 7.4 and 7.5.

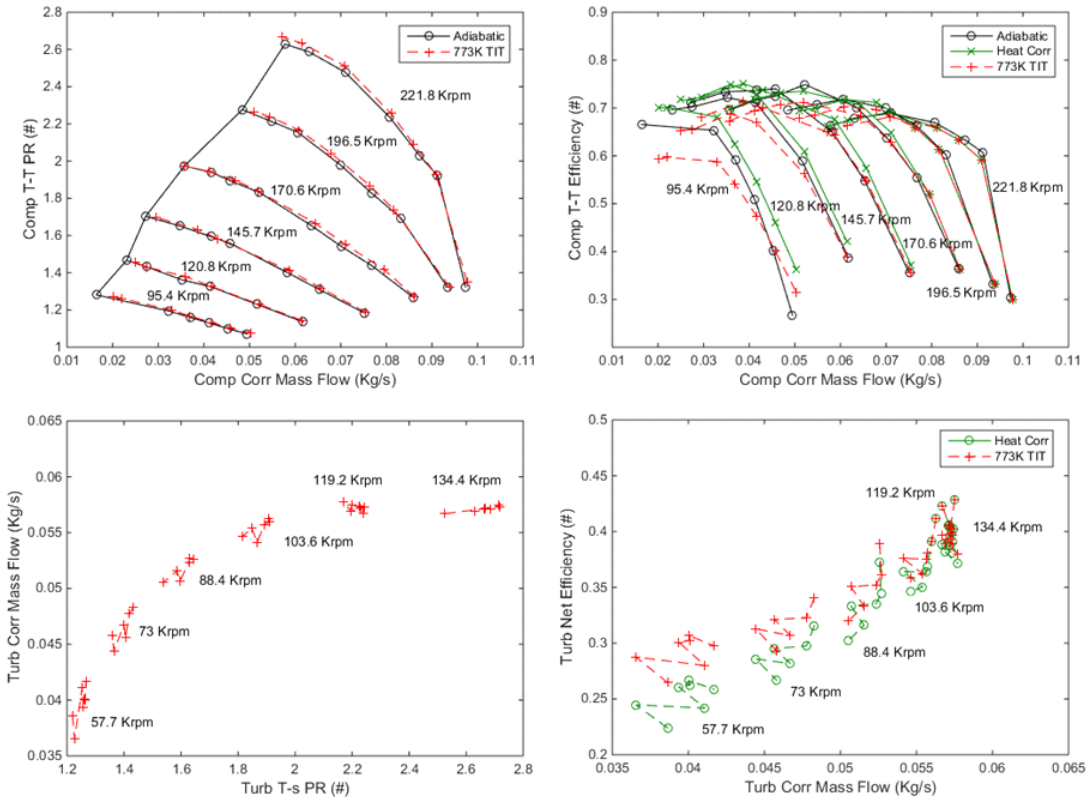

Figure 7. 4: HP compressor, at the top, and turbine, at the bottom, performance maps, as adiabatic, diabatic and heat corrected are shown

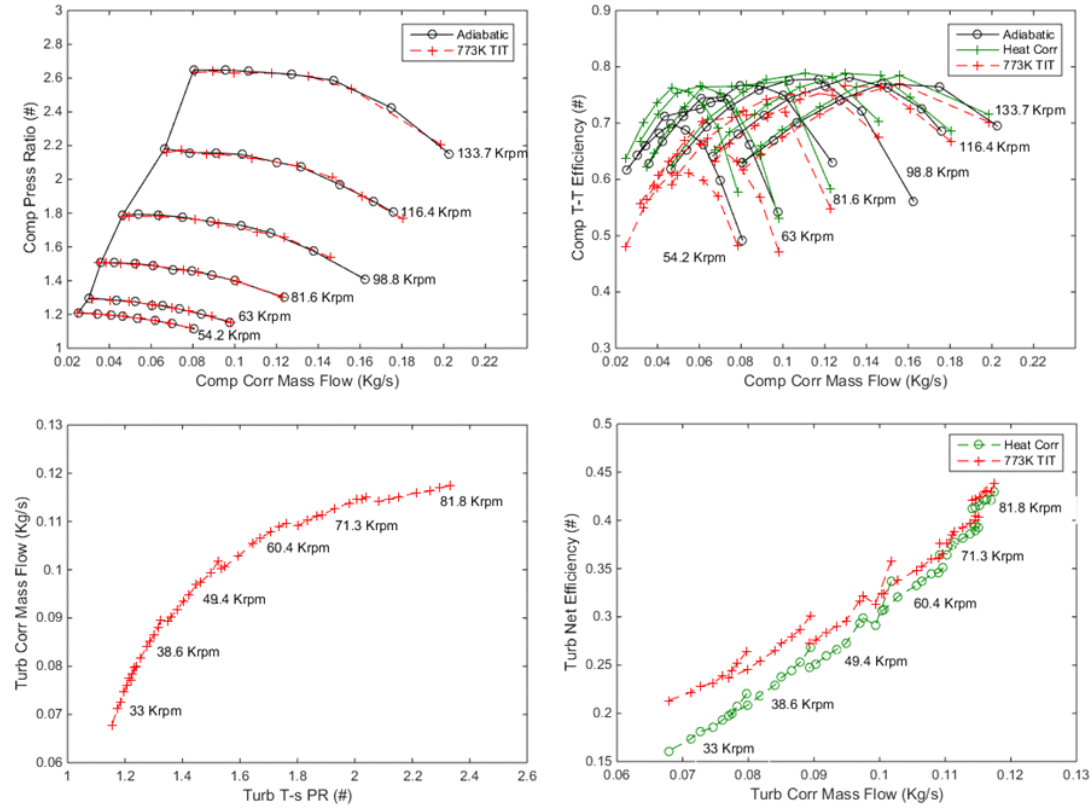

Figure 7. 5: LP compressor, at the top, and turbine, at the bottom, performance maps, as adiabatic, diabatic and heat corrected are shown

In figures 7.4 and 7.5, variations in compressor efficiency can be noticed between adiabatic and diabatic conditions for both HP and LP turbochargers. Specifically, the diabatic efficiency decreases significantly, at low corrected compressor mass flow rates, in comparison to the adiabatic efficiency. In the case of turbines, the adiabatic map could not be generated, due to varying TIT and corrected speed terms. Furthermore, heat corrected efficiencies have been calculated for both turbine and compressor. As visible in both figures 7.4 and 7.5, compressor efficiency is closer to adiabatic operations, when heat corrections are applied. On the other side, a reduction of turbine net efficiency is obtained with heat correction, due to lower power required by HP and LP compressors, in figures 7.4 and 7.5, respectively.

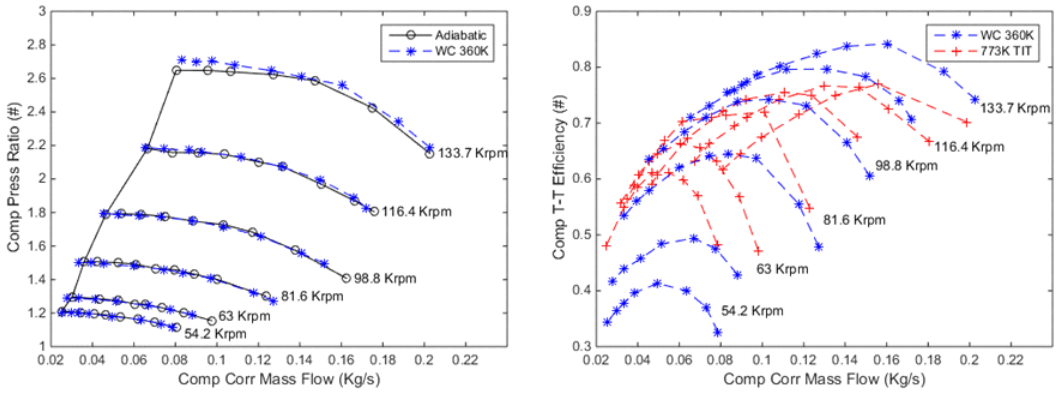

Figure 7. 6: At the left hand-side, LP compressor performance map for adiabatic and water-cooled conditions at 90degC (WC 360K). At the right hand-side, apparent LP compressor T-T efficiency

Due to the variation experienced with the equivalent two-stage compressor efficiency in figure 7.3, the effect of water-cooling on LP compressor performance has been analysed. In figure 7.6, the maximum speed line tested on the LP compressor has shown a rise in pressure ratio, in comparison to adiabatic conditions. In fact, in the presence of water-cooling, a significant increase in apparent compressor efficiency is recorded. Specifically, the apparent compressor efficiency reaches values higher than 0.8 at 133.7Krpm. Meanwhile, peak efficiency at 54.2Krpm reduces from 0.6, at diabatic operations, to 0.4, at water-cooled conditions.

Applying the correction for heat and cooling power to the temperature related LP compressor efficiency (apparent) in the gas-stand can lead to the analysis of water-cooling effects on the compression process. In figure 7.7, the variation of

compressor efficiency, due to water-cooling system controlled at a downstream water-flow temperature of 360K, is shown. As visible in figure 7.7, the efficiency corrected for water-cooling power (Cool Corr) is higher than adiabatic and heat corrected efficiency values at mass flow operations lower than peak efficiency points at 116.4Krpm and 133.7Krpm. At lower speeds of the LP turbocharger, the water-cooling system is not able to extract heat from the compression process, due to compressor outlet temperatures unable to reach 360K. In addition, owing to a more efficient compressor, the cool corrected turbine net efficiency is affected.

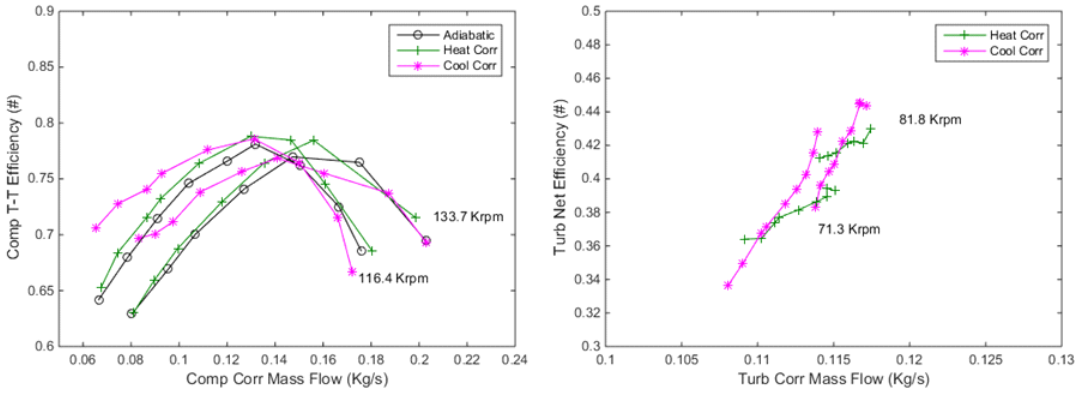

Figure 7. 7: At the left hand-side, adiabatic, heat and coolant corrected compressor T-T efficiency. At the right hand-side, heat and coolant corrected turbine net efficiency for the two highest LP turbine corrected speeds tested in gas-stand

7.3.3 Map correction

The turbocharger gas-stand is extremely important for the performance evaluation of compressors and turbines. However, the small distances between turbine and compressor wheels in turbochargers can cause the measurement of diabatic compression and expansion processes, in case of heat sources introduced at the turbine inlet [34]. In this scenario, corrections of performance would have to be performed, in order to distinguish between heat and thermodynamic work. The evaluation of adiabatic maps in the turbocharger gas-stand reduces the requirements for heat transfer models [62]. However, adiabatic and diabatic maps would have to be experimentally measured, in the steady gas-stand, increasing the testing time. It is important to state that the focus of the investigation here is with regard to the comparison of equivalent and combined maps for two-stage turbocharging systems. In addition, the map correction procedure is adopted to differentiate between turbocharger shaft power and heat. Therefore, after assuming

the total energy balance across the turbocharger operating in adiabatic operations, the friction power can be calculated for HP and LP turbochargers. Specifically, the turbochargers are non-insulated, while, ducts around the turbochargers are covered with thermal blankets. Therefore, a small amount of heat is able to escape to the ambient by the turbocharger housing.

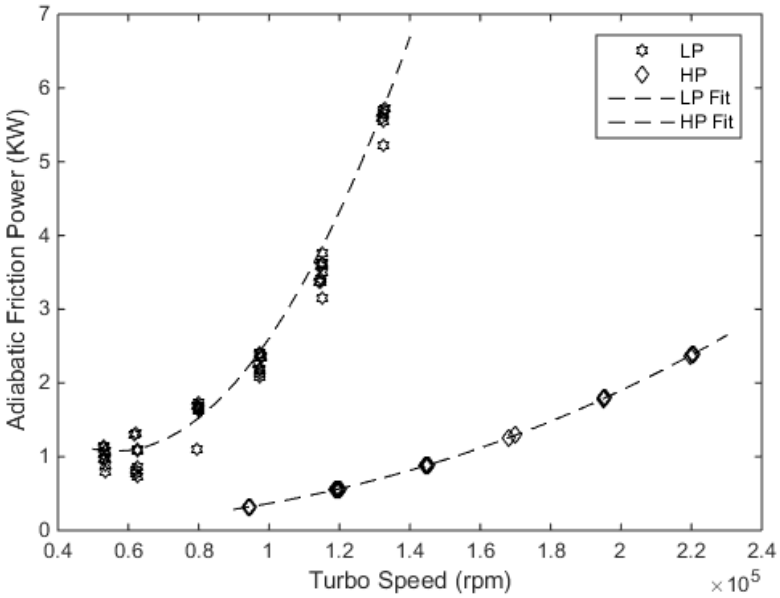

Figure 7. 8: Relationship between adiabatic friction power and turbo speed for HP and LP turbochargers. Best-fit curves for HP and LP turbochargers as dashed lines

The difference in turbocharger sizes has resulted in a different magnitude of friction losses, as presented in figure 7.8. Specifically, although the HP turbocharger is tested at rotating speeds of about 220Krpm, the friction losses account for about 2.5KW. In the case of LP turbocharger, the same amount of friction power is achieved at about 100Krpm. Moreover, the relationship between shaft speed and friction power develops differently for the two turbochargers.

$$Power_f = Power_{T,adia} - Power_{c,adia} \tag{7.9}$$

$$Power_c = \dot{m}_c\left(h_{t,2} - h_{t,1}\right) = \dot{m}_c\left(c_{p2}T_{t,2} - c_{p1}T_{t,1}\right) \tag{7.10}$$

$$Power_T = \dot{m}_T\left(h_{t,3} - h_{s,4}\right) = \dot{m}_T\left(c_{p3}T_{t,3} - c_{p4}T_{s,4}\right) \tag{7.11}$$

The friction power for both the HP and LP turbochargers is calculated, assuming an energy balance between measured compressor and turbine powers at adiabatic conditions. In equation 7.9, assuming that heat transfer is not occurring at adiabatic conditions, friction power ($Power_f$) is equal to the difference between adiabatic turbine ($Power_{T,adia}$) and compressor ($Power_{c,adia}$) powers. As expressed in equation 7.10, compressor power is given by the total enthalpies difference at inlet ($h_{t,1}$) and outlet ($h_{t,2}$) and the compressor mass flow rate ($\dot{m}_c$). In addition, equation 7.11 expresses the turbine expansion power ($Power_T$), depending on turbine mass flow rate ($\dot{m}_t$), total inlet ($h_{t,3}$) and static outlet ($h_{s,4}$) enthalpies. In both equations 7.10 and 7.11, enthalpy is expressed as product between specific heat capacity at constant pressure (c_p) and temperature (*T*). In this scenario, the assumption of friction independency from variation of axial trust is stated, although, this could differ between adiabatic and diabatic operations [59].

In the case of diabatic operations with a TIT of 773K, the heat correction is performed, considering the compressor and turbine performance have been measured at both adiabatic and diabatic conditions. Due to heat transfer, the compressor power at diabatic operations ($Power_{c,dia}$) is higher than the adiabatic compressor power ($Power_{c,adia}$). Therefore, the change in power ($\dot{Q}_c$) can be estimated in equation 7.12. The heat from turbine to compressor (q_c) is evaluated for HP and LP turbochargers as in equation 7.13.

$$\dot{Q}_c = Power_{c,dia} - Power_{c,adia} \tag{7.12}$$

$$q_c = \dot{Q}_c / \dot{m}_c \tag{7.13}$$

In order to calculate the total heat escaping the turbine (q_T), the same process of equations 7.12 and 7.13 is implemented, as reported in equations 7.14 and 7.15. In particular, $\dot{Q}_T$ represents the heat power escaping the turbine, $Power_{T,dia}$ and $Power_{T,adia}$ represent turbine power for diabatic and adiabatic maps, respectively.

$$\dot{Q}_T = Power_{T,dia} - Power_{T,adia} \tag{7.14}$$

$$q_T = \dot{Q}_T / \dot{m}_T \tag{7.15}$$

Furthermore, adiabatic and diabatic maps have allowed for the calculation of specific heat flow to the compressor, assuming that heat addition to the compressor is occurring after the compressor. In figures 7.9 and 7.10, the relationship between compressor and turbine heat and mass flow for HP and LP turbochargers is shown. It is visible that the specific heat flow is significantly higher in magnitude at the LP compressor, achieving about twice the amount of HP compressor energy at 0.02Kg/s. Additionally, the specific heat flow consists of 2KJ/Kg at about 0.07Kg/s, in the HP compressor, and 0.14Kg/s, in the LP compressor. A different trend is observed for the specific heat flow escaping the turbine. In fact, the amount of heat is similar between HP and LP turbines, although a shift towards higher mass flows is recorded for the LP compressor.

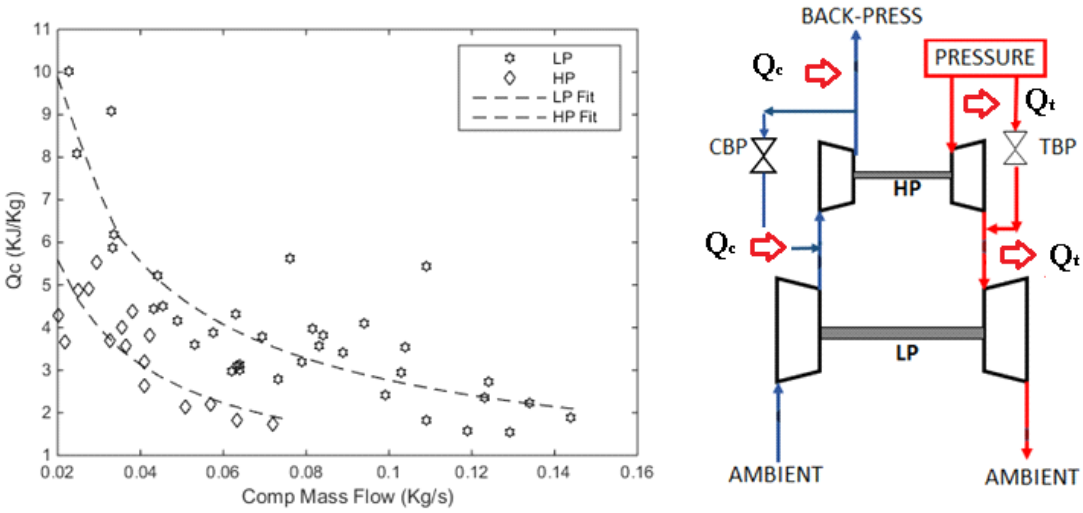

Figure 7. 9: Relationship between specific compressor heat flow and compressor mass flow for HP and LP turbochargers. Best-fit curves for HP and LP turbochargers as dashed lines. Positive specific heat flow is transmitted to the compressor

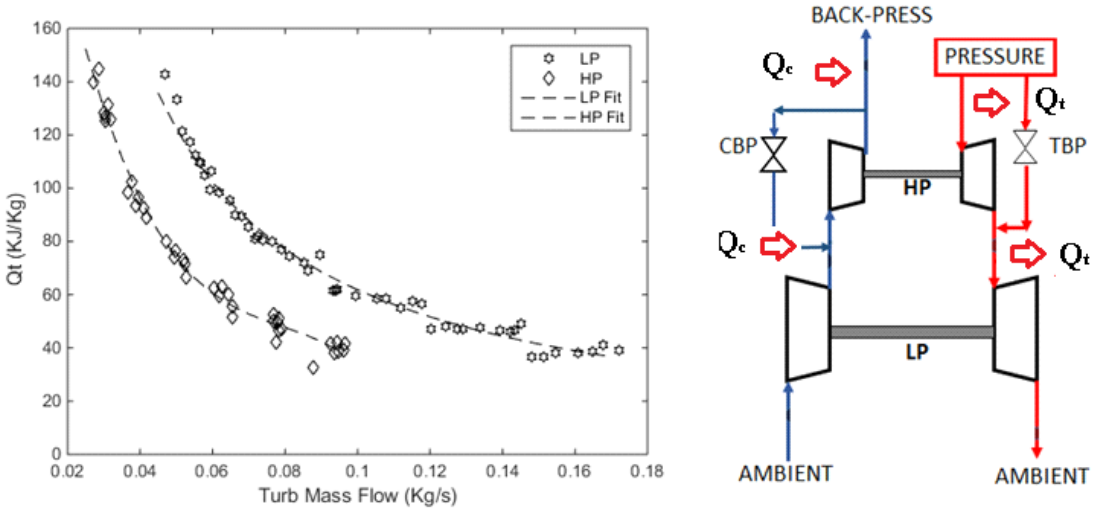

Figure 7. 10: Relationship between specific turbine heat flow and turbine mass flow for HP and LP turbochargers. Best-fit curves for HP and LP turbochargers as dashed lines. Positive specific heat flow is escaping the turbine

In order to evaluate the changes in compressor efficiency with the introduction of water-cooling systems at the LP compressor housing, the multiple effects of heat and cooling flow would have to be subtracted from the measured compressor efficiency in the gas-stand (equation 7.9). In this perspective, the cooling power is analysed from availability of friction and effective turbine powers.

In order to calculate the effective LP compressor power ($Power_{eff}$) under diabatic conditions, including the water-cooling system at the LP compressor, equation 7.16 should be applied. In fact, effective compressor power in the presence of water-cooling system would be equal to the difference between the measured apparent power in the gas-stand ($Power_{app}$) and both heat source from hot turbine ($\dot{Q}_c$) and power extraction from the water-cooling system ($Power_{cool}$). However, due to the absence of experimental data from the water-cooling unit, compressor effective power is calculated adopting equation 7.17. In this case, effective compressor power depends on the diabatic turbine power at active compressor water-cooling system ($Power_{T,dia(WC)}$), the heat source to the compressor from the turbine ($\dot{Q}_c$) and the friction power ($Power_f$). Therefore, equation 7.17 assumes a power equilibrium across the turbocharger, allowing for the calculation of the effective (coolant and heat corrected) compressor power.

$$Power_{eff} = Power_{app} - \dot{Q}_c - Power_{cool} \quad (7.16)$$

$$Power_{eff} = Power_{T,dia(WC)} - \dot{Q}_T - Power_f \quad (7.17)$$

Moreover, the cooling capacity of the LP compressor along the entire mapped operations is shown in figure 7.11. In this graph, significant benefits on compressor efficiency from the water-cooling system can be achieved at compressor speeds above 100Krpm. At high speed, cooling capacity is less dependent on compressor mass flow. At the maximum tested speed of the LP turbocharger, 1.25KW can be extracted, as shown in figure 7.11.In addition, for rotational speeds below 100Krpm, the cooling system is adding heat to the compressor, due to conditions of compressor outlet temperatures below 360K. This is supported by the positive sign on the cooling power, achieving 1.5KW.

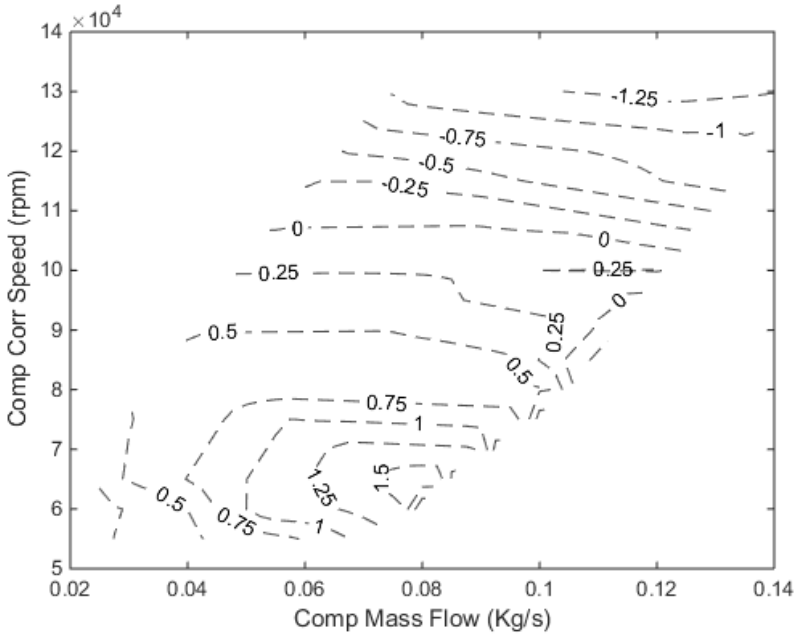

Figure 7. 11: Contour plot of cooling power (KW) in relation to compressor mass flow and LP turbocharger speed. Negative power values represent cooling action of water on compressor outlet flow

7.4 Two-stage performance prediction

7.4.1 Equivalent and combined maps

In order to evaluate the gap in performance prediction of the two-stage turbocharging system, analysis of equivalent two-stage and combined stand-alone HP and LP maps could provide accurate information. In fact, inter-stage phenomena occurring between HP and LP turbochargers could affect the performance of the entire two-stage system. In this scenario, the equivalent two-stage maps for compressors and turbines generated under diabatic conditions should be compared to combined maps of the two turbochargers. The process of maps combination is performed in a 1D model of the steady turbocharger gas-stand, similarly to figure 6.9. HP and LP turbochargers are represented by the stand-alone maps measured in the engine gas-stand at diabatic (773K) and adiabatic conditions, including heat transfer corrections. The 1D model is adopted for the combination of maps and the analysis of boundary conditions of each turbocharging stage. The 1D modelling approach is widely adopted for the analysis of two-stage systems in automotive powertrains [16, 25, 29]. It is important to consider that inter-stage components have been included in the mapping procedures of stand-alone HP and LP turbochargers. Therefore, the inter-connecting ducts should not be represented into the 1D model as previously included in the measured maps. Specifically, measured HP and LP turbochargers speeds are imposed and performance across the two turbochargers are calculated, as shown in the diagram of figure 7.12. Due to the possibility of difference in HP and LP turbocharger speeds in the measured equivalent map, extrapolation of unmeasured speed values is done through quadratic fits to regions of the speed lines via least squares regression.

The process in figure 7.13 highlights the maps combination. Firstly, the temperature and pressure conditions at inlet of HP turbine and LP compressor are imposed, as well as, the ambient conditions at LP turbine and HP compressor outlets. Secondly, HP and LP turbocharger speeds are imposed, accordingly to speed values in the measured equivalent map. Finally, in order to generate the combined maps, the back-pressure at compressor system is imposed, matching the mass flow through turbines and compressors. Furthermore, heat correction at HP and LP turbochargers are included as heat sources, in the case of adiabatic maps.

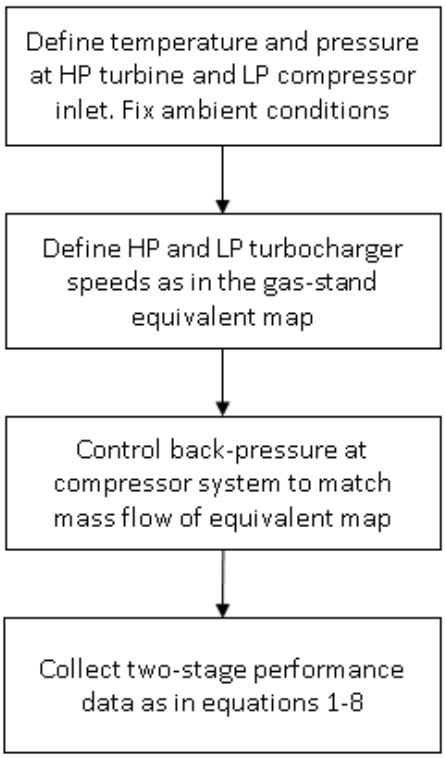

Figure 7. 12: Diagram resembling the combination process of stand-alone HP and LP maps occurring into a steady 1D model

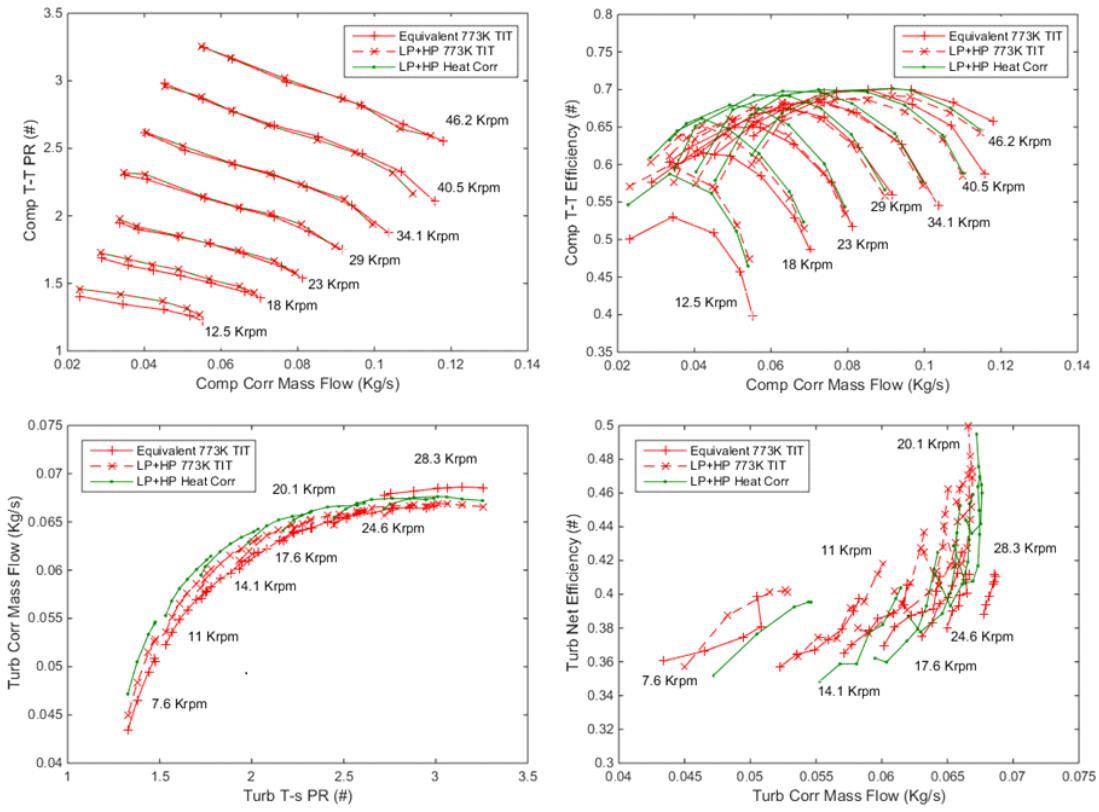

Figure 7. 13: Compressor, at the top, and turbine, at the bottom, performance maps of equivalent two-stage system at diabatic conditions and combined stages at diabatic conditions w/ and w/o heat corrections

The results of figure 7.13 show a significant different in both pressure ratio and efficiency predictions for the compressors system. In particular, equivalent two-stage compressor map measures a lower pressure ratio at 12.5Krpm and 18Krpm in comparison to combined maps w/ and w/o heat correction, as visible at the top left corner of figure 7.13. The change in pressure ratio prediction is nearly absent at equivalent speeds equal and higher than 23Krpm. The difference between equivalent and combined pressure ratios at low speeds in the HP and LP compressors could be induced by the absence of measured data with high confidence and accuracy, as supported by the results [32]. Specifically, during the mapping of the two turbochargers in stand-alone configuration, data are recorded at minimum speed of 54.2Krpm, for the LP compressor (figure 7.5), and 95.4Krpm, for the HP compressor (figure 7.4). The equivalent mapping approach would reduce the absolute error in performance variables. Instead of measuring performance for each of the two compressors with combination of values and errors due to sensors accuracy, performance data result in higher accuracy for equivalent two-stage maps with measurements at inlet and outlet of the entire compression system. Additionally, a similar trend to pressure ratios in figure 7.13 is recorded in the estimation of compressor efficiency. In these conditions, a maximum change in efficiency for about 0.05 is monitored at 12.5Krpm between equivalent and combined compressors. Furthermore, combined map estimate a difference in the swallowing capacity of the two-stage turbines in relation to the equivalent two-stage map measured directly in the turbocharger gas-stand. Differently from the compressors case, the turbine net efficiency obtained by the combination of HP and LP maps is overestimated at high equivalent speed values, as visible in figure 7.13. The increase in turbine efficiency prediction could be explained in the underestimation of the isentropic turbine power. This can be supported by the variation of the swallowing capacity between equivalent and combined turbine maps in figure 7.13. In fact, the definition of corrected turbine mass flow in the stand-alone HP and LP turbine maps could introduce source of errors due to the temperature, mass flow and pressure sensor accuracy. Above all, the implementation of heat correction to diabatic operations of HP and LP turbochargers is not able to significantly improve predictions of two-stage system performance. Therefore, an additional proof could be given by the comparison of an adiabatic equivalent two-stage map. However, this experiments has not been performed in this study.

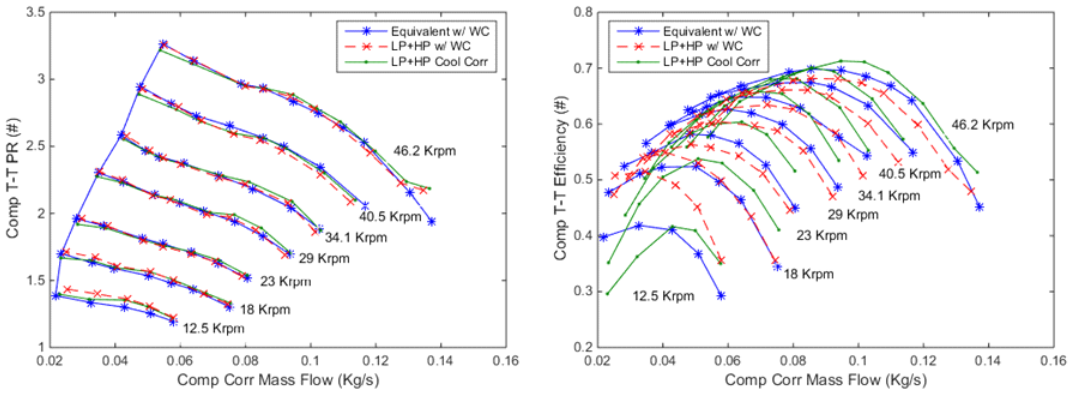

Figure 7. 14: Compressor performance maps of equivalent two-stage system with water-cooling at LP stage, combined stand-alone HP and water-cooled LP stages w/ and w/o cooling corrections

The heat and cooling correction of the LP compressor map is able to improve the prediction of the two-stage system performance, in relation to the equivalent configuration, as visible in figure 7.14. In fact, in the case of equivalent compressor pressure ratio, combination of HP and LP maps with cooling corrections can reduce the gap with the measured equivalent map at low rotating speeds. Accordingly, compressor efficiency estimation is improved in parts of the lowest compressor speed, when cooling power correction is applied at the LP stage. Specifically, higher efficiency is monitored for the two-stage in the gas-stand at low mass flows across the analysed speed lines. However, the absence of cooling correction factors at the LP stage is not able to predict compressor efficiency at 12.5Krpm. Furthermore, it is important to notice that the combination of stand-alone turbochargers maps is unable to confidently predict two-stage turbocharging performance at low operating speeds and pressure ratios.

In order to analyse the effect of heat and cool corrections to stand-alone maps, HP and LP compressors powers are investigated in combined two-stage maps. Figure 7.14 shows the relationship between HP and LP powers under diabatic conditions w/ and w/o water-cooling at the LP turbocharger. Moreover, the introduction of heat and cooling power corrections in relation to the two diabatic cases highlights variation of trends in figure 7.14. Accordingly to plots in figures 7.13 and 7.14, a higher influence to compressors power is achieved in the implementation of corrections of the water-cooled LP turbocharger. In fact, in conjunction to the low

speed operations analysed in figure 7.15, LP compressor power is reduced with correction for heating effects by the water-cooling system controlled at 360K. Moreover, the application of a correction for heat flux from the turbine to the compressor reduces both HP and LP compressor powers, although a smaller effect is recorded in figure 7.15.

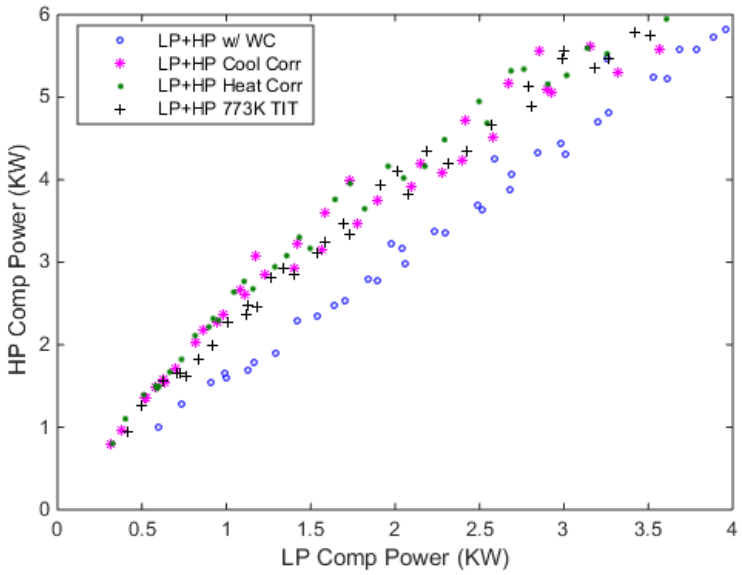

Figure 7. 15: HP and LP compressor power in combined stand-alone maps at diabatic conditions, with water-cooling at LP stage (w/ WC), with heat and cooling corrections

7.5 Chapter summary and conclusions

In this chapter, the following conclusions can be listed:

- Firstly, the equivalent mapping approach has been able to measure complete two-stage system performance. The equivalent speed has been defined, capturing constant speed trends and operations of the two turbochargers. In the equivalent compressor map, variation between diabatic operation w/ and w/o water-cooling is visible, reaching about 0.1 efficiency points difference at 12.5Krpm.

- Secondly, differences between equivalent and combined two-stage maps recorded. In fact, compressor performance differ at low equivalent speeds, due to inaccuracies from the extrapolation of stand-alone compressors performance in the low speed regions. Furthermore, the combined two-stage turbine map shows increased efficiency, due to an underestimation of equivalent swallowing capacity and isentropic power, in comparison to the equivalent map. Additionally, the equivalent two-stage mapping approach improves accuracy, monitoring conditions upstream and downstream the turbocharging system.

- Thirdly, heat corrections and adiabatic maps affect efficiencies and powers of each turbocharging stage. In fact, in comparison to apparent efficiencies of diabatic maps, compressor power is higher for the heat corrected case. Similarly, the variation is visible in the presence of water-cooling at LP stage.

- Lastly, the investigation is performed for constant positions of the two turbochargers VGTs. It would necessary to expand the analysis to different VGT positions, analysing the capabilities of the equivalent mapping approach in capturing complete operating conditions of the turbocharging system.

Chapter 8 – Equivalent two-stage system maps in engine gas-stand

In this chapter, 1D simulation models of the engine gas-stand are developed in order to evaluate the effectiveness of the equivalent two-stage mapping methodology. Initially, the two-stage system of chapter 8 is tested in the engine gas-stand facility under pulsating and transient operations. Subsequently, 1D simulations of the engine gas-stand including the two-stage system are performed. In fact, stand-alone diabatic and heat transfer corrected maps are implemented into 1D models and evaluated against the equivalent two-stage maps. Conclusively, boundary conditions of compressors and turbines, such as temperature, pressure and mass flow, are analysed for the three two-stage modelling approached. Furthermore, these are compared to engine gas-stand measurements for pulsating and transient operations of the turbocharging system.

8.1 Two-stage system in the engine gas-stand

8.1.1 System layout

The two-stage sequential turbocharging system, previously tested in the steady-flow turbocharger gas-stand, has been coupled to a 2.2L Diesel engine in order to evaluate performance of the turbocharging system. In figure 8.1, a photo of the fully instrumented two-stage turbocharging system in the engine gas-stand facility is reported. For this experiment, the single stage turbocharger with VGT and the standard exhaust manifold for the engine configuration are removed, in order to be replaced by the two stage system and the relative exhaust manifold. Therefore, a bespoke mechanical connection to couple the cylinders exhaust ports and the new exhaust manifold is required, consisting of a transition plate with thickness of approximately 25mm.

Moreover, due to cooling requirement of the LP compressor, the LP turbocharger unit is connected to the engine cooling circuit. At warm engine operating conditions, coolant is introduced into the LP compressor at approximately 90degC. In this way, the cooling circuit at the LP compressor is able to extract heat from the compression for flow temperatures above 90degC. On the other side, the hot coolant could add heat to the flow in the LP compressor for lower temperatures achieved during compression. Furthermore, the two-stage turbocharging system requires oil lubrication for both HP and LP stages. In fact, in order to avoid variation of friction behaviour of turbochargers between the measured performance in the steady turbocharger gas-stand and the engine gas-stand, SAE 5W-30 oil has been implemented, maintaining a temperature of about 90degC, during the experiments.

Figure 8. 1: Fully instrumented two-stage turbocharging system in the engine gas-stand

In the engine gas-stand layout of figure 8.2, the turbocharging system is connected to the engine exhaust with turbines powered by the hot combusted gases. Operation and load on HP and LP compressors are controlled via a CB valve. In addition, due to the missing connection between turbochargers compressors and the engine intake, in order to provide adequate boost to the engine, an external boost rig supply allowing for control of pressure, temperature and flow is included in the experimental test rig. Owing to the presence of an EGR valve for the reduction of harmful pollutants by the engine combustion process, engine intake conditions could be influenced. Therefore, in order to perform the experiments on the two-stage system, the EGR valve has been locked in the close position.

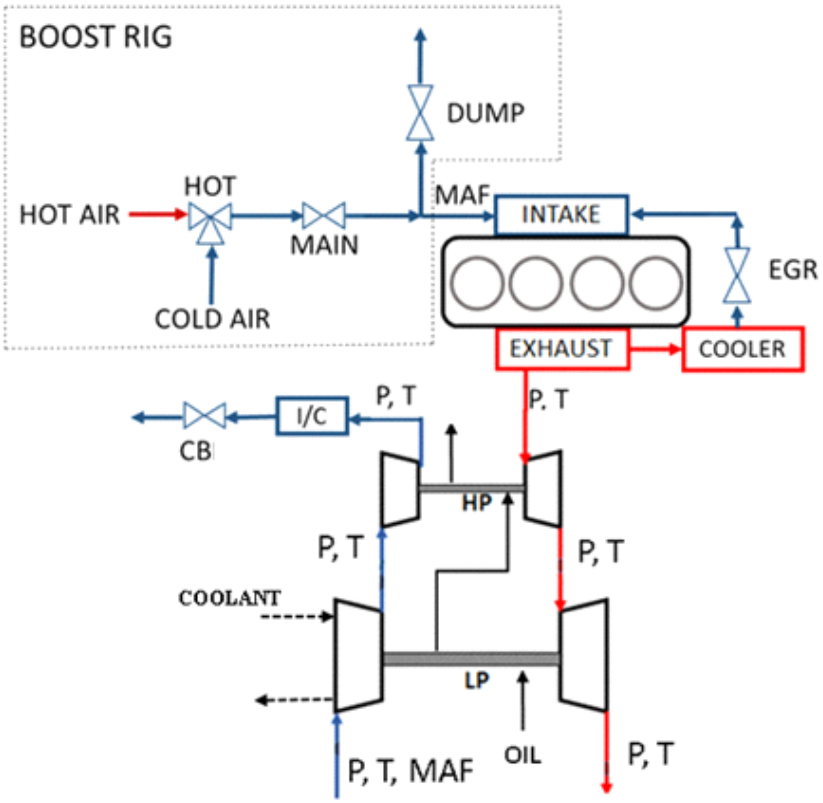

Figure 8. 2: Engine gas-stand with two-stage turbocharging system

8.1.2 Experimental procedure

In order to evaluate the effectiveness of equivalent and stand-alone two-stage maps, experiments of the turbocharging system under pulsating and transient conditions have been performed in order to serve for validation. Therefore, two operating conditions of engine gas-stand and turbocharging system, highlighted as cases A and B, have been defined in order to monitor pulsating operations. In table 8.1, main performance parameters of the engine gas-stand operating conditions are reported. In both operations of cases A and B at 1500rpm and 2000rpm, intake conditions have been controlled at 1.8barA and 311K through the boost rig. Due to the presence of VGT in both HP and LP turbochargers, the experiments have been performed at fixed VGT positions in order to resemble the experiments in the turbocharger gas-stand (chapter 7). In fact, the VGT actuators on both the turbochargers are maintained fixed at a position of 50%, as in chapter 7. Moreover, regulating valves at turbines and compressors are closed for exploring the system as fully sequential.

Table 8. 1: Operations of the engine gas-stand

VARIABLE	CASE A	CASE B
Engine speed	1500 rpm	2000 rpm
Engine torque	210 Nm	185 Nm
Intake pressure	1.8 barA	
Intake temperature	311 K	
Intake flow	182 Kg/h	250 Kg/h
Lambda	1.8	2
EGR valve	100% shut	
Engine oil temperature	365 K	
HP turbine inlet	775 K	
VGT position	50% shut	
CB valve	70% shut	
HP speed	140200 rpm	165400 rpm
LP speed	54100 rpm	69100 rpm
Equivalent speed	20880 rpm	28870 rpm

In order to maintain similar heat transfer conditions as in the steady turbocharger gas-stand, a temperature of 775K at the inlet of the HP turbine is controlled through the combustion events of the 2.2L Diesel engine. In fact, as engine intake and speed conditions are set, the total amount of injected fuel and the air-to-fuel concentration are adjusted to the correct turbocharger operations. In addition, due to different engine speed in the two cases analysed, two pulsating frequency of the exhaust flow, as well as, amplitude of pulsations at the turbine inlet are generated. Furthermore, in order to control the load on the compressors side of the two-stage turbocharging system, a CB valve is restricting the flow at the outlet of the HP compressor, allowing flow passage for 30% of the 3” opening area. Furthermore, single turbochargers speeds are different between the two cases, resulting in equivalent speeds of the turbocharging system of about 21Krpm and 29Krpm.

In order to evaluate the different mapping approaches, the performance of the two turbochargers are monitored under transient operations. In this scenario, a load step of the engine at constant rotating speed of 2000rpm is evaluated. The target operating condition at the end of the load step would be represented by the case B of table 8.1. In addition, the operating conditions at the start of the load step are kept identical in the engine gas-stand, apart from the injected fuel and lambda. In fact, constant boost condition of 1.8barA at 311K persists between start and end of the transient. In order to maintain validity of the two-stage equivalent maps measured in the steady gas-stand, regulating valves of the turbocharging system are closed and VGTs are 50% shut. In this way, the load and operation of engine and

turbocharging system are varied due to an increase of injected fuel and lambda being reduced to the target value of 2:1.

In figure 8.3, performance variables representing the transient load change in the engine gas-stand can be analysed. The starting and finishing target engine loads during transient are included in figure 8.3a. In this scenario, HP and LP turbochargers are subjected to acceleration, as visible in figures 8.3d and 8.3e. This allows the compressor outlet pressure and mass flow to increase to the target value. According to figures 8.3b and 8.3c, both mass flow and outlet pressure at compressor increase at maximum rate to about 1.2sec, following a slower rise in speed to achieve the final steady-state values. For completeness, the value of equivalent speed is included in figure 8.3f.

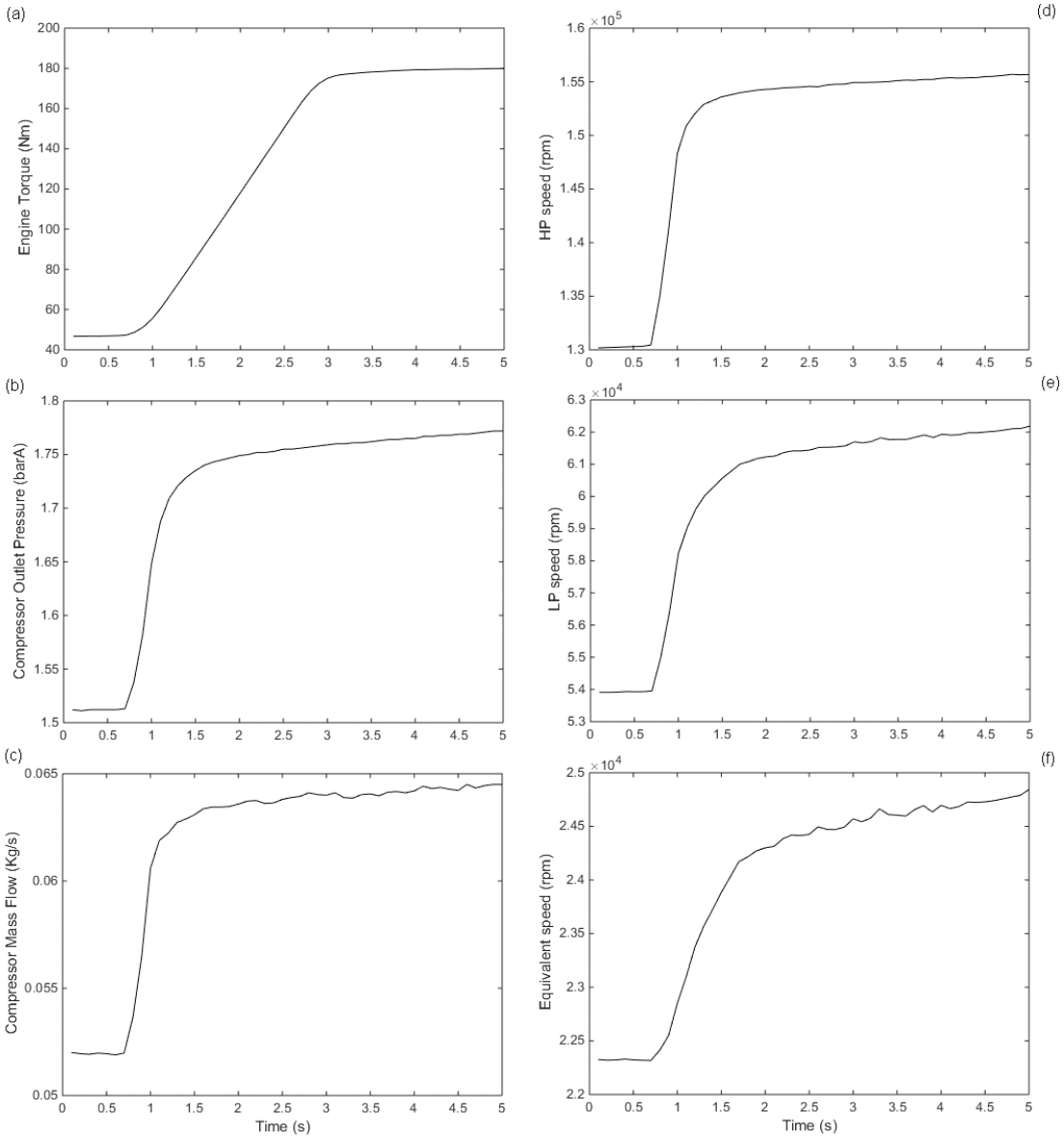

Figure 8. 3: Parameters during a transient engine load change at 2000rpm: engine torque (a), compressor outlet pressure (b), compressor mass flow (c), HP speed (d), LP speed (e) and equivalent speed (f)

8.2 Modelling approaches

The pulsating and transient operations of the engine gas-stand and turbocharging system are modelled by representing the entire system into a 1D simulation. Particularly, compressors and turbines maps as measured in the steady turbocharger gas-stand are included into the model. In order to evaluate the optimal modelling approach for representing the behaviour of the two-stage turbocharging system, stand-alone and equivalent maps are included in different simulations. In particular, two approaches are considered regarding the introduction of stand-alone maps, consisting of diabatic and heat transfer (HT) corrected compressors and turbines maps, available in section 3 of chapter 7. In diabatic maps, steady turbocharger gas-stand measurements of compressors and turbines are performed at turbine inlet temperature of 773K. In this case, efficiency terms include heat transfer across the turbochargers, due to temperature imbalance between compressor and turbine. In addition, the water-cooling action influencing the LP compressor performance is also integrated into the efficiency value of the compressor. In HT corrected maps, efficiencies of the turbomachine represent the real aerodynamic power of compressors and turbines. Additionally, heat transfer terms are added to the flow downstream the compressor, while, heat is extracted upstream the turbine. Due to the presence of LP compressor cooling, effects are included as heat transfer terms at the compressor outlet. Specifically, figures 8.4, 8.5 and 8.6 show the 1D models, including diabatic, corrected and equivalent performance maps of the two turbochargers, respectively.

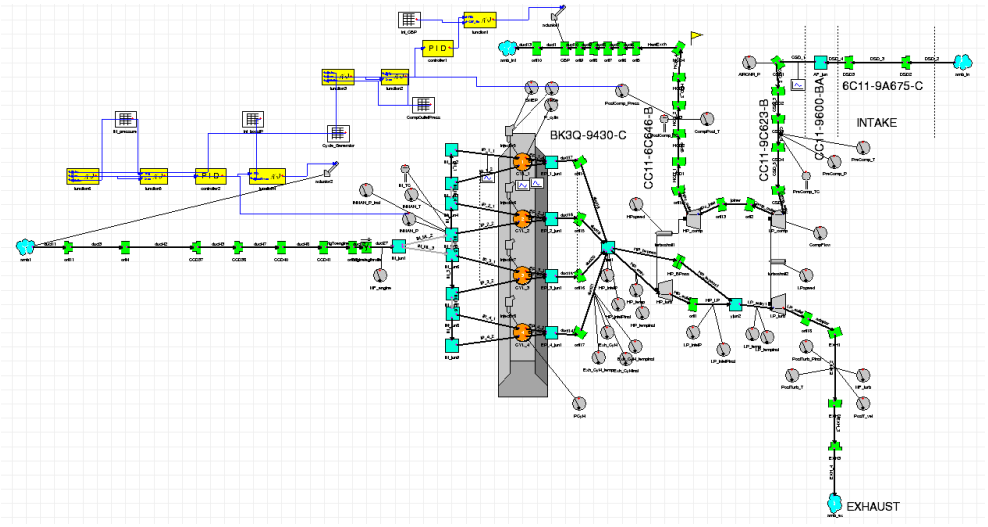

Figure 8. 4: Layout of 1D model representing the engine gas-stand with diabatic stand-alone maps of turbochargers

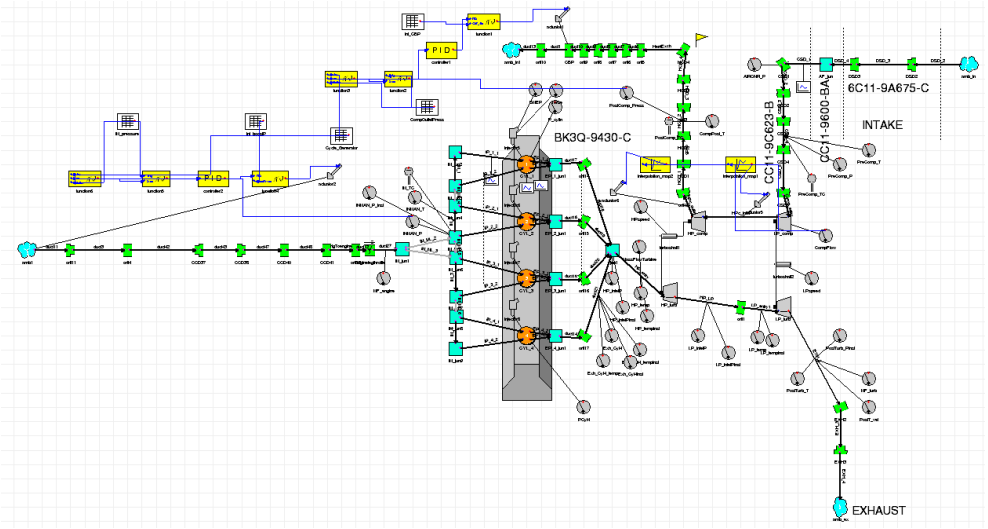

Figure 8. 5: Layout of 1D model representing the engine gas-stand with corrected stand-alone maps of turbochargers

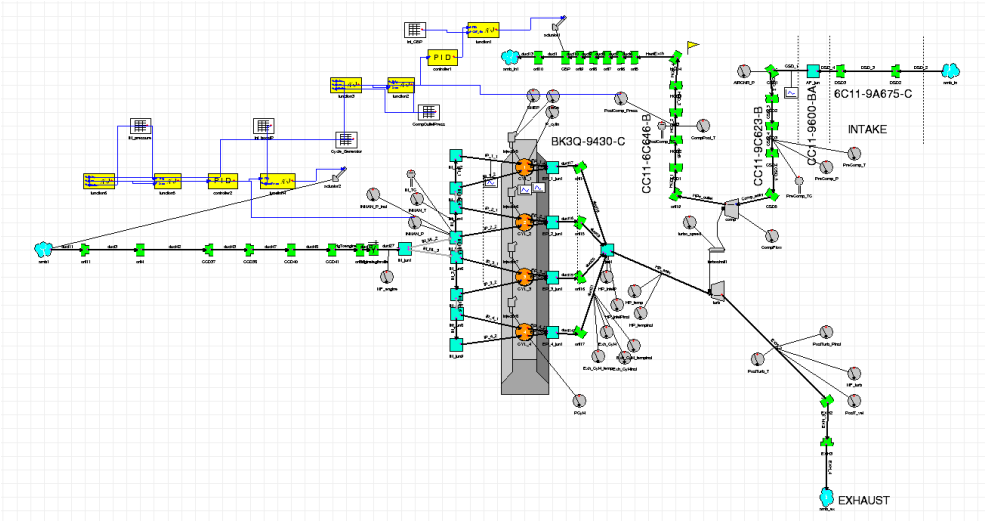

Figure 8. 6: Layout of 1D model representing the engine gas-stand with equivalent two-stage maps

Furthermore, the equivalent two-stage maps for turbines and compressors have been considered as measured in chapter 7. In this scenario, a turbine inlet temperature of 773K is adopted with the presence of water-cooling at the LP compressor. Specifically, equivalent maps are able to include the effects of the two-stage turbocharging system into single maps for compressors and turbines. In this chapter, 1D simulations representing operations of engine gas-stand, as cases A and B, and transient load step are evaluated including diabatic, HT corrected and equivalent maps of the system.

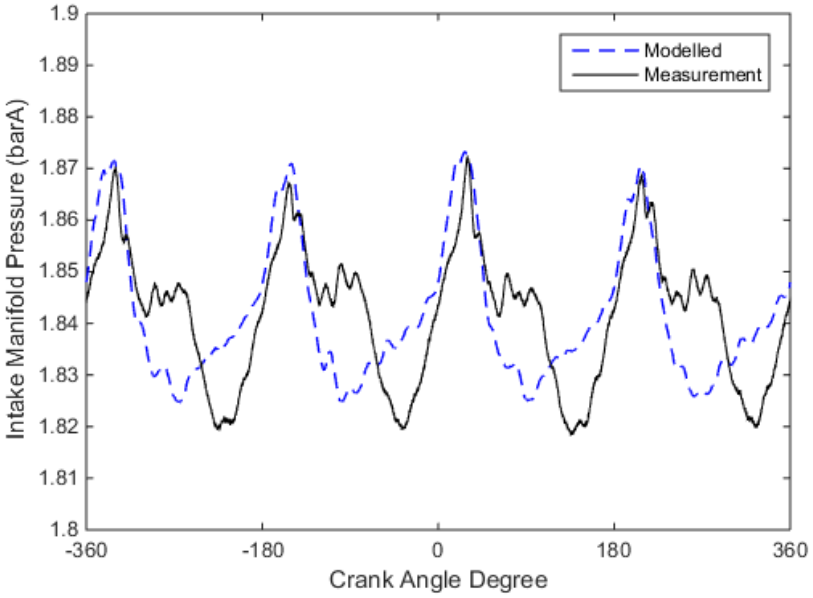

Figure 8. 7: Example of measured and modelled intake manifold pressure for case A

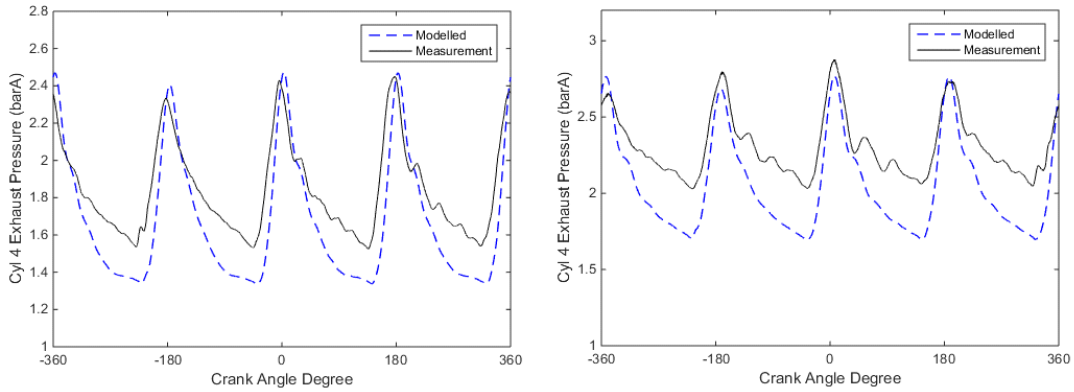

Figure 8. 8: Example of measured and example of modelled cylinder four exhaust manifold pressure at 1500rpm, at the left hand-side, and 2000rpm, at the right hand-side

Engine boundaries such as pressures at intake and exhaust have been analysed in order to check for correct representation of the engine gas-stand operation. In figure 8.7, modelled and measured pressures in the intake manifold are closely matched in amplitude, assuming adequate modelled conditions of the intake. At the same time, the exhaust pressure is monitored at the outlet of the engine cylinder four. Figure 8.8 shows the correlation between modelled and measured pressures at the exhaust manifold at 1500rpm and 2000rpm. The simulated pressures at the exhaust show higher amplitude of pulsation in both the operating conditions.

8.3 Evaluation of mapping approaches

8.3.1 Pulsating exhaust flow

In order to evaluate the capabilities of the modelling approaches in representing the turbocharging system, pressure and temperatures at both turbine and compressor sides would have to be investigated. Thus, figure 8.9 shows pressures at the inlet of HP and LP turbines, as well as, downstream of the turbocharging system in the tailpipe. Measured instantaneous pressures in the engine gas-stand operating at cases A and B with the engine at 1500rm and 2000rpm, respectively. Therefore, in figure 8.9, pressure values measured in the engine gas-stand are compared to the pressure values obtained by the 1D simulations. In fact, approaches using diabatic, HT corrected and equivalent maps for representing performance of the turbocharging system are included in figure 8.9. Specifically, figures 8.9a and 8.9d show predictions and measurements of the HP turbine inlet pressures at 1500rpm and 2000rpm. In figures 8.9b and 8.9e, the LP inlet pressure is visible but without data from the equivalent approach, due to a single map adopted for both HP and LP stages. Moreover, pressure measured downstream the turbines in the tailpipe is compared to predicted instantaneous values in figures 8.9c and 8.9f for cases A and B of table 8.1.

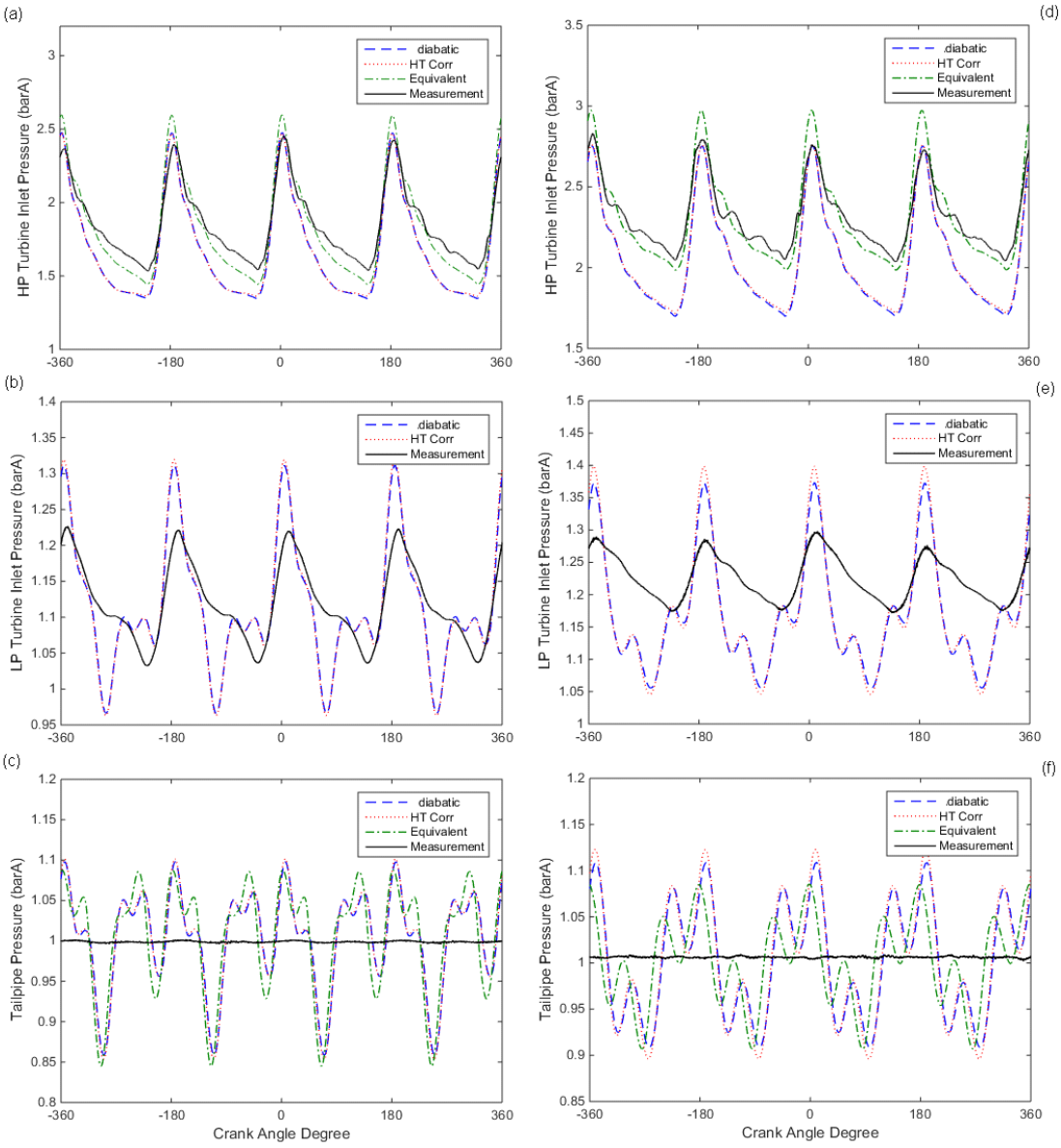

Figure 8. 9: Measured and modelled HP (a), LP (b) turbine inlet and tailpipe (c) pressures at 1500rpm, at the left hand-side, and HP (d), LP (e) turbine inlet and tailpipe (f) pressures at 2000rpm, at the right hand-side

In figures 8.9a and 8.9d, the equivalent approach for HP and LP turbochargers maps shows a different trend compared to the modelling approaches involving the adoption of single maps for each turbocharger. In addition, an improved pressure prediction might be obtained through the adoption of equivalent maps. In the case of the LP inlet pressure, adiabatic and HT corrected models generate a significant difference with the measured pressure values. In fact, the pressure oscillations are significantly lower in the recorded experiments, accordingly to figures 8.9b and 8.9e. In the case of tailpipe pressure, figures 8.9c and 8.9f highlight the stability of the

measured values at 1500rpm and 2000rpm. On the other side, modelling approaches react similarly, including more predominant pressure oscillations. These could be caused by the difficulties in accounting for the complete volume of the extraction system of the actual engine gas-stand facility, in order to be represented into the 1D model.

As well as pressures, temperatures in the exhaust system around HP and LP turbines are evaluated. In tables 8.2 and 8.3, temperatures at tailpipe, high pressure turbine (HPT) and low pressure turbine (LPT) inlets are collected for the two operating conditions explored in the engine gas-stand as cases A and B, at 1500rpm and 2000rpm, respectively. In the case of the equivalent approach, an over-estimation of the inlet and outlet temperature is recorded. Specifically, although the temperature at HPT inlet might not differ more than 6K between equivalent models and measurements, the predicted tailpipe temperature could be 20K higher than the monitored values in the engine gas-stand. In the case of diabatic turbochargers modelling, the temperature predictions differ for a maximum of 10K from the measured values. In addition, temperature difference seems to be constant across the flow path, suggesting that the turbine modelling approach would reduce the source of errors in the predictions. However, this scenario can be valid for similar heat transfer conditions in turbochargers between the measured maps and represented application. In fact, in this particular study, a temperature of 775K at inlet of HPT is maintained in the engine gas-stand operations, similarly to the temperature adopted during the turbochargers mapping, in chapter 8. Lastly, the HT correction approach provides the highest temperature difference with the recorded temperatures in the engine gas-stand, suggesting that the approach for including heat transfer into the 1D model would have to be improved.

Table 8. 2: Temperature differences between modelled and measured values at case A

	MEASUREMENT	DIABATIC	HT CORRECTED	EQUIVALENT
HPT inlet	775 K	+10 K	-14 K	+6 K
LPT inlet	714 K	+9 K	+14 K	NA
Tailpipe	661 K	+10 K	-2 K	+20 K

Table 8. 3: Temperature differences between modelled and measured values at case B

	MEASUREMENT	DIABATIC	HT CORRECTED	EQUIVALENT
HPT inlet	775 K	+1 K	-14 K	+6 K
LPT inlet	704 K	+2 K	+17 K	NA
Tailpipe	649 K	+5 K	+10 K	+14 K

At the opposite side of the turbochargers, compressors are subjected to steady flow operations due to the absence of pressure fluctuations. In both the analysed engine gas-stand operations, the back-pressure valve has been set to 70% shut. In order to evaluate the effectiveness of the two-stage modelling approaches, the 1D simulations control the back-pressure valve to match pressure ratio of the complete two-stage compression. In this way, the outlet pressure at the HP compressor is matching the measured pressure values of 1.58barA and 1.93barA at cases A and B, respectively. Therefore, the model evaluation is based on the accuracy of the predicted mass air flow (MAF) through the system. In table 8.4, the percentage of errors between measured and predicted values in diabatic, HT corrected and equivalent approaches are shown. Specifically, the results of case B vary from a perfect match in the diabatic approach to a -7% error in the equivalent system approach. In addition, the data in the table suggest that the equivalent approach can give a better performance prediction in case A with a low -1.8% difference in MAF. In fact, this could be explained by higher accuracy of the equivalent modelling approach at low turbochargers speed, comparing to diabatic and HT corrected approaches. Moreover, the adoption of individual maps at HP and LP stages with a model for heat transfer is able to predict MAF values with sufficient accuracy. In addition, the error is reduced at higher rotational speeds where heat transfer has a small influence on the compressor performance, suggesting improvements on the introduction of heat transfer into the simulation model would have to be made.

Table 8. 4: Percentage of error between modelled and measured values of compressor mass air flow (MAF)

OPERATION	MEASUREMENT	DIABATIC	HT CORRECTED	EQUIVALENT
Case A	0.056 Kg/s	-5.4%	+6%	-1.8%
Case B	0.071 Kg/s	0%	+2.8%	-7%

8.3.2 Transient operations

In order to investigate the effectiveness of two-stage modelling approaches in the 1D simulation, a transient model is used for evaluating pressure at the outlet of the HP compressor and mass flow through the two compressors. Considering that the steady-state operations of the engine gas-stand at the end of the load step matches pulsating of case B, the focus has been set on the start and initial progress of transient. In addition, the compressor back-pressure valve has been maintained constant at a position of 70% shut, while, the fuel amount injected into the engine has been instantaneously increased. Figures 8.10 and 8.11 highlight the progress of transient in the initial 1.2sec from the start of transient for pressure and mass flow, respectively.

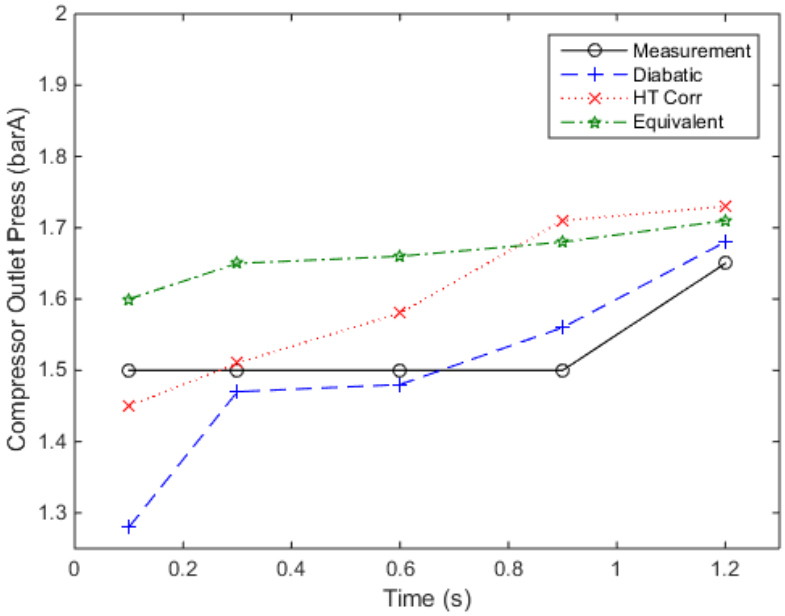

Figure 8. 10: HP compressor outlet pressure at several instants following the start of transient load change at 2000rpm

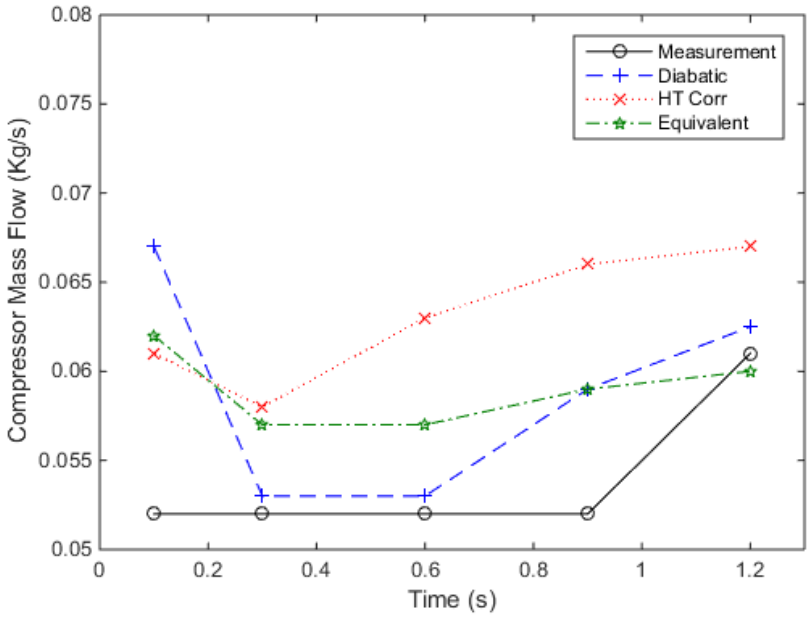

Figure 8. 11: Compressors mass flow at several instants following the start of transient load change at 2000rpm

The plot in figure 8.10 suggests that the diabatic modelling approach would be adequate to represent pressure at the outlet of the HP compressor. Meanwhile, the HT corrected and equivalent approaches could be over or under-predicting the measured pressure values in the first 0.9sec of the transient. In fact, diabatic and equivalent approaches are able to predict pressure at the outlet of the compressor system. A similar trend is reported with regards to the mass flow predictions in figure 8.11. Specifically, the HT corrected modelling approach is over-predicting the measured values of compressor mass flow. At 0.3sec and 0.6sec, the diabatic model generates a mass flow value of about 0.054Kg/s, similarly to the measurements in the engine gas-stand. Furthermore, the mass flow through the compressors at the start of transient is poorly modelled in the three approaches.

8.4 Chapter summary and conclusions

In this chapter, the equivalent maps of the two-stage turbocharging system in chapter 7 are evaluated through 1D simulations of the engine gas-stand facility. Stand-alone diabatic and HT corrected maps are also implemented for the evaluation under pulsating flows and transient operations. In summary, main conclusions of the chapter are drawn as follows:

- Under pulsating conditions of the turbine, the adoption of equivalent maps into the 1D model allows a better prediction of instantaneous pressure at the inlet of the HPT. However, the adoption of stand-alone maps could reduce the ability of the model to represent instantaneous pressures, specifically, for the LP turbine.

- In both cases A and B, optimal temperature prediction around turbines is achieved through the implementation of diabatic maps of stand-alone turbochargers, assuming constant heat transfer conditions. Moreover, HT corrected and equivalent maps would provide a maximum error of 20K at downstream turbine conditions in the tailpipe.

- Regarding mass flow in the compressors, a maximum error of 7% between simulations and measurements persists for both cases A and B, without a significant change across modelling approaches.

- During load steps of the engine gas-stand, a poor prediction in compressor mass flow and outlet pressure of the 1D models at 0.1s is shown. Differently, at 1.2s after start, equivalent two-stage and diabatic stand-alone maps would improve the prediction of pressure and mass flow values.

- Furthermore, analysis of low turbocharger speed operations in a two-stage turbocharged engine, including pulsations on compressors, could be able to evaluate the highest potential of the equivalent mapping approach. This would also be supported by the differences at low equivalent speed, highlighted in chapter 7.

Chapter 9 – Conclusions and Outlook

In this final chapter, conclusions of the thesis are drawn. In particular, three sections are included:

- The final summary collects the main outcomes of chapters and thesis.
- The research objectives, as defined in the first chapter, are addressed, together with the project aim.
- The outlook is described, highlighting contribution of this thesis to other projects in the research group. Moreover, future work is also proposed, expanding and validating further use of the equivalent two-stage mapping approach.

9.1 Summary

This thesis has evaluated methods regarding the characterisation of turbocharger unsteady behaviour, surge and two-stage turbocharging system performance. In fact, the focus has been on the validation of equivalent and stand-alone turbochargers maps into 1D simulations, widely adopted in the automotive industry and powertrain system investigation. Following the introduction in chapter 1, chapter 2 presents a detailed review on factors influencing performance of two-stage systems. In order to perform the experiments on the mapping methodology for two-stage turbocharging systems, the engine gas-stand of chapter 3 has been developed with the capabilities of generating steady and unsteady flows at compressor and turbine, respectively. In addition, due to absence of instantaneous mass flow and temperature measurements in the exhaust, in chapter 4, a turbine modelling approach has been evaluated for better representing the real sensors in engine test environments, exposed to pulsating flows. Moreover, the importance of compressor surge definition has led to the study presented in chapter 5. Furthermore, in order to investigate two-stage turbocharging systems, a 1D simulation study has been performed in chapter 6, defining characteristics of an equivalent map and speed. In chapter 7, the system performance under steady flows are evaluated through the use of equivalent and combined stand-alone maps. Finally, in chapter 8, the obtained performance maps are evaluated using the engine gas-stand, through comparison of 1D simulations and measurements.

9.2 Conclusions

In this section, conclusions of the thesis are reported, addressing objectives, as previously defined in chapter 1. Therefore, in order to facilitate the reader, objectives are reported in italics with comments placed below.

1. *Review of flow and heat transfer effects influencing the performance maps of turbochargers and approaches for modelling two-stage turbocharging systems into 1D simulations.*

The literature review of chapter 2 has investigated the factors, influencing the performance maps. In particular, the presence of flow motion and non-uniformity at the inlet of turbomachine due to bends and/or swirling devices will influence the performance behaviour. In the case of a compressor, surge and choke limits are perturbed as well as an influence on the achievable pressure ratio. Moreover, the diabatic operation of a turbocharger, rising the turbine inlet temperature as high as about 770K, leads to heat transfer across the turbocharger shaft and housing. In this case, an apparent reduction in compressor efficiency is induced by the additional heat flux from the turbine. Therefore, efficiency would have to be corrected during diabatic operations. For this reason, heat transfer models are applied to turbochargers. In 1D powertrain simulations, these effects are excluded from the model, accounting for pressure drops and heat transfer, while, performance maps for HP and LP compressors and turbines are referred to steady flows. Therefore, the review has resulted in the definition of a specific mapping approach to represent two-stage performance. The proposed approach consists of equivalent system maps for compressor and turbine, including inter-stage effects and heat fluxes.

2. *Develop a unique engine gas-stand facility to explore performance of turbochargers.*

A new engine gas-stand facility has been developed, including an externally boosted 2.2L Diesel engine, powering the turbocharger through the hot exhaust gasses. The

characteristics of the engine gas-stand are reported, in chapter 3, addressing the capability in generating compressor maps under steady flows. The uniqueness of the facility consists in the mapping methodology adopted using the combination of VGT and back-pressure valve. However, in the present work, the facility has not been able to capture instantaneous turbine performance due to slow response of temperature and mass flow sensors. However, unlike a turbocharger gas-stand, the engine gas-stand is able to perform controlled experiments for evaluating transient turbocharger behaviours including pulsating flow on the turbine and compressor. For the latter a rearrangement of the downstream ducts at the compressor can allow investigation of compressor performance under unsteady flow conditions, as shown in chapter 5. This is a unique and powerful capability since it is able to separate the influence of turbocharger speed fluctuation (due to turbine pulsations) and intake pressure fluctuations (due to intake valve) on compressor performance.

3. *Attempt the development of a methodology to interpret pulsating turbine performance measurements from the engine gas-stand, to capture turbine outlet temperatures into 1D models.*

Due to the difficulty in measuring instantaneous performance accurately in the engine gas-stand with the instrumentation available, the hybrid unsteady/quasi-steady turbine model has been introduced. The novelty of the method consists in the representation of turbine inlet and outlet in tapered ducts, in order to allow representation of flow temperature in the proximity of turbine rotor. Chapter 4 shows the attempt to correlate experimental measurements on the pulsating exhaust side of the engine gas-stand with 1D simulations. As well as representing turbine performance with a steady-state map, the hybrid unsteady/quasi-steady turbine model is introduced to account for mass storage at the turbine inlet and outlet. However, although a better prediction over averaged turbine outlet temperature could be achieved (maximum error of 20K), the hybrid turbine model could not generate useful predictions over the instantaneous turbine performance. Therefore, the investigation in chapter 4 suggests that the evaluation of instantaneous turbine performance in the engine gas-stand is not possible, due to the absence of accurate and responsive mass flow and temperature sensors.

4. *Develop a methodology to identify surge onset under steady and pulsating flows of the compressor, identifying the influence on stability range.*

Chapter 5 of this thesis focus on the investigation of compressor performance. In particular, a study of surge onset in the engine gas-stand has shown that compressor performs under steady flows, with turbine pulsations being transferred to the compressor. Although, in the engine gas-stand, pulsations at the compressor are small in magnitude, the surge line is affected. In comparison to steady-state resulting in lower corrected mass flow rates, in comparison to the steady-state compressor map generated in the turbocharger gas-stand, the small pulsations, being transferred from the turbine, reduce the compressor flow rate at which surge occurs. In addition, the analysis of pressure and mass flow has shown disturbances due to the surge phenomenon. However, due to controllability limits of the engine gas-stand in the standard configuration, improved degree of information could be generated through the FFT analysis in the steady turbocharger gas-stand. In addition, in the unsteady turbocharger gas-stand, the presence of pulsating flows at the compressor leads to a progressive surge onset, compared to the more sudden effect of surge onset under steady compressor flows. Most of all, the presence of significant flow pulsations at the compressor affects the surge line, shifting it to even lower corrected mass flow values. In addition, the unsteady engine gas-stand is able to consider the real engine intake process, exposing the compressor to the variation of downstream volume.

5. *Investigate performance of regulated two-stage turbocharging systems under real powertrain operations, in order to identify the system operation.*

In order to evaluate the application of an equivalent mapping methodology, the operational boundaries of the two-stage system under real powertrain operations would have to be explored. It has emerged that the two turbochargers work simultaneously below certain levels of pressure ratios and mass flows. Above the defined range, HP stage is by-passed through the TBP valve. In addition, the HP compressor is by-passed via the CBP valve, limiting the maximum pressure at the

compressor outlet. In this way, the boost level would be provided entirely by the LP turbocharger. Furthermore, chapter 6 shows that operations in the two-stage system are regulated through by-pass valves during operations, suggesting that an additional variable would have to be included in the equivalent two-stage performance map.

6. *Define a novel mapping methodology for two-stage turbocharging systems, reducing the errors in performance predictions, due to inter-stage effects.*

In order to set and define a characteristic map to represent complete behaviour of two-stage system performance, a novel testing methodology to generate equivalent two-stage maps has been proposed and demonstrated in chapter 6. The surge line of the equivalent map is affected by HP compressor at lower speeds (below 20Krpm) and LP compressor at higher speeds. Similarly, choke of the two-stage turbocharging system would be caused by the LP compressor at low speed and HP compressor at high compressor. 1D simulation of the mapping approach shows the possible equivalent two-stage map of compressors and turbines, including TBP valve position as a performance variable in the equivalent map. Moreover, performance maps of an actual two-stage system have been generated in the steady turbocharger gas-stand to acquire compressor and turbine performance, as visible in chapter 7. In this case, the turbocharging system has been mapped as a single turbocharging unit, being represented by equivalent speed lines of the entire system. In fact, this speed term would be able to represent performance of the system, obtaining high values at high mass flows and pressure ratios, such as, during the HP stage by-pass.

7. *Evaluate the effectiveness of equivalent maps in representing two-stage system performance.*

The comparison of equivalent two-stage and combined stand-alone maps of the turbocharging system highlights differences in the measured performance, as reported in chapter 7. Regarding the two compressors, the difference in

performance is mainly achieved at low equivalent speeds, where both HP and LP turbochargers operate at low pressure ratios and rotational speeds. In contrast to the stand-alone maps, the equivalent approach can improve data accuracy of compressors and turbines maps. In fact, measurement points would be required only at inlet at outlet of the turbocharging system. In the case of the LP and HP turbines, significant differences between the two mapping approaches lie at high turbine speeds, due to a change in the estimation of turbine isentropic power. In chapter 8, correlation between simulations and experiments of the two-stage turbocharging system in the engine gas-stand has been investigated, also at transient conditions. The equivalent approach has shown the ability to perform in a similar way to the use of stand-alone turbochargers maps. In fact, this could be expected as the both equivalent and combined two-stage maps could show similar performance of the turbocharging system for the operations of chapter 8. In order to fully explore the benefits of the novel equivalent two-stage maps, operating conditions of the system at low and high speeds should be evaluated, as also supported by the findings of chapter 7.

One of the main aims of this thesis has been the investigation of an equivalent mapping approach for modelling regulated two-stage turbocharging systems. The project has achieved the development of a characterisation method for two-stage systems considering several operating conditions. The equivalent two-stage map has been able to represent full characteristics of the turbocharging system, including the operations at activated turbine by-pass, as shown in simulation. The map can completely replace the stand-alone maps of HP and LP stages, including the inter-stage effects. In addition, improved accuracy is achieved by the novel approach, due to reduction of measure points for each of the two turbochargers. In order to evaluate the characterisation methodology at unsteady and transient operations, an engine gas-stand has been developed. The engine gas-stand has proved capabilities in testing automotive turbochargers, generating steady compressor maps and investigating pulsating operations of the turbine.

9.3 Outlook and further work

In order to achieve the project aim and address the project objectives, an engine gas-stand facility has been developed in the Powertrain and Vehicle Research Centre of the University of Bath. This has allowed the centre to investigate performance of turbochargers for a variety of projects at the research centre, such as, the dynamic investigation of heat transfer in automotive turbochargers, in collaboration with CMT-Motores Termicos from the Universidad Politecnica de Valencia. Moreover, the facility has allowed additional research students to perform experimental investigations, such as, Miss Qiyou Deng, being able to investigate pulsating interactions between turbocharger turbine and external waste-gate.

Additionally, the analysis on compressor surge in the engine gas-stand and the unsteady turbocharger facility has been part of a collaboration study with the research student, Mr Tomasz Duda, leading to a wide scale investigation on compressor surge, involving several turbochargers. With the surge investigation of this thesis, the analysis has been coupled to experiments in the steady and unsteady turbocharger gas-stand. In this scenario, chapter 5 of this thesis has served for validation of the surge onset analysis, involving the presence of pulsating flows at compressor outlet.

In relation to future applications of the mapping methodology, the adoption of equivalent two-stage maps could also be applied in the European research project *Thomson*, developing a mild hybrid powertrain including a two-stage boosting device. In this scenario, equivalent maps at the compressor would be able to provide an elevated degree of accuracy at low mass flows and pressure ratios. In this way, both simulation models and system calibration strategies would benefit from reliable data on the boosting devices.

Furthermore, the equivalent two-stage mapping approach could be expanded to several VGT positions of LP and HP turbines. In order to perform the study, both simulations and experiments would be able to highlight the potential of important parameters for the definition of performance maps. Furthermore, in relation to the 1D model, measurements and simulations of pulsating performance of the turbine could be improved through the adoption of temperature and mass flow sensors at adequate response time.

References

1. Fortune, 2016, "Volkswagen Scandal Pushes French Rival to Cut Back on Diesel".Available from: http://fortune.com/2016/09/06/renault-diesel-engines/ [Accessed 25th May 2017].

2. Degraeuwe, B., and Weiss, M., 2017, "Does the New European Driving Cycle (NEDC) really fail to capture the NOX emissions of diesel cars in Europe?", Environmental pollution, 222, pp. 234-241, 10.1016/j.envpol.2016.12.050.

3. Mock, P., Kuehlwein, J., Tietge, U., Franco, V., Bandivadekar, A., and German, J., 2014, "The WLTP: How a new test procedure for cars will affect fuel consumption values in the EU", The International Council on Clean Transportation, 10.1016/j.enpol.2013.12.013i.

4. Fontaras, G., Zacharof, N.-G., and Ciuffo, B., 2017, "Fuel consumption and CO 2 emissions from passenger cars in Europe – Laboratory versus real-world emissions", Progress in Energy and Combustion Science, 60, pp. 97-131, 10.1016/j.pecs.2016.12.004.

5. Zinner, K., 1978, Supercharging of internal combustion engines: fundamentals, calculations, examples, Springer, Berlin.

6. Copeland, C. D., Martinez-Botas, R., and Seiler, M., 2012, "Unsteady Performance of a Double Entry Turbocharger Turbine With a Comparison to Steady Flow Conditions", Journal of Turbomachinery, 134 (2), p. 021022, 10.1115/1.4003171.

7. BorgWarner_Turbo_Systems, 2017, "Turbocharger Products".Available from: http://www.turbos.bwauto.com/en/products/turbofacts.aspx [Accessed 15/07/2017].

8. Ricardo, 2017, "Ricardo WAVE".Available from: https://ricardo.com/software/products/wave [Accessed 15/07/2017].

9. Gamma_Technologies_LLC, 2017, "GT-Suite".Available from: https://www.gtisoft.com/ [Accessed 15/07/2017].

10. Munson, B. R., Okiishi, T. H., Huebsch, W. W., and Rothmayer, A. P., 2012, Fundamentals of Fluid Mechanics, Wiley, USA.

11. Avola, C., Copeland, C., Duda, T., Burke, R. D., Akehurst, S., and Brace, C. J., 2015, "Review of Turbocharger Mapping and 1D Modelling Inaccuracies with specific focus on Two-Stage Systems", SAE Technical Paper (2015-21-2523), 10.4271/2015-24-2523.

12. Turner, J. W. G., Popplewell, A., Patel, R., Johnson, T. R., Darnton, N. J., Richardson, S., Bredda, S. W., Tudor, R. J., Bithell, C. I., Jackson, R., Remmert, S. M., Cracknell, R. F., Fernandes, J. X., Lewis, A. G. J., Akehurst, S., Brace, C., Copeland, C., Martinez-Botas, R., Romagnoli, A., and Burluka, A. A., 2014, "Ultra Boost for Economy: Extending the Limits of Extreme Engine Downsizing", SAE Technical Paper (2014-01-1185), 10.4271/2014-01-1185.

13. Schernus, C., Dieterich, C., Nebbia, C., Sehr, A., Wedowski, S., and Weinowski, R., 2011, "Turbocharging of Downsized Gasoline DI Engines with 2 and 3 Cylinders", SAE Technical Paper (2011-24-0138), 10.4271/2011-24-0138.

14. Pflueger, F., 1998, "Regulated two-stage turbocharging - KKK's new charging system for commercial diesel engines", Sixth International Conference on Turbocharging and Air Management Systems, IMechE, London, pp. 127-141.

15. Kang, J., Lee, J., Song, H.-s., and Lee, D., 2012, "Enhancing Power Density with Two-Stage Turbochargers", SAE Technical Paper (2012-01-0709), 10.4271/2012-01-0709.

16. Saulnier, S., and Guilan, S., 2004, "Computational Study of Diesel Engine Downsizing using Two-Stage Turbocharging", SAE Technical Paper (2004-01-0929), 10.4271/2004-01-0929.

17. Choi, C., Kwon, S., and Cho, S., 2006, "Development of Fuel Consumption of Passenger Diesel Engine with 2 Stage Turbocharger", SAE Technical Paper (2006-01-0021), 10.4271/2006-01-0021.

18. Marsiglia, R. F., and Bassetti, F. B., 2012, "Thermodynamic evaluation of two-stage turbocharging system", SAE Technical Paper (2012-36-0169), 10.4271/2012-36-0169.

19. Millo, F., Mallamo, F., and Ganio Mego, G., 2005, "The Potential of Dual Stage Turbocharging and Miller Cycle for HD Diesel Engines", SAE Technical Paper (2005-01-0221), 10.4271/2005-01-0221.

20. Wik, C., and Hallbaeck, B., 2008, "Reducing emissions using 2-stage turbo charging", Waertsilae Technical Journal, 01, pp. 35-41.

21. Codan, E., and Christen, C., 2014, "Further development of two-stage turbocharging systems for large engines", 11th International Conference on Turbochargers and Turbocharging, IMechE, London, pp. 189-203.

22. Sauerstein, R., Dabrowski, R., Becker, M., and Bullmer, W., 2010, "Regulated Two-Stage Turbocharging for gasoline Engines", BorgWarner, 10/03/2015.

23. Codan, E., and Huber, T., 2012, "Application of two stage turbocharging systems on large engines", 10th International Conference on Turbochargers and Turbocharging, IMechE, London, pp. 55-69.

24. SAE-International, 1995, SAE J1826 Turbocharger Gas Stand Test Code, Society of Automotive Engineers, Inc.

25. Zhang, Q., Brace, C., Akehurst, S., Burke, R., Capon, G., Smith, L., Garrett, S., and Zhang, K., 2013, "Simulation Study of the Series Sequential Turbocharging for Engine Downsizing and Fuel Efficiency", SAE Technical Paper (2013-01-0935), 10.4271/2013-01-0935.

26. Weber, O., Christmann, R., Gauckler, V., and Sauerstein, R., 2012, "R2S - modelling and consequences for the boost control", 10th International Conference on Turbochargers and Turbocharging, IMechE, London, pp. 43-53.

27. Lee, B., Filipi, Z., Assanis, D., and Jung, D., 2009, "Simulation-based Assessment of Various Dual-Stage Boosting Systems in Terms of Performance and Fuel Economy Improvements", SAE Technical Paper (2009-01-1471), 10.4271/2009-01-1471.

28. Galindo, J., Serrano, J. R., Climent, H., and Varnier, O., 2010, "Impact of two-stage turbocharging architectures on pumping losses of automotive engines based on an analytical model", Energy Conversion and Management, 51 (10), pp. 1958-1969, DOI 10.1016/j.enconman.2010.02.028.

29. Amann, M., and Ouwenga, D., 2014, "Engine Parameter Optimization for Improved Engine and Drive Cycle Efficiency for Boosted, GDI Engines with Different

Boosting System Architecture", SAE Technical Paper (2014-01-1204), 10.4271/2014-01-1204.

30. Westin, F., and Burenius, R., 2010, "Measurement of Interstage Losses of a Twostage Turbocharger System in a Turbocharger Test Rig", SAE Technical Paper (2010-01-1221), 10.4271/2010-01-1221.

31. Westin, F., and Burenius, R., 2010, "Measurement of interstage losses of a two-stage turbocharger system in a turbocharger test rig", 9th International Conference on Turbochargers and Turbocharging, IMechE, London, 10.1243/17547164C0012010005.

32. Fitzky, G., Bothien, M., Zbinden, S., Codan, E., and Voegeli, S., 2010, "Testing and qualification of two-stage turbocharging systems", 9th International Conference on Turbochargers and Turbocharging, IMechE, London, pp. 79-94, 10.1243/17547164C0012010006

33. Serrano, J. R., Guardiola, C., Dolz, V., and Tiseira, A., 2007, "Experimental Study of the Turbine Inlet Gas Temperature Influence on Turbocharger Performance", SAE Technical Paper (2007-01-1559), 10.4271/2007-01-1559.

34. Shaaban, S., and Seume, J., 2006, "Analysis of Turbocharger Non-Adiabatic Performance", 8th International Conference on Turbochargers and Turbocharging, IMechE, London, pp. 119-130, 10.1016/B978-1-84569-174-5.50012-9.

35. Watson, N., and Janota, S., 1982, Turbocharging the internal combustion engine, The Macmillan Press Ltd, London.

36. Casey, M. V., and Fesich, T. M., 2010, "The Efficiency of Turbocharger Compressors With Diabatic Flows", Journal of Engineering for Gas Turbines and Power, 132 (072302), 10.1115/1.4000300.

37. Grigoriadis, P., Binder, E., Böttcher, L., Benz, A., and Sens, M., 2013, "Advanced Turbocharger Model for 1D ICE Simulation - Part I", SAE Technical Paper (2013-01-0581), 10.4271/2013-01-0581.

38. Cengel, Y. A., and Boles, M. A., 2001, Thermodynamics: An Engineering Approach, Mcgraw-Hill College.

39. Lueddecke, B., Filsinger, D., and Bargende, M., 2014, "Engine crank angle resolved turbocharger turbine performance measurements by contactless shaft

torque detection", 11th International Conference on Turbochargers and Turbocharging, IMechE, London, pp. 301-320.

40. Bohn, D., Heuer, T., and Kusterer, K., 2005, "Conjugate Flow and Heat Transfer Investigation of a Turbo Charger", Journal of Engineering for Gas Turbines and Power, 127 (3), pp. 663-669, 10.1115/1.1839919.

41. Deraad, S., Fulton, B., Gryglak, A., Hallgren, B., Hudson, A., Ives, D., Morgan, P., Styron, J., Waszczenko, E., and Cattermole, I., 2010, "The New Ford 6.7L V-8 Turbocharged Diesel Engine", SAE Technical Paper (2010-01-1101), 10.4271/2010-01-1101.

42. Sirakov, B., and Casey, M., 2013, "Evaluation of Heat Transfer Effects on Turbocharger Performance", Journal of Turbomachinery, 135 (021011), 10.1115/1.4006608.

43. Cormerais, M., Hetet, J. F., Chesse, P., and Maiboom, A., 2006, "Heat Transfer Analysis in a Turbocharger Compressor: Modeling and Experiments", SAE Technical Paper (2006-01-0023), 10.4271/2006-01-0023.

44. Dittus, F. W., and Boelter, L. M. K., 1985, "Heat transfer in automobile radiators of the tubular type", International Communications in Heat and Mass Transfer, 12 (1), pp. 3-22, 10.1016/0735-1933(85)90003-X.

45. Cormerais, M., Chesse, P., and Hetet, J. F., 2009, "Turbocharger Heat Transfer Modeling Under Steady and Transient Conditions", International Journal of Thermodynamics, 12 (4).

46. Baines, N., Wygant, K. D., and Dris, A., 2010, "The Analysis of Heat Transfer in Automotive Turbochargers", Journal of Engineering for Gas Turbines and Power, 132 (0402301), 10.1115/1.3204586.

47. Serrano, J. R., Olmeda, P., Páez, A., and Vidal, F., 2010, "An experimental procedure to determine heat transfer properties of turbochargers", Measurement Science and Technology, 21 (035109), 10.1088/0957-0233/21/3/035109.

48. Serrano, J. R., Dolz, V., Arnau, F. J., and Reyes Belmonte, M. A., 2013, "Determination of heat flows inside turbochargers by means of a one dimensional lumped model", Mathematical and Computer Modelling, 57, pp. 1847-1852.

49. Aghaali, H., and Angstrom, H.-E., 2012, "Improving Turbocharged Engine Simulation by Including Heat Transfer in the Turbocharger", SAE Technical Paper (2012-01-0703), 10.4271/2012-01-0703.

50. Payri, F., Olmeda, P., Arnau, F. J., Dombrovsky, A., and Smith, L., 2014, "External heat losses in small turbochargers: Model and experiments", Energy, 71, pp. 534-546, 10.1016/j.energy.2014.04.096.

51. Burke, R. D., Olmeda, P., Arnau, F. J., and Reyes Belmonte, M. A., 2014, "Modelling of turbocharger heat transfer under stationary and transient engine operating conditions", 11th International Conference on Turbochargers and Turbocharging, IMechE, London, pp. 104-112.

52. Serrano, J. R., Olmeda, P., Arnau, F. J., Dombrovsky, A., and Smith, L., 2014, "Analysis and Methodology to Characterize Heat Transfer Phenomena in Automotive Turbochargers", Journal of Engineering for Gas Turbines and Power, 137 (021901), 10.1115/1.4028261.

53. Cavalcanti de Souza, R., and Krieger Filho, G. C., 2011, "Automotive Turbocharger Radial Turbine CFD and Comparison to Gas Stand Data", SAE Technical Paper (2011-36-0081), 10.4271/2011-36-0081.

54. Grabowska, D., Palfreyman, D., and Reynolds, B., 2010, "Application of Star-CCM+ to Turbocharger Modeling at BorgWarner Turbo Systems", CD-adapco, 9th November 2010.

55. Haehndel, K., Frank, T., Christel, F. M., Spengler, C., Suck, G., and Abanteriba, S., 2013, "The Development of Exhaust Surface Temperature Models for 3D CFD Vehicle Thermal Management Simulations Part 1 - General Exhaust Configurations", SAE Technical Paper (2013-01-0879), 10.4271/2013-01-0879.

56. De Vos, S., Haehndel, K., Frank, T., Christel, F., and Abanteriba, S., 2014, "The Development of Turbine Volute Surface Temperature Models for 3D CFD Vehicle Thermal Management Simulations: Part 3: Exhaust Radial Turbine Volute Systems", SAE Technical Paper (2014-01-0648), 10.4271/2014-01-0648.

57. Romagnoli, A., and Martinez-Botas, R., 2012, "Heat transfer analysis in a turbocharger turbine: An experimental and computational evaluation", Applied Thermal Engineering, 38, pp. 58-77, 10.1016/j.applthermaleng.2011.12.022.

58. Burke, R. D., 2014, "Analysis and Modeling of the Transient Thermal Behavior of Automotive Turbochargers", Journal of Engineering for Gas Turbines and Power, 136 (101511), 10.1115/1.4027290.

59. Scharf, J., Uhlmann, T., Schernus, C., Lueckmann, D., Hoepke, B., and Schorn, N., 2012, "Extended Turbine Mapping and its Benefits for the Development of Turbocharged Internal Combustion Engines", 21st Aachen Colloquium Automobile and Engine Technology, RWTH Aachen, Aachen, 8-10 October 2012, pp. 449-473.

60. Scharf, J. S., 2010, "Extended Turbocharger Mapping and Engine Simulation ", Ph.D., RWTH, Aachen.

61. Lueckmann, D., Schernus, C., Uhlmann, T., Hoepke, B., and Nebbia, C., 2012, "Friction and Heat Transfer Effects on Turbocharger Modeling", GT 2012 Conference, GT-Suite, Frankfurt, 22nd October 2012.

62. Burke, R. D., Copeland, C., Duda, T., and Reyes Belmonte, M. A., 2015, "Lumped capacitance and 3D CFD conjugate heat transfer modelling of an automotive turbocharger", Proceedings of the ASME Turbo Expo 2015, ASME, Montreal, 10.1115/GT2015-42612.

63. Anwer, M., and So, R. M. C., 1993, "Swirling turbulent flow through a curved pipe. Part I: Effect of swirl and bend curvature", Experiments in Fluids, 14, pp. 85-96.

64. Wallace, F. J., Whitfield, A., and Atkey, R. C., 1975, "Experimental and theoretical performance of a radial flow turbocharger compressor with inlet prewhirl", ImechE Proc Instn Mech Engrs, 189 (43/75), pp. 177-186.

65. Whitfield, A., and Abdullah, A. H., 1998, "The Performance of a Centrifugal Compressor With High Inlet Prewhirl", ASME Journal of Turbomachinery, 120 (July 1998), pp. 487-493.

66. Mohtar, H., Chesse, P., Yammine, A., and Hetet, J. F., 2008, "Variable Inlet Guide Vanes in a Turbocharger Centrifugal Compressor: Local and Global Study", SAE Technical Paper (2008-01-0301), 10.4271/2008-01-0301.

67. Galindo, J., Serrano, J. R., Margot, X., Tiseira, A., Schorn, N., and Kindl, H., 2007, "Potential of flow pre-whirl at the compressor inlet of automotive engine

turbochargers to enlarge surge margin and overcome packaging limitations", International Journal of Heat and Fluid Flow, 28 (3), pp. 374-387, 10.1016/j.ijheatfluidflow.2006.06.002.

68. Kim, Y., Engeda, A., Aungier, R., and Direnzi, G., 2001, "The influence of inlet flow distortion on the performance of a centrifugal compressor and the development of an improved inlet using numerical simulations", Proceedings of the Institution of Mechanical Engineers, Part A: Journal of Power and Energy, 215 (3), pp. 323-338, 10.1243/0957650011538550.

69. Engeda, A., Kim, Y., Aungier, R., and Direnzi, G., 2003, "The Inlet Flow Structure of a Centrifugal Compressor Stage and Its Influence on the Compressor Performance", Journal of Fluids Engineering, 125 (5), p. 779, 10.1115/1.1601255.

70. Capon, G., Leong, A., and Morris, T., 2006, "The Influence of Installation Parameters on Turbocharged Automotive Engine Performance", 8th International Conference on Turbochargers and Turbocharging, IMechE, London, pp. 43-54.

71. Chen, H., and Lei, V.-M., 2013, "Casing Treatment and Inlet Swirl of Centrifugal Compressors", Journal of Turbomachinery, 135 (041010), 10.1115/1.4007739.

72. Harley, P. X. L., Spence, S. W. T., Early, J., Filsinger, D., and Dietrich, M., 2014, "Inlet recirculation in automotive turbocharger centrifugal compressors", 11th International Conference on Turbochargers and Turbocharging, IMechE, London, pp. 89-100.

73. Capon, G., and Morris, T., 2010, "The effect of air inlet system features on automotive turbocharger compressor performance", 9th International Conference on Turbochargers and Turbocharging, IMechE, London, pp. 95-113.

74. Serrano, J. R., Margot, X., Tiseira, A., and Garcia-Cuevas, L. M., 2013, "Optimization of the inlet air line of an automotive turbocharger", International Journal of Engine Research, 14 (1), pp. 92-104, 10.1177/1468087412449085.

75. Liu, Y., Zhuge, W., Zheng, X., Zhang, Y., Zhang, S., and Zhang, J., 2013, "Study of Mechanism of Counter-rotating Turbine Increasing Two-Stage Turbine System Efficiency", International Journal of Fluid Machinery and Systems, 6 (3), pp. 160-169, 10.5293/ijfms.2013.6.3.160.

76. Avola, C., Dimitriou, P., Burke, R., and Copeland, C., 2016, "Preliminary DoE Analysis and Control of Mapping Procedure for a Turbocharger on an Engine Gas-stand", ASME Turbo EXPO 2016, ASME, Seoul, South Korea, 13-17 June 2016, 10.1115/GT2016-56466.

77. Serrano, J. R., Olmeda, P., Arnau, F. J., Dombrovsky, A., and Smith, L., 2015, "Turbocharger heat transfer and mechanical losses influence in predicting engines performance by using one-dimensional simulation codes ", Energy, 86, pp. 204-218, 10.1016/j.energy.2015.03.130.

78. Serrano, J. R., Arnau, F. J., Novella, R., and Reyes Belmonte, M. A., 2014, "A Procedure to Achieve 1D Predictive Modeling of Turbochargers under Hot and Pulsating Flow Conditions at the Turbine Inlet", SAE Technical Paper (2014-01-1080), 10.4271/2014-01-1080.

79. Deligant, M., Podevin, P., and Descombes, G., 2012, "Experimental identification of turbocharger mechanical friction losses", Energy, 39 (1), pp. 388-394, 10.1016/j.energy.2011.12.049.

80. Lujan, J. M., Bermudez, V., Serrano, J. R., and Cervello, C., 2002, "Test Bench for Turbocharger Groups Characterization", SAE Technical Paper (2002-01-0163), 10.4271/2002-01-0163.

81. Bontempo, R., Cardone, M., Manna, M., and Vorraro, G., 2014, "Highly Flexible Hot Gas Generation System for Turbocharger Testing", Energy Procedia, 45, pp. 1116-1125, 10.1016/j.egypro.2014.01.117.

82. SAE-International, 1995, "SAE J1723 Supercharger Testing Standard", Society of Automotive Engineers, Inc.

83. ASME, 1997, "Performance Test Code on Compressors and Exhausters", ASME Standards.

84. Lee, E. A., and Varaiya, P., 2011, Structure and Interpretation of Signals and Systems, LeeVaraiya.org.

85. Tang, Q., Fu, J., Liu, J., Boulet, B., Tan, L., and Zhao, Z., 2016, "Comparison and analysis of the effects of various improved turbocharging approaches on gasoline engine transient performances", Applied Thermal Engineering, 93, pp. 797-812, 10.1016/j.applthermaleng.2015.09.063.

86. Roethlisberger, R. P., and Favrat, D., 2002, "Comparison between direct and indirect (prechamber) spark ignition in the case of a cogeneration natural gas engine, part II: engine operating parameters and turbocharger characteristics", Applied Thermal Engineering, 22, pp. 1231-1243, 0.1016/S1359-4311(02)00041-8.

87. Galindo, J., Luján, J. M., Serrano, J. R., and Hernández, L., 2005, "Combustion simulation of turbocharger HSDI Diesel engines during transient operation using neural networks", Applied Thermal Engineering, 25 (5-6), pp. 877-898, 10.1016/j.applthermaleng.2004.08.004.

88. Serrano, J. R., Arnau, F. J., Dolz, V., and Piqueras, P., 2009, "Methodology for characterisation and simulation of turbocharged diesel engines combustion during transient operation. Part 1: Data acquisition and post-processing", Applied Thermal Engineering, 29 (1), pp. 142-149, 10.1016/j.applthermaleng.2008.02.011.

89. Rajoo, S., and Martinez-Botas, R. F., 2010, "Unsteady Effect in a Nozzled Turbocharger Turbine", Journal of Turbomachinery, 132 (3), p. 031001, 10.1115/1.3142862.

90. Bontempo, R., Cardone, M., Manna, M., and Vorraro, G., 2015, "Steady and unsteady experimental analysis of a turbocharger for automotive applications", Energy Conversion and Management, 99, pp. 72-80, 10.1016/j.enconman.2015.04.025.

91. Winterbone, D. E., and Pearson, R. J., "Turbocharger turbine performance under unsteady flow - a review of experimental results and proposed models", Proc. Sixth International Conference on Turbocharging and Air Management Systems, C554/031/98, IMechE, 193-206.

92. Lujan, J. M., Galindo, J., and Serrano, J. R., 2001, "Efficiency Characterization of Centripetal Turbines under Pulsating Flow Conditions", SAE Technical Paper (2001-01-0272), 10.4271/2001-01-0272.

93. Lee, J., Tan, C. S., Sirakov, B., Wilkins, C., Im, H.-S., Babak, M., and Tisserant, D., "Performance Metric for Turbine Stage under Unsteady Pulsating Flow Environment", Proc. ASME Turbo EXPO 2016, GT2016-56343, ASME, 13-17 June 2016, p.^pp., 10.1115/GT2016-56343.

94. Ehrlich, D. A., Lawless, P. B., and Fleeter, S., 1997, "On-Engine Turbocharger Turbine Inlet Flow Characterization", SAE Technical Paper (971565), 10.4271/971565.

95. Marelli, S., and Capobianco, M., 2011, "Steady and pulsating flow efficiency of a waste-gated turbocharger radial flow turbine for automotive application", Energy, 36 (1), pp. 459-465, 10.1016/j.energy.2010.10.019.

96. Arenz, M. C., Weigel, B., Habermann, J., Staudacher, S., Rose, M. G., Lutum, E., and Berns, W., "Development and Application of a Fast-response Total Temperature Probe for Turbomachinery", Proc. ASME Turbo EXPO 2016, GT2016-56132, ASME, 13-17 June 2016, p.^pp., 10.1115/GT2016-56132.

97. Laurantzon, F., Tillmark, N., and Alfredsson, P. H., 2010, "A pulsating flow rig for analyzing turbocharger performance", 9th International Conference on Turbochargers and Turbocharging, pp. 363-372.

98. Capobianco, M., and Marelli, S., "Turbocharger turbine performance under steady and unsteady flow: test bed analysis and correlation criteria", Proc. 8th International Conference on Turbochargers and Turbocharging, IMechE, 193-206.

99. Kalpakli, A., Örlü, R., Tillmark, N., and Alfredsson, P. H., 2012, "Experimental investigation on the effect of pulsations on exhaust manifold-related flows aiming at improved efficiency", 10th International Conference on Turbochargers and Turbocharging, pp. 377-387.

100. Serrano, J. R., Arnau, F. J., Dolz, V., Tiseira, A., and Cervelló, C., 2008, "A model of turbocharger radial turbines appropriate to be used in zero- and one-dimensional gas dynamics codes for internal combustion engines modelling", Energy Conversion and Management, 49 (12), pp. 3729-3745, 10.1016/j.enconman.2008.06.031.

101. Piscaglia, F., Onorati, A., Marelli, S., and Capobianco, M., 2007, "Unsteady Behavior in Turbocharger Turbines: Experimental Analysis and Numerical Simulation", SAE Technical Paper (2007-24-0081), 10.4271/2007-24-0081.

102. Chiong, M. S., Rajoo, S., Romagnoli, A., Costall, A. W., and Martinez-Botas, R. F., 2014, "Integration of meanline and one-dimensional methods for prediction of

pulsating performance of a turbocharger turbine", Energy Conversion and Management, 81, pp. 270-281, 10.1016/j.enconman.2014.01.043.

103. Costall, A., and Martinez-Botas, R., "Fundamental Characterization of Turbocharger Turbine Unsteady Flow Behaviour", Proc. ASME Turbo Expo 2007, GT2007-28317, ASME, 10.1115/GT2007-28317.

104. Chiong, M. S., Rajoo, S., Romagnoli, A., and Martinez-Botas, R., "Unsteady Performance Prediction of a Single Entry Mixed Flow Turbine Usinf 1-D Gas Dynamic Code Extended with Meanline Model", Proc. ASME Turbo EXPO 2012, GT2012-69176, ASME, 11-15 June 2012, p.^pp., 10.1115/GT2012-69176.

105. Costall, A. W., McDavid, R. M., Martinez-Botas, R. F., and Baines, N. C., 2011, "Pulse Performance Modeling of a Twin Entry Turbocharger Turbine Under Full and Unequal Admission", Journal of Turbomachinery, 133 (2), p. 021005, 10.1115/1.4000566.

106. Yang, M., Martinez-Botas, R., Rajoo, S., Ibaraki, S., Yokoyama, T., and Deng, K., "Unsteady behaviours of a volute in turbocharger turbine under pulsating conditions", Proc. Global Power and Propulsion Forum 2017, GPPF-2017-54, GPPS, 16-18 Jan 2017, p.^pp.

107. Szymko, S., Martinez-Botas, R., and Pullen, K. R., "Experimental Evaluation of Turbocharger Turbine Performance under Pulsating Flow Conditions", Proc. ASME Turbo EXPO 2005, GT2005-68878, ASME, 6-9 June 2005, p.^pp., 10.1115/GT2005-68878.

108. Greitzer, E. M., Tan, C. S., and Graf, M. B., 2004, Internal flow: concepts and applications, Cambridge University Press, USA.

109. Ricardo, "WAVE 2015.1 Help - Thermocouple Element ".

110. Galindo, J., Tiseira, A., Arnau, F. J., and Lang, R., 2013, "On-Engine Measurement of Turbocharger Surge Limit", Experimental Techniques, 37 (1), pp. 47-54, 10.1111/j.1747-1567.2010.00697.x.

111. Galindo, J., Arnau, F., Tiseira, A., Lang, R., Lahjaily PhD, H., and Gimenes Md, T., 2011, "Measurement and Modeling of Compressor Surge on Engine Test Bench for Different Intake Line Configurations", SAE Technical Paper, 10.4271/2011-01-0370.

112. Chesse, P., Hetet, J. F., Tauzia, X., Roy, P., and Inozu, B., 2000, "Performance Simulation of Sequentially Turbocharged Marine Diesel Engines With Applications to Compressor Surge", ASME Journal of Engineering for Gas Turbines and Power, 122, pp. 562-569, 10.1115/1.1290587.

113. Galindo, J., Serrano, J. R., Climent, H., and Tiseira, A., 2008, "Experiments and modelling of surge in small centrifugal compressor for automotive engines", Experimental Thermal and Fluid Science, 32 (3), pp. 818-826, 10.1016/j.expthermflusci.2007.10.001.

114. Liu, A. X., and Zheng, X. Q., 2013, "Methods of surge point judgment for compressor experiments", Experimental Thermal and Fluid Science, 51, pp. 204-213, 10.1016/j.expthermflusci.2013.07.015.

115. Avola, C., Copeland, C., Duda, T., and Burke, R. D., "Compressor surge for fully and semi fluctuating flows in automtoive turbochargers", Proc. Global Power and Propulsion Forum 2017, GPPF-2017-136, GPPS, 16-18 Jan 2017, p.^pp.

116. Tang, H., Pennycott, A., Akehurst, S., and Brace, C. J., 2014, "A review of the application of variable geometry turbines to the downsized gasoline engine", International Journal of Engine Research, 16 (6), pp. 810-825, 10.1177/1468087414552289.

117. Avola, C., Copeland, C., Burke, R. D., and Brace, C. J., 2016, "Numerical Investigation of Two-Stage Turbocharging Systems Performance", ASME ICEF 2016, ASME, Greenville, SC, USA, 10.1115/ICEF2016-9449.

118. Greitzer, E. M., 1976, "Surge and Rotating Stall in Axial Flow Compressors. Part I: Theoretical Compression System Model", ASME Journal of Engineering for Power, APRIL 1976, pp. 190-198, 10.1115/1.3446138.

119. Greitzer, E. M., 1976, "Surge and Rotating Stall in Axial Flow Compressors. Part II: Experimental Results and Comparison With Theory", ASME Journal of Engineering for Power, APRIL 1976, pp. 199-211, 10.1115/1.3446139.

120. Hansen, K. E., Jorgensen, P., and Larsen, P. S., 1981, "Experimental and Theoretical Study of Surge in a Small Centrifugal Compressor", ASME Journal of Fluids Engineering, 103, pp. 391-395, 10.1115/1.3240796.

121. Fink, D. A., Cumpsty, N. A., and Greitzer, E. M., 1992, "Surge Dynamics in a Free-Spool Centrifugal Compressor System", Journal of Turbomachinery, 114 (April 1992), pp. 321-332, 10.1115/1.2929146.

122. Dehner, R., Selamet, A., Keller, P., and Becker, M., 2011, "Prediction of Surge in a Turbocharger Compression System vs. Measurements", SAE International Journal of Engines, 4 (2), pp. 2181-2192, 10.4271/2011-01-1527.

123. Theotokatos, G., and Kyrtatos, N. P., 2001, "Diesel Engine Transient Operation with Turbocharger Compressor Surging", SAE Technical Paper (2001-01-1241), 10.4271/2001-01-1241.

124. Galindo, J., Serrano, J. R., Guardiola, C., and Cervelló, C., 2006, "Surge limit definition in a specific test bench for the characterization of automotive turbochargers", Experimental Thermal and Fluid Science, 30 (5), pp. 449-462, 10.1016/j.expthermflusci.2005.06.002.

125. Marelli, S., Carraro, C., Marmorato, G., Zamboni, G., and Capobianco, M., 2014, "Experimental analysis on the performance of a turbocharger compressor in the unstable operating region and close to the surge limit", Experimental Thermal and Fluid Science, 53, pp. 154-160, 10.1016/j.expthermflusci.2013.11.025.

126. Andersen, J., Lindström, F., and Westin, F., 2008, "Surge Definitions for Radial Compressors in Automotive Turbochargers", SAE Technical Paper (2008-01-0296), 10.4271/2008-01-0296.

127. Galindo, J., Climent, H., Guardiola, C., and Tiseira, A., 2009, "On the effect of pulsating flow on surge margin of small centrifugal compressors for automotive engines", Experimental Thermal and Fluid Science, 33 (8), pp. 1163-1171, 10.1016/j.expthermflusci.2009.07.006.

128. Marelli, S., Carraro, C., and Capobianco, M., 2012, "Effect of Pulsating Flow Characteristics on Performance and Surge Limit of Automotive Turbocharger Compressors", SAE International Journal of Engines, 5 (2), pp. 596-601, 10.4271/2012-01-0715.

129. Barrera-Medrano, M. E., Newton, P., Martinez-Botas, R., Rajoo, S., Tomita, I., and Ibaraki, S., "Effect of exit pressure pulsation on the performance and stability limit of a turbocharger centrifugal compressor", Proc. ASME Turbo EXPO 2016,

GT2016-56109, ASME, ed., ASME, 13-17 June 2016, p.^pp., 10.1115/GT2016-56109.

130. An, B., and Shiraishi, T., 2010, "Development of Variable Two-stage Turbocharger for Passenger Car Diesel Engines", Mitsubishi Heavy Industries Technical Review, 47 (4).

131. Kaufmann, A., 2014, "Using Turbocharger maps in gas exchange simulation and engine control units", Forschung im Ingenieurwesen, 78 (1-2), pp. 45-57, 10.1007/s10010-014-0171-0.

132. Avola, C., Copeland, C. D., Burke, R. D., and Brace, C. J., 2017, "Effect of inter-stage phenomena on the performance prediction of two-stage turbocharging systems", Energy, 134, pp. 743-756, 10.1016/j.energy.2017.06.067.

133. Zamboni, G., and Capobianco, M., 2012, "Experimental study on the effects of HP and LP EGR in an automotive turbocharged diesel engine", Applied Energy, 94, pp. 117-128, 10.1016/j.apenergy.2012.01.046.

134. Bermúdez, V., Lujan, J. M., Pla, B., and Linares, W. G., 2011, "Effects of low pressure exhaust gas recirculation on regulated and unregulated gaseous emissions during NEDC in a light-duty diesel engine", Energy, 36 (9), pp. 5655-5665, 10.1016/j.energy.2011.06.061.

135. Galindo, J., Ruiz, S., Dolz, V., and Royo-Pascual, L., 2016, "Advanced exergy analysis for a bottoming organic rankine cycle coupled to an internal combustion engine", Energy Conversion and Management, 126, pp. 217-227, 10.1016/j.enconman.2016.07.080.

136. Al-Hinti, I., Samhouri, M., Al-Ghandoor, A., and Sakhrieh, A., 2009, "The effect of boost pressure on the performance characteristics of a diesel engine: A neuro-fuzzy approach", Applied Energy, 86 (1), pp. 113-121, 10.1016/j.apenergy.2008.04.015.

137. Bernasconi, S., Codan, E., Yang, D., Jacoby, P., and Weisser, G., "Two-stage Turbocharging Solutions for Tier 4 Rail Applications", Proc. ASME 2015 Internal Combustion Engine Division Fall Technical Conference, ASME, ed., ASME, November 8-11, 2015, p.^pp., 10.1115/ICEF2015-1076.

138. Grönman, A., Sallinen, P., Honkatukia, J., Backman, J., and Uusitalo, A., 2016, "Design and experiments of two-stage intercooled electrically assisted turbocharger", Energy Conversion and Management, 111, pp. 115-124, 10.1016/j.enconman.2015.12.055.

139. Numakura, R., 2012, "Performance of a small-size two-stage centrifugal compressor", 10th International Conference on Turbochargers and Turbocharging, IMechE, London, UK, pp. 307-318, 10.1533/9780857096135.6.307.

140. Emekli, M. E., and Güvenç, B. A., 2016, "Explicit MIMO Model Predictive Boost Pressure Control of a Two-Stage Turbocharged Diesel Engine", IEEE Transactions on Control Systems Technology, PP (99), 10.1109/TCST.2016.2554558.

141. Galindo, J., Tiseira, A., Navarro, R., Tarí, D., and Meano, C. M., 2017, "Effect of the inlet geometry on performance, surge margin and noise emission of an automotive turbocharger compressor", Applied Thermal Engineering, 110, pp. 875-882, 10.1016/j.applthermaleng.2016.08.099.

142. Liu, Y. B., Zhuge, W. L., Zhang, Y. J., and Zhang, S. Y., 2016, "Numerical analysis of flow interaction of turbine system in two-stage turbocharger of internal combustion engine", IOP Conference Series: Materials Science and Engineering, 129, p. 012004, 10.1088/1757-899x/129/1/012004.

143. Serrano, J. R., Olmeda, P., Arnau, F. J., Reyes-Belmonte, M. A., and Tartoussi, H., 2015, "A study on the internal convection in small turbochargers. Proposal of heat transfer convective coefficients", Applied Thermal Engineering, 89, pp. 587-599, 10.1016/j.applthermaleng.2015.06.053.